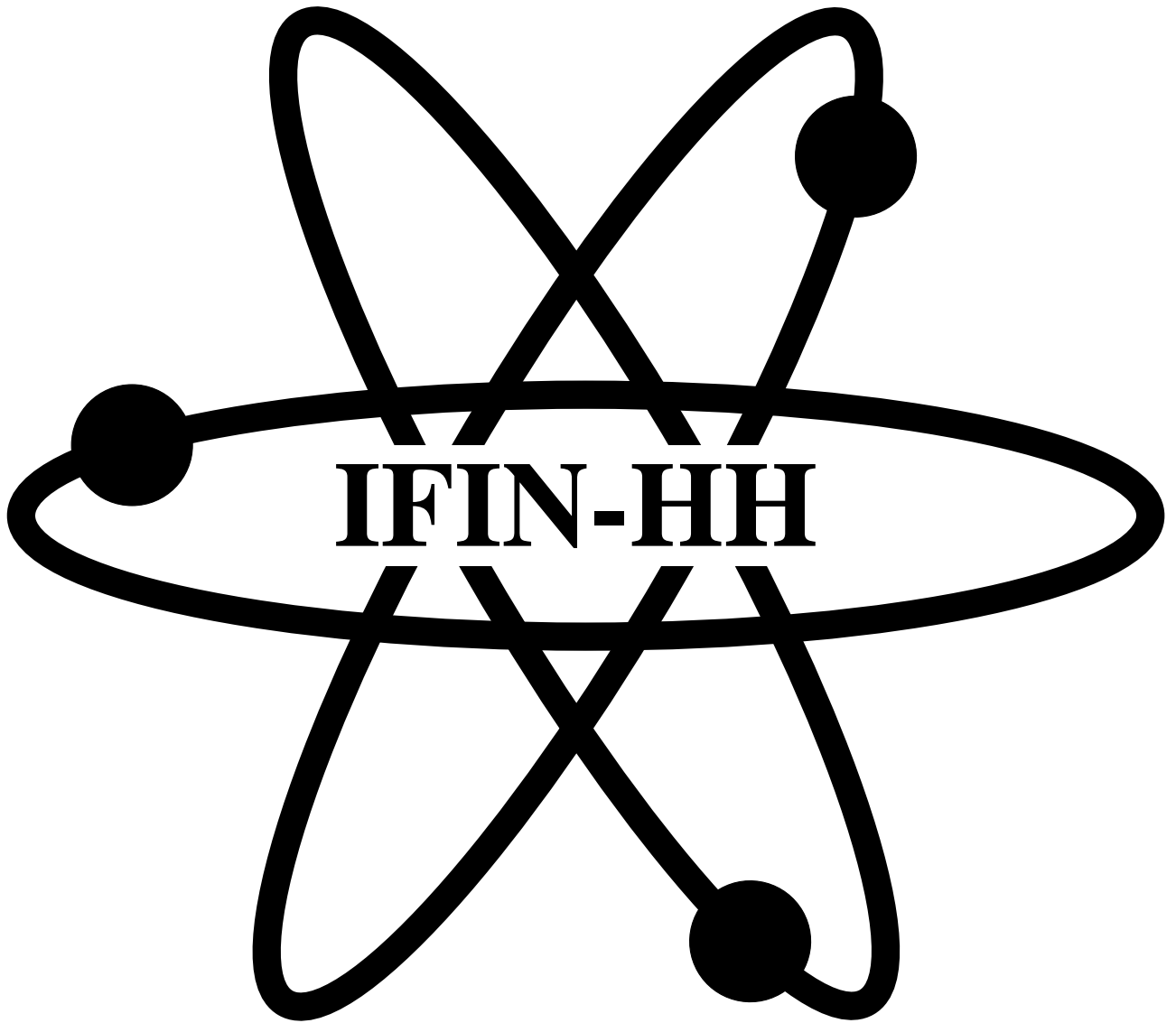


SCIENTIFIC REPORT 2000



Bucharest, Romania, 2001

ISSN 1454-2714
IFIN-HH-AR-2001

Publisher: Horia Hulubei National Institute for Physics and Nuclear Engineering
Str. Atomistilor no. 109
P.O. Box MG-6
RO-76900 Bucharest-Măgurele
Romania
Telephone: +40 1 780 70 40
Fax: +40 1 423 17 01
E-mail: ifin.nipne.ro
WWW home page: <http://www.nipne.ro>

Editors: Felicia Drăgulici, Sanda-Elena Enescu, Margareta Oancea, Mihaela Preda, Lucia Prodan, Adriana Răduță, Doina Sandu, Claudiu Șchiaua

The editors have not modified the text of the contributions, not even for spelling or grammar. Changes were only made in the title of some contributions by converting some capital-case letters to lower-case for case uniformity, and in the spelling of some author's names to assure the correct building of the author index.

Contents

Theoretical Physics	7
Nuclear and Atomic Physics	9
Mathematical Physics, Field Theory and Elementary Particles	10
Physics of Information	14
Nuclear Physics	21
Nuclear Structure	23
Nuclear Reactions	35
Atomic Physics	44
Cosmic Rays and Nuclear Astrophysics	51
Inertial Fusion, Physics of Neutrons and Nuclear Transmutations	54
Nuclear Instruments and Methods	59
Particle Physics	71
Health and Environmental Physics	85
Applied Physics	95
Tracers, Radiopharmaceuticals and Radiometry	111
Waste Management and Site Restoration	123
Standardisation	127
Appendix	131
Publications	133
In Journals	133
Books and Chapter in Books	138
Preprints	138
International Conferences	139
PhD Theses	145
Scientific Exchanges	145
Foreign Visitors	145
Invited Seminars	146

	5
Visits Abroad	146
Seminars Abroad	148
Research Staff	149
Author Index	153

Results included in the following are progress reports of research projects and therefore should be considered as preliminary communications.

Theoretical Physics

Nuclear and Atomic Physics	9
Mathematical Physics, Field Theory and Elementary Particles	10
Physics of Information	14

Nuclear and Atomic Physics

Influence of the absorptive part of the complex potential on the S-Matrix poles

C. Grama¹, N. Grama¹, I. Zamfirescu¹

¹ IFIN-HH

Although the polology of the S-matrix has been extensively studied, it occurred that some aspects remained disputable in the case of complex central potential $\mathcal{V}(r) = gV(r)$, $g \in \mathbf{C}$. These aspects are related to the origin of the observed narrow Σ -hypernuclear states that have been interpreted by Gal, Toker and Alexander [1] as states which correspond to S-matrix poles situated in the second k -plane quadrant. From the analytical properties of the S-matrix for a real potential it results that there is no pole in the first and second k -plane quadrants, except for the imaginary k -axis. By switching on the absorption the S-matrix poles for real potential can evolve into the second quadrant of the k -plane. A critical study of the Σ -hypernuclear states needs the analysis of the motion of the S-matrix poles in the k -plane for variable complex coupling strength g . Recently contradictory opinions relative to the S-matrix poles trajectories in the complex k -plane for a complex square potential occurred. According to some authors [1, 2, 3] the poles in the second quadrant can occur either from bound state poles moving anticlockwise, or from virtual state poles and capture resonant state poles moving clockwise as the absorption is switched on. Dąbrowski [4] argues that the statement made by [1, 2, 3] concerning the movement of the virtual poles with increasing absorptive potential is in general not correct. Dąbrowski [4, 5] relates the direction in which the pole moves when the potential absorption increases to the direction in which the pole moves with increasing the real part of the potential, without clarifying this last question. For example, two poles moving in opposite directions along the imaginary k -axis are associated in [4, 5] to the same state. This is a wrong result, because one should associate a single pole to each quantum state.

The aim of our work is to study the influence of the absorptive part of the potential on the S-matrix poles for the non-relativistic scattering in the framework of the Riemann surface approach for bound and resonant states.

The Riemann surface approach has been presented in details in [6]. It consists in constructing the Riemann surface $R_g^{(l)}$ of the pole function $k = k^{(l)}(g)$ over the complex g -plane on which the pole function $k = k^{(l)}(g)$ is single-valued and analytic. $R_g^{(l)}$ is di-

vided into sheets $\Sigma_n^{(l)}$ and the images $\Sigma_n'^{(l)}$ of these sheets in the k -plane are constructed. In this way the sheet $\Sigma_n^{(l)}$ of $R_g^{(l)}$ is associated to a given state with quantum numbers (l, n) . The number n that labels the sheets, their images and the corresponding quantum states (l, n) counts the solutions of the pole function at $g \rightarrow 0$ [6].

The global method allows the unique identification of the poles that can occur in the second quadrant of the k -plane by switching on the absorption of the potential. By a detailed analysis of the Riemann surface $R_g^{(l)}$ of the pole function for a central rectangular potential we have found that the poles that can support the Σ -hypernuclear states occur on the sheet images $\Sigma_{-n}^{(l)}$, $n \geq (l+1)/2$ for odd l and $n \geq l/2$ for even l . They originate from those poles that for a real potential are bound or capture resonant state poles.

As a result of our analysis a complete answer is given to the disputable problem of the direction in which a virtual pole moves when the absorption is introduced. Our analysis shows that the virtual poles do not always move towards the third quadrant of the k -plane, as stated in [2, 3]. For example, for $l = 0$ the virtual poles on the sheet images $\Sigma_n^{(0)}$, $n \leq 0$, move clockwise into the third quadrant of the k -plane, while on the sheet images $\Sigma_n'^{(0)}$, $n > 0$, they move anticlockwise into the fourth quadrant of the k -plane when the absorption is switched on.

References

- [1] Gal A, Toker G and Alexander Y 1981 *Ann. Phys., NY* **137** 341
- [2] Bonetti R, Koning A J, Accermans J M and Hodgson P E 1994 *Phys. Rep.* **247** 1
- [3] Oset E, de Córdoba P F, Salcedo L L and Brockmann R 1990 *Phys. Rep.* **188** 79
- [4] Dąbrowski J 1996 *Phys. Rev. C* **53** 2004
- [5] Dąbrowski J 1997 *J. Phys. G:Nucl. Part. Phys.* **23** 1539
- [6] C.Grama, N.Grama and I.Zamfirescu, *Phys. Rev. A* **61** (2000) 032716

Mathematical Physics, Field Theory and Elementary Particles

Factorization of unitary matrices

P. Diță¹

¹ Theoretical Physics Department

Matrix factorization is a live subject of linear algebra and no general theory is available yet. Our goal is to obtain a factorization of unitary matrices that are very useful tools in solving many problems in mathematical and theoretical physics. Factorization is closely related to parametrization of unitary matrices and the classical result by Murnaghan [1] gives the parametrization of an $n \times n$ unitary matrix as a product of a diagonal matrix containing n phases and $n(n-1)/2$ matrices whose main building block is essentially two-dimensional. A selection of a specific set of angles and/or phases has no theoretical significance because all the choices are mathematically equivalent, however a clever choice may shed some light on important qualitative issues. In the same time many new problems require a more elaborate factorization, one of them being that suggested by Chaturvedi and Mukunda and Mathur and Sen [2] who obtained a factorization of $SU(3)$ matrices as a product of two matrices each one being generated by a complex vector. Our aim was to elaborate such a factorization for $n \times n$ unitary matrices as a product of n diagonal matrices containing phases and $n-1$ orthogonal matrices, each one generated by a n -dimensional real vector. The result is contained in the following:

Theorem: Any element $A_n \in U(n)$ can be factored into an ordered product of $2n-1$ matrices of the following form

$$A_n = d_n^0 \mathcal{O}_n d_{n-1}^1 \mathcal{O}_{n-1}^1 \dots d_2^{n-2} \mathcal{O}_2^{n-1} d_1^{n-1}$$

where d_{n-k}^k are diagonal matrices of the form $d_{n-k}^k = (1_{n-k}, e^{i\psi_1}, \dots, e^{i\psi_k})$, $k \leq n$, where 1_{n-k} means that the first $(n-k)$ diagonal entries are equal to unity,

\mathcal{O}_{n-k}^k are orthogonal matrices whose columns are generated by real $(n-k)$ -dimensional unit vectors. The condition $\sum_{i=1}^{n(n+1)/2} \psi_i = 0$, imposed on ψ_i the arbitrary phases entering the parametrization of A_n , gives the factorization of $SU(n)$ matrices. If $w_n = \mathcal{O}_n d_{n-1}^1 \mathcal{O}_{n-1}^1 \dots d_2^{n-2} \mathcal{O}_2^{n-1} d_1^{n-1} = \mathcal{O}_n d_{n-1}^1 w_{n-1}$ then

$$W_n = w_n^* d_n w_n \quad (11)$$

is one (of the many possible) Weyl representation of unitary matrices. If all the phases entering A_n are zero $\psi_i = 0$, $i = 1, \dots, n(n+1)/2$, one gets the factorization of rotations $R_n \in SO(n)$

$$R_n = \mathcal{O}_n \mathcal{O}_{n-1}^1 \dots \mathcal{O}_2^{n-1} \quad (12)$$

More details and proofs are given in [3]

References

- [1] F.D. Murnaghan, *The Unitary and Rotation Groups*, (1962), Spartan Books, Washington, D.C.
- [2] S. Chaturvedi and N. Mukunda, *Parametrizing the Mixing Matrix: a Unified Approach*, arXiv: hep-ph/0004219
M Mathur and D Sen, *Coherent States For $SU(3)$* , arXiv: quant-ph/0012099
- [3] P. Diță, *Factorization of Unitary Matrices*, arXiv: math-ph/0103005

Off-shell extrapolation for $B \rightarrow \pi^+ \pi^-$ decay

I. Caprini¹, L. Micu¹, C. Bourrely²

¹ NIPNE-HH, Theoretical Physics Department

² Centre de Physique Théorique, CNRS-Luminy, Marseille, France

The inclusion of the strong interaction effects in the theory of exclusive nonleptonic B decays is a very difficult task. The problem has been investigated recently by many authors, in particular, for charmless decays into light pseudoscalar mesons, since the strong phases of these amplitudes are crucial for the determination of CP-violating phases in present and future experiments.

Recent calculations of the $B \rightarrow \pi^+ \pi^-$ decay amplitude were performed either in the generalized QCD factorization approach [1] and the conventional perturbative QCD [2], or in a hadronic approach [3], [4]. We consider the decay amplitude

$$A(p, k_1, k_2) = \langle \pi^+ \pi^-, \text{out} | \mathcal{H}_w(0) | B_d^0, \text{in} \rangle, \quad (1)$$

where the “in” and “out” states are defined with respect to the strong interactions and \mathcal{H}_w is the weak effective hamiltonian. The decay amplitude (1) can be splitted as

$$A = V_{ud} V_{ub}^* A_u + V_{cd} V_{cb}^* A_c, \quad (2)$$

with the CP violating phase $\gamma = \text{Arg}(V_{ub}^*)$ appearing in the first term.

The physical amplitude (1) is calculated for $p = k_1 + k_2$ at on-shell values of the momenta, $p^2 = m_B^2$, $k_1^2 = m_\pi^2$, $k_2^2 = m_\pi^2$. The extrapolation to off-shell external momenta can be achieved by the LSZ reduction formalism [5]. In Ref. [4] this procedure was applied to the expression (1) of the amplitude. However, it is more convenient to start from the S -matrix element of the decay and apply the LSZ reduction to the B meson and one of the final pions. This method allows us to make an analytic continuation either with respect to in the squared momentum p^2 of the B -meson, or with respect with the squared momentum k_1^2 of one final pion. We obtain in both cases dispersion relations with spectral functions describing final state and initial state interactions, which involve complicated off-shell amplitudes. Actually, one can derive dispersion relations for each of the amplitudes A_u and A_c appearing in (2). In particular, the dispersion relations with respect to the momentum squared k_1^2 of one final meson can be written as

$$A_j = A_{j,0} + \frac{\sigma_{j,FSI}}{\pi} \ln \left[\frac{m_\pi^2}{(m_B - m_\pi)^2} - 1 \right], \quad (3)$$

for $j = u, c$. In this relation, $\sigma_{j,FSI}$ is the on-shell

spectral function describing the final state interactions

$$\sigma_{j,FSI} \approx \sum_n \delta(k_1 + k_2 - p_n) M^*(n \rightarrow \pi\pi) A_j(B \rightarrow n), \quad (4)$$

where $M(A_j)$ denote strong (weak) amplitudes, respectively, and $A_{j,0}$ is the amplitude in the limit of vanishing final state interactions. Using arguments based on quark-hadron duality, one can show that the dominant contribution to $A_{j,0}$ is given by the factorized amplitude [1].

The representation (3), combined with the Regge model for the high-energy strong interactions, can be used to derive corrections to the factorized amplitude, produced by the final state interactions in the heavy quark limit. We notice that in the hadronic formalism the real part of the final state interaction amplitude is suppressed by two powers of the heavy mass, compared to the imaginary part. The dominant corrections to the imaginary part are given by the next to leading logarithmic term of the pomeron contribution. Other sources of large power corrections to the factorized amplitude are not found, assuming that multiparticle effects are qualitatively taken into account by the Goldberger-Treiman method of calculating the spectral functions. Using for illustration a numerical input suggested by QCD factorization [1], the results indicate that the phase and the modulus of the ratio A_c/A_u are not drastically modified by the final state interactions. With the improved results of QCD factorization calculations, expected in the future, it will be possible to test the dispersion relations conjectured in the present work and, more generally, the validity of quark-hadron duality.

References

- [1] M. Beneke, G. Buchalla, M. Neubert, and C.T. Sachrajda, Phys. Rev. Lett. **83**, 1914 (1999).
- [2] D. Du, D. Yang and G. Zhu, Phys. Lett. B. **488**, 46(2000).
- [3] J.F. Donoghue et al, Phys. Rev. Lett. **77**, 2178 (1996).
- [4] I. Caprini, L. Micu, and C. Bourrely, Phys. Rev. D **60**, 074016 (1999); Phys. Rev. D **62**, 034016 (2000).
- [5] H. Lehmann, K. Symanzik, and W. Zimmermann, Nuovo Cimento, **1**, (1956) 205; **2**, (1957) 425.

A convergent non-power QCD perturbative series based on analytic continuation

I. Caprini¹, J. Fischer²

¹ NIPNE-HH, Theoretical Physics Department

² Institute of Physics, Academy of Sciences of the Czech Republic, 182 21 Prague 8, Czech Republic

We consider the standard perturbative expansion of a generic QCD amplitude

$$A(a) = \sum_{n=0}^{\infty} a_n a^n, \quad (1)$$

where $a = \alpha_s(\mu^2)/\pi$ is the renormalized coupling constant. This expansion is known to be plagued by several deficiencies. The coefficients a_n exhibit a typical factorial increase, $a_n \sim \xi^n n! n^\delta$ with nonalternating signs, which shows that the series (1) is divergent and Borel non-summable. The truncated, fixed order perturbative expansion is afflicted also with the problem of renormalization scheme dependence and violates explicitly, due to the Landau singularities, the rigorous momentum plane analyticity imposed by the general principles of field theory. Several resummations or reformulations of the perturbative expansion have been considered recently, trying to reduce these deficiencies.

In the present work, we propose a novel, non-power series replacing the standard power expansion (1). We start from the divergence pattern of perturbative quantum chromodynamics, which suggests for the Borel transform $B(u)$ of the correlator $A(a)$ a structure of branch-point singularities along the real axis in the complex u -plane, with a gap of nonvanishing width containing the origin. We define the expansion functions $W_n(a)$ as

$$W_n(a) = \frac{1}{a} \int_{\mathcal{C}} e^{-u/a} (w(u))^n du, \quad (2)$$

where $w(u)$ is the conformal mapping of the cut Borel plane onto the unit disk [1] and \mathcal{C} is a contour avoiding the singularities along the real axis. The intrinsic ambiguity of perturbative QCD manifests itself in this prescription dependence of the expansion functions $W_n(a)$. The modified perturbative expansion replacing (1) is

$$A(a) = \sum_0^{\infty} c_n W_n(a), \quad (3)$$

where c_n are the Taylor coefficients of the expansion of the Borel transform in powers of the variable w [1].

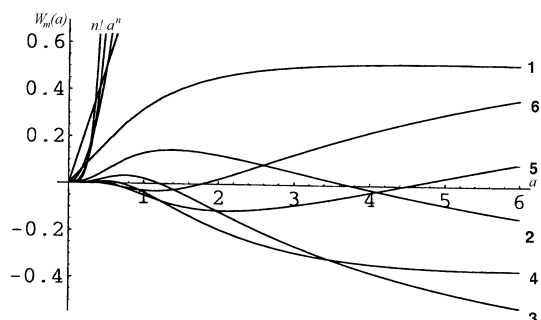


Figure 1: The functions $W_n(a)$ for $n = 1, \dots, 6$ and a in the interval $(0, 6)$.

One can show that the expansion (3) is a straightforward generalization of the conventional series (1), and reproduces the known result [3] in the case of a Borel summable series. The functions $W_n(a)$ have interesting properties (see Figure 1): they are bounded, sign-changing, and vanish when a tends to infinity. For large n they behave as

$$W_n(a) \approx n^{\frac{1}{4}} \zeta^n e^{-2^{3/4}(1+i)(n/a)^{1/2}}, \quad (4)$$

where ζ is a constant. This shows that the new expansion (3) has remarkable convergence properties [1]. One can prove also that for small a the n -th order function $W_n(a)$ behaves like a^n , thereby retaining the fundamental feature of a perturbative expansion. On the other hand, the Taylor expansion of $W_n(a)$ in powers of a is a divergent asymptotic series, with an analyticity domain resembling that of the correlator $A(a)$ [2]. By the modified expansion (3), one obtains a better estimate of the intrinsic ambiguity of the perturbative QCD due to the infrared regions in Feynman diagrams, which will be eventually compensated in the full theory by the nonperturbative terms.

References

- [1] I. Caprini and J. Fischer, Phys.Rev D**60**, 054014 (1999); Phys. Rev. D**62**, 054007 (2000).
- [2] G. 't Hooft, in: *The Whys of Subnuclear Physics*, Plenum Press, New York, 1979, p. 943.
- [3] J. Zinn-Justin, *Quantum Field Theory and Critical Phenomena* (Oxford University Press, 1995)

Yang-Mills theories in the causal approach

D. R. Grigore¹

¹ NIPNE-HH, Department of Theoretical Physics

The mathematical formulation of perturbative renormalization theory starts from Bogoliubov axioms imposed on the S -matrix (or equivalently on the chronological products). The S -matrix is formal series of operator valued distributions:

$$S(\mathbf{g}) = 1 + \sum_{n=1}^{\infty} \frac{i^n}{n!} \int dx_1 \cdots dx_n T_{j_1, \dots, j_n}(x_1, \dots, x_n) g_{j_1}(x_1) \cdots g_{j_n}(x_n) \quad (1)$$

where $\mathbf{g} = (g_j(x))_{j=1, \dots, P}$ is a multi-valued tempered test function in the Minkowski space \mathbf{R}^4 that switches the interaction and $T_{j_1, \dots, j_n}(x_1, \dots, x_n)$ are operator-valued distributions acting in the Fock space of some collection of free fields with a common dense domain of definition D_0 . These operator-valued distributions are called *chronological products* and verify some properties called *Bogoliubov axioms*. One starts from a set of Wick monomials $T_j(x)$, $j = 1, \dots, P$ and tries to construct the whole series T_{j_1, \dots, j_n} , $n \geq 2$.

The most convenient method of proving the existence of solutions is based on the analysis of Epstein and Glaser [1]; the construction is purely recursive using the causal support properties of various distributions appearing in the theory and distribution splitting theory. For some models describing higher spin particles one uses unphysical degree of freedom and the elimination of the unphysical states in the Hilbert space is made imposing the gauge invariance condition.

The gauge invariance condition on the chronological products can be expressed in such a way that infrared divergences are not considered (see [5] and [6]):

$$[Q, T(x_1, \dots, x_n)] = i \sum_{l=1}^n \frac{\partial}{\partial x_l^\mu} T_l^\mu(x_1, \dots, x_n), \quad (2)$$

for some chronological products $T(X)$, $T_l^\mu(X)$ which are convenient linear combinations of the expression T_{j_1, \dots, j_n} ; here $n = 1, 2, \dots$ and $l = 1, \dots, n$. The obstructions to such a factorisation process are called *anomalies*.

We can generate the Hilbert space for the standard model as follows: one considers a set of masses m_a , $a = 1, \dots, r$ and splits the indices in two types:

(I) $m_a \neq 0$. In this case we apply to the vacuum Ω the free fields $A_{a\mu}$, u_a , \tilde{u}_a , Φ_a $a = 1, \dots, r$ all of them of mass m_a , where the first one has vector transformation properties with respect to the Poincaré group and the others are scalars. In other words, every vector field has three scalar partners. Also the fields

u_a , \tilde{u}_a $a = 1, \dots, r$ are Fermionic and A_μ , Φ_a $a = 1, \dots, r$ are Bosonic.

(II) $m_a = 0$. In this case we have three possibilities: (IIa) $A_{a\mu}$, u_a , \tilde{u}_a , $\Phi_a \neq 0$; the scalar field Φ_a can have a non-zero mass: $m_a^H \geq 0$. (IIb) $\Phi_a \equiv 0$; (IIc) $A_{a\mu}$, u_a , $\tilde{u}_a \equiv 0$. In the cases (IIa) and (IIb) the fields $A_{a\mu}$, u_a , \tilde{u}_a have null mass. The statistics assignment is the same as in case (I). The auxiliary Hilbert space \mathcal{H}^{gh} is generated in this way. In this Hilbert space we can define a sesquilinear form $\langle \cdot, \cdot \rangle$ such that:

$$\begin{aligned} A_{a\mu}(x)^\dagger &= A_{a\mu}(x), & \Phi_a(x)^\dagger &= \Phi_a(x) \\ u_a(x)^\dagger &= u_a(x), & \tilde{u}_a(x)^\dagger &= -\tilde{u}_a(x). \end{aligned} \quad (3)$$

One can define the BRST *supercharge* Q by:

$$\begin{aligned} \{Q, u_a\} &= 0 & \{Q, \tilde{u}_a\} &= -i(\partial_\mu A_a^\mu + m_a \Phi_a) \\ \{Q, A_a^\mu\} &= i\partial^\mu u_a & \{Q, \Phi_a\} &= im_a u_a, \end{aligned} \quad (4)$$

and

$$Q\Omega = 0. \quad (5)$$

One can consider also a set of Dirac fields describing the matter and commuting with the supercharge. Then one can justify that the **physical** Hilbert space of the Yang-Mills system is a factor space

$$\mathcal{H}_{YM}^r \equiv \text{Ker}(Q)/\text{Ran}(Q); \quad (6)$$

the sesquilinear form $\langle \cdot, \cdot \rangle$ induces a *bona fide* scalar product on the Hilbert factor space and spontaneous symmetry breaking is taken into account from the very beginning. The field content of this model consists of matter and massive and massless Bosons.

One can prove that the condition (2) for $n = 1, 2, 3$ gives the usual expression for the Yang-Mills interaction Lagrangian and for the axial anomaly [2], [3], [4].

References

- [1] H. Epstein, V. Glaser, Ann. Inst. H. Poincaré **19** A (1973) 211-295
- [2] D. R. Grigore, Romanian Journ. Phys. **44** (1999) 853-913
- [3] D. R. Grigore, Journ. Phys. **A 33** (2000) 8443-8476
- [4] D. R. Grigore, hep-th/9903206
- [5] M. Dütsch, T. Hurth, F. Krahe, G. Scharf, Il Nuovo Cimento **A 106** (1993) 1029-1041
- [6] M. Dütsch, T. Hurth, F. Krahe, G. Scharf, Il Nuovo Cimento **A 107** (1994) 375-406

Physics of Information

Exchange and spin-fluctuation superconducting pairing in the strong correlation limit of the Hubbard model

N. M. Plakida¹, L. Anton^{1,3,4}, S. Adam^{1,2}, Gh. Adam^{1,2}

¹JINR, 141980 Dubna, Moscow, Russia

²IFIN-HH, Department of Theoretical Physics; E-mail: adamg@ifin.nipne.ro, adams@ifin.nipne.ro

³INFLPR, Lab.22 PO Box MG-36, Bucharest, Romania

⁴Inst. Theor. Phys., Univ. Stellenbosch, Private Bag X1, 7602 Matieland, South Africa

A microscopical theory of superconductivity in the two-band singlet-hole Hubbard model, in the strong coupling limit in a paramagnetic state, is developed. The model Hamiltonian is obtained by projecting the p - d model to an asymmetric Hubbard model with the lower Hubbard subband occupied by one-hole Cu d -like states and the upper Hubbard subband occupied by two-hole p - d singlet states [N.M. Plakida, R. Hayn, J.-L. Richard, Phys. Rev. B **51**, 16599 (1995); L.F. Feiner, J.H. Jefferson, R. Raimondi, Phys. Rev. B **53**, 8751 (1996)]. The model requires two microscopical parameters only, the p - d hybridization parameter t and the charge-transfer gap Δ . It was previously shown to secure an appropriate description of the normal state properties of the high- T_c cuprates.

To treat rigorously the strong correlations, the Hubbard operator technique within the projection method for the Green function is used. The Dyson equation is derived. In the molecular field approximation, d -wave superconducting pairing of conventional hole (electron) pairs in one Hubbard subband is found, which is mediated by the exchange interaction given by the interband hopping, $J_{ij} = 4(t_{ij})^2/\Delta$.

The normal and anomalous components of the self-energy matrix are calculated in the self-consistent Born approximation for the electron-spin-fluctuation scattering mediated by kinematic interaction of the second order of the intraband hopping. The derived numerical and analytical solutions predict the occurrence of singlet $d_{x^2-y^2}$ -wave pairing both in the d -hole and singlet Hubbard subbands. The gap functions and T_c are calculated for different hole concentrations.

The exchange interaction is shown to be the most important pairing interaction in the Hubbard model in the strong correlation limit, while the spin-fluctuation coupling results only in a moderate enhancement of T_c . The smaller weight of the latter comes from two specific features: its vanishing inside the Brillouin zone (BZ) along the lines $|k_x| + |k_y| = \pi$ pointing towards the hot spots and the existence of a small energy shell within which the pairing is effective. By contrast, the exchange interaction is maximal along the above-mentioned lines inside BZ and it couples the electrons (holes) in a much broader energy shell, of the order of

the bandwidth $W = 8t_{eff}$, due to the interband hopping where the retardation effects are unimportant.

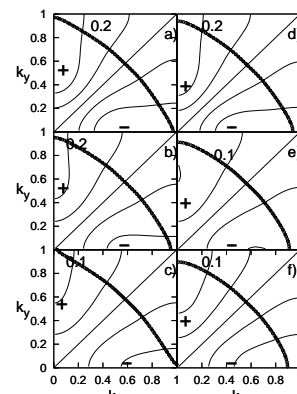


Figure 1: Combined effect of the kinematic and exchange interactions to the temperature dependence of the order parameter $\Phi^{22}(\mathbf{k})$ over the first quadrant of the BZ: at optimum doping ($\delta = 0.13$) $\{T = 0$ (a); $0.5T_c$ (b); $0.9T_c$ (c) $\}$ and at overdoping ($\delta = 0.2$) $\{T = 0$ (d); $0.5T_c$ (e); $0.9T_c$ (f) $\}$.

Samplings of the wave-vector behavior of the order parameters $\Phi^{22}(\mathbf{k})$ over the first quadrant of the BZ (Fig. 1) at several temperatures show the occurrence of a peculiar $d_{x^2-y^2}$ -wave gap pattern which strongly depends on the type of the involved interactions.

In conclusion, the present investigation points to the existence of a singlet $d_{x^2-y^2}$ -wave superconducting pairing for holes or electrons in the two-band Hubbard model mediated by the exchange interaction and antiferromagnetic spin-fluctuation scattering induced by the kinematic interaction, characteristic to the Hubbard model. These mechanisms of superconducting pairing are absent in the fermionic models [P.W. Anderson, Adv. in Physics **46**, 3 (1997)].

Our results agree with the recent investigations of the Hubbard model within the dynamical cluster approximation, where the self-energy has been calculated in the non-crossing approximation for the 4-cluster model [Th. Maier, M. Jarrel, Th. Pruschke, J. Keller, Phys. Rev. Lett. **85**, 1524 (2000); A.I. Lichtenstein M.I. Katsnelson, Phys. Rev. B **62**, R9283 (2000)].

{The full version of the paper is available on the site <http://xxx.lanl.gov/abs/cond-mat/0104234>}

Increasing reliability of Gauss-Kronrod quadrature by Eratosthenes' sieve method

Gh. Adam¹, S. Adam¹

¹ IFIN-HH, Department of Theoretical Physics; E-mail: adamg@ifin.nipne.ro, adams@ifin.nipne.ro

Within a modern quadrature algorithm, the quality of the implemented local error estimates influences, to a large extent, both the efficiency and the reliability of an automatic algorithm, either adaptive or non-adaptive. Particularly successful Gauss-Kronrod (GK) quadrature algorithms with improved heuristic QUADPACK-GK (QDP) local error estimates have been reported in QUADPACK [R. Piessens, E. de Doncker-Kapenga, C. W. Überhuber, D. K. Kahaner, QUADPACK, a subroutine package for automatic integration, Springer Verlag, Berlin, 1983] which has been incorporated in most major program libraries. The QDP approach extended the genuine Gauss-Kronrod (GGK) local error estimates previously proposed by Kronrod.

The present paper reports some rules of thumb which have been found to be very effective in increasing the output reliability of the automatic adaptive quadrature algorithms based on QDP local error estimates. The discussion is limited to GK 7-15 and GK 10-21 quadrature rules, the general description of which is given in QUADPACK. With minor reformulation, the derived results hold true for other quadrature rules as well.

Let I denote the actual value of the integral to be solved numerically. A subroutine which implements a Gauss-Kronrod quadrature rule for solving I provides at output a pair $\{r_K, e_K\}$. In the present context, r_K is the *computed approximation* of I by Kronrod quadrature sum, while e_K is the *local error estimate*.

Then the local GGK error estimate is given by

$$e_{ggk} = |r_K - r_G|.$$

Let \tilde{f} denote the computed value of the average of $f(x)$ over $[a, b]$ at the knots of r_K and Δ denote the computed value of the integral $\int_a^b |f(x) - \tilde{f}| dx$, which measures the area covered by the deviations of $f(x)$ around \tilde{f} . The local QDP error estimate is then

$$e_{qdp} = \Delta \times \min\{(200e_{ggk}/\Delta)^{3/2}, 1\}.$$

The values e_{ggk} and e_{qdp} are taken for error estimates provided they do not fall below the attainable accuracy limit imposed by the relative machine precision. The latter threshold is defined as the product

$$e_{roff} = \tau_0 \epsilon_0 Q_K [|f|].$$

The present study shows that an analysis of some key features of the integrand, done within the subroutine which implements the quadrature rule of interest,

provides significant hints on the reliability of the local error estimate.

In the case of GK 7-15 and GK 10-21 quadrature rules, a local error estimate *self-validates itself* according to the following scheme:

$$e_K = \begin{cases} \max[e_{roff}, \min(e_{ggk}, e_{qdp})] & \text{iff reliability} \\ & \text{conditions fulfilled} \\ e_{qdp} \text{ \textit{\textless} error flag} & \text{otherwise} \end{cases}$$

When a self-validating quadrature rule is incorporated in an automatic adaptive quadrature program, substantial increase of the correctness of the automatic decisions is obtained for difficult integrands.

The *reliability conditions* entering this definition have been derived by the use of Eratosthenes' sieve method to the analysis of sets of data obtained over families of elementary integrals. This allowed us to identify characteristic trends of the error behaviour with the integrand variation and to formulate rules of thumb in agreement with the general theory of the Riemann integral.

If the computation results in a value $|r_K|$ exceeding the machine underflow, the error estimates e_{qdp} and e_{ggk} may be taken for reliable provided that

$$\rho_{qdp} < \tau_{qdp} \phi_d, \quad \tau_{qdp} = 0.5,$$

and respectively

$$\rho_{ggk} < \tau_{ggk} \phi_d, \quad \tau_{ggk} = 0.005,$$

where ρ_{qdp} and ρ_{ggk} denote relative errors.

Here, the constants τ_{qdp} and τ_{ggk} simply trace the line between error estimates carrying significant figures at output and error estimates which do not carry out any significant figure under the integration of *continuous monotonic integrands*.

The discouraging factor $\phi_d = 10^{\min(\lambda, \mu, \nu)} \leq 1$, is a quantity inferred from the analysis of the integrand structure. It secures sharper reliability thresholds in the case of *continuous non-monotonic integrands*.

The quantities λ and μ measure the consistency of the integrand profile inferred from its values at the Gauss and Kronrod abscissas respectively from the study of the integrand extrema and its intersections with the average integrand value \tilde{f} . Finally, the quantity ν provides a measure to the asymmetry of the distribution of the interpolatory polynomial values at the GK quadrature abscissas around the computed average.

CP methods for the Schrödinger equation

L. Gr. Ixaru¹

¹ Institute of Physics and Nuclear Engineering, Department of Theoretical Physics, POBox MG - 6, Bucharest, Romania, Email : ixaru@theor1.theory.nipne.ro

After a short survey over the efforts in the direction of solving the Schrödinger equation by using piecewise approximations of the potential function, the paper focuses on the piecewise perturbation methods in their CP implementation. The presentation includes a short list of problems for which CP versions are available, a sketch of the derivation of the CPM formulae, a description of various ways to construct or identify a

certain version and also the main results of the error analysis. One of the most relevant results of the latter is that the energy dependence of the error is bounded, a fact which places these methods on a special position among the numerical methods for differential equations. A numerical illustration is also included in which a CPM based code for the regular Sturm-Liouville problem is compared with some other, well-established codes.

Highly accurate eigenvalues for the distorted Coulomb potential

L. Gr. Ixaru¹, H. De Meyer², G. Vanden Berghe²

¹ Institute of Physics and Nuclear Engineering, Department of Theoretical Physics, POBox MG - 6, Bucharest, Romania, Email : ixaru@theor1.theory.nipne.ro

² Department of Applied Mathematics and Computer Science, Universiteit Gent, Krijgslaan 281-S9, B-9000 Gent, Belgium

We consider the eigenvalue problem for the radial Schrödinger equation with potentials of the form $V(r) = S(r)/r + R(r)$ where $S(r)$ and $R(r)$ are well behaved functions which tend to some (not necessarily equal) constants when $r \rightarrow 0$ and $r \rightarrow \infty$. Formulae (14.4.5–8) of Abramowitz and Stegun, corresponding to the

pure Coulomb case, are here generalized for this distorted case. We also present a complete procedure for the numerical solution of the problem. Our procedure is robust, very economic and particularly suited for very large n . Numerical illustrations for n up to 2000 are given.

Three-dimensional walking spatiotemporal solitons in quadratic media

D. Mihalache¹, D. Mazilu¹, L.-C. Crasovan¹, L. Torner², B. A. Malomed³, F. Lederer⁴

¹ Department of Theoretical Physics, Institute of Atomic Physics, National Institute of Physics and Nuclear Engineering, P.O. Box MG-6, Bucharest, Romania

² Laboratory of Photonics, Department of Signal Theory and Communications, Universitat Politècnica de Catalunya, Barcelona ES 08034, Spain

³ Department of Interdisciplinary Sciences, Faculty of Engineering, Tel Aviv University, Tel Aviv 69978, Israel

⁴ Institute of Solid State Theory and Theoretical Optics, Friedrich-Schiller University Jena, Max-Wien-Platz 1, Jena, D-07743, Germany

Two-parameter families of chirped stationary three-dimensional spatiotemporal solitons in dispersive quadratically nonlinear optical media featuring type-I second-harmonic generation are constructed in the presence of temporal walk-off. Basic features of these walking spatiotemporal solitons, including their dynamical stability, are investigated in the general case of unequal group-velocity dispersions at the fundamental and second-harmonic frequencies. In the cases when

the solitons are unstable, the growth rate of a dominant perturbation eigenmode is found as a function of the soliton wave number shift. The findings are in full agreement with the stability predictions made on the basis of a marginal linear-stability curve. It is found that the walking three-dimensional spatiotemporal solitons are dynamically *stable* in most cases; hence in principle they may be experimentally generated in quadratically nonlinear media.

Localized multidimensional femtosecond optical pulses in an off-resonance two-level medium

I. V. Melnikov¹, D. Mihalache², N.-C. Panoiu^{2,3}

¹ General Physics Institute of the Russian Academy of Sciences, ul. Vavilova 38, Moscow 117942, Russian Federation

² Department of Theoretical Physics, Institute of Atomic Physics, National Institute of Physics and Nuclear Engineering, P.O. Box MG-6, Bucharest, Romania

³ Department of Physics, New York University, 4 Washington Place, New York, NY 10003, USA

The propagation of a femtosecond optical pulse in a multidimensional off-resonance two-level material is studied. In the case of quasiadiabatic following, the evolution of the pulse is governed by the equation of generalized Kadomtsev-Petviashvili type with coupling of the spatial profile to temporal structure. The

presence of this coupling can have a dramatic effect on the dynamics of the optical pulse which cannot be observed within the framework of slowly-varying envelope approximation. In particular, we show that stable localized multidimensional pulses can arise through interaction of the transient diffraction with electrodynamic absorption.

Adiabatic perturbative analysis of symmetry-endowed two-soliton solutions

N.-C. Panoiu^{1,2}, D. Mihalache², D. Mazilu², L.-C. Crasovan², I. V. Melnikov³, F. Lederer⁴

¹ Department of Physics, New York University, 4 Washington Place, New York, NY 10003, USA

² Department of Theoretical Physics, Institute of Atomic Physics, National Institute of Physics and Nuclear Engineering, P.O. Box MG-6, Bucharest, Romania

³ General Physics Institute of the Russian Academy of Sciences, ul. Vavilova 38, Moscow 117942, Russian Federation

⁴ Institute of Solid State Theory and Theoretical Optics, Friedrich Schiller University Jena, Max-Wien-Platz 1, Jena, D-07743, Germany

A comprehensive analysis of the propagation of symmetry-endowed two-soliton solutions under the influence of various perturbations important in nonlinear optics is presented. Thus, we begin by introducing the analytical expressions of these two-soliton solutions. Then, by considering perturbations which preserve the initial symmetry of the two-soliton solutions, the dependence of the soliton parameters on the prop-

agation distance is determined by using an adiabatic perturbation method. As perturbations of this kind and important for soliton-based communication systems we consider the bandwidth-limited amplification, nonlinear amplification, amplitude and phase modulation. Moreover, the analytical predictions are compared with the results obtained by direct numerical simulations of the corresponding governing differential equations.

Three-dimensional spinning solitons in the cubic-quintic nonlinear medium

D. Mihalache^{1,3}, D. Mazilu¹, L.-C. Crasovan¹, B. A. Malomed², F. Lederer³

¹ Department of Theoretical Physics, Institute of Atomic Physics, National Institute of Physics and Nuclear Engineering, P.O. Box MG-6, Bucharest, Romania

² Department of Interdisciplinary Sciences, Faculty of Engineering, Tel Aviv University, Tel Aviv 69978, Israel

³ Institute of Solid State Theory and Theoretical Optics, Friedrich Schiller University Jena, Max-Wien-Platz 1, Jena, D-07743, Germany

We find one-parameter families of three-dimensional spatiotemporal bright vortex solitons (doughnuts, or *spinning light bullets*), in bulk dispersive cubic-quintic optically nonlinear media. The spinning solitons display a symmetry-breaking azimuthal instability, which

leads to breakup of the spinning soliton into a set of fragments, each being a stable nonspinning light bullet. However, in some cases the instability is developing so slowly that the spinning light bullets may be regarded as virtually stable ones, from the standpoint of an experiment with finite-size samples.

Azimuthal instability of spinning spatiotemporal solitons

D. Mihalache^{1,3}, D. Mazilu¹, L.-C. Crasovan¹, B. A. Malomed², F. Lederer³

¹ Department of Theoretical Physics, Institute of Atomic Physics, National Institute of Physics and Nuclear Engineering, P.O. Box MG-6, Bucharest, Romania

² Department of Interdisciplinary Sciences, Faculty of Engineering, Tel Aviv University, Tel Aviv 69978, Israel

³ Institute of Solid State Theory and Theoretical Optics, Friedrich Schiller University Jena, Max-Wien-Platz 1, Jena, D-07743, Germany

We find one-parameter families of three-dimensional spatiotemporal bright vortex solitons (doughnuts, or *spinning light bullets*), in dispersive quadratically nonlinear media. We show that they are subject to a

strong instability against azimuthal perturbations, similarly to the previously studied (2+1)-dimensional bright spatial vortex solitons. The instability breaks the spinning soliton into several fragments, each being a *stable* nonspinning light bullet.

Stable solitons of quadratic Ginzburg-Landau equations

L.-C. Crasovan^{1,3}, B. A. Malomed², D. Mihalache^{1,3}, D. Mazilu¹, F. Lederer³

¹ Department of Theoretical Physics, Institute of Atomic Physics, National Institute of Physics and Nuclear Engineering, P.O. Box MG-6, Bucharest, Romania

² Department of Interdisciplinary Sciences, Faculty of Engineering, Tel Aviv University, Tel Aviv 69978, Israel

³ Institute of Solid State Theory and Theoretical Optics, Friedrich Schiller University Jena, Max-Wien-Platz 1, Jena, D-07743, Germany

We put forward a physical model based on coupled Ginzburg-Landau equations that supports *stable* temporal solitary-wave pulses. The system consists of two parallel-coupled cores, one having a quadratic nonlinearity, the other one being effectively linear. The former core is active, with bandwidth-limited amplification built into it, while the latter core has only losses. Parameters of the model can be easily selected so that the zero background is stable. The model has non-generic exact analytical solutions in the form of soli-

tary pulses ("dissipative solitons"). Direct numerical simulations, using these exact solutions as initial configurations, show that they are unstable; however, the evolution initiated by the exact unstable solitons ends up with nontrivial stable localized pulses, which are very robust attractors. Direct simulations also demonstrate that the presence of group-velocity mismatch (walk-off) between the two harmonics in the active core makes the pulses moving at a constant velocity, but does not destabilize them.

Non-destructive beam characterization at an electron source exit

S. Marghitu², C. Dinca², M. Rizea¹, C. Oproiu², M. Toma², D. Martin², E. Iliescu²

¹ Department of Theoretical Physics, National Institute of Physics and Nuclear Engineering (NIPNE), P.O. Box MG-6, Bucharest, Romania

² Accelerators Laboratory, National Institute for Laser, Plasma and Radiation Physics (NILPRP), P.O. Box MG-6, Bucharest, Romania

The method, experimental set-up, and experimental results, referring to the non-destructive beam emittance at an electron source exit, as well as to the beam envelope determination, are presented. The method consists in an interactive use of both the beam cross-section measurements, realized in the three-gradient arrangement, and the K-V equation. The important parts of the experimental set-up are: the electron source

(a Pierce convergent diode, working in a pulse mode), an axially symmetric magnetic lens, and two beam profile monitors (wire scanners). The electron source is of the type frequently used in linear accelerators, particularly in our accelerators ALIN - 10 and ALID - 7 at NILPRP, and works in the energy range of 20-70 keV, with 4 μ s pulse duration and 0.1 - 1 A pulse intensity.

Nuclear Physics

Nuclear Structure	23
Nuclear Reactions	35
Atomic Physics	44
Cosmic Rays and Nuclear Astrophysics	51
Inertial Fusion, Physics of Neutrons and Nuclear Transmutations	54
Nuclear Instruments and Methods	59

Consequences of the center-of-mass correction in large scale nuclear structure calculations

A. Petrovici^{1,2}, K.W. Schmid², A. Faessler²

¹NIPNE-HH, Department of Nuclear Physics

²Institut für Theoretische Physik, Univ. Tübingen, D-72076 Tübingen, Germany

The coexistence phenomena dominating the structure of medium mass nuclei at low and intermediate spins are rather well described in the frame of the *complex* VAMPIR (variation after projection) models which can account for the delicate interplay between collective and single-particle degrees of freedom, treat like-nucleon and neutron-proton pairing correlations on the same footing and are numerically feasible for rather large model spaces and general two-body forces [1, 2, 3]. The spherical-deformed shape coexistence identified in the N=Z nucleus ⁵⁶Ni was investigated within the *complex* Excited Vampir approach using a rather large valence space including in addition to the full 1p0f-shell the $0g_{9/2}$ and $1d_{5/2}$ oscillator orbits for both protons and neutrons. Therefore, we have to worry about effects due to the broken Galilean invariance. Obviously the latter could be restored by projecting into the center of momentum rest frame before variation, but this procedure requires an additional 3-dimensional integration and is for the moment numerically not possible. In order to study the effects of contaminations due to the center of momentum motion we applied a rough method to eliminate them at least approximately. Instead of minimizing the usual Hamiltonian H we have complemented it with a penalty function and used in the minimization

$$\tilde{H} = H + \lambda H_{COM} \quad (1)$$

where

$$H_{COM} \equiv \frac{\hat{P}^2}{2MA} + \frac{1}{2}MA\omega^2\vec{R}^2 \quad (2)$$

is the usual (many-body) harmonic oscillator Hamiltonian of the center of momentum. H_{COM} is positive definite, and, for a complete $n\hbar\omega$ space, has eigenvalues $3/2\hbar\omega$, $5/2\hbar\omega$, etc. corresponding to the center of momentum being in its ground (the 0s) or some excited state. By choosing λ sufficiently large one therefore penalizes the excitations of the center of momentum. Fig. 1 shows the results for λ -values of 0 (this corresponds to the normal calculation, not worrying about the center of momentum motion), 1, 5 and finally 10. The numbers on top of the levels denote the expectation values of H_{COM} for the corresponding solutions in units of $\hbar\omega$. Thus 1.5 corresponds to a completely nonspurious state. As expected, indeed the increase of λ leads to a decrease of the spurious admixtures. However, neither the relative spacings of the deformed

band nor of the upper part of the yrast band seem to be considerably effected. An exception is the 0^+ ground state. Here, for $\lambda = 0$ a considerably larger contamination than in the higher spin states of the yrast band is seen. As a consequence the $0^+ - 2^+$ energy difference becomes almost one MeV smaller when increasing λ from 0 to 10. In the deformed band the H_{COM} expectation values are rather similar for all angular momenta and hence the relative position of those states does hardly change.

Our investigations revealed also the importance of the center of momentum motion for medium mass nuclei manifesting oblate-prolate mixing.

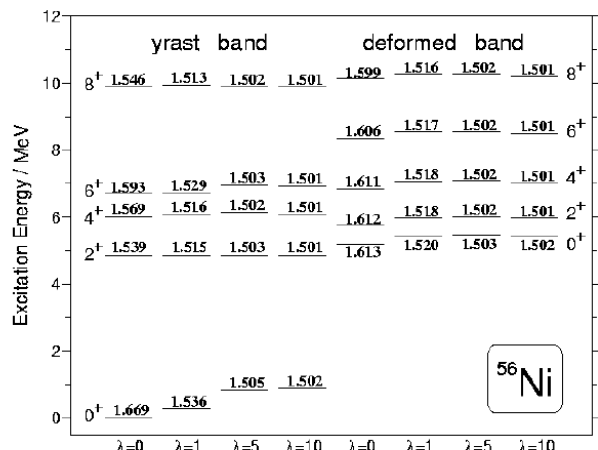


Figure 1: The yrast and the first deformed band in ⁵⁶Ni calculated for different λ . The levels have been normalized to the yrast 2^+ energy.

In a complete $n\hbar\omega$ model space the above procedure would be correct. Whether it remains a good approximation within rather small model spaces it is not clear and can probably only be decided by an exact restoration of Galilean invariance via projection. Similar effects are to be expected in large scale Hartree-Fock or Hartree-Fock-Bogoliubov calculations.

References

- [1] A. Petrovici *et al*, Progr. Part. Nucl. Phys. **43**, 485 (1999)
- [2] A. Petrovici *et al*, Nucl. Phys. **A665**, 333 (2000)
- [3] A. Petrovici *et al*, Nucl. Phys. **A**, (2001) (in press)

Static quadrupole moment of the $K^\pi=14^+$ isomer in ^{176}W

M. Ionescu-Bujor¹, A. Iordăchescu¹, F. Brandolini², D. Bucurescu¹, M. De Poli³, S.M. Lenzi²,
N. Mărginean^{1,3}, N.H Medina⁴, D.R. Napoli³, Zs. Podolyak⁵, P. Pavan², R.V. Ribas⁴, C. Rossi Alvarez²,
C.A. Ur^{1,2}

¹ NIPNE-HH, Department of Nuclear Physics, Bucharest, Romania

² Dipartimento di Fisica and INFN, Sezione di Padova, Padova, Italy

³ INFN, LNL, Legnaro, Italy

⁴ Instituto de Fisica, Universidade di Sao Paulo, Sao Paulo, Brazil

⁵ Department of Physics, University of Surrey, Guildford, UK

The investigation of high-K isomeric states in the deformed nuclei of the $A \approx 180$ region has found renewed interest in recent years. Much experimental and theoretical work was devoted to understand the mechanisms which govern their decay to lower-lying states, particularly the anomalous strong decays to low-K states. Other questions of great importance are the quenching of the pairing correlations and the shape polarization effects in the high-seniority multi-quasiparticle excitations.

Our interest focused on the 41 ns $K^\pi=14^+$ 3746 keV isomeric state with anomalous decay in ^{176}W [1]. On the basis of a precise g-factor measurement we assigned to this isomer a pure four-quasiparticle configuration, composed by two protons in the $\frac{7}{2}^+$ [404] and $\frac{9}{2}^-$ [514] orbitals and two neutrons in the $\frac{7}{2}^+$ [633] and $\frac{5}{2}^-$ [512] orbitals [2]. In the present work the measurement of its static quadrupole moment has been performed. Prior to our experiment, static quadrupole moments have been measured only for three high-K isomeric states of seniority ≥ 4 in the $A \approx 180$ region: 16^+ in ^{178}Hf [3], $\frac{35}{2}^-$ in ^{179}W [4] and 25^+ in ^{182}Os [5]. A deformation very similar to that of the ground state has been deduced for the 16^+ isomer in ^{178}Hf , while for the high-K isomers in ^{179}W and ^{182}Os significantly smaller deformations were reported.

The quadrupole interaction of the 14^+ isomeric state in ^{176}W has been investigated in the electric field gradient (EFG) of the polycrystalline lattice of metallic Tl by applying the time-differential perturbed angular distribution method. For W impurities in Tl host the EFG strength and its temperature dependence have been recently reported [4]. The isomer was populated in the $^{164}\text{Dy}(^{16}\text{O},4n)^{176}\text{W}$ reaction using a 83 MeV ^{16}O pulsed beam (pulse width 1.5 ns, repetition period 800 ns) delivered by the XTU-Tandem of Laboratori Nazionali di Legnaro. The target consisted of 0.5 mg/cm² metallic ^{164}Dy on thick Tl backing in which both the recoiling ^{176}W nuclei and the projectiles were stopped. The target has been heated at 464 K in a special oven. This temperature was chosen in order to assure an EFG strength convenient for the observation of the quadrupole interaction pattern on time scale given by the isomeric lifetime. The γ -

rays were detected by Ge detectors of 25% efficiency placed at the angles 0° and 90° with respect to the beam direction. The 240, 351, 440, and 558 keV γ -lines of the ^{176}W yrast band which collects practically all the isomeric decay branches [1] have been analysed. The experimental modulation ratio is illustrated in Fig. 1 together with the least-squares fit. A quadrupole frequency $\nu_Q=92(10)$ MHz has been determined, which corresponds, with the EFG calibration of [4], to a spectroscopic quadrupole moment $Q_s=6.3(1.4)$ eb. Assuming the strong coupling scheme, a value of $Q_o=7.7(1.8)$ eb is obtained for the intrinsic quadrupole moment of the 14^+ isomer. This value fits very well into the systematics of the ground-state quadrupole moments of W nuclei [6] what indicates that no shape polarization occurs in the multi-quasiparticle structure of ^{176}W .

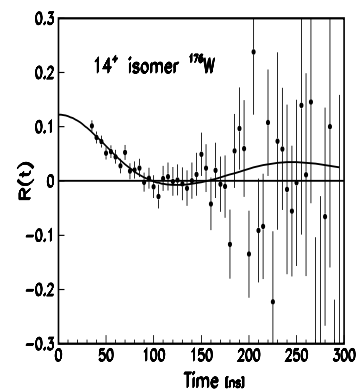


Figure 1: Quadrupole interaction spectrum for the 41 ns 14^+ isomer in ^{176}W implanted in polycrystalline Tl at a temperature of 464 K.

References

- [1] B. Crowell et al., Phys. Rev. Lett. **72** (1994) 1164.
- [2] M. Ionescu-Bujor et al., Phys. Lett. B **495** (2000) 289.
- [3] N. Boos et al., Phys. Rev. Lett. **72** (1994) 2689.
- [4] D.L. Balabanski et al., Phys. Rev. Lett. **86** (2001) 604.
- [5] C. Broude et al., Phys. Lett. B **264** (1991) 17.
- [6] S. Raman et al., At. Data Nucl. Data Tables **36** (1987) 1.

Reflection asymmetric nuclear shapes obtained by solving a differential equation

D.N. Poenaru¹, R.A. Gherghescu¹, W. Greiner², J.H. Hamilton³, A.V. Ramayya³

¹ NIPNE-HH

² Institut fuer Theoretische Physik der Universitaet, Frankfurt am Main, Germany

³ Department of Physics, Vanderbilt University, Nashville, Tennessee, USA

The equilibrium nuclear shapes in fission theory are usually obtained by minimizing the deformation energy for a given surface equation [1]. In the following we present a method allowing to obtain a very general equilibrium (saddle-point) shape as a solution of a differential equation without an *a priori* introduction of a shape parametrization. In the approach based on a pure liquid drop model (LDM) [2], saddle-point shapes are always reflection symmetric: the deformation energy increases with the mass-asymmetry parameter $\eta = (A_1 - A_2)/(A_1 + A_2)$, as is illustrated in Fig.1, where η is replaced by an almost linear dependent quantity $(d_L - d_R)/R_0$. In this way the well established experimentally fission fragment mass asymmetry can not be explained. By adding the shell corrections δE to the LDM deformation energy, $E_{def} = E_{LDM} + \delta E$, we succeeded to obtain the minima shown in Fig.1.

The nuclear surface equation of an axially symmetric body $u(x)$ is a solution of the following differential equation:

$$u'' = 2 + \frac{1}{u}[u'^2 + (x - d + \hat{V}_s)(4u + u'^2)^{3/2}] \quad (1)$$

where d is an input parameter which determines the deformation.

In our present approach we included in the deformation energy

$$E(R) = E_{LD}(R) + \delta E(R) - \delta E^0 \quad (2)$$

a phenomenological shell corrections δE inspired from [3], and the above written differential equation is solved iteratively by using Runge-Kutta method. The procedure is repeated until the solution of the variational problem leads to the minimum of the deformation energy which is the sum of the surface and Coulomb energies plus shell corrections.

At a given deformation we find the fragment volumes and the corresponding number of protons and neutrons $Z_i(R)$, $N_i(R)$ ($i = 1, 2$). For every fragment we add contributions from protons and neutrons

$$\delta E(R) = \sum_i \delta E_i(R) = \sum_i [\delta E_{pi}(R) + \delta E_{ni}(R)] \quad (3)$$

given by

$$\delta E_{pi} = Cs(Z_i); \quad \delta E_{ni} = Cs(N_i) \quad (4)$$

where

$$s(Z) = F(Z)/[(Z)^{-2/3}] - cZ^{1/3} \quad (5)$$

and a similar equation for $s(N)$, where

$$F(n) = \frac{3}{5} \left[\frac{N_i^{5/3} - N_{i-1}^{5/3}}{N_i - N_{i-1}} (n - N_{i-1}) - n^{5/3} + N_{i-1}^{5/3} \right]$$

in which $n \in (N_{i-1}, N_i)$ is the actual number of protons or neutrons Z or N , and N_{i-1}, N_i are the neighbouring magic numbers. The parameters $c = 0.2$, $C = 6.2$ MeV were determined by fit with experimental masses and deformations.

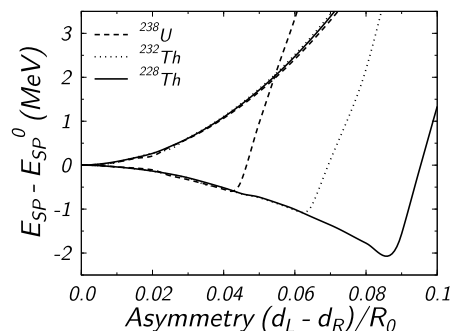


Figure 1: Saddle-point deformation energy versus mass asymmetry parameter for the binary fission of ^{238}U and $^{232,228}\text{Th}$ nuclei. One can see a monotonous increase within a pure liquid drop model and minima when the shell corrections are included.

By introducing shell corrections we obtained minima of deformation energy illustrated in Fig.1 for parent nuclei ^{238}U , $^{232,228}\text{Th}$ at a finite mass asymmetry giving for the three nuclei the same mass number of the heavy fragment $A_1 = 125$.

References

- [1] D. N. Poenaru and W. Greiner, in *Nuclear Decay Modes*, (IOP Publishing, Bristol, 1996), Chap. 6, pp. 275–336; and in *Handbook of Nuclear Properties*, (Oxford University Press, 1996), Chap. 5, pp. 131–182.
- [2] V.M. Strutinsky, N.Ya. Lyashchenko and N.A. Popov *Nucl. Phys.* **46** (1963) 639.
- [3] W.D. Myers and W.J. Swiatecki, *Nucl. Phys. A* **81** (1966) 1.

General utility computer programs for nuclear structure experiments

M. Colci¹, Gh. Căta-Danil¹

¹ IFIN-HH, Department of Nuclear Physics, Bucharest, Romania

The Nuclear codes package contains several theory programs which allow the calculation of many quantities needed in nuclear structure experiments. These codes were initially created to run on Vax Machines. Therefore, many errors result at their compilation on Linux Machines. We fixed these errors and verified the result with input parameters that generate known output quantities. The following programs are available on the Linux network at the Department of Nuclear Physics.

1. BASS -Program to calculate fusion barriers and the limiting angular momentum for complete fusion of heavy ions, using the Bass model [1].
2. BM1BE2 -Program to calculate the ratio of the reduced transition probabilities:

$$\frac{B(M1; I \rightarrow I-1)}{B(E2; I \rightarrow I-2)} = \frac{\langle I, I | M1 | I-1, I-1 \rangle^2}{\langle I, I | E2 | I-2, I-2 \rangle^2}$$

and the mixing ratio of $\Delta I = 1$ transitions:

$$\delta = 0.799 \cdot E_\gamma (MeV) \cdot \frac{\langle I, I | E2 | I-1, I-1 \rangle}{\langle I, I | M1 | I-1, I-1 \rangle}$$

The Program uses the semi-classical formalism of Dönau and Frauendorf [2].

The extension to multi-quasiparticle structures follows Radford's prescription [3].

3. CLEBSCH -Program to calculate the Clebsch-Gordan coefficients:

$$\langle j_1 \ m_1 \ j_2 \ m_2 | j \ m \rangle$$

4. CLEB -Calculates only the following Clebsch-Gordan coefficients:

$$\langle I \ K \ 1 \ 0 | I-1 \ K \rangle$$

$$\langle I \ K \ 2 \ 0 | I-2 \ K \rangle$$

5. DEDX -Based on an old Oak Ridge code, this program calculates stopping powers and ranges. It works with all chemical elements, plus the compounds *ISOBUTANE* and *MYLAR*.

6. EPSBET - The program makes conversion between Nilsson epsilon deformations and Warsaw betas, i.e. shape defined in terms of epsilons will be expanded in terms of betas. Originally written by W. Nazarewicz.

7. GOSTOP -This program allows the calculation of electronic and nuclear stopping powers. Data for the stopper material density is taken from the American Institute of Physics handbook.

8. QUAD -Program which extracts β_2 and ϵ_2 values from a given quadrupole moment Q_0

9. STIME -Program to calculate stopping times for ions in materials.

10. WU -Program to calculate the reduced electromagnetic transition rates B(EL), B(ML) and the ratios

$$\frac{B(EL)}{B(EL)_w} \quad \text{and} \quad \frac{B(ML)}{B(ML)_w} \quad (\text{in Weiskopf units}).$$

Source codes and theoretical references are provided at request at the electronic address: mcolci@tandem.nipne.ro

References

- [1] Bass, R-Nucl.Phys.A231(1974)45
- [2] F.Dönau-Nucl.Phys.A471(1987)469
- [3] D. C.Radford et al-NPA 545, 665(1992)

Nuclear structure of doubly - odd ^{150}Pm nucleus

E. Dragulescu¹, G. C. Serbanut¹, P. Racolta¹, D. Moisă¹, F. Baci¹, C. Besliu¹, I. Iftimia², G. Semenescu¹

¹ NIPNE-HH, Department of Nuclear Physics

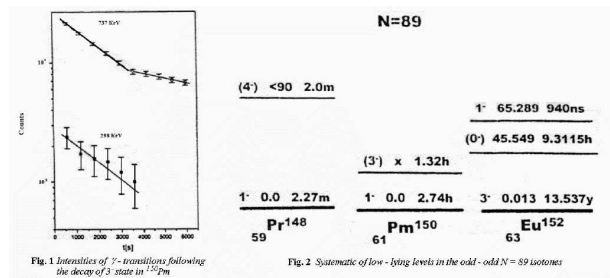
² Clemson University, USA

It has been suggested [1] that in rare - earth nuclei around $N = 88$ one may expect octupole correlation similar those found in the actinide nuclei around $Z = 88$. The experimental study of nuclei with $Z = 54 - 62$ and populated by α - induced reactions and fission [4, 5] has been revealed the presence of interleaved negative- and positive- parity yrast bands there are coupled by enhanced E1 transitions. A review on both experimental and theoretical progress in this area was done by Butler and Nazarewicz [1].

Octupole deformation can be established in special cases depending on the arrangement and the strength of the octupole interaction between $\Delta l = 3$ and $\Delta J = 3$ opposite orbitals. The maximum effect of octupole coupling might be expected at $Z \approx 62$ and $N = 90$ since the Fermi level lies both between the $f_{7/2}$ and $i_{13/2}$ neutron orbitals and between the $d_{5/2}$ and $h_{11/2}$ orbitals [2].

Drach and Salamon [3] suggested the possibility of using elemental abundance of Tc ($Z = 43$) and Pm ($Z = 61$), which no stable isotopes, as cosmic ray clocks. The abundance of their isotopes in the solar system have arisen from a combination of several different astrophysical sources. For example, there are thought to be three main nucleosynthesis processes that produced the solar system abundance for elements heavier than iron (the so - called s-, r- and p- process). We can investigate the details of the s - process by examining properties of so - called "branch point" [4].

The present study of low spin states of ^{150}Pm by means of $(p, n\gamma)$ reaction is an extension of previous systematic investigation of octupole correlation in the transitional odd - even $^{145-149}\text{Pm}$ and odd - odd $^{144-148}\text{Pm}$ [1].



The low spin structure for ^{148}Pm has been previously obtained from the $(p, n\gamma)$ reaction [17]. No excited states for ^{150}Pm have been reported up to now in the literature.

Nuclear levels in ^{150}Pm have been firstly investigated with the $^{150}\text{Nd}(p, n\gamma)$ reaction using beams of 5 - 8 MeV protons. A series of measurements, including excitation function $\gamma\gamma$ coincidence and lifetime measurements were performed. From our activation measurements of β decay of ^{150}Pm were determined the half - lives for: ground state (1^-), and new isomeric state (3^-) (see Fig. 1), 2.74(2) h and 1.31(1) h, respectively. This new 3^- state in ^{150}Pm is observed in the neighbouring odd - odd $N = 89$ isotones shown in Fig. 2.

Several new levels have been identified in ^{150}Pm and interpreted in the framework of theoretical models.

References

- [1] P. A. Butler and W. Nazarewicz, Rev. Mod. Phys. **88**, 349 (1996)
- [2] W. Urban et al., Phys. Lett. **B247**, 238(1996)
- [3] J. Drach and M. H. Salamon, Astrophys. J. **319**,237(1987)
- [4] K.T. Lesko et al., Phys. Rev. **C39**, 619(1989)

Nuclear structure of the $N=Z$ odd - odd nuclei around $N=28$ closed shell interpreted with IBFFM

E. Dragulescu¹, I. Serbanut², G. C. Serbanut¹

¹ NIPNE-HH, Department of Nuclear Physics

² University of Bucharest, Faculty of Physics, section of Nuclear Interactions and Elementary Particles Physics

INTRODUCTION

In the very recent years the knowledge of the level structure at lower and higher energies in the fpg shell $N=Z$ nuclei has renewed a growing interest due to major improvements in the theoretical techniques. Going away from closed shell, the shell model calculations rapidly exhaust computer capabilities and we must resort to the model observed on collective phenomena. The fpg odd-odd $N = Z$ around the doubly magic ⁵⁶Ni nuclei are good candidates to investigate the competition between collective and single-particle excitation [1-3].

Here is presented a part of results obtained from an exhaustive sistematic study [4,5] of the selfconjugate doubly-odd nuclei with $A > 62$: ⁶²Ga and ⁶⁶As nuclei using the interacting - boson - fermion - fermion - model (IBFFM) [6-8].

RESULTS AND DISCUSSION

The odd-odd nuclei are described in the framework of the IBFFM by coupling valence shell proton and neutron quasiparticles to even-even core described in the interacting - boson model. Inthe first step of the calculations the core parameters for ⁶⁰Zn and ⁶⁴Ge cores were fitted to the energies of their excited states.

In the second step of calculations, I have adjusted the IBFM proton hamiltonian to the low - lying levels of ⁶³Ga and ⁶⁷As nuclei and IBFM neutron hamiltonian of low - lying levels of ⁶¹Zn and ⁶⁵Ge nuclei involved in the casees of the structure of odd-odd ⁶²Ga and ⁶⁶As nuclei. We have finally calculated the level spectra and electromagnetic properties of above mentioned nuclei. The IBFFM positive - parity energy spectra are compared with experimental ones in Fig. 1. These calculations show a resonable agreement with experimental data and existing shell - model calculations.

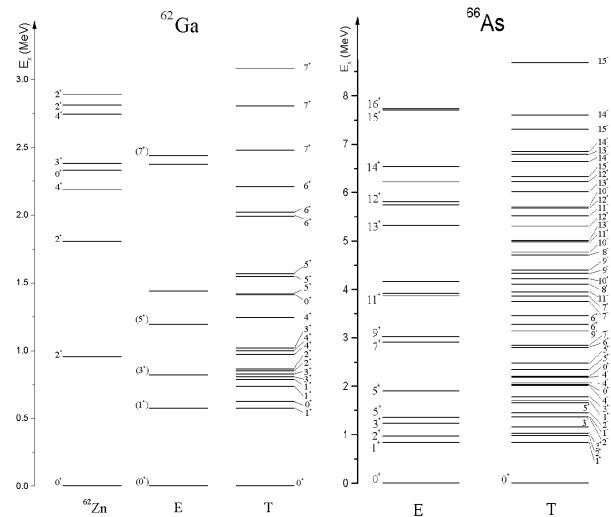


Figure 1: Low - lying experimental levels in ⁶²Ga [2] and ⁶⁶As [1,7] compared with the present IBFFM calculations.

References

- [1] R. Grzywacz et al., Phys. Lett., **B429**, 247 (1998).
- [2] S. M. Vincent et al., Phys. Lett., **B437**, 264 (1998).
- [3] D. Rudolph et al., Phys. Rev. Lett., **80**, 3018 (1998).
- [4] E. Dragulescu, in Proceedings "International Workshop Pingst 2000 - Selected Topics on $N = Z$ Nuclei", June 6 - 10, 2000, Lund, Sweden, Eds. D. Rudolph and M. Hellstrom (Bloms i Lund AB, 2000), p. 210.; E. Dragulescu to be published.
- [5] R. Grzywacz et al., in Proc. Int. Conf. "Nuclear Structure 2000", August 15 - 19, 2000, East Lansing, in press.
- [6] V. Paar et al., Z. Phys., **A327**, 291 (1987).

Algebraic and geometric description of the collectivity evolution in the even-even Yb nuclei

Al. Negreț¹, Gh. Căta-Danil¹

¹ IFIN-HH, Department of Nuclear Physics, Bucharest, Romania

We have studied the $^{160-174}\text{Yb}$ isotopes in the frame of the Interacting Boson Model (IBA-1) and the Geometric Collective Model (GCM). The existing experimental information in these nuclei refers mainly to the ground state and gamma bands. The information is not so rich on the excited $K=0$ bands. Our aim was to describe the structure of the low lying states.

The energy of the first excited state of the ground-state band (2_1^+) lowers continuously from $E=243$ KeV in ^{160}Yb to $E=77$ KeV in ^{174}Yb . The energy of the band-head of the gamma band increases from $E=820$ KeV in ^{160}Yb to $E=1634$ KeV in ^{174}Yb and the energy of the $K=0$ band-head (the 0_2^+ level) is almost constant [1].

IBA and GCM are two different approaches to the nuclear structure. IBA represents the algebraic point of view and GCM the geometric one. It has been shown that they describe the same physical structure [2]. We used this study also to find out how far the similitude between the two models can go.

The IBA computer codes "PHINT" and "FBEM" have been employed with the CQF parametrisation [3]. It has been shown [2] that the GCM can also reproduce the three known symmetries (symetric rotor, vibrator and γ -unstable rotor) using only the first three terms in the potential part of the hamiltonian. Therefore, in the GCM code we retained only four parameters - C_2 , C_3 and C_4 for potential, and the mass parameter B_2 [4].

The first nucleus where the calculations have been performed was ^{172}Yb , which is situated very close to the rotor limit. We obtained good fits, both in IBA and GCM. The procedure was extended as follows: for each nucleus we firstly employed the parameters from the neighbour isotope. Then, slowly varying the parameters we looked for the best agreement with the

experimental level scheme and the $B(E2)$ values. The main problem of this procedure appears between the isotope with $A=170$ and the isotope with $A=168$. Here, the relative position of the gamma band and of the $K=0$ band changes. Therefore we had to accept a leap of the parameters in this point in order to reproduce this effect.

In conclusion, we obtained acceptable agreement with the experimental values, both in IBA and GCM. The model parameters were kept in a narrow range. As we expected, the most difficult problem is the description of the $K=0$ bands. Their nature seems more complex than the simple assumptions of the pure collective models and we can observe a disagreement both for $B(E2)$ values and the parameter of inertia of $K=0$ bands of some isotopes.

Althought the calculations in the two models have been developed independently, the results are similar. Differences appear in details such as the moments of inertia of the excited $K=0$ bands.

Further on, we are planning experiments guided by these calculations.

References

- [1] Nuclear Data Sheets - www.nndc.bnl.gov
- [2] J. Zhang, R.F. Casten, N.V. Zamfir, Phys. Lett. B 407 (1997) 201
- [3] R.F. Casten, D.D. Warner, Rev. Mod. Phys. 60 (1988) 389
- [4] Computational Nuclear Physics, eds. K.Langanke, J.A.Maruhn and S.E. Koonin (Springer, Berlin, 1991)

Polarized neutron reflectivity on CoO/Co exchange biased multilayers

F. Radu^{1,2}, M. Etzkorn², V. Leiner^{2,3}, A. Schreyer², K. Westerholt², H. Zabel²

¹ NIPNE-HH, Department of Nuclear Physics, Romania

² Institut für Experimentalphysik/Festkörperphysik, Ruhr-Universität Bochum, Germany

³ Institute Laue-Langevin, France

The exchange bias (EB) phenomenon is associated with interfacial coupling between ferromagnetic and antiferromagnetic layers, which results in an unidirectional magnetic anisotropy. The macroscopic effects related to exchange biased systems are the shift of the hysteresis loop towards positive or negative directions and an increase of the coercivity field as upon cooling the system in an applied magnetic field. However, another macroscopic effect, namely, time relaxation of the exchange bias field has gained little attention so far [1,2,3].

The system we used for measuring the three macroscopic effects and, especially, the time relaxation one is a CoO/Co multilayer. The sample was prepared by rf-sputter on an a-plane sapphire substrate. The growth parameters were optimised as to obtain a low interface roughness, in expense of the crystallinity. The measurements were carried out at the ADAM reflectometer (ILL) by Polarised Neutron Reflectometry. The samples have been characterised by x-ray reflectivity and MOKE measurements. Neutron hysteresis loops [Fig. 1] were measured at 310 K (TN of CoO is 291 K) and 240 K by scanning the magnetic field and detecting the 4 reflectivities (R++, R+-, R-, R-) at the position of the first multilayer peak. From such curves we see that the reversal of magnetisation in the sample occurs not by in-plane rotation but rather through domain walls movement. In-plane magnetic moment rotation would have induced an increase of the spin-flip reflectivities (R+- and R-) at the crossing-point. There was no difference of the behaviour of the magnetisation reversal process from room temperature to low temperature and from the positive to the negative part of the hysteresis loop. We noticed, as well, that the exchange bias field was not stable in time [Fig. 2]. It decreases from about 180 Oe towards 0 Oe. The half-life time obtained by fitting the time dependence of the exchange bias field (TDEBF) curve with a "exponential decay" type of function was 580 sec.

[2] J. Nogues, I. K. Schuller, Exchange bias, J MAGN MAGN MATER **192**: (2) 203-232 FEB 1999

[3] R. L. Stamps, Mechanisms for exchange bias, J PHYS D APPL PHYS **33**: (23) R247-R268 DEC 7 2000

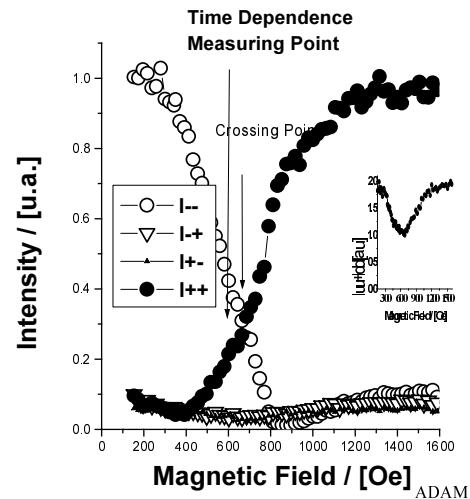


Figure 1: Neutron hysteresis loop taken at $T=240\text{K}$ after field cooling ($HFC=2\text{KOe}$) through Neel temperature of the antiferromagnet. In the inset: the sum of I_{++} and I_{--} which shows a dip on the zero magnetization region.

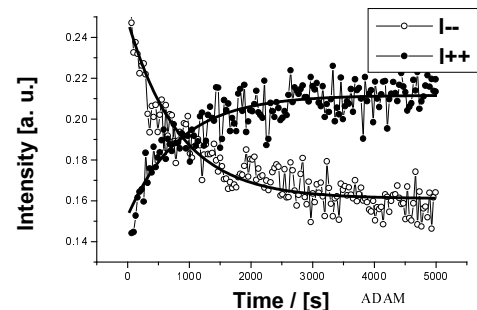


Figure 2: Time dependence of the neutron intensities I_{uu} and I_{dd} of the first multilayer peak.

References

- [1] W. Meiklejohn and C. P. Bean, Phys. Rev. **102**, 1413 (1956); **105**, 904 (1957)

Time and temperature effects on exchange biased CoO/Co bilayers

F. Radu^{1,2}, M. Etzkorn², T. Schmitte², A. Schreyer², K. Westerholt², H. Zabel²

¹ NIPNE-HH, Department of Nuclear Physics, Romania

² Institut für Experimentalphysik/Festkörperphysik, Ruhr-Universität Bochum, Germany

Considering the stability of magnetic configurations near ferromagnetic/antiferromagnetic interfaces, it is important to understand how the exchange bias (EB) and the coercivity field are affected by thermal fluctuations [1,2]. We have studied the time and temperature dependence of natural CoO/Co bilayers prepared by rf-sputtering and oxidized in air. The growth parameters were optimised in order to obtain a low interfacial roughness. We observed two striking peculiarities when studying the temperature dependence of the hysteresis loops after field cooling: a) the exchange bias starts out with a positive value at the blocking temperature of $T_B=180\text{K}$, and becomes negative below 160K . b) the coercive force increases drastically below 210K . Thus there is a temperature region where the coercive force is enhanced while the EB is suppressed [Fig. 1]. The last observation is in agreement with a thermal activation model proposed by Wee and Stamps [3].

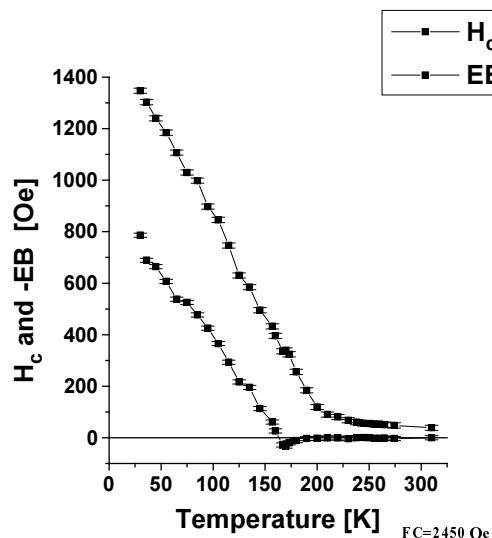


Figure 1: The -EB and coercivity field versus the temperature. The sample was cooled in $FC=2440\text{ Oe}$.

The time dependence of the EB was evidenced by its sweeping rate dependence at finite temperature. Taking advantage of the fact that for our system the first magnetisation reversal branch of the hysteresis loop is mainly causing the shift of the hysteresis loop

(as shown by the training effect) we stopped the magnetic field sweep at different points around the coercive force. We then determined the magnetic relaxation [Fig. 2] and, after magnetisation reversal, closed the loop by sweeping the magnetic field again. We noticed that in the region of positive EB the hysteresis loop is enlarged, while in the negative EB region it is narrowed. The training effects show the same behaviour.

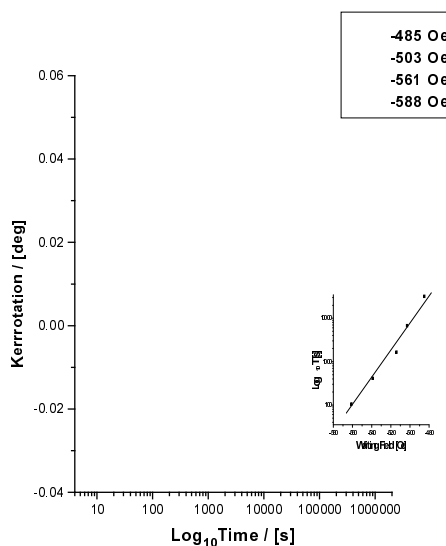


Figure 2: The evolution of Kerr rotation versus the time. The field scan was stopped at several waiting magnetic fields before the magnetization reversal one. In the inset: the dependence of time relaxation versus the waiting field.

References

- [1] W. Meiklejohn and C. P. Bean, Phys. Rev. **102**, 1413 (1956); **105**, 904 (1957)
- [2] J. Nogues, I. K. Schuller, Exchange bias, J MAGN MAGN MATER **192**: (2) 203-232 FEB 1999
- [3] R. L. Stamps, Mechanisms for exchange bias, J PHYS D APPL PHYS **33**: (23) R247-R268 DEC 7 2000

A new shape isomer in the N=Z nucleus ^{72}Kr

F. Becker^{1,2}, B. Blank³, C. Borcea⁴, E. Bouchez¹, I. Emsallem⁵, G. de France², J. Genevey, K. Hauschild¹, A. Hurstel⁵, W. Korten¹, Y. Le Coz¹, M. Lewitowicz², R. Lucas¹, I. Macovei², F. Negoita⁴, F. de Oliveira², D. Pantelică¹, J. Pinston⁶, P. Rahkila⁸, M. Rejmund¹, M. Stanoiu², Ch. Theisen¹

¹ CEA Saclay, France

² GANIL Caen, France

³ CENBG Bordeaux, France

⁴ IFIN-HH

⁵ IPN Lyon, France

⁶ ISN Grenoble, France

⁷ CSNSM Orsay, France

⁸ Univ. of Juvaskyla, Finland

The neutron-deficient Kr isotopes have a long history as candidates for the occurrence of coexistence between well-deformed prolate and oblate shapes [1]. The pronounced shell gaps for large prolate and oblate deformations at proton number $Z=36$ [2] play a major role for the structure of the Kr isotopes. Different shell gaps for neutron numbers between 36 and 42 lead to a pronounced deformation in the more neutron-deficient isotopes. Close to the N=Z line prolate and oblate shapes are generally expected within a few hundred keV of excitation energy. The shape of the ground state depends very much on the details of the effective interaction, including the possible influence of proton-neutron pairing when approaching the N=Z line. Detailed measurements of the properties of shape coexisting states in light Kr isotopes therefore constitute an important test of the nuclear models.

A systematic study of the properties of neutron-deficient Kr isotopes has been performed by our collaboration over few years. In-beam γ -ray and conversion-electron (CE) spectroscopy after fusion-evaporation reactions was used to study ^{74}Kr [3], while Coulomb excitation was performed on ^{78}Kr . In the most recent experiment, we have investigated isomeric states in very neutron-deficient nuclei around $A=70$, using for the first time combined CE and γ -ray spectroscopy after fragmentation reaction. Here, a 73 MeV/A ^{78}Kr beam, delivered by the GANIL cyclotrons, was fragmented on a Be target. The fragments were mass and charge analysed by the LISE3 spectrometer and implanted in thin Kapton foil. γ -ray were measured with a set up of segmented Clover detectors from EXOGAM collaboration, while the CE were detected with a large area Si(Li) detector mounted close to the implantation foil. With this method isomer transition can be assigned on an event-by-event basis to a given fragment. In this way an isomeric 0^+ state in ^{74}Kr , first observed in an earlier GANIL experiment without CE detection [4], could be firmly established by its E0 decay to the ground state. Moreover, a new 0^+ isomer was identi-

fied as the first excited state of the N=Z nucleus ^{72}Kr . This finding constitutes the first observation of a shape isomer in an N=Z nucleus.

References

- [1] R. Piercey et al., Phys. Rev. Lett. 47(1981)1514.
- [2] W. Nazarewicz et al., Nucl. Phys. A435(1985)397.
- [3] F. Becker et al., Eur. Phys. J A4(1999)103 and Phys. Scripta 17(2000).
- [4] C. Chandler et al., Phys. Rev. C61(2000)044309 and Phys. Rev C56(1997)R2924.

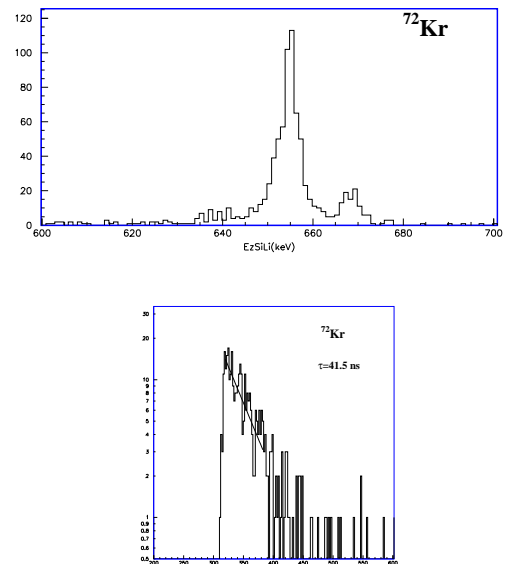


Figure 1: Upper figure: an CE spectrum corresponding to the $0^+ \rightarrow 0^+$ E0 transition. Bottom: the decay curve of the 0^+ excited level.

The investigation of magnetic phase transitions in a Fe/Gd bilayer embedded in a multilayer resonator

F. Radu^{1,2}, Yu. V. Nikitenko³, V Syromyatnikov⁴, H. Lauter⁵, V. Leiner⁵, V. L. Aksenov³

¹Departamentul de Fizica Nucleara, Institutul de Fizica si Inginerie Nucleara, 76900 Magurele, Romania

²Institut für Experimentalphysik/Festkörperphysik, Ruhr-Universität Bochum, D-44780 Bochum, Germany

³Frank Laboratory of Neutron Physics of Joint Institute for Nuclear Research, 141980, Dubna, Russia

⁴Petersburg Nuclear Physics Institute, 188350 Gatchina, Russia

⁵Institute Laue-Langevin, 38042 Grenoble Cedex 9, France

The experiment reported hitherto aimed at observation of magnetic phase transition in a Fe/Gd bilayer embedded in a multilayer neutron resonator. Polarised neutron reflectivity (PNR) measurements were carried out using the ADAM reflectometer at the Institute Laue Langevin. The magnetic structure of Fe/Gd multilayers is the result of the competition between the ferromagnetic coupling in Fe (bcc ferromagnet) and in Gd (bcc ferromagnet) layers and an antiferromagnetic coupling at the interface. It was shown [1,2] that three magnetic phases can take place: twisted, aligned-Fe, aligned-Gd. The aligned states are unstable against a strong enough magnetic field and, for a critical one, the magnetic moments leave the aligned states and will make an angle in respect to the external field. At low temperatures only 2 phases are expected to occur: one at low fields when the Gd moments are aligned in the direction of the field, and iron moments are antiparallel; at high enough external magnetic field the system undergoes a transition towards a state where the magnetisation of Fe and Gd are kept antiparallel between themselves but under an angle to the external field. As the neutron spin-flip reflectivities are sensitive to such an angle, one would expect a direct evidence of such a transition by direct comparison of the reflectivities corresponding to the aligned-Gd and twisted magnetic phases. Taking advantage of the neutron density probability enhancement in the neutron multilayer resonator [3,4], we have measured the neutron reflectivities (R₊₊, R₊₋, R₋₊, R₋) from the following sample: Cu(100 Å)/Ti(500 Å)/Gd(30 Å)/Fe(120 Å)/Ti(1500 Å)/Cu(1000 Å)/Glass at 3 different temperatures (93 K, 50K, 1K). For each temperature point, 2 sets of reflectivities were collected at 500 Oe and 5 KOe. The magnetic field was applied parallel to the sample surface. The measurements at (H=5 KOe, T=95 K) are shown in fig 1. Plotted lines are the collected neutron intensities I_{uu}, I_{dd}, I_{ud}, I_{du} which after data manipulation according to Ref. 5 will turn out in reflectivities R₊₊, R₋, R₋₊, R₊₋. One can notice that there are dips in total reflection region for I_{dd} and I_{uu}, mainly due to the neutron absorption in Gd layer. It shows that for different neutron wavelengths the neutron density probability is enhanced, thus the absorption and spin-flip probability (if any)

is enhanced, as well.

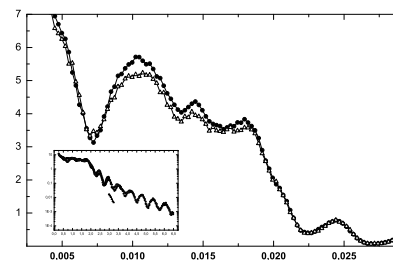


Figure 1: The I_{uu} (R₊₊) neutron intensities at T=95 K for 2 different magnetic fields: H=500 Oe and, respectively, H=5 KOe. In the inset: The I_{uu}, I_{dd}, I_{du}, I_{ud} neutron intensities at T=95 K and H=5 KOe. The magnetic field was applied parallel to the sample surface. In fig. 2 the intensities I_{uu} at T=95, H=500 Oe and (T=95, H=5 KOe) points in phase diagram are plotted against the wave vector transfer. The difference between them is well seen in the total reflection region while in the Kissing fringes regime it is hardly distinguishable. The origin of the difference of the two reflectivities is connected with the change of magnetic configuration of the Fe/Gd system. The Fe/Gd bilayer at H=500 Oe is more noncollinear than at H=5 KOe. Quantitative analysis of the data based on fitting to the neutron reflectivities is now under development.

References

- [1] R. E. Camley and D. R. Tilley, Phys. Rev. B, 37, 3413, 1988
- [2] C. Dufour, K. Cherifi, G. Marchal, Ph. Mangin, M. Hennion, Phys. Rev. B, 47, 14 572, 1993
- [3] V. L. Aksenov, Yu. V. Nikitenko, F. Radu, Yu. M. Gledenov, P. V. Sedyshev, Physica B, 276-278, pp. 946-947, 2000
- [4] F. Radu, V. K. Ignatovich Physica B, 292, pp. 160-163, 2000
- [5] C. F. Majkrzak, Physica B 221, 342, 1996

Nuclear Reactions

Pre-equilibrium emission surface effects in activation reactoins

V. Avrigeanu¹, M. Avrigeanu¹, A.J.M. Plompen²

¹ IFIN-HH, Department of Nuclear Physics, Bucharest, Romania

² EC/JRC/IRMM, Neutron Physics Unit, Geel, Belgium

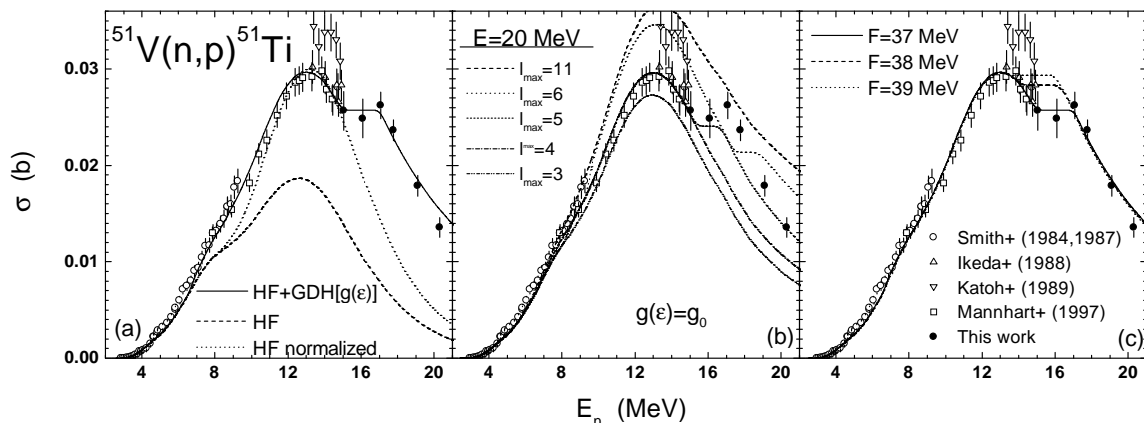
Improved cross-section calculations are reported in this work [1], based on updated particle-hole level density formalism including energy-dependent single-particle level densities as well as surface effects [2].

The often low predictive power of the statistical and pre-equilibrium (PE) nuclear reaction models has recently been underlined by IRMM studies [3] of both absolute cross sections and shape of excitation functions of fast neutron-induced reactions on medium mass nuclei. A better description of the high-energy side of activation excitation functions, most sensitive to PE modeling (e.g. Fig. 1a), is obtained especially within the geometry-dependent hybrid (GDH) model by means of averages of the imaginary potential and nuclear density over projectile trajectories for various partial waves in order to determine the intranuclear transition rates ([4] and references therein). At the same time it is assumed that the reactions are localized within spherical shells determined by the projectile impact parameter. Actually, the discussion of the nuclear surface localization of preequilibrium reactions at low energy [5], by means of the semiclassical method, has confirmed the geometry effect taken into account within the GDH model (Fig. 1b,c). Moreover, Kalbach's [6] recent phenomenological re-analysis of the surface localization of the initial target-projectile

interaction provides an increased effect for lower energy neutrons, in close agreement with the results obtained by using the improved particle-hole level density within the GDH formalism.

References

- [1] EURATOM–NASTI-Romania Association Contract; EFDA-2001 Ref. TTMN-001 (Deliverable 3).
- [2] M. Avrigeanu and V. Avrigeanu, *Comp. Phys. Comm.* **112**, 191 (1998); Computer code PLD, CPC Program Library, The Queen's University of Belfast; A. Harangozo, I. Stetcu, M. Avrigeanu, and V. Avrigeanu, *Phys. Rev. C* **58**, 295 (1998).
- [3] A. Fessler, E. Wattecamps, D.L. Smith, and S.M. Qaim, *Phys. Rev. C* **58**, 996 (1998).
- [4] M. Blann and H.K. Vonach, *Phys. Rev. C* **28**, 1475 (1983).
- [5] M. Avrigeanu, A. Harangozo, V. Avrigeanu, and A. N. Antonov, *Phys. Rev. C* **54**, 2538 (1996).
- [6] C. Kalbach, *Phys. Rev. C* **62**, 044608 (1996).



Vanadium cross section measurements by the activation technique and evaluations from threshold to 20 MeV

P. Reimer¹, A.J.M. Plompen¹, V. Avrigeanu², S.M. Qaim³

¹ EC/JRC/IRMM, Neutron Physics Unit, Geel, Belgium

² IFIN-HH, Department of Nuclear Physics, Bucharest, Romania

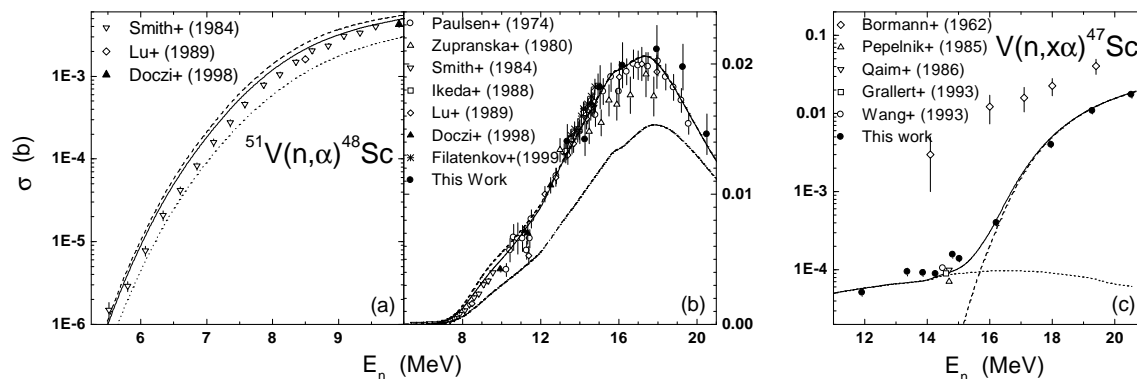
³ FZ-Jülich, INC, D-52425 Jülich, Germany

Vanadium is of interest as a candidate low-activation structural material in devices with a hard neutron flux. Recent measurements of the ^{47}Sc production in benchmark irradiations of vanadium alloys showed discrepancies with calculations using data from the EAF-97 library of $C/E=1.5$ or more depending on the neutron spectrum used. In the present work [1, 2] the reaction $^{nat}\text{V}(n,\alpha)^{47}\text{Sc}$ is studied from threshold to 20.5 MeV with the aim to improve the data base and resolve the above discrepancies. Simultaneously, new measurements were done for the $^{51}\text{V}(n,\alpha)^{48}\text{Sc}$ reaction as well, e.g. Fig. 1(a,b), and some additional experimental data were added to those obtained recently for the $^{51}\text{V}(n,p)^{51}\text{Ti}$ [3]. Calculations were performed using a revised version (e.g. [4]) of the STAPRE-H95 statistical model code [5] with pre-equilibrium contributions calculated using the geometry dependent hybrid model. A physically consistent description of all pertinent experimental information was attempted. In most cases a description of the experimental data is obtained that is sufficiently accurate to consider adopting all the new model calculations in evaluated data files. Disagreement with earlier estimates for the

$^{51}\text{V}(n,n'\alpha)^{47}\text{Sc}$ cross sections is attributed to a misinterpretation of the dominant process that is ongoing around 14.8 MeV incident energy, e.g. Fig. 1(c).

References

- [1] FP5/PECO Project EC/JRC/IRMM-14a "Neutron Data Measurement and Evaluation Activities" (2000-2002).
- [2] EURATOM-NASTI-Romania Association Contract; EFDA-2001 Ref. TTMN-001 (Deliverable 3).
- [3] A. Fessler, A.J.M. Plompen, D.L. Smith, J.W. Meadows, and Y. Ikeda, Nucl. Sci. Eng. **129**, 164 (2000).
- [4] M. Avrigeanu and V. Avrigeanu, Comp. Phys. Comm. **112**, 191 (1998).
- [5] M. Avrigeanu and V. Avrigeanu, J. Phys. G **20**, 613 (1994); M. Avrigeanu and V. Avrigeanu, Report NP-86-1995, IPNE, Bucharest, 1995; NEA-DB Index: IAEA0971/03.



On consistent description of nuclear level density

V. Avrigeanu¹, T. Glodariu¹, A.J.M. Plompen², H. Weigmann²

¹ IFIN-HH, Department of Nuclear Physics, Bucharest, Romania

² EC/JRC/IRMM, Neutron Physics Unit, Geel, Belgium

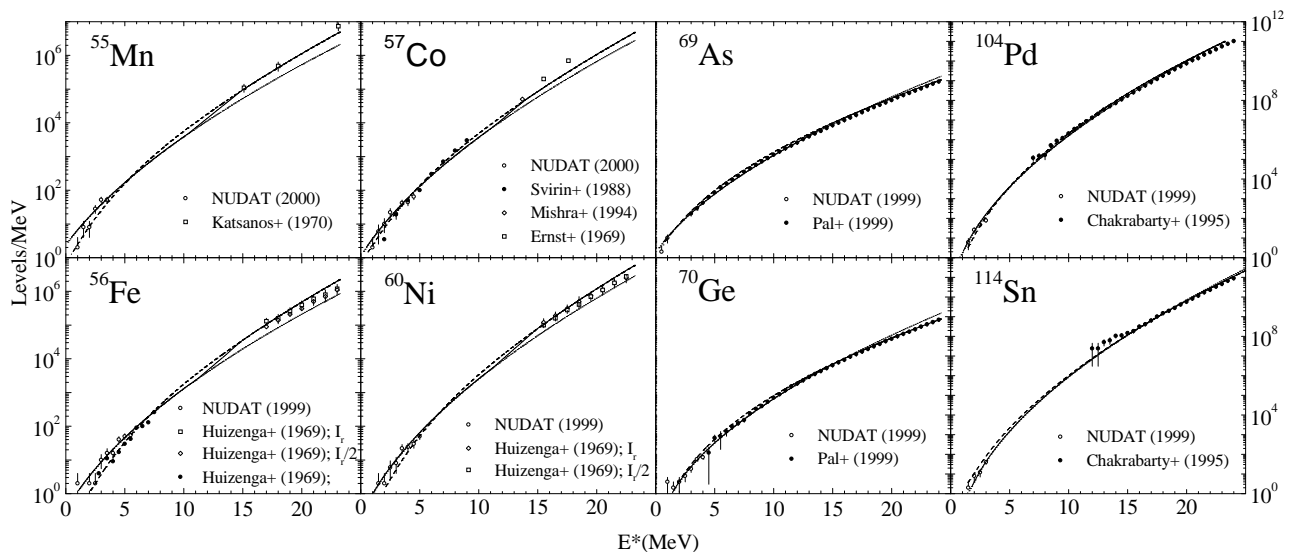
A consistent description of all experimental data related to the nuclear level density of medium-heavy nuclei, i.e. the low-lying discrete levels, the nucleon-resonance data, and the level density data above the nucleon binding energy, has been obtained [1]. The back-shifted Fermi gas (BSFG) model has been used for the description of the nuclear level density at excitation energies lower than the nucleon binding energy by fitting the latest experimental low-lying discrete levels and average s -wave nucleon resonance spacings D_0 . While recent studies [2] indicate that the effective moment of inertia of the nucleus is about half the widely used rigid-body value I_r , the analysis of the ratio of the proton and neutron resonance spacings corresponding to the same compound nucleus [3] has led to the value $I/I_r = (0.75 \pm 0.06)$ for the nucleus ^{51}V . Moreover, following theoretical predictions we have adopted a variable ratio I/I_r that ranges from 0.5 at the ground state energy to 0.75 at the binding energy and 1 at 15 MeV, while remaining constant above.

Also, various approaches developed for the energy-dependent level density parameter are reviewed, pointing out the usefulness of the method proposed by Koning and Chadwick [4] for choosing the appropriate shell correction energy. A consistent description of both the s -wave nucleon-resonance data and the level density data above 10-15 MeV, for nuclei with $A=55-$

70 and $A=104-114$ has been obtained. A smooth transition range from the BSFG formula description (dotted curves, Fig.1) to the approach adopted for the higher energies (dashed curves) has been chosen between the binding energy and the value of 15 MeV. The difference still existing at the binding energy is due to the different (i) effective energies, and (ii) forms of the two approach denominators. The partial removal of the former effect could be obtained by using a correction factor given by the ratio of the nuclear temperatures corresponding to the two formulas.

References

- [1] EURATOM-NASTI-Romania Association Contract; EFDA-2001 Ref. TTMN-001 (Deliverable 3).
- [2] S.F. Mughabghab and C. Dunford, Phys. Rev. Lett. **82**, 4083 (1998); B.K. Agrawal, S.K. Samaddar, A. Ansari, and J.N. De, Phys. Rev. C **59**, 3109 (1999).
- [3] H. Weigmann, C. Wagemans, A. Emsallem, and M. Asghar, Nucl. Phys. **A368**, 117 (1981).
- [4] A.J. Koning and M.B. Chadwick, Phys. Rev. C **56**, 970 (1997).



Fast neutron distributions from Be and C thick targets bombarded with 80 and 160 MeV deuterons

N. Pauwels¹, S. Brandenburg², H. Laurent¹, J.P.M. Beijers², F. Clapier¹, H. Lebreton³, M. Mirea⁴,
M.G. Saint-Laurent³, R.G.T. Zegers²

¹ Institut de Physique Nucleaire, Orsay Cedex, France

² Kernfysisch Versneller Instituut, Groningen, The Netherlands

³ Grand Accelérateur National d'Ions Lourds, Caen Cedex, France

⁴ NIPNE-HH, Experimental Physics Departement

Production of fast neutrons studies have come to the fore in the past few years because of the great interest for the possible applications of induced fission to produce neutron rich ion beams. In this context, the main objective of the SPIRAL II (Système de Production d'Ions Radioactifs Accélérés en Ligne) and PARRNe (Production d'Atomes Radioactifs Riches en Neutrons) R&D projects is the investigation of the feasibility and of the optimum parameters for a neutron rich isotope source. Special attention is dedicated to the energy and angular distributions of the neutrons obtained through deuteron break-up in different types of converters and different incident energies. Analysis and modelization of such behaviors, together with the study of the yields of neutron induced fission [1], can be used to optimize the productivity of the fissioning target its geometry and designing it accordingly. The present report continues our previous studies realised for 17, 20, 28 [2] and 200 MeV [3] deuteron energies and it is focused on deuteron incident energies of 80 and 160 MeV.

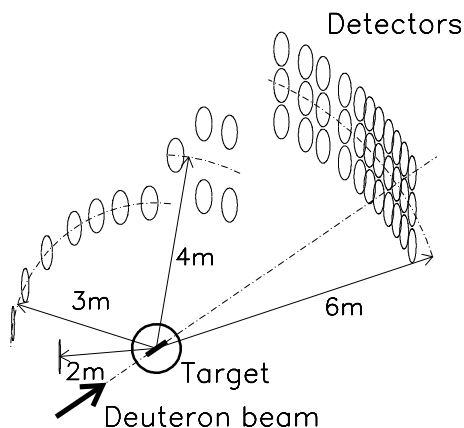


Figure 1: Experimental set-up

In the experiment, the double differential cross section for neutron production induced by 80 and 160 MeV deuterons impinging on thick C and Be targets, in which the incident deuterons were completely stopped,

have been measured. The energy of the neutrons was determined from the time-of-flight (TOF) measurement. To obtain an energy resolution of about 4% for the fastest, forward-emitted neutrons, which have approximately beam velocity, the length of the flight-path for the detectors at angles up to 30° was chosen to be 6 m. At backward angles, where the neutron energies are lower, a shorter flightpath was chosen. A schematic drawing of the setup is shown in Fig. 1. A 100 mm thick Be target and a 70 mm thick C target were used.

Results are exemplified with the angular and energy distributions of neutron obtained for Be target at 80 MeV in Fig. 2.

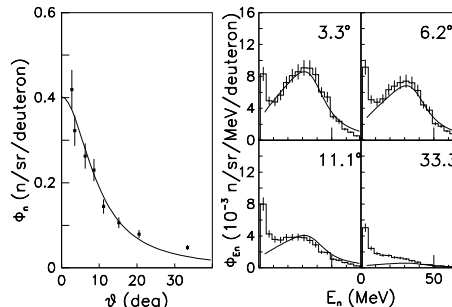


Figure 2: Experimental angular and energy neutron distributions.

References

- [1] M. Mirea, F. Clapier, N. Pauwels, and J. Proust, *Nuovo Cimento* **111A** (1998) 267.
- [2] S. Menard, M. Mirea, F. Clapier, N. Pauwels, J. Proust, C. Donzaud, D. Guillemaud-Mueller, I. Lhenry, A.C. Mueller, J.A. Scarpaci and O. Sorlin, *Phys. Rev. ST Accel. Beams* **2** (1999) 033501.
- [3] N. Pauwels, F. Clapier, P. Gara, M. Mirea and J. Proust, *Nucl. Instr. Meth. B* **160** (2000) 315.

${}^3\text{H}/{}^3\text{He}$ squeeze-out - a signature of the fireball's isospin distribution?

M. Petrovici^{1,2}, G. Stoicea^{1,2}, Y. Leifels², A. Andronic^{1,2}, N. Herrmann², K.D. Hildenbrand²,
Collaboration FOPI²

¹NIPNE-HH Bucharest, Department of Nuclear Physics

²GSI-Darmstadt, Germany

The Phase I FOPI data evidence for highly central Au + Au collisions at 100, 150 and 250 A·MeV systematically larger mean kinetic energies for ${}^3\text{He}$ fragments relative to the ${}^3\text{H}$ values [1]. The EOS Collaboration find the same trend with somewhat larger size [2]. Microscopic transport models [3] and hybrid hydrodynamical models, including pure Coulomb repulsion at the freeze-out moment [4] do not succeed to explain quantitatively this difference. Similar findings are recently reported by the INDRA Collaboration [5] for ${}^{129}\text{Xe} + {}^{119}\text{Sn}$ at 50 A·MeV. At a higher incident energy 1.15 A·GeV it seems that this difference disappears. Both types of fragments have the same mean kinetic energy, following a trend as a function of the fragment mass only, which is specific for the emission from an expanding source.

Corroborating these facts, based on the dynamics of the expansion suggested by hydrodynamical models, one could imagine that due to the Coulomb repulsion, the outer layers of the initial fireball are to some extent more proton rich than the inner zones. If this is the case, then one expects ${}^3\text{He}$ fragments originating with higher probability from these regions of the fireball and consequently having larger expansion velocities as far as the expansion has an almost linear dependence as a function of the distance from the center of the fireball [3, 4]. Within such a scenario, the ${}^3\text{He}$ fragments are supposed to be emitted preferentially in earlier phases of the expansion than the ${}^3\text{H}$ fragments, and feel a larger shadowing from the spectators passing by. For mid-central collisions this may lead to a difference in the squeeze-out signal. In order to check this, we analysed data of Ru + Ru collision at 400 A·MeV obtained with the Phase II - FOPI experimental configuration.

The mass and charge identification of A=3 fragments is achieved using the combined information from the central drift chamber (CDC) and the time-of-flight Barrel surrounding the CDC. The low momentum range cannot be used due to the geometrical gap between the CDC and HELITRON. However, the kinetic energy distribution of ${}^3\text{He}$ and ${}^3\text{H}$, for highly central collisions (1% cross section), show similar trends as those observed in Au + Au collision [1]. The selection of the collision geometry and reaction plane determination are explained in a different contribution to this report. The azimuthal distributions are obtained in the reference frame rotated by the sideward flow angle relative to the collision axis. Due to geometrical cuts the

experimental data are analysed in the angular range 0° - 60° and 300° - 360° . The angular distributions are obtained by symmetrising these results relative to 90° and 270° , respectively. For an impact parameter range of $b = 2$ -4 fm one observes a much larger squeeze-out signal for ${}^3\text{He}$ relative to ${}^3\text{H}$. The two azimuthal distributions are normalised at 0° . A second order Fourier expansion ($f(\Phi) = a_0(1 + a_2\cos(2\Phi))$) is used to fit the azimuthal distributions. The resulting a_2 coefficients for all fragments from A=1 to A=4 are presented in Fig.1. While p,d and ${}^4\text{He}$ show the well known enhancement of the squeeze-out signal as a function of mass, larger a_2 values for ${}^3\text{He}$ relative to ${}^3\text{H}$ can be observed. Different cross-checks and comparisons with microscopic model predictions are in progress. However, this preliminary result seem to indicate that the relative value of the squeeze-out signal of ${}^3\text{H}$ and ${}^3\text{He}$ could be related to the isospin distribution in the fireball at the freeze-out moment. Obviously, other contributions (like Coulomb focusing) to the observed effect are not excluded.

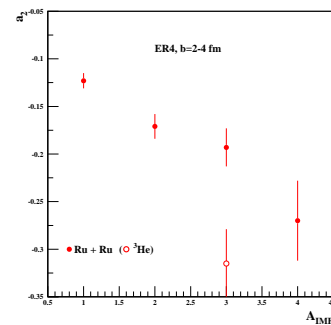


Figure 1: a_2 values as a function of mass of the reaction products for Ru + Ru collision for the same geometry and $p_t^{(0)}$ values as for Fig. 1

References

- [1] G. Poggi et al., Nucl. Phys. **A586**, 755 (1995)
- [2] M. Lisa et al., Phys. Rev. Lett. 7526621995
- [3] P. Danielewicz, et al., Phys. Rep. 517161995
- [4] M. Petrovici, FOPI Collaboration, "Heavy Ion Physics at Low Intermediate and Relativistic Energies", World Scientific, 1997, p. 216
- [5] D. Gorio et al., Eur. Phys. J. A7,245(2000)
- [6] A. Andronic et al., Nucl. Phys. **A679**, 765 (2001)

Incident energy and A_{part} dependence of the fireball expansion in Au+Au collisions

G. Stoicea^{1,2}, M. Petrovici^{1,2}, A. Andronic^{1,2}, N. Herrmann², K.D. Hildenbrand², Y. Leifels², W. Reisdorf²,
Collaboration FOPI²

¹NIPNE-HH Bucharest, Department of Nuclear Physics

²GSI-Darmstadt, Germany

A unified representation of the squeeze-out trends can be done in terms of the azimuthal distribution of the kinetic energy [1, 2]. A comprehensive description of the squeeze-out phenomena in the energy range 0.25 - 1.15 A·GeV is based on the parametrisation of the transverse mass spectra with an expression describing a radially symmetric expanding shell [1]. As far as such a situation can hardly be encountered in heavy ion collisions and is not specific at all for mid-central collisions, a presentation of the experimental information free of any model is preferred.

In this contribution we present results on azimuthal distributions of the collective flow β ($=v/c$) which is extracted from the rise of the experimental mean kinetic energy $\langle E_{kin}^{cm} \rangle$ with the mass of the reaction products. We use the full coverage of the FOPI experimental device in order to extract as precise as possible this experimental information. Therefore, we have to combine the information from the forward plastic wall detector where the reaction products are identified only by their charge with the one from the central drift chamber (CDC) where the reaction products are identified by their mass. This is achieved by using the information obtained during earlier Phase I experiments when Si-CsI telescopes delivered a very good mass and charge separation of the light products within the acceptance of the plastic wall [3]. The collision geometry definition is based on CDC charged particle multiplicity and the ratio of transversal to longitudinal energies [4]. The analysis is performed in a reference frame with the z axis along the sideways flow direction and within $80^\circ \leq \Theta_{cm} \leq 100^\circ$ polar angular range. The azimuthal distributions are symmetric with respect to 90° and 270° , hence, we overlap 0° - 90° and 270° - 360° azimuthal ranges to decrease the statistical errors, make five bins in azimuth and reflect the results in order to cover the full angular range 0° - 360° . The average flow value, β_o , and the out-of-plane - in-plane difference, $\Delta\beta$, are taken from a fit to the flow ($\beta=v/c$) azimuthal distributions using the following expression:

$$\beta(\Phi) = \beta_o - \Delta\beta \cdot \cos 2\Phi$$

The elliptic flow characterised by the major axis perpendicular to the reaction plane rises continuously from 90 to 400 A·MeV for mid-central collisions (Fig. 1). At 90 A·MeV the in-plane and out-of-plane flow values are very similar, specific for the E_{tran} region [4]. At all energies the flow β_o increases with the centrality, namely with increasing the baryonic content of

the fireball (A_{part}), while $\Delta\beta$, the difference between out-of-plane and in-plane flow, decreases showing the shadowing effect of the spectator matter. At lower centralities, i.e. larger impact parameters, the spectator matter being more compact, the bulk of products detected in the reaction plane emitted by the fireball and not hindered by the spectators correspond to the late phase of the expansion when the flow is weaker and the spectators moved apart from the collision zone.

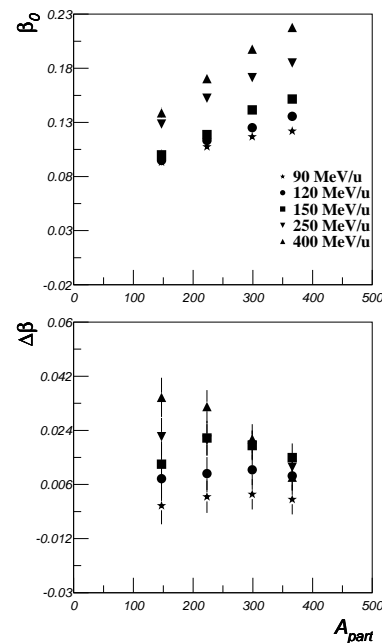


Figure 1: The average, β_o , and in-plane - out-of-plane difference, $\Delta\beta$, of the flow value as a function of centrality, for 90, 120, 150, 250, 400 A·MeV

These experimental trends can be followed in Fig.1. The continuation of these studies at higher energies and detailed comparisons with microscopic transport model predictions are in progress.

References

- [1] S. Wang et al., Phys. Rev. Lett. **76**, 3911 (1996)
- [2] M. Petrovici, FOPI Collaboration, "Heavy Ion Physics at Low, Intermediate and Relativistic Energies using 4π Detectors", World Scientific, 1997, p. 216
- [3] G. Poggi et al., Nucl. Phys. **A586**, 755 (1955)
- [4] A. Andronic et al., Nucl. Phys. **A679**, 765 (2001)

New results from two times double gap strip lines read-out RPC

M. Petrovici^{1,2}, N. Herrmann², K.D. Hildenbrand², P. Braun-Munzinger², I. Cruceru¹, M. Duma¹,
D. Moisă¹, M. Petriș¹, G. Stoicea¹

¹ NIPNE-HH Bucharest, Department of Nuclear Physics

² GSI-Darmstadt, Germany

This contribution is aimed to be a continuation of the previous report [1], where it was proposed a new type of structure of a MRPC and presented preliminary results obtained with it.

Besides the 30 cm long counter (short version), we tested also a 90 cm long version, a size appropriate for the time of flight barrel, surrounding the CDC, in the FOPI experimental device.

Different of our first prototype, all resistive electrodes are made from normal transparent glass, 2 mm thick for the short version and 1 mm thickness for the long version.

The electrode's width remained the same while the intermediate read-out printed circuit has for the long version only 12 strips relative to 16 used in the 30 cm counter.

As spacers we used for these tests two fishing roads along the floating glass electrode at about 5 mm from the lateral edges, on both sides of it. The long version was also tested with discrete spacers, every 5 cm, 5 mm long, fixed on the edges of the intermediate electrode.

A ⁶⁰Co source was used for tests and Fig. 1 shows the experimental configuration.

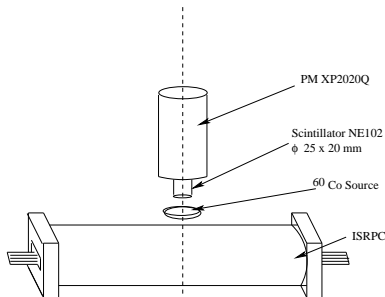


Figure 1:

While the electronic scheme is similar with that used in the previous tests, this time we equipped 4 strips - 8 channels, to see in which extend there is some influence on the results as a function of number of operated channels. The standard ORTEC421 fast amplifiers were replaced by 810L old GSI version.

Taking only the amplitudes larger than a given value and narrow conditions in the position (of about 30 mm), the sum time spectra $t = 1/2(t_{left} + t_{right})$ was obtained.

The measurements done with the short prototype reproduced the previous results [1] in terms of time resolution.

The result of Gaussian fit and the final time resolution, corrected for the contribution of the plastic

scintillator for the long prototype tests can be followed in Fig. 2.

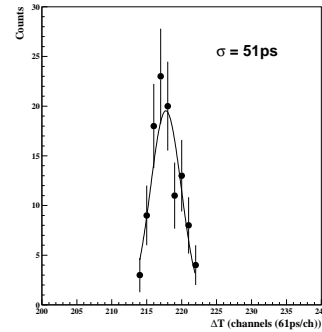


Figure 2:

The main conclusions of the present tests can be summarized as follows:

- the proposed structure gives reproducible results
- the time resolution does not depend on the lengths of the counter and does not show any position dependence
- the time resolution performance does not depend on the operated number of strips
- preliminary studies of the electronic cross-talk show that such counters could be operated in multiple hit environment if the distance between hits is larger than the number of strips fired due to the avalanche size. However, quantitative answer can be delivered after detailed tests using MIPs in multiple hit environment.
- normal transparent glass plates can be used for such a counter without a visible effect on the time resolution. Other aspects like the life time and the dependence of the performance as a function of operating time have to be studied in the future
- a better concept for the spacers has to be worked out and this seems to be much easier if the floating glass electrode will have a larger width relative to the others.

The results of present tests, in terms of time resolution, confirm the one of the previous report arguing the urgent need of in-beam tests using MIPs.

References

- [1] M. Petrovici et al, IFIN-HH Scientific Report (1999)59.
- [2] ALICE - TDR of the TOF, CERN/LHCC 2000

Array of photoelectric cells for Coulomb excitation experiments

M. Colci¹, D. Moisă¹

¹ IFIN-HH, Department of Experimental Physics, Bucharest, Romania

Since their development as practical detectors in the early 1960s, silicon diodes have become the detectors of choice for the majority of applications in which heavy charged particles are involved.

Some of the more common applications involve the spectroscopy of alpha particles and fission fragments and the measurement of energy loss of charged particles in transmission detectors.

If a measurement of the radiation energy is not required, simple counting of charged particle radiation can be carried out with silicon diode detectors which have quite good timing characteristics.

Silicon Sensors Inc. offers a wide range of standard photocell configurations. We have several low capacitance ($LC=12.57$) cells of 1 inch long and 0.2 inch width, having the following electrical characteristics (measured at 25° Celsius):

Active Area Dimensions = $4.42 \times 25.17 \text{ mm}^2$

Dark Current: for $VR = 2V, I = 4000 \text{ pA}$

and for $VR=10 \text{ V}, I=20000 \text{ pA}$

Junction Capacitance: for $VR = 0V, C=2220 \text{ pF}$

and for $VR=5 \text{ V}, C=555 \text{ pF}$.

We used four such photo-electric cells to detect backward scattered beam particles in Coulomb excitation experiments. These were arranged as indicated in Fig.1 and positioned 4.5 cm far from the target position.

We tested the energetic resolution and the timing characteristics of these photoelectric cells. They were connected through 4 charge sensitive preamplifiers to four spectroscopic amplifiers and were operated with different negative bias voltages. The energetic resolution improves with increasing voltage and we established an optimum value at 80V.

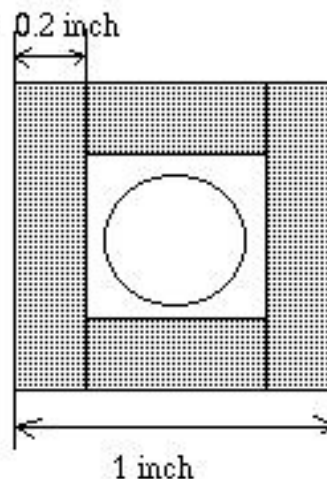


Figure 1: Schematic drawing of the arrangement of the 4 element array of photoelectric cells in Coulomb excitation experiment

States in ^{76}Ge were Coulomb excited by a 45 MeV ^{16}O beam delivered by the FN Tandem accelerator in Bucharest. The cells covered angles from 156° to 170° with respect to the beam direction. Detection of γ -rays in coincidence with ^{16}O scattered at these angles provided information about the time resolution of the photocells, which was $\approx 34 \text{ ns}$.

We also tested the detectors performance by recording the fission fragment spectrum from the spontaneously fissioning isotope ^{252}Cf in coincidence with γ rays. The time resolution was $\approx 25 \text{ ns}$.

We intend to use these detectors for further in-beam experiments.

Recent results on timing properties of CVD diamond detectors for MIPs

M. Petrovici^{1,2}, E. Berdermann², G. Caragheorghopol¹, M. Petriş¹, P. Braun-Munzinger², V. Catanescu^{1,2}, M. Ciobanu^{1,2}, M. Duma¹, D. Moisă¹, P. Moritz¹, J. Schukraft³, V. Simion¹, H. Stelzer², G. Stoicea¹

¹ NIPNE-HH, Bucharest, Department of Nuclear Physics

² GSI-Darmstadt, Germany

³ CERN, CH-1211 Geneva 23

The diamond has proper electrical properties for being used as a particle radiation detector. Due to its radiation hardness and fast charge collection speed, the CVD diamond detectors have been investigated and developed in the last decade for possible use as trackers in high luminosity hadron colliders [1]. Recent results demonstrate the excellent timing properties and extremely high counting rate capability of CVD diamond detectors in heavy ion experiments [2].

We have reported our preliminary results on timing properties of CVD diamond detectors for minimum ionizing particles (MIPs) [3].

We continued our investigations with a better quality CVD material. For the results presented here, two polished CVD diamond samples grown to a thickness of 500 μm were used (samples D1 and D2). The charge collection distances measured by us for these samples are about 200 μm . As in our previous communications, the results have been obtained using a ^{90}Sr β source with an end point energy of 2.28 MeV. The observed energy loss of the β particles in the diamond sample is a good approximation to the energy loss of minimum ionizing particles [4]. Using walk corrections for the D1 detector and selecting amplitudes between channel 750 and channel 1000 for the second detector (see Fig.1a) in order to have a reference signal not influenced by the walk effect, the intrinsic time resolution of 95ps was obtained, without any amplitude cut in the correspondingly sample (Fig.1b).

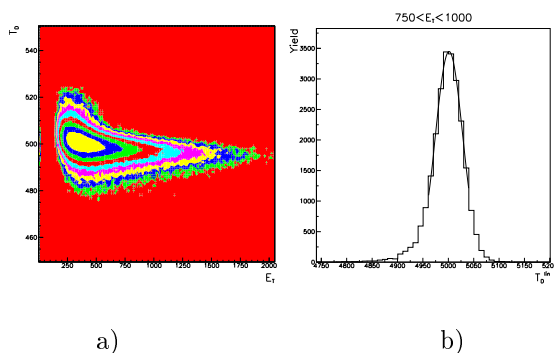


Fig.1

The detection efficiency is an other important parameter studied in the present work. Using the fast preamplifier developed for CVD diamond counters [5], for which the best time resolution was found, an CF4000

discriminator, the detection efficiency is very low ($\sim 3\%$). There are many signals just below the threshold of the discriminator setting at the noise level (Fig.2a). A much better value of about 90% was obtained using a charge sensitive preamplifier, characterized by a much better signal to noise ratio (Fig.2b).

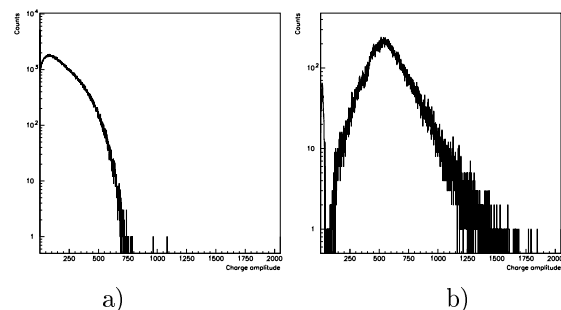


Fig.2

In conclusion, the results reported here show that using high quality CVD material and appropriate electronics for signal processing, diamond detectors could become serious candidates for being used as T0 detectors for MIPs with a time resolution below 100 ps.

The main effort should be concentrated now on developing the proper electronics in terms of signal to noise ratio preserving the timing properties of the present generation.

References

- [1] RD42 Collaboration, Nucl.Instr.and Meth. in Phys.Res. **A434**(1999)131
- [2] E. Berdermann et al, Nucl.Phys.B(Proc. Suppl.),**78**(1999)533
- [3] M. Petrovici et al., "Preliminary results on timing properties of CVD diamond detectors for MIPs", IFIN-HH Scientific Report 1999, p.60
- [4] S. Zhao, Ph.D.Thesis, The Ohio State University, 1994
- [5] P. Moritz et al., "Diamond Detectors for Beam Diagnostics in Heavy Ion Accelerators" DIPAC III, Frascati (1997)

Atomic Physics

Charge state distribution of highly charged ions passing through microcapillaries

D.E. Dumitriu^{1,2}, Y. Kanai², Y. Iwai², Y. Morishita², Y. Yamazaki²

¹ NIPNE-HH, Bucharest, Romania

² RIKEN, Wako, Japan

The properties of hollow atoms related with their formation mechanism have been intensively studied. In typical ion-surface experiments the study of the intrinsic nature of hollow atoms in the first generation-hollow atom above the surface (HAA)-is difficult, because the time interval between the HAA formation and its arrival at the surface is shorter than its intrinsic lifetime. Beam Capillary Spectroscopy (BCS) is a new and powerful method recently developed¹ which allows direct observation of HAA in vacuum by using a thin microcapillary as a target. q_f . 22 keV O^{q+} and N^{q+} ions ($q = 5, 6, 7$) from RIKEN 14.5 GHz ECR ion source were used as incident projectiles. The charge states of the ions transmitted through the target were separated and analyzed by a new charge state analyzer built in Atomic Physics Lab. at RIKEN. It consists of two sets of deflectors arranged in a "cascade" type configuration so they can guide the ions towards a channeltron. The Ni microcapillary target (area: 4mm^2 , length: $3.8\ \mu\text{m}$) is set in front of the analyzer. Results are shown in Fig. 1 and they present the following features: (a) One electron capture ($q_f = q - 1$) dominates in the charge changed fractions, independent of the projectile and initial charge state. (b) Almost neutralized projectiles ($q = 1$) are produced in large quantities and comparable to that for one electron capture. (c) The other charge states fractions ($1 < q_f < q - 1$) are lower than those for $q_f = 1$ and $q_f = q - 1$. (d) For the same initial charge state q , almost similar behavior was found in the final charge state distributions.

The total fraction CF of the all transmitted ions who captured electrons from microcapillary walls can be estimated by $CF = 2d_c/\rho$ with $d_c = (2q)^{1/2}/W$, where d_c is the critical distance for one electron capture, ρ is the nominal radius of the microcapillary and W is the binding energies of the target valence electrons. The CF formula is available under assumptions that the beam is entering parallel with the capillary axis and with the capillaries being of perfect cylindrical shape. The present target has capillaries with radii varying between 50nm on the backside and 90 nm on the front side. Considering a nominal radius of 50nm the expected CF is $\sim 4.1\%$ for $q = 7$ and decrease to 3.5% for $q = 5$. The total fraction CF measured is larger, due to different conditions of the beam and the

capillary from the ideal conditions as mentioned above.

The present results are in qualitative agreement with the theoretical one³. The measurements for N^{6+} ion beam can be also qualitatively compared with a previous measurement with N^{6+} (28 keV) incident projectile on a Ni microcapillary target⁴ with a different nominal radius and length. We found an overall agreement for final charge states distribution pattern in both cases.

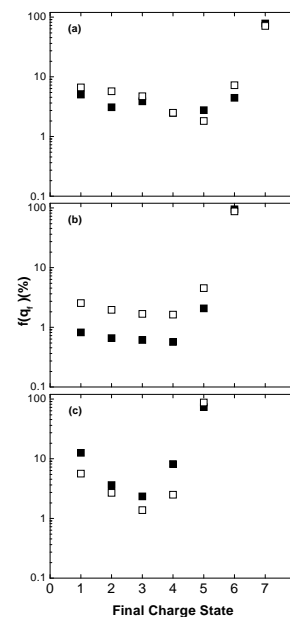


Figure 1: Charge state distribution for N^{q+} - full symbols and O^{q+} - open symbols; $q = 7, 6, 5$ - charge of the incident projectile on Ni microcapillary target

References

- [1] Y. Yamazaki et al.: J. Phys. Soc. Jpn. **65**, 1199 (1996)
- [2] Y. Yamazaki: Int.J. Mass Spectrom. **192**, 437 (1999)
- [3] K. Tókési et al.: NIM B **154-165**, 504 (2000)
- [4] S. Ninomiya et al.: Phys. Rev. Lett. **78**, 4557 (1997)

PIXE and ICP analysis of chemical elements in the downer cow syndrome

G. Dima², I. V. Popescu¹, T. Badica¹, A. Olariu¹, C. Stihl², M. Petre¹, E. D. Jianu³

¹National Institute of Physics and Nuclear Engineering, Bucharest, Magurele

²Valahia University of Targoviste

³S.C. TAROM S.A., Bucharest

The aim of this study was the microelemental analysis of blood serum samples collected from healthy and ill cows (downer cow syndrome DCS). The origin of this syndrome is uncertain but the clinical experience denotes that the DCS is advanced by the hypocalcemic paresis of parturition. The diminution of some nutritive elements from food can be a cause of DCS. The cows are more sensitive to the diminution of P in food in comparison with the diminution of Ca. Another interesting aspect about the origin of DCS is the ratio Ca/P in food.

The samples were collected from cows at some animal farms: 20 healthy cows and 12 DCS cows breeds

on the same conditions. Concentrations of P, Cl, K, Ca and Fe elements were obtained by using particle induced X - ray emission (PIXE) and inductively coupled plasma (ICP).

The mineral concentrations in the serum have values in normal limits for healthy cows even during the winter, when the mineral content of drying food is very poor. On the other hand, we can observe important decreases under the normal limits of the amount of Ca, P and Mg in the blood serum of DCS cows. It is easy to see the tendency of the DCS animals to have hypocalcemia and hypophosphatemia. Those perturbations can be the causes of the installations of the ill cows in the lypostatic and decubital attitudes.

Gamma-ray critical scattering on Rb_2ZnCl_4 around the normal-incommensurate phase transition point

S.E. Enescu¹, I. Bibicu², M.N. Grecu², C. Ciortea¹, Al. Enulescu¹, A. Kluger¹

¹NIPNE-HH, Nuclear Physics Department, Bucharest, Romania

²NIMP, Bucharest, Romania

Careful measurements of recoilless Rayleigh scattering of ^{57}Fe -14.4 keV radiation on Rb_2ZnCl_4 crystals can provide valuable information on the normal-incommensurate phase transition.

The 14.4 keV ^{57}Fe photons from a Mössbauer source of ^{57}Co in rhodium, scattered at 5.82° with respect to the (*ac*) plane, were measured at different temperatures around T_i . Details of the experimental set-up and the method used to discriminate the photons scattered elastically from those which undergoes inelastic scattering are described in [1]. Clear discontinuities in the resonance effects ϵ and in the ratio f_{in}/f_{el} (Fig. 1) are observed at T_i .

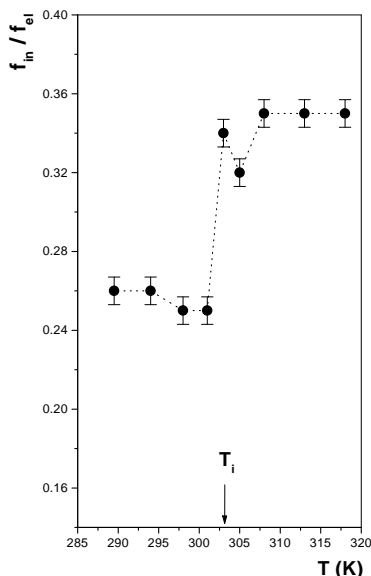


Figure 1: The temperature dependence of the ratio f_{in}/f_{el} of the Mössbauer radiation scattered on Rb_2ZnCl_4 ; dotted curve is a guide line.

Two models have been proposed in order to describe the normal-incommensurate phase transition in insulators of the A_2BX_4 family: the displacive one and the order-disorder one [2]. In the displacive model the

incommensurate phase is characterized by the appearance of a modulation of the atoms positions with a periodicity which is an irrational fraction of the periodicity of the underlying lattice. In the order-disorder model the potential energy surface of the atoms is considered to have two minima in the incommensurate phase. The probability of finding an atom in a specific minimum is modulated.

The ratio f_{in}/f_{el} gives especially information on the dynamics of the lattice. According to the differential cross-section for coherent inelastic scattering of photon [3], the magnitude of the coherent inelastic intensity increases with decreasing the frequency $\omega_{\mathbf{q}j}$ of the lattice mode (\mathbf{q},j). Thus, the modes with low frequency have an important contribution to the f_{in} .

The displacive model predicts a critical regime of the inelastic scattering of photons around T_i [4]. Our results are consistent with this model. In a simplified picture, the critical regime of the inelastic scattering is related to the critical soft mode whose contribution to the differential cross section is important due to its frequency approaching "zero". In our experiment the scattering vector \mathbf{Q} is approximately perpendicular to the (*ac*) plane. Hence the soft mode oscillates perpendicular to the (*ac*) plane and involves the motion of the Rb atoms which are by far the most efficient scattering atoms of Rb_2ZnCl_4 .

In conclusion, we reported a new critical phenomenon related to the normal-incommensurate phase transition of Rb_2ZnCl_4 : the inelastic scattering of Mössbauer radiation. This result proves that a significant change in the lattice dynamics occurs at the transition temperature.

References

- [1] Enescu S. E., Bibicu I, Zoran V., Kluger A., Stolica A. D. and Tripadus V., Eur.Phys.J.AP **3**, 119 (1998)
- [2] de Pater C.J. and van Dijk C., Phys.Rev. B **18**, 1281 (1978)
- [3] Donovan B. and Angress J. F., Lattice Vibrations, Chapman and Hall LTD, London, 1971, p.127
- [4] Andrews S. R. and Mashiyama H., J.Phys.C:Solid State Phys. **16**, 4985 (1983)

Investigation of the heavy metal pollution of Danube delta sediments by TTPIXE analysis

I. David¹, L. Dinescu², C. Ciortea¹, S.E. Enescu¹, D. Fluerasu¹, D.E. Dumitriu¹, A. Stochioiu³

¹ NIPNE-HH Nuclear Physics Department

² Nuclear Engineering and Vacuum Department

³ Environmental and Life Sciences Department

The elemental composition of sediments collected from some Danube Delta lakes (Malita, Furtuna, Lund, Mester and Sinoe), which are located in active sedimentary zones, was investigated by using two complementary methods: thick target proton-induced X-ray emission (TTPIXE) [1] and instrumental neutron activation analysis (INAA) or X-ray fluorescence (XRF) [2]. The goal was to obtain a complete survey of heavy metal pollution and reconstruct recent pollution history in these Danube Delta lakes. Vertical distribution was analyzed, except for the case of Sinoe Lake, from which samples were only collected at the surface. During PIXE measurements, the pellets of 12 mm diameter and $\sim 1,5$ mm thickness were bombarded using 3 MeV proton beams delivered by the FN-Tandem accelerator of IFIN-HH. The X-ray spectra were measured with a Ge-HP detector of 180 eV/5.9 KeV energy resolution for some micro.C charge accumulation. Control samples of reference sediments (IAEA, SL-1 and SOIL-7) prepared in the same conditions were also measured. Corrections were made for proton stopping and X-ray self-attenuation in the thick samples. Thirty-eight samples from the first four lakes and 7 samples from Sinoe Lake were analyzed, and the concentrations of 27 elements in every sample were determined by TTPIXE method. The following elements: S, Ca, Ti, Mn, Ni, Ga, Pb, and Hg could not be determined by INAA in our conditions. figure 1 shows a typical measured spectrum where the presence of various pollutant elements could be pointed out. Five elements - As, Br, Cr, Sb and Zn - were identified as pollutants by INAA method, showing concentrations about 1.5-2 times larger at the sediments surface. The vertical distribution of the presumed pollutant elements generally reflected the pollution history of the Danube Delta, namely a steady increase in pollution till the end of the 1980s, which can be associated with intense industrialization of Central and Eastern European countries prior to 1990. We think the interplay with TTPIXE

method will lead to an accurate picture of the heavy metal pollution of the Danube Delta.

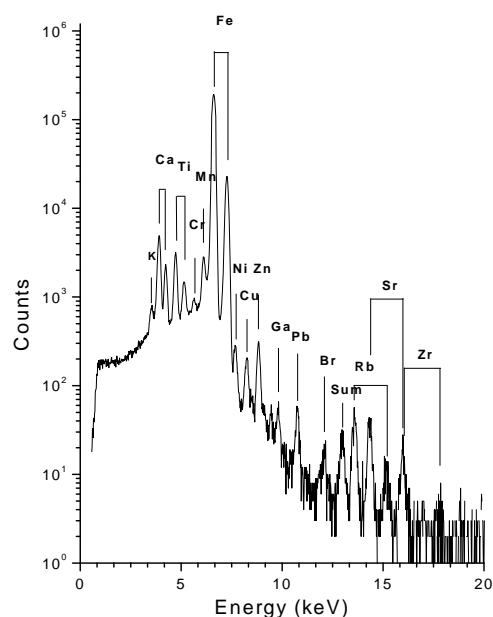


Figure 1: Typical X-ray spectrum obtained as result of irradiation of a sediment sample from Danube Delta

References

- [1] F. Araujo, T. Pinheiro, L. Alves, P. Valerio, F. Gaspar, J. Alves NIM B **136-138**, (1998) 1005-1012
- [2] V. Cojocaru, B. Constantinescu, I. stefanescu, C. Petolescu, Journal of Radional. and Nucl. Chem. **246** (2000) 185 -190

Improved PIXE analysis of micro- and trace elements in dental composites

E.A. Preoteasa¹, C. Ciortea², D. Flueraşu², S.E. Enescu², E. Preoteasa³

¹ NIPNE-HH, Bucharest, Romania

² NIPNE-HH, Nuclear Physics Department, Bucharest, Romania

³ Helident Ltd. Bucharest, Dental Surgery Branch, Bucharest, Romania

Due to the interactions occurring at the solid-solid and solid-liquid interfaces of a tooth's filling in the mouth, the mineral elements of the restorative composite may induce a complex response of the organism. To study such problems, sensitive surface trace element analysis is required. Particle-induced X-ray emission (PIXE) has a detection limit one order of magnitude lower than XRF [1] and has been used for hard dental tissues [2], but not yet for dental composites.

We evaluated the potential of PIXE in a study of ten types of composites used in restorative dentistry, some of them with two color shades each. The samples were prepared as described for XRF. The measurements were performed with 3 MeV protons from a van de Graaf tandem linear accelerator, using a hyper pure Ge detector and collecting the spectra for 1,5-4 hours. The spectra were processed with the program Leone. The protons' route in the sample calculated with the Trim program (~ 50 - $100 \mu\text{m}$) exceeded the size of mineral particles (0.02 - $30 \mu\text{m}$), thus granularity did not affect the analysis.

The PIXE analysis detected $Z \geq 19$ elements in all composites, and $Z \geq 14$ elements in only one low Z material (Fig. 1). PIXE detected generally the same dominant elements, but many more trace elements than XRF. Thus both Charisma (Kulzer) and Pekafill (Bayer) contained Ba as the major element, but trace elements were Ni, Zn, In, in the first, and Fe, Cu, Zn, Sr, Ag in the second. In other glass- and ceramics-based materials we found: Ca, Zr, Ba, Yb and traces of Sr, In, and possibly Ti in Tetric Ceram and in Ariston (both from Vivadent); Ca, Zr, Ba, Hf, possibly Mn, and traces of Ni, Ho, Ti, Fe, Cr in Valux Plus (3M Dental); Sr, Ba (major), K, Fe, Mn (minor), and traces of Ni, Zn, In, in F2000 Compomer (3M Dental); Ba (major) and traces of Fe, Ni, Sr in Surefil (Dentsply). In quartz-based materials we detected: Si, Ca, Ti, Fe and traces of K, Cl, Cr, Ni, Cu, Zn in Evicrol (Spofa); low and trace levels of Ca, Ti, Cr, Mn, Fe, Cu in Alphaplast (DGM) and Concise (3M Dental). Color shades were dependent on the ratio (Fe, Ni)/Cu/(Ti, Cr) in Evicrol; but were composition-

invariant in Tetric Ceram, Valux Plus and Surefil.

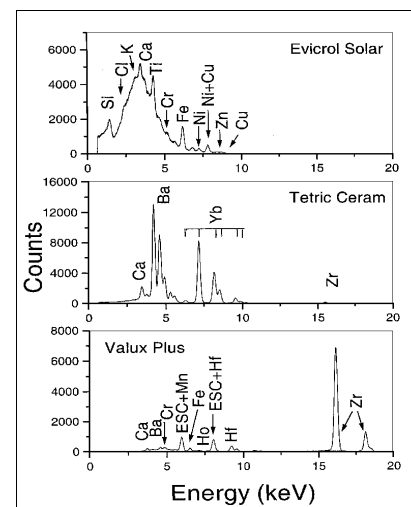


Figure 1: PIXE spectra of three dental composites showing major, minor and trace elements.

Some traces were impurities (as Sr accompanying Ba and Ca); they may influence the properties of nanoparticles in the materials.

The ability of PIXE for trace detection in dental composites was due both to better sensitivity and to careful analysis of spectra. However, spectral overlap caused a degree of uncertainty on some trace elements [1]. Caution is necessary to avoid trace contamination of samples. The method could serve also in new materials development and in forensic expertise.

References

- [1] R.P.H. Garten, Trends Analyt. Chem. **3**, 152 (1984)
- [2] M. Chaudri, Nutrition **11**, 538 (1995)

Potential of ERDA for analysis and depth profiles of light elements in dental composites

E.A. Preoteasa¹, D. Pantelica¹, F. Negoita¹, E. Preoteasa²

¹NIPNE-HH, Nuclear Physics Department, Bucharest, Romania

²Helident Ltd. Bucharest, Dental Surgery Branch, Bucharest, Romania

In the elemental analysis of dental composites, XRF and PIXE failed to detect low Z elements. The light elements from these biomaterials can be detected, however, by various ion beam analysis techniques. Among them, elastic recoil detection analysis (ERDA) is a fairly new method for simultaneous analysis of light and medium mass elements at the surface and for the determination of their depth profile [1].

In view of evaluating the potential of ERDA for the analysis of dental composites, Tetric Ceram (Vivadent) was chosen because it contains many light elements, i.e. H, C, N, O, F, Al, Si [2]. A flat surface sample was prepared as for XRF and PIXE. The ERDA measurements were carried out using a van de Graaf tandem accelerator. The projectiles were 80 MeV $^{63}\text{Cu}^{10+}$ ions. The detector was a compact $\Delta E(\text{gas})\text{-}E(\text{solid})$ telescope. The angles of incidence and exit were 75° relative to the sample normal.

The ΔE - E spectrum evidenced H, B, C, N, O, F, Na, Al and Si (Fig. 1). The elements' total energy spectra were analyzed with our program SURFAN [2], showing the relative atomic concentrations H : B : C : N : O : F : Na : Al : Si, to be in the ratios 0.8 : 0.1 : 0.8 : 0.03 : 1.4 : 0.18 : 0.004 : 0.09 : 0.4. Levels of the organic H and C were high, and Si dominated the inorganic elements, followed by F, B and Al. The ratios H/C and B/Al were equal to ~ 1 . Levels of N (organic) and Na (inorganic) were low. Oxygen high level came both from the organic polymer and the inorganic particles.

The ratios between elements were not uniform within the depth of 1-1.5 μm penetrated by the $^{63}\text{Cu}^{10+}$ ion beam, evidencing depth profiles by deviations of the experimental energy spectra with respect to the theoretical calculations for homogenous distributions. Thus H, C, N were increased for a depth of $\sim 0.25\text{-}0.35 \mu\text{m}$, Al and Si decreased for $\sim 0.35\text{-}0.40 \mu\text{m}$, and F decreased for $\sim 0.2 \mu\text{m}$.

This showed the local concentrations near surface to be higher for the organic polymer and lower for the inorganic phase, and the latter to show a faster decrease for F than for Al and Si. The near surface opposite trends of the organic/inorganic phases indi-

cates competition between their filling factors within a depth equal to the mean radius of the inorganic particles, where additional interstitial space becomes available and is filled by the polymer. A mean radius of 0.35 μm specified by the producer [3] supports this view. The more abrupt decrease of F suggest a smaller mean size of the YbF_3 crystals than of the Al,Si-containing particles.

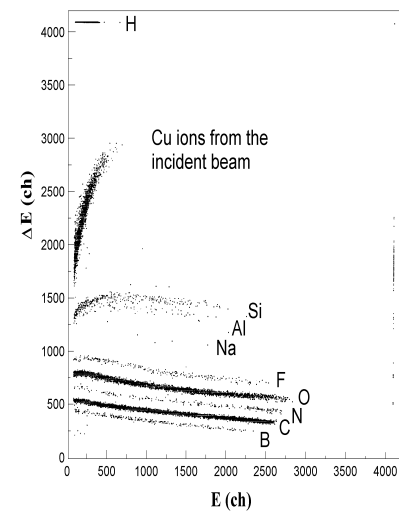


Figure 1: The E - ΔE spectrum of the dental composite analyzed by ERDA.

References

- [1] L.R. Doolittle, Nucl. Instr. and Meth., B **9**, 344 (1985)
- [2] Tetric Ceram product information, Vivadent Ets., Schaan, Lichtenstein (1999)
- [3] F. Negoita, C. Borcan, D. Pantelica, NIPNE Scientific Report, p. 120 (1996)

Experiment on the KVI 14 GHz ECR ion source with a metal-dielectric liner

L. Schächter¹, S. Dobrescu¹, A. G. Drentje², H. Fraiquin², G. Rodrigues³

¹NIPNE-HH, Nuclear Physics Department, Bucharest, Romania

²KVI, Groningen, The Netherlands

³NSC, New Delhi, India

The metal-dielectric (MD) structures with high secondary electron emission properties were developed in Bucharest [1]. First promising tests of these structures in an ECRIS were performed at IKF, Frankfurt, Germany [2]. The purpose of the present experiment made in November 2000 on the 14 GHz ECR ion source at KVI, Groningen, The Netherlands was: (1) to observe the effect of the MD structure on the intensity of high argon charge states, (2) to compare its effect on the ECRIS output beam charge state distribution (CSD) with the well known effect of gas mixing.

The source fed with pure argon, but without liner, was optimized on the Ar^{12+} peak. A stable source operation was obtained at 320 Watt RF power. Contaminants like oxygen, nitrogen and carbon were extremely small, so that the effect of gas mixing was really negligible. Then, natural oxygen was fed as mixing gas into the source, again optimizing on the 12+ peak and using 730 W RF power. The improvements were: stability at higher RF power, a shift of the CSD maximum from 9+ to 11+ and for Ar^{16+} an increase from 0.002 to 0.180 $e\mu\text{A}$.

A cylindrical MD structure ($\text{Al-Al}_2\text{O}_3$) was installed as a liner in the source plasma chamber. After one day of outgassing, the CSD-E presented in Fig. 1 was obtained at 320 W of RF power and optimizing on Ar^{12+} . The intensities of beam charge states 12+ ... 14+ were equal with those obtained in the case of gas mixing while the Ar^{16+} intensity had almost doubled to 0.32 $e\mu\text{A}$. Carefull source optimization gave even a spectrum with 0.38 $e\mu\text{A}$ of Ar^{16+} and 0.015 $e\mu\text{A}$ of Ar^{17+} , while the Ar^{12+} peak was lower.

Some low intensity oxygen peaks were clearly present in the spectra, implying that an effect of gas mixing could exist. After a few days of outgassing, the oxygen peaks had not reduced, so that we made the assumption that some oxygen is escaping from the MD structure. The effect of mixing small amounts of oxygen into an argon plasma (without liner) was studied in two situations: (i) the amount of oxygen was slightly lower than in E; the result is shown in the CSD-L in Fig. 1. (ii) the amount of oxygen was slightly higher, see CSD-M. In both cases the RF power was 320 Watt

and the argon gas feed was adjusted to have the same Ar^{12+} current as in spectrum E. In both situations the argon beam intensities of charge states higher than 12+ were smaller than those obtained in the presence of the MD liner.

The conclusion is that the cylindrical MD structure leads to a significant increase of the high charge state current output of ECRIS. The increase is not due to the introduction of a small amount of oxygen in the plasma but to other physical phenomena. The ECR ion source was remarkably stable in the presence of the MD structure.

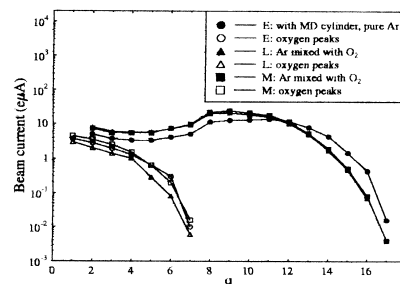


Figure 1: Argon and Oxygen beam CSD's.

The Romanian group acknowledges the Romanian National Agency for Science and Technology for the Grant nr. 6126/2000 that allowed to realize this experiment in collaboration.

References

- [1] L. Schächter, S. Dobrescu and Al. I. Badescu-Singureanu, *Rev. Sci. Instrum.* **69**, 706 (1998)
- [2] L. Schächter, K. E. Stiebing, S. Dobrescu, Al. I. Badescu-Singureanu, L. Schmidt, O. Hohn and S. Runkel, *Rev. Sci. Instrum.* **70**, 1367 (1999)

Cosmic Rays and Nuclear Astrophysics

Simulation studies of the information content of muon arrival time observations of high energy extensive air showers

I. M. Brancus¹, H. Rebel², M. Duma¹, A. F. Badea¹, C. Aiftimie¹, J. Oehlschlaeger²

¹ NIPNE-HH, Department of Nuclear Physics, Bucharest

² Forschungszentrum Karlsruhe, Institut für Kernphysik, Germany

By extensive Monte Carlo calculations, using the air shower simulation code CORSIKA [1], EAS muon arrival time distributions and EAS time profiles up to 320 m distances from the shower centre have been generated, for proton, oxygen and iron induced showers using different hadronic interaction models as Monte Carlo generators. The model dependence and mass discriminating features have been scrutinised for three energies ranges, (1.-1.78) 10^{15} eV, (1.-1.78) 10^{16} eV and (1.78-3.16) 10^{16} eV. The present studies [2] have been focussed to the exploration of the information carried by EAS time observables and their correlations in view of features discriminating the mass of the cosmic primary and different hadronic interaction models. Advanced non-parametrical statistical methods based on Bayesian decision rules have been applied to scrutinise the EAS observables [3] and to specify quantitatively the results. A first inspection allows some tentative conclusions:

1. The correlations of the local muon arrival time variables with the local muon density improves the true classification rate and discrimination features. It turns out that the correlation can be replaced by a single parameter: $\Delta\tau_q/\rho_\mu$. The classification gets improved by the correlating the muon arrival times with the shower age, the shower size N_e and N_μ^{tr} , see Fig.1.
2. Correlating the observation of $\Delta\tau_q/\rho_\mu$ for two radial distances, the mass discrimination of the primaries get only slightly improved, different from our previous result [4] analysing the (global) arrival times of the foremost muon correlated at two different radial distances.
3. Comparing the classification rates for different muon arrival time quantities: the first quartile, the median and the third quartile, by both considered models QGSJET and VENUS similar results have been obtained. The analysis of the median $\Delta\tau_{0.50}$ and of the slow component of the arrival time distribution, represented by $\Delta\tau_{0.75}$, improves the true-classification rate of the oxygen component.

From the present results an enhancement of the discriminative features may be expected at larger distances from the shower core (>150 m) and to higher primary energies ($>10^{16}$ eV). This finding is of actual interest in view of the KASCADE collaboration to extend the detector array to a larger area, KASCADE GRANDE.

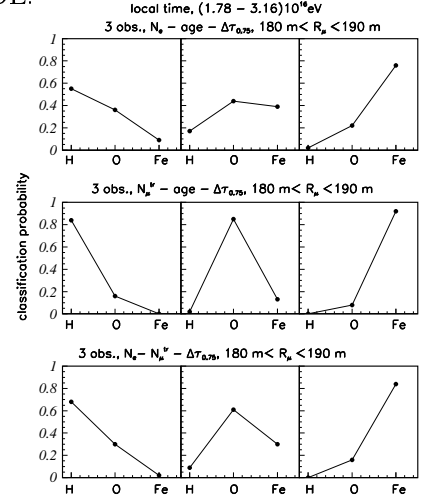


Figure 1: The classification and misclassification probabilities correlating the observation of muon arrival times with N_e , N_μ^{tr} and the shower age.

References

- [1] P. Capdevielle et al: KfK-Report 4998, Forschungszentrum Karlsruhe (1992); D.Heck et al: FZKA-Report 6019, Forschungszentrum Karlsruhe (1998);
- [2] I.M.Brancus: Interner Bericht KASCADE-09/2000-02, 51.02.03, sept.2000;
- [3] A.A.Chilingarian: ANI Reference Manual,(1999); A. A. Chilingarian: Comp. Phys. Comm. 54 (1989);
- [4] I.M.Brancus, B.Vulpescu, H.Rebel, M.Duma, A.A.Chilingarian: Astropart. Phys.7 (1997) 343;

The modification and the installation of WILLI detector as a rotatable device

I. M. Brancus¹, J. Wentz², B. Vulpesu¹, H. Rebel², A. F. Badea¹, A. Bercuci², H. Bozdog¹, M. Duma¹,
H. J. Mathes², M. Petcu¹, C. Aiftimiei¹, B. Mitrica¹

¹ NIPNE-HH, Department of Nuclear Physics, Bucharest

² Forschungszentrum Karlsruhe, Institut für Kernphysik, Germany

The compact WILLI device, built in IFIN-HH Bucharest (44026'N latitude and 26004'E longitude) at a vertical cut-off rigidity of 5.6 GV, has been used for measurements of the charge ratio in the vertical atmospheric flux at momenta below 1 GeV/c [1]. In this low energy range the studies of muon charge ratio provide information useful for the discussion of the so-called atmospheric neutrino anomaly and for studies of atmospheric neutrino and antineutrino fluxes [2]. The experimental method is based on the observation of the reduced effective lifetime of the negative muons, stopped in matter, as compared to the lifetime of positive muons. Avoiding the difficulties and the systematic errors of magnetic spectrometers, results are obtained with high accuracy [3], indicating a decrease of the muon charge ratio from 1.30 (at 0.87 GeV/c) to 1.15 (at 0.24 GeV/c).

Super-Kamiokande [4] and other experiments find that the ratio of muonic to electronic neutrinos is much smaller than the theoretical production, the effect depending on the incidence angle of the neutrinos. The interpretation of such so-called "neutrino anomaly" in terms of neutrino oscillations is based on theoretical predictions of the fluxes of the neutrinos of different flavour, based on different hadronic interaction models. A possibility to verify such models is to compare the theoretical predictions for muon flux, which plays a key role in neutrinos chain, with the experimental data [2]. Thus, the ratio of the flux of positive to negative muons could provide a sensitive test for models regarding muon and neutrino production.

The WILLI detector is a suitable instrument for further investigation of the modulation of muon charge ratio and the neutrino fluxes by the geomagnetic cut-off. The details about the geomagnetic influence have not been explored using the observation of muons with

different angles of incidence in zenithal and azimuthal plane. The WILLI detector is now modified in a rotatable set-up, see Fig.1, which will allow precise measurements of the East-West effect, caused by the anisotropy of the primary proton flux and the local magnetic field, deflecting the trajectory of charged particles in the atmosphere. With such perspective a systematic "muon charge ratio spectroscopy" may provide interesting geophysical observation.

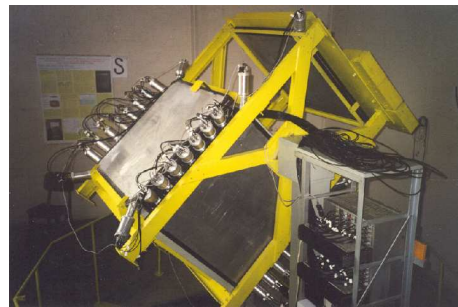


Figure 1: The WILLI detector transforms in a rotatable device

References

- [1] B.Vulpescu et al: Nucl.Instr.and Meth. in Phys.Res. A414 (1998);
- [2] J.Wentz et al: J.Phys.G.Nucl.Part.Phys, in print;
- [3] Y.Fukuda et al: Phys.Lett.B433 (1998)9; Phys.Rev.Lett 81 (1988) 1562;
- [4] B. Vulpescu et al: J.Phys.G.Nucl.Part.Phys, in print

A new experiment on $^{12}\text{C}(\alpha, \gamma)^{16}\text{O}$ reaction for astrophysics

C. Grama¹, M. Assunção², A. Coc², F. Hannachi², J. Kiener², A. Korichi², D. LeDu², A. Lopez-Martens², A. Lefebvre², R. Meunier², C. Pelissier², V. Tatischeff², J.P. Thibaud², J.W. Hammer³, M. Fey³, R. Kunz³, D. Malcherek³, C. Beck⁴, S. Courtin⁴, F. Haas⁴, N. Rowley⁴, M. Rousseau⁴, S. Szilner⁴, S. Harissopulos⁵, E. Galanopoulos⁵, G. Kriembardis⁵, T. Paradellis⁵, G. Staudt⁶, J. Weil⁷, F. Fleurot⁸

¹ IFIN-HH

² CSNSM, IN2P3-CNRS et Université de Paris Sud, Orsay, France

³ Institut für Strahlenphysik, Universität Stuttgart, Germany

⁴ IRes, IN2P3-CNRS et Université Louis Pasteur, Strasbourg, France

⁵ Institute of Nuclear Physics, N.C.S.R. "Demokritos", Athens, Greece

⁶ Physikalisches Institut, Universität Tuebingen

⁷ University of Kentucky, Lexington, USA

⁸ KVI, University of Groningen, Holland

The $^{12}\text{C}(\alpha, \gamma)^{16}\text{O}$ reaction is one of the key reactions in stellar evolution, as its reaction rate determines the abundance ratio of ^{12}C and ^{16}O after the helium burning, and therefore the abundances of heavier elements up to Fe. Due to the extremely low cross section (estimated to 0.01 fb at the Gamow window for central He combustion) the direct measurements at astrophysically relevant energies are impossible and an extrapolation from higher energies is necessary. This extrapolation is particularly complicated due to the superposition of E1 and E2 captures and to the presence of two levels 1^- and 2^+ just below the $^{12}\text{C}+\alpha$ threshold that interfere with a higher energy 1^- resonance and with the direct capture contribution. One of the best methods to separate the E1 and E2 contributions is to measure the γ -ray angular distributions in a wide energy range. In the present experiment the γ -ray angular distributions have been measured in the range $E_{cm}=1.39 - 2.80$ MeV of the excitation function by using a 4π setup with nine EUROAM HPGe detectors, each equipped with an active BGO shielding, in a close geometry, as described in [1]. The IFS DYNAMITRON accelerator was used to provide a high intensity alpha beam. The detector efficiencies have been measured using standard calibrated γ sources and the $^{27}\text{Al}(p, \gamma)$ resonance at $E_p=992$ keV. The isotopically ^{12}C enriched targets used in this experiment have been obtained by different implantation techniques with various thickness and depth profile

of the carbon layer. The ^{13}C content of each target has been determined using the well known $^{13}\text{C}(p, \gamma)$ resonance at $E_p=1748$ keV. The ^{12}C profile and the homogeneity of the targets have been analysed by using RBS technics with a 1.2 MeV incident α beam at the ARAMIS Orsay accelerator. In the energy range $E_{cm}=1.39 - 2.80$ MeV 28 angular distributions have been taken - each with eight or nine points at once - using target currents between 100 and 340 μA . Particularly the region around the 2^+ resonance at $E_{cm}=2.69$ MeV has been covered with smaller energy steps in order to analyse the interference effects with the sub-threshold 2^+ resonance. The angular distributions have been fitted in order to extract the cross sections σ_{E1} and σ_{E2} , as well as the relative phase ϕ , that will be used in the R-matrix fits and extrapolation to lower energies.

References

- [1] A. Lefebvre, J. Kiener, V. Tatischeff, A. Coc, C. Grama, F. Hammache, F. Hannachi, A. Korichi, A. Lopez-Martens, J.P. Thibaud, J.W. Hammer, M. Fey, R. Kunz, D. Malcherek, F. Haas, C. Beck, S. Courtin, M. Rousseau, N. Rowley, S. Szilner, E. Galanopoulos, S. Harissopoulos, G. Kriembardis, T. Paradellis, G. Staudt, J. Weil, F. Fleurot, IFS Annual Report 1999, p.38

Inertial Fusion, Physics of Neutrons and Nuclear Transmutations

Neutron spectrometry on low-concentrated zirconium hydride

A. Radulescu¹, R.E. Lechner², I. Padureanu¹, C. Postolache³

¹ NIPNE-HH, Departament of Nuclear Physics, Bucharest

² Hahn-Meitner-Institut, BENSC, Berlin

³ NIPNE-HH, Radioisotope Production Center, Bucharest

Vibrational modes in $ZrH_{0.1}$ were studied by neutron spectroscopy at room temperature (where α -Zr and γ -hydride were present) and around 528K, the FCO γ -phase to FCC δ -phase conversion temperature given by the literature. The inelastic neutron scattering measurements were performed by using the NEAT spectrometer set-up at BER II reactor of BENSC [1]. The analysis of optical modes in terms of H vibrations specific to different crystallographic phases shown by Zr-H system agrees with recent neutron diffraction [2] and specific heat [3] measurements and indicates in fact a lower temperature for this phase transition.

Using different experimental resolutions (0.175, 0.057 and 0.011 meV) the inelastic scattering was well-separated by the quasielastic one. Additional low-frequency modes (Fig.1) were revealed around 5 meV by spectra measured at all temperatures. Due to the complex structure of the sample the exactly nature of these modes is difficult to be stated. However, two possible explanation could be taken into account, with the mention that for a better understanding of the mechanism leading to such a low-lying frequencies further studies are still necessary:

a) A similar phenomenon like the Kohn anomaly shown by some of metal lattices. The Kohn anomaly occurs for a lattice phonon q vector that coincides with the k vector for electrons at the Fermi Surface and clearly evidences a strong electron-phonon interaction; adding hydrogen to the lattice it will change the Fermi Surface diameter by adding electrons. The low energy peak revealed by experimental spectra around 5 meV is not present in the case of pure Zr [4, 5] so, it can be assumed that it is due to the presence of H.

b) Strong overdamped phonons characteristic of resonant vibrations. The introduction of an interstitial atom into an ideal lattice disturbs the ideal coupling in the neighbourhood of the defect. The nearest neighbouring host atoms will be coupled to each other by a longitudinal spring only, whereas the interstitial will be coupled to every surrounding host atom by both a longitudinal and a transversal spring. From the simple

definition of a resonant mode frequency

$$\omega_{res}^2 = \frac{F_{eff}}{M_{eff}} \quad (1)$$

where F_{eff} and M_{eff} are the effective mass and effective force constant, respectively, of the cluster oscillator (interstitial plus surrounding nearest neighbours), it is apparent that apart from a heavy defect mass, also a weakening of the effective force constant can lead to resonant modes.

The analysis of experimental results in terms of mechanisms above presented is in progress.

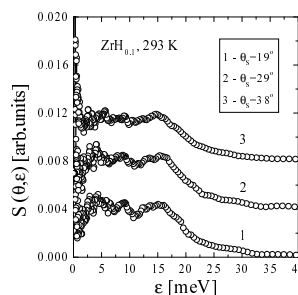


Figure 1: The dynamic structure factor of $ZrH_{0.1}$ in the range of acoustic vibrations

References

- [1] R.E. Lechner, *Physica B* **180-181**, 973 (1992)
- [2] W.M. Small et al., *J. Nucl. Matter.* **256**, 102 (1998)
- [3] I.O. Bashkin et al., *Z. Phys. Chem.* **179**, 289 (1993)
- [4] C. Stassis et al., *Phys. Rev. B* **18**, 2632 (1978)
- [5] A. Radulescu, I. Padureanu, S.N. Rapeanu and A. Beldiman, *Phys. Status Solidi b* **217**, 777 (2000)

Microscopic mechanisms in the liquid-glass transition of glycerol

I. Pădureanu¹, D. Aranghel¹, M. Ion¹, R. Lechner², A. Desmedt², J. Pieper²

¹ NIPNE-HH, Department of Nuclear Physics, Bucharest

² Hahn-Meitner-Institut, Neutron Scattering Center, Berlin

In this report we present the temperature dependence investigation of the dynamic function $S(Q, h\nu)$ of glycerol in its liquid and glassy states. Neutron scattering experiment has been carried out at the time of flight spectrometer NEAT, using cold neutrons of $\lambda=5.1$ Å, corresponding to an energy of 3.145 meV and a resolution of 98 μeV (FWHM of the elastic line of the vanadium sample). The inelastic neutron scattering spectra (INS), were measured at 6 temperatures between 50-400 K in the kinematic space with the wave vector transfer Q range $Q=0.33-2.31$ Å⁻¹ and a energy transfer $h\nu = 0 - 21.74$ meV (Fig.1).

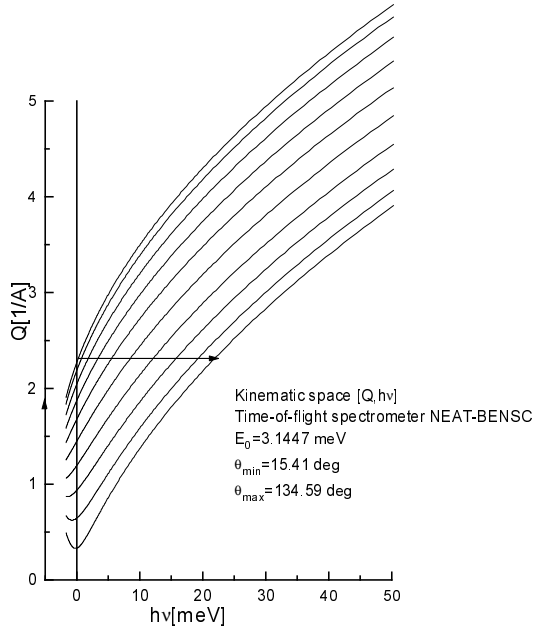


Fig. 1. Kinematic region covered in the experiment

Figure 1: Kinematic region covered in the experiment

The topic presented here concerns the temperature dependence of the low energy features in glycerol under various states: liquid, supercooled and glassy. For a correct interpretation of the results regarding the existence of the peaks at finite energies, a time of flight data have to be put on a $h\nu=\text{constant}$ and $Q=\text{constant}$ scale. Following this procedure, the dynamic function $S(Q, h\nu)$ for a constant $Q=2.20$ Å⁻¹ as a function of energy is presented in Fig.2 at 3 temperatures.

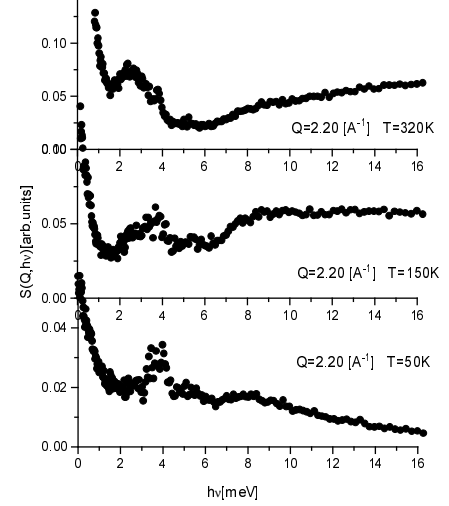


Figure 2: Dynamic scattering function for glycerol at constant $Q=2.2$ Å⁻¹

The main conclusions derived from these preliminary results can be summarised as follows:

1. A well-resolved peak located at the low but finite energy as $h\nu=2.4-4.0$ meV is observed for all investigated temperatures in the Q range between $Q=1.6-2.28$ Å⁻¹;
2. A such as feature has been also observed in other condensed matter systems investigation earlier by us, such as liquid Ga [1], Zr-H [2], superionics [3];
3. The position of this feature is continuously decreasing as a function of temperature from about 4 meV at 50K to 2.4 meV at 400K.

References

- [1] I.Pădureanu, A.Rădulescu, A.Beldiman, M.Ion, A.G.Novikov, V.V.Savostin, Zh.A.Kozlov, Physica B 276,459 (2000);
- [2] A.Rădulescu, I.Pădureanu, A.Beldiman, Zh.Kozlov, V.A.Semenov, Physica B 276,841 (2000);
- [3] A.Rădulescu, I.Pădureanu, A.Beldiman, M.Ion, Zh.A.Kozlov, Phys.Rev.B,59,3270 (1999).

On the dynamics and site occupation of D atoms in δ and ε Zr-deuterides

A. Rădulescu¹, I. Pădureanu¹, S. Râpeanu¹, Zh.A. Kozlov², V.A. Semenov³

¹NIPNE-HH, Department of Nuclear Physics

²JINR Dubna, FLNP Laboratory

³IPPE-Obninsk, Neutron Scattering Laboratory

The vibrational frequencies of D in δ and ε Zr deuterides have been measured by inelastic neutron scattering. From the experimental data analyzed in terms of the generalized vibrational density of states new information on the H(D) potential in Zr have been obtained. Performing an accurate analysis of the high energy range of scattering spectra the distribution of D atoms on the available interstitial sites in FCC and FCT Zr lattices has been studied. Recent results obtained by INS [1, 2] revealed that H behaviour in Zr-H system is still far from a complete knowledge. In this paper we continue a study started few years ago reporting new results obtained by INS investigation of the vibrational properties of D in two Zr lattices (FCC and FCT) at room temperature. The samples contain one-phase δ and ε deuterides of Zr. These results are related to the investigation of the energy range higher than that characteristic to the host lattice vibrations. An accurate analysis of the latter at the transition from pure α -Zr to the hydride(deuteride) phases has been reported in a previous paper [3]. Inelastic neutron scattering measurements of the vibrational fre-

quencies of D in δ and ε Zr deuterides clearly reveal the anharmonicity of H(D) potential in FCC and FCT Zr lattices, thus improving our understanding of the H(D) dynamics in a metal-hydrogen system with a rich phase diagram as the Zr-H system is. Additional information on the D distribution in Zr lattices has been obtained. For a clear explanation of some of them further investigations are still necessary.

References

- [1] A. Rădulescu, S. N. Râpeanu, I. Pădureanu, A. Beldiman, *Balkan Phys.Lett. (Suppl.)* 5, 334 (1997).
- [2] A. Rădulescu, I. Pădureanu, A. Beldiman, S. N. Râpeanu, Zh. A. Kozlov, V. A. Semenov, *Physica B* 276-278, 841 (2000).
- [3] A. Rădulescu, I. Pădureanu, S. N. Râpeanu, A. Beldiman, *Phys. Stat. Sol. (b)* 217, 777 (2000).

Elastic recoil detection analysis with improved resolution

H. Petrascu¹, A. Isbasescu¹, F. Negoita¹, D. Pantelica¹, M. Petrascu¹, N. Scantei¹, A. Tudorica¹

¹ HH-NIPNE, Dept. of Nucl. Phys., Bucharest, Romania

Tests for improving the resolution, by coupling directly the preamplifier to the anode of the $(\Delta E, E)$ ionization chamber used in the ERDA measurements, were performed. The achieved preamplifier consists of integrated circuits with very few external components. In Fig.1 the preamplifier scheme is presented. The essential part of this scheme is the CSAM integrated circuit. It has large amplification (5000) and very low noise. It proved to be very stable. It could be operated in high vacuum without presenting a notable heating. The $(\Delta E, E)$ ionization chamber was of the type used for the first time in ERDA measurements [1]. The entrance window of the chamber was made of mylar, $2 \mu\text{m}$ thickness. It was operated by using a mixture of 90% Argon + 10% Methan at pressures between 100 and 200 mbarr. The measurements in the new arrangement in which the preamplifier was directly coupled to the anode of the chamber were done with an ^{233}U α source and with a heavy ion beam. The measurements with the α source have shown that the resolution of the ionization chamber was improved by 25 % comparing with the best results obtained by using an external preamplifier. This was confirmed by the identification map shown in Fig.2, obtained with ^{63}Cu beam on a glass probe.

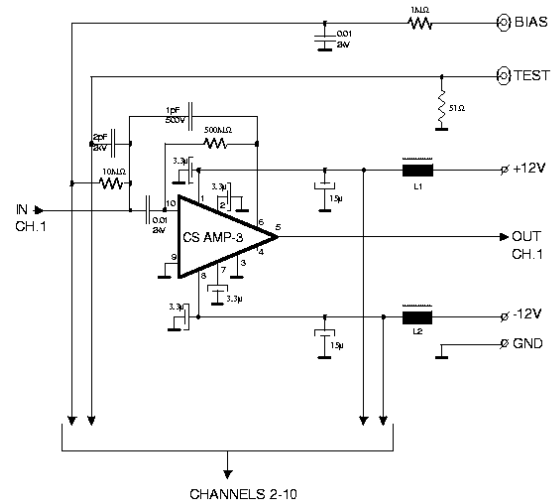


Figure 1:

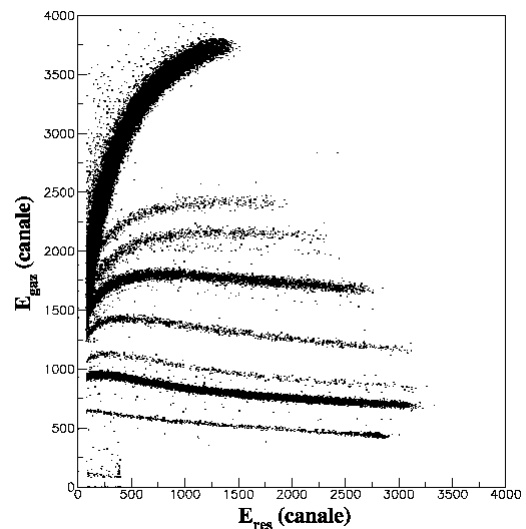


Figure 2:

References

- [1] M.Petrascu *et al*, *NIM B4* 396 (1984)

Neutron pair pre-emission in the fusion of ^{11}Li halo nuclei with light targets

M. Petrascu¹, I. Tanihata², T. Kobayashi³, M. Giurgiu², K. Morimoto², K. Katori², I. Cruceru¹, A. Isbacescu¹, H. Petrascu¹, R. Ruscu¹, M. Chiba², Y. Nishi², S. Nishimura², A. Ozawa², T. Suda², K. Yoshida², A. Constantinescu⁴, C. Bordeanu⁵, A. Tudorica⁶

¹ HH-NIPNE, Bucharest, Romania

² RIKEN, Wako-shi, Saitama, Japan

³ Tohoku University, Japan

⁴ Bucharest University, Romania

⁵ Weizmann Institute, Rehovot, Israel

⁶ SUNY at Stony Brook, Chemistry Dept., NY-11774, USA

The pre-emission of neutron pairs in the fusion of ^{11}Li halo nuclei with Si targets was first mentioned in ref. [1, 2]. However the statistics of n-n coincidences was rather low due to the fact that the detection system was not optimal for such measurements. Here, we report results of a recent experiment performed using of a new array detector, revealing a notable n-n coincidence effect. After subtraction of the cross-talk background, a number of about 300 n-n coincidences remained within the range of the narrow neutron group. The measurement with the array detector allowed a new determination with increased resolution of the transverse momentum distribution for the neutrons within the narrow group. The best fit of the experimental data was obtained by including a background term in the Gauss function. In this case the transverse momentum p_{\perp} expressed by σ of the distribution is $p_{\perp} \cong 6 \pm 1.2$ MeV/c. About 2 times larger value of σ was obtained by forcing the fit without a background term. The n-n coincidence data processed by considering a background on which the narrow neutron group is superposed allowed to obtain P_{nn} , the percentage for the neutron pair pre-emission, with the value $P_{nn} = (72 \pm 10)\%$. Without subtraction of this background P_{nn} turns out to be $P_{nn} = (22 \pm 3)\%$.

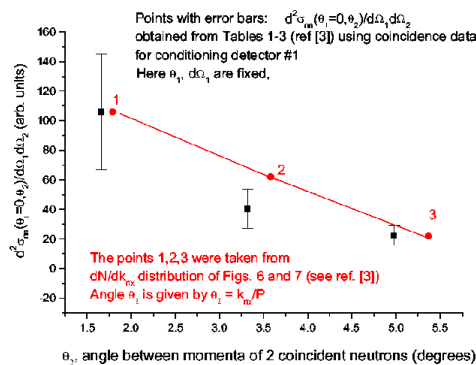


Figure 1:

From the coincidence results, also the differential

$d^2\sigma_{nn}(\theta_1, \theta_2)/d\Omega_1 d\Omega_2$ cross-section, for 2 neutron pre-emission was obtained. It was found that the $d^2\sigma_{nn}(\theta_1, \theta_2)/d\Omega_1 d\Omega_2$ values are close to the slope characterizing the neutron transverse momentum distribution (Fig1). In contrast to the n-n coincidence data, the cross-talk data processed in same manner for getting the cross-sections, are totally in disagreement with the slope of the neutron transverse momentum distribution (Fig2) (see ref. [3]). It was also observed a change in the slope of n-n coincidence data, by interchanging det #1 with det #2,4,6,8 and #3,5,7,9. This may be an indication for n-n correlation. It is estimated that a 2-3 times larger n-n coincidence effect may be expected in the case of $^{11}\text{Li} + \text{C}$ detector-target fusion interaction. The present approach may be of interest also for the borromean ^6He nucleus investigation.

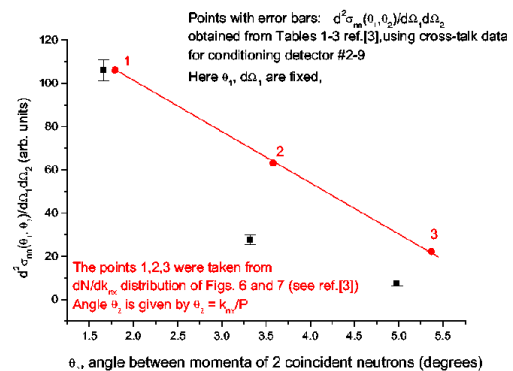


Figure 2:

References

- [1] M.Petrascu *et al*, *Phys.Lett.* **B405**, 224 (1997).
- [2] M.Petrascu *et al*, *Rom.J.Phys.* **43**, 307 (1998).
- [3] M.Petrascu *et al*, *RIKEN Rep.* AF - NP 395, April 2001.

Nuclear Instruments and Methods

PIXE (particle induced X-ray emission) and ICP (inductive coupled plasma) in microelemental study of vegetal-biological samples

C. Stihl², I. V. Popescu¹, G. Busuioc², T. Badica¹, A. Olariu¹, G. Dima², M. Petre¹, E. D. Jianu³

¹National Institute of Physics and Nuclear Engineering, Bucharest, Magurele

²Valahia University of Targoviste

³S. C. TAROM S. A., Bucharest

A fundamental aspect in agriculture and in plant growing is the relationship between plant nutrient concentration and growth conditions: light, temperature, water supply and fertilisers supply. The different fertilisers are different chemical compounds and they act in different ways in nutrient concentration of plants. A plant cultivated as a vegetable in tropical areas, which

have curative purposes - gastric dressing, in hepatic tumour and ganglion tumour treatment is the Basella Alba L. plant. Six leaves groups of this plant grown in different conditions at the Variety Testing Center (VTC) in Targoviste (Table 1) were analysed by using PIXE and ICP methods. We identified and determined the concentration of P, S, Cl, K, Ca, Mg, Fe, Cu, Zn and Sr. Using a

Sample	Growth conditions
B1 (VTC) - July	Soil without fertiliser
B2 (VTC) - July	Natural fertiliser(a)
B3 (VTC) - July	NKP fertiliser(b)
B4 (VTC) - August	Soil without fertiliser
B5 (VTC) - August	Natural fertiliser
B6 (VTC) - August	NKP fertiliser
C(c)	Green house soil without fertiliser

Table 1: (a) Sheep excrements, (b) Nitrogen- phosphorus-potassium fertiliser in 14/11/26 ratio, (c) Control group

A natural fertiliser the Mg concentration increased in the plants and also the Cl concentration became higher. Using the NKP fertiliser the P and K concentrations increased but the Mg and Fe concentrations decreased in plant. The other elements did not show

much change. Using NKP fertiliser we have observed an increase of the Sr concentration. This increase cannot be due to the chemical components of NKP fertiliser, but it might be possible that the NKP fertiliser rises the affinity of Basella Alba L. plant for environmental Sr.

ERDA characterization of AlN thin films deposited by reactive pulsed laser deposition

D. Pantelica⁴, F. Negoita⁴, A. Tudorica³, M. Petrascu⁴, Eniko Gyorgy², Carmen Ristoscu², I.N. Mihailescu², Argyro Klini⁴, N. Vainos⁴, C. Fotakis⁴

¹ IFIN-HH

² Institute for Laser, Plasma and Radiation Physics, Bucharest-Magurele

³ SUNY at Stony Brook, Chemistry Dept., NY-11774, USA

⁴ Foundation for Research and Technology -Hellas, Institute of Electronis Structure and Laser, P.O. Box 1527, Heraklion 711 10, Crete, Greece

The growth of metal-nitride thin films is of interest because of their important applications: AlN films are promising materials for microelectronics and optoelectronics devices.

Several methodes have been used to grow and deposit AlN thin films. In the present work the AlN thin films were deposited on Si wafers using reactive pulsed laser deposition from Al targets in nitrogen and from AlN target in vacuum and low presure nitrogen. Two UV excimer laser sources were used: a ns system and, for the first time, a sub ps system. ERD analysis with ions has been systematically applied to determine the influence on the composition of the main deposition parameters: laser pulse duration, fluence and gas presure. The ERDA measurements were caried out at 8.5 MV Tandem accelerator of IFIN-HH using a ⁶³Cu beam at 80 MeV. The detector consisted in a compact $\Delta E(\text{gas})-E(\text{solid})$ telescope [1], placed at 30° with respect to the beam. For the calibration of the telescope, the response of the passivated, ion implanted Si detector to different ions between H and Cu was measured. The quantitative analysis of ERDA spectre has been performed using our computer code SURFAN [2]. A typical $\Delta E-E_r$ spectrum in shown in Figure 1. Besides N and Al, in the film are also present: H, C and O. The energy spectra for all these components are shown in Figure 1 and compared with the simulated spectra.

Our analysis showed that the samples deposited using Al target consisted of AL only, with samll traces of AlN. The samples prepared using AlN target are stoichiometric. However, films deposited using the ns laser source contain a detectable amount of Al.

References

- [1] Petrascu et al., Nucl. Instrum. Meth. 84(1984)396.

- [2] F. Negoita, Cristina Borcan, D. Pantelica, NIPNE Scientific Report 1996, P.120.

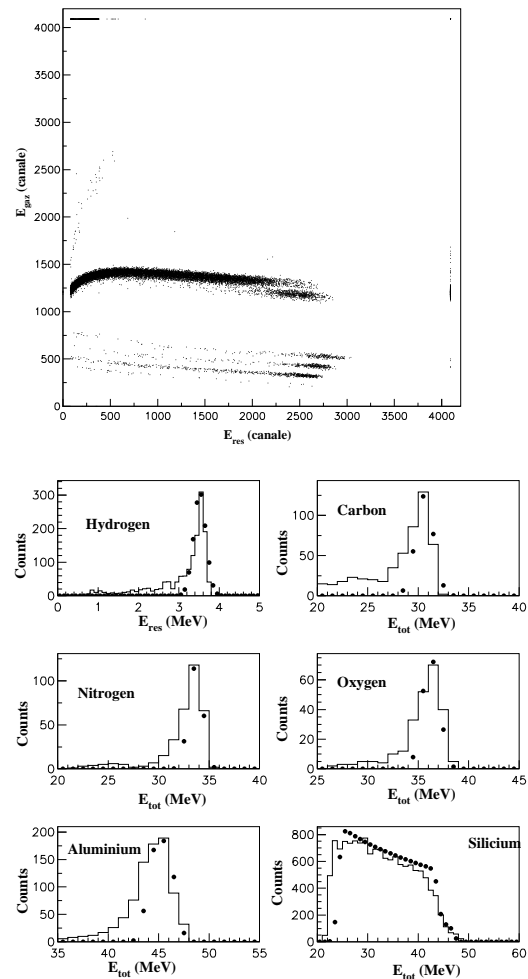


Figure 1: A typical $\Delta E-E$ spectrum and the energy spectra for H, C, N, O, Al and Si (histogram) together with the corresponding simulated spectra.

ERDA characterization of semi-insulating oxygen doped GaAs

M.F. Lazarescu¹, D. Pantelică², A.S. Manea¹, R.V. Ghita¹, F. Negoita²

¹ National Institute for Materials Physics, Bucharest-Magurele

² IFIN-HH

The role of oxygen in GaAs is the subject of many studies in part due to the possibility that doping process with oxygen caused GaAs to become semi-insulating [1].

Optical quality, oxygen doped GaAs grown by liquid encapsulation Czochralski method till about 2 inches diameter was produced to be used as a substrate for infrared CO₂ lasers at 10.6 μm devoted to industrial applications. In this contribution we report result obtained using ERDA technique for characterization of GaAs:O single cristal samples.

The GaAs single crystals were grown in the National Institute for Material Physics by two different procedures, namely horizontal Bridgman and liquid encapsulation Czochralski.

The GaAs synthesis by liquid encapsulation Czochralski was performed in a single working cycle using a Malvern MSR-6 pulling machine. High purity (minimum 99.9999%) gallium and arsenic were used as raw materials. The two components were encapsulated in conventional quartz crucibles of 75 mm diameter with different amounts of Ga₂O₃ (99.999%). The Ga₂O₃/GaAs mass ratio was varied between 0.001 and 0.002. The presence of amounts of Ga₂O₃ during the crystal growth leads to an oxygen doped GaAs with higher semi-insulating properties.

The ERDA measurements were carried out at the 8.5 MV Tandem accelerator of IFIN-HH using ⁶³Cu¹⁰⁺ beam at 80 MeV. The detector consisted in a compact ΔE(gas)–E(solid) telescope [2], placed at 30° with respect to the beam. The total energy spectra were analysed using our code SURFAN [3]. A ΔE–E_{res} spectrum of GaAs:O sample is presented in Figure 1. Besides C and O, the ⁶³Cu scattered by Ga and As (as well as Ga and As recoils) can be seen. The C represents a contamination. A hydrogen contamination is also present in the sample, but not in the bidimensional spectrum in figure 1, because the energy loss of hydrogen recoils in gas is less than the threshold of the analog-to-digital convertor. For hydrogen, only

E_{res} the signal is detected.

The doping oxygen has a rather uniform depth distribution with a mean Ga₁As₁O_{0.02}C_{0.1}H_{0.1} stoichiometry. The results of ERDA measurements are in good agreement with the results of Hall measurements, indicating a high value of the resistivity as a consequence of the semi-insulating character of the material.

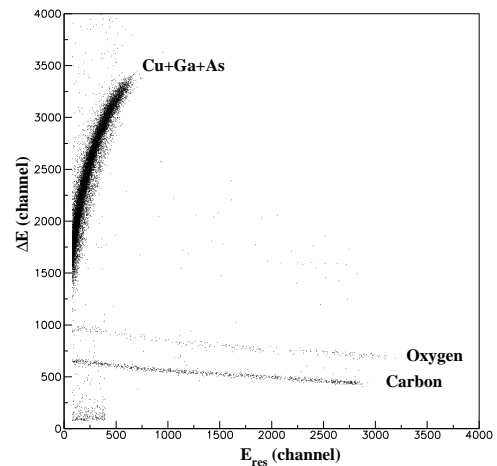


Figure 1: ΔE–E spectrum of a doped GaAs sample.

References

- [1] S.T. Neild and M. Skowrowski, Appl. Phys. Lett. 58(1991)859.
- [2] Petrascu et al., Nucl. Instrum. Meth. 84(1984)396.
- [3] F. Negoita, Cristina Borcan, D. Pantelica, NIPNE Scientific Report 1996, P.120.

Air alpha monitoring device and system for the calibration of the track detectors

A. Danis¹, M. Oncescu¹, M. Ciubotariu¹

¹ NIPNE-HH, Nuclear Engineering and Vacuum Department

The radon measurement plays a critical role:

- in the monitoring human health and safety, due to radon destructive health effects. Sustained exposures of humans to high concentration of radon, in fact to high concentrations of its decay products, can produce lung cancer;
- in a variety of geophysical, geochemical, hydrological and atmosphere purposes, such as exploring resources of uranium or hydrocarbons. The transport of radon within the earth, waters and atmosphere makes it a useful tracer in these purposes.

In both cases, the reliable long-term measurements are required because usual short-term variations in concentration need to be averaged. These variations are caused by factors such as relative humidity, temperature, atmospheric pressure and their seasonal variations, moisture content in the air, or ventilation in the dwelling or working places. The integrating measurement methods meet these requirements. Among them, the alpha track method is one of the adequate and useful method and it is used by authors in radon measurements in dwelling and working places including mines and house cellars.

CR-39 detector, that proved to be the best etched track alpha detector for radon measurements due to: its sensitivity to alpha particles emitted by radon/its decay products, its stability against various environmental factors and its high degree of optical clarity, was used in a proper device for alpha monitoring in air [1]. Its calibration for radon measurements was performed in the proper calibration system [2]. The general descriptions and specifications are given in detail at references. Only some characteristics of these devices are given here.

For *air alpha monitoring device*: i) equipped with filter, during alpha exposure, the alpha particles of *radon* are registered in the etched track detector mounted inside (ρ_{Rn} - track density); ii) without filter, the alpha particles emitted by *radon + its alpha decay products/their aerosols* are registered in the detector (ρ_{tot} - track density). After the etching of the detectors and study of the tracks, using these two track densities, it is possible to determine :

- the activity concentrations of the radon in air;
- the equilibrium factor for radon and its decay products in air, using the ratio ρ_{tot}/ρ_{Rn} and the

Planinic and Faj equation, for the case when the values of the ratio are $1 < \rho_{tot}/\rho_{Rn} < 3$, where ρ_{tot} is the track density in the detector mounted in the device without the filter and ρ_{Rn} is the track density in the detector mounted in the device with filter.

The system for the calibration of the track detectors and charcoal detectors used in radon measurements assures:

- a constant volume concentration of radon activity, by a continuous generation of the radon, at constant rate. The radon is generated by a calibrated ²²⁶Ra source of (236 ± 19) kBq activity, which is in radioactive equilibrium with all its decay products;
- the radioprotection against the alpha particles of radon and its decay products, the system being an airtight one. For gamma and beta radiations, the radioprotection is assured by the 5 cm Pb shielding of the source flat bottom flask;
- for radon measurements, for the specified etching conditions, the calibration constant is expressed in [tracks cm⁻²/kBq m⁻³ h].

Both the air alpha monitoring device and the system for track detector calibration will be used by authors for the radon monitoring in dwelling and working places. For this, we try at present to meet all the requirements for Testing and Approval of Processing Laboratories in conformity with International Radon Metrology Programme.

References

- [1] A. Danis, M. Ciubotariu, I. Mocsy, V. Tomulescu, N.D. Murariu-Magureanu. On the diffusion and deposition in air of the gaseous and solid alpha radionuclides genetically related. (under press *Sci. Techn. for Environ. Protection*, 2001).
- [2] A. Danis, M. Oncescu, M. Ciubotariu. System for calibration of track detectors used in gaseous and solid alpha radionuclides monitoring. (accepted to be published in *Radiat. Meas.*, 2001).

Ge(HP) detectors repair

D. Dorcioman¹, Al. Negreț¹

¹ NIPNE-HH, Department of Nuclear Physics, Bucharest, Romania

During in-beam spectroscopy experiments the Ge(HP) detectors are usually exposed to neutron flux. The interaction between neutrons and the germanium crystal leads to the damage of the crystal structure.

The γ -rays interaction with the semiconductor creates a number of electron-hole pairs proportional to the absorbed energy of the incident photon. Electrons

and holes are swept to opposite contacts by the electric fields in the depletion region of the detector element. If the crystal structure is damaged, the electrons and the holes will interact with the flaws and the electric charge will not be entirely collected. As a result, the photopeaks in the spectrum will get tails on the left side and the energy resolution will worsen.

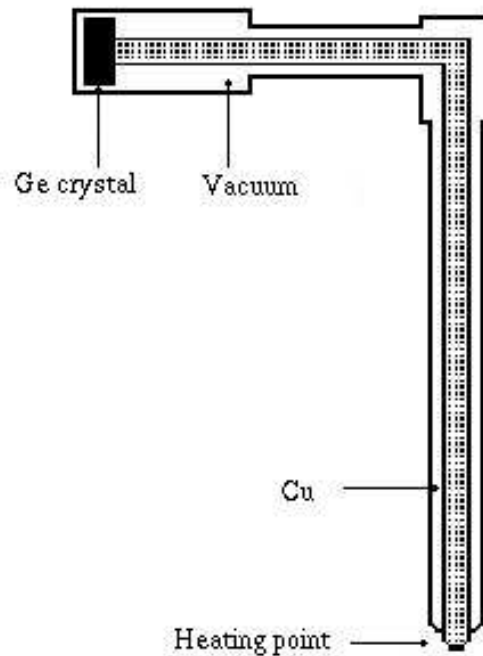


Figure 1: The cryostat of a detector

A neutron-damaged detector can be repaired. It is necessary to repair the crystal structure, i.e. to supply a quantity of energy so that the flaws vanish. If one heats enough the crystal the atoms will get back to their normal position. The procedure requires to keep the crystal a certain time at $\sim 105^\circ\text{C}$, in vacuum conditions. For the available Ge(HP) detectors this can

be done without dismantling the crystal by heating up only the end of the Cu bar (see the figure).

We built a setup that makes possible this procedure. Basically, it contains a vacuum turbomolecular pump and a furnace. The temperature of the crystal is carefully monitored during the heating.

Using this procedure we periodically recover our Ge(HP) detectors.

Preamplifier/shaper for ALICE TRD

M. Ciobanu¹, V. Cătănescu¹, Collaboration ALICE²

¹ NIPNE-HH, Bucharest, Department of Nuclear Physics

² CERN, CH-1211 Geneva 23

The preamplifier/shaper is the first block of the front end electronics, receiving the signals from the detector pads of the Transition Radiation Detector (TRD).

The main requirements of the preamplifier/shaper for the TRD ALICE front end electronics and readout are given in Table 1.

Parameter	Value
Number of channels	1200000
Number of samplings/event	30
Sampling rate	15 – 20 MHz
ADC with	8-10 bits
Max. power consumption/ch.	60-80 mW

Table 1: Preamplifier/shaper requirements

From the Table 1 results that the preamp/shaper must be very fast, with a low power consumption, and the big amount of channels impose a very good reproducibility of specifications at a low price.

The first two models of preamplifier/shaper were built in NIPNE - Bucharest, and the third at GSI-Darmstadt with discrete components in an 8 channel structure. All were tested also in a beam with the detector prototype.

The first one had as main component the current feedback type MAX 4182 operational amplifier.

The preamp/shaper contain the following blocks:

- Input protection - I/U converter - R-C shaper;
- Voltage amplifier - RC shaper;
- Output voltage amplifier;
- DC baseline restorer.

With this model it was processed eight detector pads signals. Having input impedance changing capability it was also useful in finding the optimum input impedance for a good signal/noise ratio and crosstalk determination. The main specifications for 1600 Ohms input impedance:

- Gain 0.7 mV/fC;
- ENC (equivalent noise charge) about 11000 e;
- Crosstalk between adjacent channels 10%.

The second preamplifier/shaper was built also around MAX 4182 operational amplifier, but in a current type configuration. Having a low input impedance, about 160 ohms, it exhibited a low crosstalk for adjacent channels (only 2%). Other specifications: gain 1.3 mV/fC, noise about 7000 e.

The third preamplifier/shaper was a charge-sensitive type. With a gain of 2 mV/fC, CR-RC shaping time and a noise of only 1500 e, it was possible to estimate the rejection ratio between TRs and pions.

Analog-microchip for ALICE TRD

V. Cătănescu¹, M. Ciobanu¹, Collaboration ALICE²

¹ NIPNE-HH, Bucharest, Department of Nuclear Physics

² CERN, CH-1211 Geneva 23

For the ALICE Transition Radiation Detector (TRD) a first version of an analog chip was implemented and tested. It consists of a number of analog channels, and is the first block of the front end electronics receiving the signals from the detector pads. The current signals of the detector pads are first amplified by a charge-sensitive preamplifier. It is followed by a pole-zero cancellation circuit and a second order shaper-filter assuring a shaped output pulse with about 125ns FWHM. The last functional element of the analog channel chain is the output amplifier. It delivers an output signal accordingly to the ADC requirements concerning driving capability and output levels.

The overall gain of the analog channel is 5.2 mV/fC and the shaping type is CR-(RC)². The output amplifier acts as an external 8-bit 2V range fast ADC (National type NS 08351).

From the point of view of the implementation, in the first version of the TRD analog chip were 21-analog channels, basically the same. The only difference refers to the value of input pad resistance. There are 8 channels with 0 Ohms, 8 channels with 50 Ohms, 2 channels with 200 Ohms and 2 channels 500 Ohms, to estimate the influence of the pad input resistance to overall noise. One additional channel with 50 Ohms input resistance (probe channel) allows monitoring of the signal in each main part of the analog channel, not only to the output.

The first results obtained from the measurements of the analog channels of the chip are very similar with those from simulation. The main results are given in Table 1.

The signals in the probe channel, corresponding to preamplifier, pole-zero circuit, shaper and output amplifier are shown in Fig. 1.

Parameter	Value
Gain	5.2 mV/fC
Shaping time (FWHM)	~125 ns
Shaping Type	CR-(RC) ²
Equivalent input noise	1700 e
Input dynamic range	330 fC
Output pulse level	0.2 – 2 V
Integral nonlinearity	0.8%
Max. power consumption/ch.	7.5 mW

Table 1: Main results of the first version of the analog chip for ALICE TRD

The first version of the analog chip for ALICE TRD was built and tested. The results are in concordance with initial requirements. Now the chips of this first version are used in the multichip module card (MMC), containing ADCs and a digital chip, which is the whole configuration of the front end electronics.

Very soon will be submitted the 2nd version of the analog chip. For this the shaping type is CR-(RC)⁴, the estimated equivalent of 700 e, the input dynamic range of 165 fC, the gain of about 6.1mV/fC, and the output of differential type.

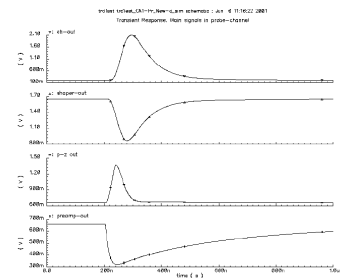


Figure 1: The main signals in the probe analog channel of the chip

Array detector for neutron pre-emission investigations

M. Petrascu¹, I. Tanihata², K. Morimoto², I. Cruceru¹, M. Giurgiu², A. Isbasescu¹, H. Petrascu¹,
R. Ruscu¹, A. Constantinescu³, C. Bordeanu⁴

¹ HH-NIPNE, Bucharest, Romania

² RIKEN, Wako-shi, Saitama, Japan

³ Bucharest University, Romania

⁴ Weizmann Institute, Rehovot, Israel

The array detector built within the cooperation agreement between the Institute of Physics and Nuclear Engineering-Romania and RIKEN-Japan is shown in Picture 1. The design and expected characteristics of this detector are presented in ref. [1]. This detector was recently used in an experiment performed at the RIKEN-RIPS facility for investigation of neutron pair pre-emission, in the fusion of ^{11}Li halo nuclei with Si targets (see the abstract in the present progress report and also ref. [2]. In Fig.2 it is illustrated a single neutron spectrum measured in Si(^{11}Li , fusion), by using the detectors #1 - #9 of the array. The vertical lines #2 and #3 in Fig.2 mark the energy range (12.2 ~ 14.2) MeV of the selected ^{11}Li incoming beam. The vertical line #1 marks the limit due to the energy loss of the 12.2 MeV incoming beam into the 0.5 mm thick Si target-detector. It follows from Fig.2 that the main contribution to the spectrum within the (9-14) MeV neutron energy range is due to the pre-emission effect. It is to be underlined that the incoming beam is almost uniformly distributed within the (12.2 ~ 14.2) MeV energy range.



Figure 1: A view of the neutron array detector built within the cooperation agreement between the NIPNE, Romania and RIKEN, Japan. It consists of 81 detectors made of $4 \times 4 \times 12 \text{ cm}^3$ BC-400 crystals, mounted on XP2972 phototubes.

References

- [1] M.Petrascu *et al*, *Rom. Journal of Phys.* **44**, no.1-2, Supplement, 115 (1999).
[2] M.Petrascu *et al*, *RIKEN Rep.* AF ~ NP ~ 395, April 2001.

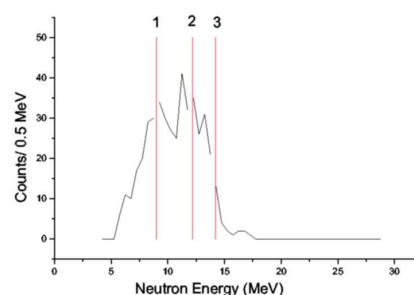


Figure 2:

Conducted and radiated noise in detection devices

D. Moisă¹

¹ NIPNE-HH Bucharest, Department of Nuclear Physics

Conducted and radiated noise is an external noise which affects the quality of the signals of the detectors. An external noise can be reduced, usually, by shielding. This was the situation with "older fashion" devices which uses boxes and coaxial cables. As the devices becomes more complex, the shielding of the detectors is more and more difficult and the transmission lines evolves from coaxial cables to twisted pair cables which are no more shielded. In such situation, it becomes important the conducted and radiated noise (C&R noise).

Due to complexity of a real detector, the main work is based on experiments with components and by simulation of some specific problems, associated with CDC detector.

The first experiment was done to understand how the C&R noise is propagated. The emission device was a set of coils (between 3 and 5 turns with diameter from 10 to 50 mm) feed by an 74S140 driver. A pulse of about 8 ns width was generated. A coil of reception about the same physical characteristics was used to see the emitted pulse. When the two coils are separated by about 80 cm, the receiver generated about no signal. But, if along the two coils, a conductive material is put (a wire for instance), the receiver sense a signal. This signal is not changed too much if the wire is or not connected to ground. The explanation is simple: the pulse in the emitting coil produces a EM pulse which spreads in space. If a conductive material is around, the EM energy is received by that conductor and is propagated at tens of meters with small attenuation. When this energy reach the end of the conductor, it radiated in space. If some others conductors are around, the energy is received and propagated by that conductors.

This experiment was done for about 20 kinds of conductors (different coax cables, twisted-pair ribbons, power cables, metallic bars) and with many coils (different diameters and numbers of turns). It was measured the pk-to-pk level, decay constant and frequencies of oscillations (eigen frequencies). Because a Fourier analyzer was not available, the eigen-frequencies were just evaluated by the scope.

The conclusions are:

1. For a 8 ns width pulse, the oscillation is damping in time with a constant between about 100 ns for

cooper bars and double-shielded coaxes and up to around 600 ns for twisted-pair ribbons;

2. The frequency of these oscillations depends on the conductor under test and so they are eigen-frequencies of that conductor. For a RG 59BU cable (F&G) the dominant EF was 20 MHz as for the same RG59U (Amphenol) the EF was 69 MHz. This is so because the technology to make the shielding is different. For a cooper bar for instance EF was measures as 46 MHz for 3.7 mm diameter and 26 MHz for 2.35 mm diameter.

To understand if these EM pulses which propagates everywhere are important or not we have to remind that these pulses are propagating on the surface of the conductors. For a shielded coax, they cannot go inside to change the signal. The situation in totally different when such pulse reach a twisted-pair cable. The signal is superimposed on the useful signal and is propagated as a "normal" signal. For this situation, the receiver of a twisted pair cable is differential so that the common mode signal could be rejected by a proper designed receiver. This is so only at the receiver side. If such noise propagates toward the source of signal (the output of the preamplifier for instance), when this EM energy go inside the transmitter, the electronic device reacts at this EM pulses. Its reaction can be a signal which goes back to line and this is impossible to be rejected by receiver because is like a normal differential signal. For a user it looks like being generated by the detector.

In an experiment, a real preamplifier, a real ribbon (about 5 meter long) and a real receiver were connected on a table. A 8 ns pulse was inserted somewhere on that 5 meter twisted-pair cable and the signal on the receiver was monitored. The input of the preamplifier was connected to ground. Due to simulated noise, on the line receiver it was measured a signal. When the power of the preamplifier was cut-off, the noise reduced by a factor of 8.

The problems to be solved are in connection with the eigen-frequencies of different cables and other kinds of F&G-noise transporters (gas, water or beam pipes). Also, the effect of the C&R noise which propagates inside the electronic devices on output-side of them, is important to be understood.

Angular momentum coherence in $^{19}\text{F} + ^{27}\text{Al}$ deep inelastic collision

I. Berceanu¹, A. Andronic¹, M. Duma¹, D. Moisă¹, M. Petrovici¹, A. Pop¹, V. Simion¹, A. Del Zoppo², G. d'Erasmus^{4,5}, G. Immé^{2,3}, G. Lanzanò^{2,3}, A. Pagano^{2,3}, G. Pantaleo⁴, G. Raciti^{2,3}

¹ NIPNE-HH Bucharest, Department of Nuclear Physics

² INFN, LNS - Catania, Italy

³ Dipart. di Fisica, Univ. di Catania, I-95129 Catania, Italy

⁴ Sez. di Bari, v. Amendola 173, 70125 Bari, Italy

⁵ Dipart. di Fisica, Univ. di Bari, Italy

In ref. [1] it has been shown that the energy-averaged cross section for deep inelastic heavy ion collision can be described by a coherent superposition of partial-wave amplitudes in a Δ window. The number of interfering partial waves (coherence length) λ_c increases with the mass of interacting nuclei and decreases with interaction time:

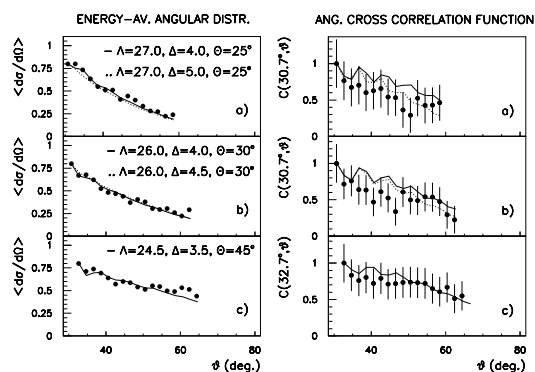
$$\lambda_c = 2J/\hbar\delta\tau, \quad (1)$$

where J is the moment of inertia and δ represents the dispersion of the wave-packet during the interaction time τ . Analytical expressions for energy-averaged cross section and angular cross correlation function (ACCF) have been obtained in [2]. It was also indicated that the same coherence effects which govern the angular dependence give rise to interference effects in the excitation function (EF) for particular cases ($\vartheta = 0$ and π). The role of the angular momentum in explaining the presence of intermediate structures in the EF of dissipative heavy ion collisions (DHIC) in general case has been addressed in ref. [3] after their experimental discovery [4].

The EF for $^{19}\text{F} + ^{27}\text{Al}$ DHIC has been measured and studied in details by our group. Intermediate structures with an average energy coherence width $\Gamma = 170 \pm 65$ keV have been evidenced [5]. Good angular resolution of our detector (0.5°) and the large statistics give the possibility to obtain angular distribution (AD) and to perform angular correlation analysis for $Z = 6 - 8$ fragments in the same windows of total kinetic energy loss (TKEL), 20 ± 2.5 , 30 ± 2.5 and 40 ± 2.5 , as for energy correlation studies. This analysis has been done on the energy range 116.76 - 129.75 MeV. Part of the results, namely the description of the energy-averaged AD and ACCF with analytical formulae from [2], are illustrated for $Z = 6$ in the following table and figure. The panels a), b) and c) of the figure correspond to TKEL windows centred on 20, 30 and 40 MeV, respectively. The continuous lines correspond to parameter values which give good description of AD: the width of angular momentum window Δ ; $\Lambda = l_o + 1/2$, where l_o is angular momentum on which Δ is centred and the mean deflection angle Θ . The dotted lines represent the results of the description with changed values of Δ (bracketed values) in order to obtain better

description of ACCF. λ_c is evaluated using the relation $1/\Gamma_\vartheta = (1/\Delta^2 + 1/\lambda_c^2)^{1/2}$, where Γ_ϑ ($1/\Gamma_\vartheta$ gives the width of AD) is obtained from ACCF. The dependence of Λ , Δ and Θ on TKEL (Z) is in agreement with expectation based on phenomenological considerations. The obtained values of angular momentum coherence width λ_c are in good agreement with value of (1.6 ± 0.6) given by Eq. (1) taking $\Gamma = 170 \pm 65$ keV from our previous studies and the relation $\tau = \hbar/\Gamma$. J is calculated taking into account the deformation as in [5]. Low values of λ_c are expected for light systems [1] (see Eq. (1)). As far as we are aware, it is for the first time when an experimental study of λ_c dependence on TKEL (Z) is realized.

TKEL (MeV)	20 ± 2.5	30 ± 2.5	40 ± 2.5
Λ (\hbar)	27.0	26.0	24.5
Δ (\hbar)	4(5)	4(4.5)	3.5
Θ ($^\circ$)	25	30	45
Γ_ϑ	2.33	2.32	1.86
λ_c	2.9(2.6)	2.7(2.4)	2.2



References

- [1] A. Y. Abul-Magd, M. H. Simbel, Phys. Lett., **B83**, 27 (1979)
- [2] K. M. Hartmann, W. Dünneweber, W. E. Frahn, Nucl. Phys. **A380**, 170 (1982)
- [3] D. M. Brink and K. Dietrich, Z. Phys. **A326**, 7 (1987)
- [4] A. De Rosa et al, Phys. Lett. **B160**, 239 (1985)
- [5] I. Berceanu et al, Phys. Rev. **C57**, 2359 (1998)

Gamma-ray multiplicity measurements for light heavy ion reactions

A. Pop¹, M. Petrovici¹, I. Berceanu¹, M. Duma¹, D. Moisă¹, V. Simion¹, A. Del Zoppo², R. Coniglione², P. Piatelli², P. Sapienza²

¹ IFIN-HH, Department of Nuclear Physics

² INFN, Laboratorio Nazionale del Sud, v. S. Sofia 44 I-95100, Catania, ITALY

Experiments on gamma-ray multiplicities are designed to probe the gamma multiplicity distribution associated with the decay of systems formed for instance in a (heavy ion,xn) reaction or in deep inelastic scattering of heavy ions [1, 2]. A method for obtaining information about the multiplicity distributions of gamma rays emitted by nuclei is based on the use of gamma-ray multicounter systems in multiple-coincidence experiments. The gamma-ray multiplicity filter used in our experiment consists of 12, 2" (diameter)x2" NaI(Tl) scintillation counters [3]. A new spherical reaction chamber has been specially constructed for this type of measurements [4]. The existing gamma-ray filter has been partially modified to fit the DRACULA set-up Phase I infrastructure [5], in order to provide the right detection geometry. Thus, the scintillation counters have been placed at 11 cm from the target, above and below the horizontal plane, each with its symmetry axis passing through the target centre, and were positioned at the polar angles: 135° (6), 45° (4), 0° (1) and 90° (1). The counters are mounted into 3 mm thick stainless steel housings which can also support lead shields in order to reduce the detection of gamma-rays scattered between neighbouring counters. The NaI(Tl) crystals are coupled to RCA 8575 photomultipliers. The selective counters are the two big ionization chambers (IC) of the DRACULA experimental device. Two Ge(Li) counters were placed in the horizontal plane. Timing signals from two large area PPADs in front of the big ICs give the reference time by starting the TDCs. An OR of the anode signals from the 12 NaI(Tl) counters gives the stop signal. The lower threshold in the time discriminators was set to a level so as to accept NaI pulses ≥ 100 keV. The timing resolution of the detectors in the filter is sufficient to allow separation of prompt gamma-rays and neutrons by time of flight (Fig.1). The energy resolution of the NaI(Tl) detectors varied from 3.33% to 9.8% for 662 keV and from 2.27% to 7.62% for 1332 keV. Using a ⁶⁰Co source, the ratio between one-fold true coincidence yield and two-fold coincidence yield coming from cross-talk, due to the 1173 keV transition, gated by photopeak events in the germanium detector corresponding to the 1332 keV transition, is found to be negligible. The absolute efficiency at an appropriate energy has been determined from the experimental ratio of the number of NaI-Ge(Li) events and the number of singles obtained with a ⁶⁰Co source, for

multiplicity M=2, in the same geometry as for the experiment and the efficiency as a function of energy and response linearity have been measured with calibrated sources.

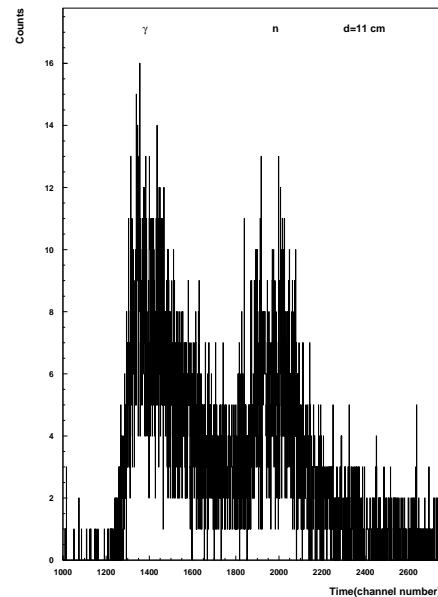


Figure 1:

Using the gamma-ray multiplicity filter coupled with the big ionization chambers, the multiplicity distribution in coincidence with products emitted in the deep inelastic reactions: ¹⁹F(136.9 MeV)+²⁷Al and ²⁷Al(140.14 MeV)+²⁷Al, has been measured.

References

- [1] G. B. Hagemann et al., Nucl. Phys. **A245**(1975)166
- [2] K. A. Geoffroy et al., Nucl. Phys. **A302**(1978)333
- [3] G. Russo et al., Phys. Rev. **C39**(1989)2462
- [4] M. Petrovici et al., INFN-LNS Activity Report 1994-1995 and NIPNE Scientific Report 1996, p. 125
- [5] M. Petrovici et al., IPNE Preprint NP-55-1986; V. Simion, Rom. J. Phys. **38**(1993)513

Prototype tests for the ALICE TRD

A. Andronic^{1,4}, H. Appelshäuser², C. Blume¹, P. Braun-Munzinger¹, D. Bucher³, V. Cătănescu⁴, M. Ciobanu⁴, H. Daues¹, A. Devismes¹, Ch. Finck¹, N. Herrmann², T. Lister³, T. Mahmoud², T. Peitzmann³, M. Petrovici⁴, K. Reygers³, R. Santo³, R. Schicker², S. Sedykh¹, R.S. Simon¹, J. Stachel², H. Stelzer¹, J. Wessels², O. Winkelmann³, B. Windelband², C. Xu², Collaboration ALICE⁵

¹ GSI-Darmstadt, Germany

² Universität Heidelberg, Germany

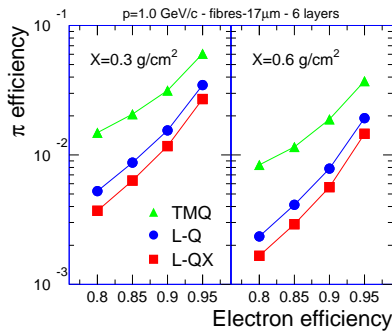
³ Universität Münster, Germany

⁴ NIPNE-HH, Bucharest, Department of Nuclear Physics

⁵ CERN, CH-1211 Geneva 23

The ALICE Transition Radiation Detector (TRD) has been designed to improve the pion rejection capability of the ALICE detector by at least a factor of 100 for momenta above 2 GeV/c [1]. To demonstrate that this goal is achievable, during the last year we have conducted prototype tests at the pion (with natural electron content) beam facility at GSI Darmstadt. A complete description of the experimental setup and of the results (including references) can be found in [2]. Many types of radiators were tested, composed of foils, fibres and foams. Here we summarize the results concerning the pion rejection performance in case of a fibres (of 17 μm diameter) radiator, which was established to be the best candidate for the final radiator.

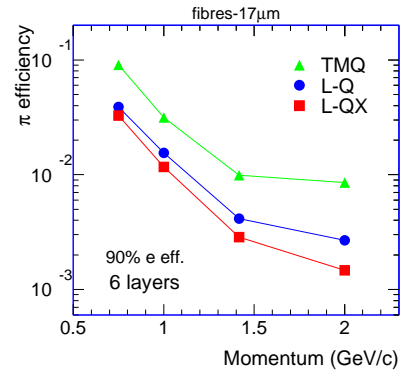
To extract the pion rejection factor we have studied three different methods: i) truncated mean of integrated energy deposit, TMQ; ii) likelihood on integrated energy deposit, L-Q; iii) bidimensional likelihood on energy deposit and position of the largest cluster found in the drift region of the DC, L-QX.



In Fig. 6 we present the pion efficiency (the inverse of the rejection factor) as function of electron efficiency (90% electron efficiency is the commonly used value) in case of fibres radiators for the momentum of 1 GeV/c. The truncated mean method, although it delivers sizeably worse identification, has the advantage of being very easy to use, being advantageous especially for an on-line identification. The bidimensional likelihood delivers the best rejection factor. In general, the three methods employed here give results in good agreement with earlier studies.

By doubling the equivalent thickness of the radiator (see Fig. 6) one gains a factor of about 2 in

pion rejection power. However, it remains to be seen how the additional material will influence (by producing secondary particles) the performance of the TRD itself and of other ALICE sub-detectors.



The pion efficiency at 90% electron efficiency as function of momentum is shown in Fig. 6. The steep decrease of pion efficiency at momenta around 1 GeV/c is due to the onset of TR production. Towards our highest momentum value, 2 GeV/c, the pion efficiency reaches a saturation, determined by the TR yield saturation and by the pion relativistic rise. Due to these effects the pion rejection is expected to get slightly worse for momenta above 3 GeV/c. As one can see in Fig. 6, at the momentum of 2 GeV/c the pion rejection factor of 300 to 600 achieved during these tests is better than the required value for the ALICE TRD. However, one has to bear in mind that a significant worsening of TRD performance has been registered when going from prototype tests to real detectors. On the other hand, impressive pion rejection factors of 1000 and above have been achieved in full size TRDs, i.e. by the HERMES experiment.

References

- [1] TRD Proposal, CERN/LHCC 99-13, available at <http://www.gsi.de/~alice>
- [2] A. Andronic et al., nucl-ex/0102017, IEEE Trans. Nucl. Sc., vol. 48, no. 4 (August 2000)

Particle Physics

Cryogenic setup for kaonic nitrogen (DEAR experiment)

M. Bragadireanu^{1,2}, C. Curceanu^{1,2}, C. Guaraldo², I. Iliescu^{1,2}, V. Lucherini², T. Ponta¹, D. Sirghi¹

¹ NIPNE, Elementary Particle Physics Dept.

² LNF-INFN, Frascati, Italy

Achieving, in the last DEAR runs, the best "expected signal"/ "measured background" ratio with the NTP setup, in the actual machine conditions, suggested, as next setup, the use of the cryogenic setup also for measuring kaonic nitrogen. The installation of the cryo setup, already in this phase of the scientific programme of DEAR, will allow an enhancement both of the signal and of the shielding factor. This due to a bigger detector solid angle and intrinsic efficiency, to an increased rate of kaonic atoms formation for the higher density and to a better compactness of the cryogenic setup, allowing a more efficient shielding.

A Monte Carlo study shown [1] that with the cryogenic setup equipped with 8 CCD-22 and 4 CCD-05, filled with nitrogen at 5 equivalent bars at room temperature, it is possible to identify the 7.6 keV line of kaonic nitrogen with only few thousands nb⁻¹ of integrated luminosity, if the signal/ background ratio is at least of the order of 1/20, by applying a suitable background subtraction technique.

After the last period of DEAR runs, which took advantage of a fully shielded NTP setup (what practically saturated any further possibility of shielding this setup), the background measured at the position of the 7.6 keV line of the kaonic nitrogen spectrum turned out about 2.6 X/nb⁻¹ [2], for an expected signal of about 0.05 X/nb⁻¹, which means a ratio still far from the above threshold. It was therefore decided to install the cryogenic setup - foreseen for the hydrogen measurement - already for the nitrogen measurement, with an additional special shielding, based on what learned - and positively applied - on the NTP setup. The expected increasing of the signal - due to the increased number of detectors, 4 CCD-05 and 8 CCD-22, the latter with larger area and higher depletion layer, as well as due to the increased density should allow, in principle, to reach a signal/background ratio such to allow to measure a kaonic nitrogen transition.

We used an octagonal target cell, placed in the cen-

ter of the vacuum chamber . The density of the target was optimized in order to reach a compromise between yield and absorption of the lines. The optimum yield for the 7.6 keV line of kaonic nitrogen (6 → 5 transition) is obtained at the equivalent pressure at room temperature of about 5 bars, which can be reached with a relatively low pressure in the target (about 2 bars) by cooling nitrogen gas down to about 120 K. The temperatures reached are 177 K for CCD-22, 166 K for CCD-05 and 118 K for the target cell, which, for the pressure of 2 bars, corresponds to a density about 5 times the NTP density.

We used both an external and an internal shielding. The external shielding is composed by a lead wall to shield the DEAR interaction region, a lead-reinforced platform for the setup and also a shielding around the setup. The internal shielding is intended to shield of all those parts of the setup which fall within the solid angle seen by the CCDs. "Golden rule" for the internal shielding - whose application allowed to obtain the best performance on the NTP setup [3] - is the use of sandwich-type structures, made by initial high Z / high density materials to finish with low Z materials. Typically, the sequence of layers is lead-aluminium-polyethylene.

Two types of CCD were mounted inside the setup : 8 CCD-22 and 4 CCD-05-20 . The readout is done with a special electronics and the DAQ is performed using two independent PCs.

The optimisation of the degrader is required to center the kaons stopping points distribution in a region with maximized solid angle and minimized absorption with respect to the CCDs position. For this goal the calculation was carried out using the Monte-Carlo program. The program took into account the present geometry of the setup and the resulting degrader is made of a layer of plexiglass and 2 layers of mylar, optimized for a density of nitrogen which corresponds to the equivalent pressure of 5 bars at room temperature.

References

[1] C. Petrascu, DEAR Note-IR-33, November 7, 2000.

[2] M. Bragadireanu et al., DEAR Note-IR-35, February 5, 2001.

[3] M. Bragadireanu et al., DEAR Note-IR-34, January 9, 2001.

A non-parametrical method for hadron energy reconstruction in ATLAS calorimetry

V. Boldea¹, S. Constantinescu², S. Dita¹, D. Pantea¹, Collaboration ATLAS

¹ NIPNE, Elementary Particle Physics Dept.

² NIPNE, Informatics and Computing Dept.

The ATLAS central (barrel) combined calorimeter prototype setup composed from three electromagnetic liquid Argon accordion modules and five hadronic iron scintillator tiles modules has been tested in the H8 beam line of the CERN SPS. The data taken with pions of energy 10, 20, 40, 50, 80, 100, 150, and 300 GeV have been used to test a non-parametrical method of the energy reconstruction. The non-parametrical method utilizes only the known e/h ratios and the electron calibration constants and does not require the determination of any parameters by a minimization technique. The results are compared with the benchmark and cells weighting methods, used previously for reconstruction.

The total energy is reconstructed as the sum of the energy deposit in the electromagnetic compartment (E_{LAR}), the deposit in the hadronic calorimeter (E_{Tile}), and that in the passive material between the LAr and Tile calorimeters (E_{dm}):

$$E = \frac{1}{e_{LAR}} \left(\frac{e}{\pi} \right)_{LAR} R_{LAR} + E_{dm} + \frac{1}{e_{Tile}} \left(\frac{e}{\pi} \right)_{Tile} R_{Tile}, \quad (1)$$

where R_{LAR} (R_{Tile}) is the measured response of the LAr (Tile) calorimeter compartment and $1/e_{Tile}$ and $1/e_{LAR}$ are energy calibration constants for the LAr and Tile calorimeters respectively. Similarly to the procedure in Refs. [1, 2], the E_{dm} term is taken to be proportional to the geometrical mean of the energy released in the third depth of the electromagnetic compartment and the first depth of the hadronic compartment ($E_{dm} = \alpha \cdot \sqrt{E_{LAR,3} \cdot E_{Tile,1}}$).

$$\frac{e}{\pi} = \frac{e/h}{1 + (e/h - 1) \cdot f_{\pi^0}}, \quad (2)$$

where f_{π^0} is the fraction of electromagnetic energy of the shower whose dependence on the incident hadron energy can be parameterized as:

$$f_{\pi^0} = E_e/E = k \cdot \ln E. \quad (3)$$

The reconstructed mean values of the hadron energies are within $\pm 1\%$ of the true values (see Fig. 1).

The fractional energy resolution (see Fig. 2) is $[(58 \pm 3)\%/\sqrt{E} + (2.5 \pm 0.3)\%] \oplus (1.7 \pm 0.2)/E$.

References

- [1] S. Akhmalaliev et al., (ATLAS Collaboration; Calorimetry and Data Acquisition), NIM **A499**, 2000, 461.
- [2] Z. Ajaltouni et al., (ATLAS Collaboration; Calorimetry and Data Acquisition), NIM **A387** (1997) 333.

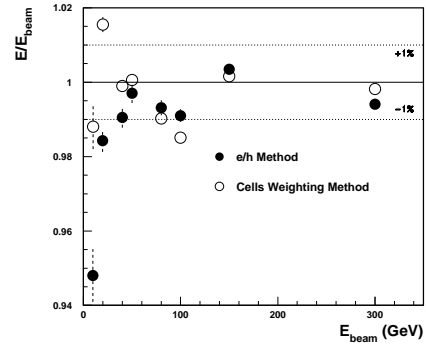


Figure 1: Energy linearity as a function of the beam energy for the e/h method (black circles) and the cells weighting method (open circles)

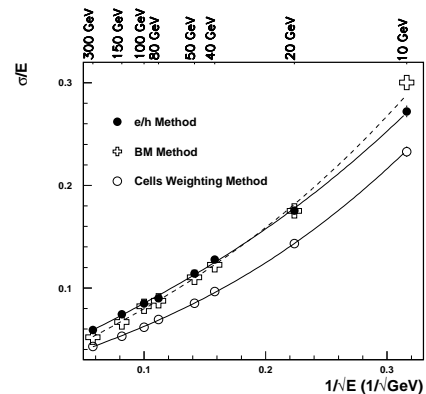


Figure 2: The energy resolutions obtained with the e/h method (black circles), the benchmark method (crosses) and the cells weighting method (circles).

Strong evidences for correlated nonextensive quantum statistics in hadronic scatterings

D.B. Ion¹, M.L. Ion²

¹ National Institute for Physics and Nuclear Engineering, IFIN-HH

² Bucharest University, Department of Atomic and Nuclear Physics

In this paper [1] the degrees of nonextensivity of the quantum systems composed from (J or θ)-quantum states in the spin ($0^{-\frac{1}{2}+} \rightarrow 0^{-\frac{1}{2}+}$) hadron-hadron scatterings are investigated. So, first we presented a complete statistical description of the nonextensive quantum systems from the ($0^{-\frac{1}{2}+} \rightarrow 0^{-\frac{1}{2}+}$)-scatterings in terms of the scattering entropies $S_J(p)$ and $S_\theta(q)$, $p, q \in R$. Then, the nonextensivity indices of quantum states from the pion-nucleon and pion-nucleus scatterings, determined by the fit of the scattering entropies $S_J(p)$ and $S_\theta(q)$ with the optimal scattering entropies $S_J^{\circ 1}(p)$ and $S_\theta^{\circ 1}(q)$, are calculated from the available *pion-nucleon* experimental phase shifts. Therefore, we consider the *maximum-entropy* (MaxEnt) problem

$$\max\{S_J(p), S_\theta(q)\} \text{ when } \sigma_{el} = \text{fixed}, \frac{d\sigma}{d\Omega}(1) = \text{fixed} \quad (1)$$

as criterion for the determination of the *equilibrium distributions* p_i^{me} and $P^{me}(x)$ for the quantum states from the ($0^{-\frac{1}{2}+} \rightarrow 0^{-\frac{1}{2}+}$)-scattering. For the *J-quantum states*, in the spin ($0^{-\frac{1}{2}+} \rightarrow 0^{-\frac{1}{2}+}$) scattering case, these distributions are given by [1]

$$p_J^{me} = p_J^{\circ 1} = \frac{1}{(J_o + 1)^2 - 1/4}, \text{ for } \frac{1}{2} \leq J \leq J_o \quad (2)$$

while, for the *theta-quantum states*, these distributions are as follows

$$P^{me}(x) = P^{\circ 1}(x) = \left[\frac{K_{\frac{1}{2}\frac{1}{2}}^2(x, 1)}{K_{\frac{1}{2}\frac{1}{2}}(1, 1)} \right] \quad (3)$$

where $d_{\frac{1}{2}\frac{1}{2}}^J(x)$ are the d-spin rotation functions [1] for the spin 1/2 particles, $\overset{\circ}{P}_l(x) \equiv dP_l(x)/dx$, the *reproducing kernel* $K_{\frac{1}{2}\frac{1}{2}}(x, y)$ is given by: $K_{\frac{1}{2}\frac{1}{2}}(x, y) = \frac{1}{2} \sum_{1/2}^{J_o} (2J+1) d_{\frac{1}{2}\frac{1}{2}}^J(x) d_{\frac{1}{2}\frac{1}{2}}^J(y)$, while the J_o is given by $(J_o + 1)^2 - 1/4 = 2K_{\frac{1}{2}\frac{1}{2}}(1, 1) = \frac{4\pi}{\sigma_{el}} \frac{d\sigma}{d\Omega}(1)$.

Hence, by a straightforward calculus we obtain that the solution of the MaxEnt problem is given by

$$S_J^{\max}(p) = S_J^{\circ 1}(p) = \left[1 - [2K_{\frac{1}{2}\frac{1}{2}}(1, 1)]^{1-p} \right] / (p-1), \quad (4)$$

$$S_\theta^{\max}(q) = S_\theta^{\circ 1}(q) = \left[1 - \int_{-1}^{+1} dx [P^{me}(x)]^q \right] / (q-1) \quad (5)$$

where $P^{me}(x) = P^{\circ 1}(x)$ is given by Eq. (3).

The *nonextensivity indices* p and q corresponding to the *J-statistics* and *theta-statistics*, respectively, are proved to be correlated via the *Riesz-Thorin relation*

$$\frac{1}{2p} + \frac{1}{2q} = 1, \text{ or } q = p/(2p-1) \quad (6)$$

The main results and conclusions obtained in Ref. [1] can be summarized as follows:

(i) In this paper [1] we obtained a complete nonextensive statistical description of the quantum state in the ($0^{-\frac{1}{2}+} \rightarrow 0^{-\frac{1}{2}+}$)-scatterings. The *equilibrium (or MaxEnt) distributions* and optimal (J or θ)-scattering entropies are obtained [1] in terms of the spin $d_{\mu\nu}^J(x)$ -functions and of corresponding reproducing kernel functions;

(ii) The experimental determination of statistical behavior of the quantum scattering states in the pion-nucleon scattering was performed by the experimental fit of the (p, q)-*nonextensivity indices* using the available *pion-nucleon* experimental phase shifts. Hence, a separate p-fit of the experimental data on the scattering entropies $S_J(p)$, $p \in (1/2, \infty)$ with the "equilibrium" entropy $S_J^{\circ 1}(p)$ [Eq. (25) in Ref. [1]] allowed us to conclude that the (J, p)-statistics of the system of J -quantum states are *subextensive* with an index p slightly above 1/2, while a separate q-fit of the experimental entropies $S_\theta(q)$, $q \in (1/2, \infty)$ with the optimal entropy $S_\theta^{\circ 1}(q)$ [Eq.(26) in Ref. [1]] proved that (θ, q)-statistics of the θ -quantum states are *superextensive* with $q \geq 2$ (see Table 1 and Fig. 1 from [1]);

(iii) A two-parameter (p, q)-fit of the scattering entropies $S_J(p)$ and $S_\theta(q)$ with the optimal scattering entropies $S_J^{\circ 1}(p)$ and $S_\theta^{\circ 1}(q)$ advanced the conclusion that the best values for p are also in the range ($0.5 \leq p \leq 0.6$) but with the *q-nonextensivities* correlated by the Riesz-Thorin relation: $1/p + 1/q = 2$ (see Tables 1 and Fig. 1 of Ref. [1]);

(iv) The strong experimental evidence obtained here for the *nonextensive statistical behavior of the (J, theta) - quantum scatterings states* in the pion-nucleon scattering can be interpreted as an indirect manifestation the presence of the *quarks and gluons* as fundamental constituents of the scattering system having the *strong-coupling long-distance regime required by the Quantum Chromodynamics*.

[1] M. L. D. Ion and D. B. Ion, Lett. **B 482** (2000) 57-64.

Limited entropic uncertainty as new principle of quantum physics

D.B. Ion¹, M.L. Ion²

¹National Institute for Physics and Nuclear Engineering, IFIN-HH

²Bucharest University, Department of Atomic and Nuclear Physics

The *Uncertainty Principle* (UP) of quantum mechanics discovered by Heisenberg which constitute the corner-stone of quantum physics, asserts that: (UP) "there is an irreducible lower bound on the uncertainty in the result of a simultaneous measurement of non-commuting observables". In order to avoid this *state-dependence* many authors proposed to use the *information entropy* as a *measure of the uncertainty* instead of above standard quantitative formulation of the *Heisenberg uncertainty principle*.

In this paper [1] the *Principle of Limited Entropic Uncertainty (LEU-Principle)*, as a new principle in quantum physics, is proved. Then, consistent experimental tests of the *LEU-principle*, obtained by using the available 49 sets of the pion-nucleus phase shifts, are presented for both, *extensive* ($q = 1$) and *nonextensive* ($q = 0.5$ and $q = 2.0$), *statistics* cases. Moreover, some results obtained by the application of *LEU-Principle* to the *diffraction phenomena* are also discussed.

In particular, using the results of Refs. [2] for the *Tsallis-like scattering entropies*, in this paper [1] we proved the following quantitative formulation of the *LEU-Principle*.

LEU-Principle for scattering: Let σ_{el} and $\frac{d\sigma}{d\Omega}(y)$ be fixed from experiment for a fixed $y \in [-1, +1]$. Let $V_{\theta L}(q) = \exp[S_{\theta L}(q)]$ be the *statistical variances* corresponding to the Tsallis-like scattering entropies $S_{\theta L}(q)$. Then, the *LEU-inequalities* can be given in the following general form:

$$\exp[(1 - 2^{1-q})/(q - 1)] \leq V_{\theta L}(q) \leq V_{\theta L}^{oy}(q), \quad (1)$$

for $q > 0$, and

$$\exp[(1 - 2^{1-q})/(q - 1)] \leq V_{\theta L}^{oy}(q) \leq V_{\theta L}(q), \quad (2)$$

for $q < 0$, where

$$V_{\theta L}^{oy}(q) = \exp[S_{\theta L}^{oy}(q)] \quad (3)$$

$$S_{\theta L}^{o1}(q) = \frac{1}{q-1} \left[1 - \sum (2l+1) [p_l^{o1}] \int_{-1}^{+1} dx [P^{o1}(x)]^q \right]$$

$$p_l^{o1} = \frac{P_l^2(x)}{2K(1,1)}, \quad P(x) = \frac{[K(x,y)]^2}{K(y,y)}$$

and the *reproducing kernels* $K(x, y)$ and $K(y, y)$ for *two-body scattering* are given by

$$K(x, y) = \frac{1}{2} \sum_{l=0}^{L_{oy}} (2l+1) P_l(x) P_l(y) \quad (4)$$

$$K(y, y) = \frac{1}{2} \sum_{l=0}^{L_{oy}} (2l+1) P_l^2(y) \quad (5)$$

while the *optimal angular momentum* L_{oy} can be obtained by solving the implicit algebraic equation

$$\frac{d\sigma}{d\Omega}(y) = K(y, y) \frac{\sigma_{el}}{2\pi} \quad (6)$$

The main results and conclusions of our paper [1] can be summarized as follows:

(i) In the paper [1] we introduced a *new principle* in quantum physics namely the *Principle of Limited Entropic Uncertainty (LEU-Principle)*. This new principle includes in a more general and exact form not only the old Heisenberg *uncertainty principle* but also introduce an *upper limit* on the magnitude of the uncertainty in the quantum physics. The *LEU-Principle* asserts that: "there is an irreducible lower bound as well as an upper bound on the uncertainty in the result of a simultaneous measurement of non-commuting observables for any extensive and nonextensive ($q \geq 0$) quantum systems.

(ii) Two important concrete realizations of the *LEU-Principle* are explicitly obtained in this paper, namely, (a) the *LEU-inequalities* [see Eqs. (2)-(5) in [1]] for the *quantum scattering of spinless particles*, and, (b) the *LEU-inequalities for the diffraction on single slit of width 2a* [see Eqs. (19)-(22)]. In particular from our general results, in the limit $y \rightarrow +1$, we recovers in an exact form all the results previously reported in Refs. [2]. In our paper [1], an experimental illustration of the *LEU-Principle* is presented in Figs. 1-3 for the cases $y=1$ and $q=0.5, 1$, and 2 .

(iii) For the nonextensive quantum systems with negative q we also proved the validity of the *state independent entropic uncertainty relations*: $\exp\{(1 - 2^{1-q})/(q - 1)\} \leq V_{\theta L}(q)$. Moreover, in this case we get [see Eqs.(14) in [1]] that the *optimal Tsallis-like entropies* (if they exists for $q < 0$) provides only an important improvement of the above state independent entropic uncertainty relations.

[1] M. L. D. Ion, D. B. Ion, Phys. Lett. **B 474** (2000) 395-401.

[2] D. B. Ion and M. L. D. Ion, Phys. Rev. Lett. **81** (1998) 5714-5717; D. B. Ion and M. L. D. Ion, Phys. Rev. **E 60** (1999) 5261-5274; M. L. D. Ion and D. B. Ion, Phys. Rev. Lett. **83** (1999) 463-467; D. B. Ion and M. L. D. Ion, Phys. Lett. **B 466** (2000) 27-32.

A precise measurement of 180 GeV muon energy losses in iron

C. Alexa¹, V. Boldea¹, S. Constantinescu², S. Dita¹, D. Pantea¹, Collaboration ATLAS

¹NIPNE-HH, Particle Phys. Dept.

²NIPNE-HH, Computing Center

The detection and measurement of muons with energies in excess of 100 GeV at the Large Hadron Collider present a special interest for the investigation of a wide variety of physics processes (intermediate boson decays, jets with heavy flavor tags, etc.). In the ATLAS detector, muons will be measured by tracking chambers within a toroidal air-core magnet after they have crossed more than 100 radiation lengths of material in the electromagnetic and hadronic calorimeters. It is, therefore, important to check precisely the theoretical predictions for muon energy losses in iron or higher Z materials.

In an earlier experiment [5], the energy loss spectrum of 150 GeV muons in 1 meter long prototype modules of the ATLAS Tile Calorimeter was studied. The spectrum of muon energy losses was found to be in very good agreement with theoretical predictions, and an indication of a non-zero value of the nuclear size correction to the bremsstrahlung process was found. The main limitation on the precision of the measurement was due to the systematic uncertainty of the calorimeter energy scale calibration.

A new measurement was performed with 180 GeV positive muons incident on a preseries module of the ATLAS Tile Calorimeter (Module 0). A detailed description of the calorimeter concept, the Module 0 and prototypes is given elsewhere [1]. For the purpose of this measurement, the Module 0 and the 1-meter small modules of the calorimeter were placed in the H8 beam of the CERN SPS, and oriented so that particles cross the tiles of Module 0 at perpendicular incidence. The 5.6 m long Module 0 was surrounded at the downstream end by three small modules on the bottom and two on the top. The beam entered in the center of the Module 0. In this setup muons traversed 5.6 m of finely segmented iron and scintillators, thereby providing high statistics and high granularity data. Compared to the past study, the fiducial region for observing large energy losses is much longer (115.3 radiation lengths, *vs.* 17.6 r.l. in Ref. [5]) and contamination from hadron and muon decays in flight are eliminated using the first 1.5 m of the muon track in the calorimeter.

The quantity to be compared to theoretical estimates is the differential probability dP/dv of fractional muon energy loss v per radiation length. The fractional energy loss v is expressed as $v = \Delta E_\mu / (E_\mu - \epsilon)$, where the muon energy E_μ is corrected by the energy losses ϵ in layers preceding the shower signal.

ΔE_μ is the shower energy, which is calculated excluding the underlying contribution from the minimum-ionizing track. To obtain ΔE_μ the signals in three consecutive layers centered on the maximal signal are summed and then corrected by subtracting the contributions from the muon track ionization and low energy showers overlapping in the three signal cells.

The differential probability dP/dv of muon fractional energy loss per radiation length of iron has been measured in the range $0.025 \leq v \leq 0.97$ and it is compared with theoretical predictions for energy losses due to bremsstrahlung, production of electron-positron pairs, energetic knock-on electrons and photonuclear interactions. Particular attention is given to muon bremsstrahlung which is the dominant process leading to large energy losses. The theoretical values, which are the sum of the predictions for the four processes mentioned above, are in very good agreement with the experimental results over the range of fractional energy losses v from 0.025 to 0.12. This is the region of screening of the nucleus by the electron cloud while the region $v \geq 0.12$ is the region of no screening where the dominant process for muon energy losses is bremsstrahlung. The sensitivity achieved in this experiment for higher fractional energy losses allowed to measure for the first time the effect on muon bremsstrahlung of the nuclear elastic form factor. The theoretical predictions vary from no effect to a -30% effect at the upper end of the energy loss spectrum. The results are precise enough to discriminate between different theoretical calculations; specifically, they are in agreement with two sets of predictions ([2, 4] and [3]), while they differ from three other sets by 2.3 to 3.5 standard deviations.

References

- [1] Tile Calorimeter TDR, CERN/LHCC 96-42
- [2] S.R. Kelner, R.P. Kokoulin, A.A. Petrukhin, preprint 024-95, Moscow Tech. University, 1995.
- [3] Yu.M. Andreev, L.B. Bezrukov, E.V. Bugaev, Phys. Atom. Nucl. 57 (1994) 2066.
- [4] R.P. Kokoulin and A.A. Petrukhin, Acta Phys. Acad. Sci. Hung. 29 Suppl. 4 (1970) 277.
- [5] E. Berger et al., Z. Phys. C73 (1997) 455-463; CERN-PPE/96-115, CERN 1996

The dependence of the anomalous J/Ψ suppression on the number of participant nucleons

C. Alexa¹, V. Boldea¹, S. Constantinescu², S. Dita¹, Collaboration NA50

¹ NIPNE-HH, Particle Phys. Dept.

² NIPNE-HH, Computing Center

The observation, reported by the NA50 collaboration, of an anomalous J/Ψ suppression in Pb-Pb collisions represents one of the most striking indications of the occurrence of the deconfinement of quarks and gluons at SPS energies. In this report we determine the J/Ψ suppression pattern as a function of the forward energy E_{ZDC} measured in a Zero-Degree Calorimeter (ZDC). Exploiting the direct connection between E_{ZDC} and the geometry of the collision, we calculate, within a Glauber approach, the relationship between the number of participants nucleons N_{part} and E_{ZDC} . We also verify the consistency of this approach with results from VENUS and RQMD event generators. Taking into account the resolution on our centrality measurement, we check if the experimental data can be better explained by a sudden or a smooth onset of the anomalous J/Ψ suppression in the N_{part} variable.

The data analyzed in this report have been collected with the NA50 set-ups of 1996 and 1998. A description of the NA50 experimental apparatus can be found in [1, 2, 3]. Details on data taking conditions and the event selection procedure can be found in Refs. [4, 5].

The geometry of a nucleus-nucleus collision is usually characterized by the value of the impact parameter b , which is not directly accessible to the experiment, but can be deduced from the measured E_{ZDC} distribution. The link between N_{part} and the impact parameter b , has been obtained with a calculation based on a Glauber model of nucleus-nucleus collisions, using Woods-Saxon nuclear profiles, with the parameters tabulated in [6]. The same N_{part} vs b dependence has been reproduced using the VENUS 4.12 [7] and RQMD 2.3 [8] event generators. In Fig.1 we plot the E_{ZDC} spectrum, for the 1996 data sample, together with the result of our Glauber calculation. The good description of the measured spectrum allows to conclude that our approach satisfactorily reproduces the connection between E_{ZDC} and the geometry of the collision. The distribution of N_{part} vs E_{ZDC} is particularly relevant for the J/Ψ suppression analysis. Two complementary techniques, the "standard analysis" and "minimum bias analysis" have been employed to extract the J/Ψ suppression pattern vs E_{ZDC} . They have been already used for the analysis of J/Ψ suppression, as a function of the neutral transverse energy and have been explained in detail in [4, 5].

The two-step pattern of the J/Ψ suppression, already established as a function of the neutral transverse energy E_T and interpreted as an evidence for deconfinement at SPS energy [5], has been confirmed.

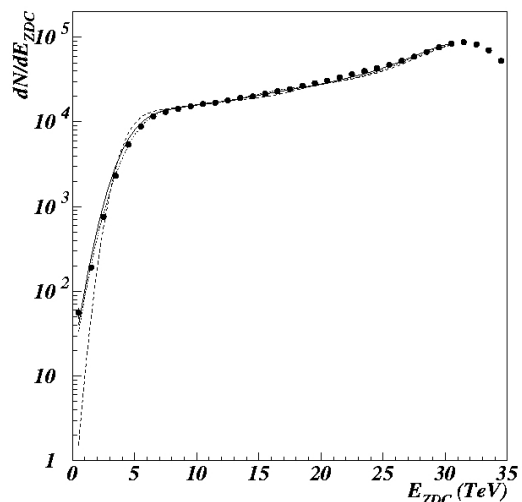


Figure 1: Comparison of the minimum bias E_{ZDC} spectrum with the result of the Glauber calculation (full line), and the Monte Carlo simulations based on VENUS (dashed line) and on RQMD (dotted line).

References

- [1] NA50 Collaboration, M.C.Abreu et al., Phys.Lett. B 410 (1997) 327
- [2] R.Arnaldi et al., Nucl. Instr. and Meth. A 411 (1998) 1
- [3] F. Bellaiche et al., Nucl. Instr. and Meth. A 398 (1997) 180
- [4] NA50 Collaboration M.C.Abreu et al., Phys. Lett.. B 450 (1999) 456
- [5] NA50 Collaboration, M. C. Abreu et al., Phys. Lett. B 477 (2000) 28
- [6] C. W. de Jager et al., Atomic Data and Nuclear Data Tables 14 (1974) 485
- [7] K. Werner, Phys. Rep. 232 (1993) 87
- [8] H. Sorge, Phys.Rev. C52 (1995) 3291

Beam-test results of the LHC-B hadron calorimeter prototype

C. Coca¹, C. Magureanu¹, T. Preda¹, A. Rosca¹, I. Ajinenko²

¹NIPNE, Elementary Particle Physics Dept.

²IHEP, Protvino, Russia

The hadron calorimeter (HCAL) of the LHC-B spectrometer [1, 2] will provide information for the event triggering and background suppression on reconstruction of B mesons decays. The overall dimension of the active area of the detector is foreseen to be $3.4 \times 6.3 \text{m}^2$.

The technology chosen for the HCAL design is a scintillator/iron sampling structure with scintillating tiles arranged in parallel to the beam axis. It has been tested two variants. They differ by the cell size (8 cm and 16 cm), by their depths ($7.3 \lambda_I$ and $5.6 \lambda_I$) and by different light collection designs (double and single sampling depth) that have been equipped with two types of fibers: Pol.Hi.Tech.(S250) and BICRON BCF-92. Results have been obtained, at CERN, in a combined run with SPD/PS, ECAL and HCAL, reading out the ECAL and HCAL with fast 25 ns sampling electronics.

For HV system has been used a prototype designed and constructed in IFIN-HH to power in parallel a group of 9PMTs FEU-115m10 with booster sources for the dynodes D7...D10. It supports a high counting rate (approx. 40 MHz) by supplying additional current to the last four dynodes of the PMT. The HV differences can be independently adjusted up to 10% of the nominal value, in the automatic mode.

Iron plates are passive radiators, and it is known that iron calorimeters are non-compensating ones. This feature is determined by increasing of π^0 's with energy: $\pi^0/\text{all} \sim 0.23 \ln(E)$ (E in GeV) that results in an increase of detected energy E with respect to the incident particle energy E_b :

$$E/E_b \approx 1 + \gamma \ln(E_b/E_c) \quad (1)$$

where E_c is the calorimeter response for the calibration energy.

The other source of non-linear behaviour could be the shower leakage behind the detector. This causes two opposite effects: it decreases the detected energy due to leakage, but on the other hand, it can generate Cerenkov light in the fiber bundle just in front of the PMT.

The energy dependence of the resolution for sampling hadron calorimeter is described by two parameters: the stochastic and constant term. The first re-

fects the statistical fluctuation in the energy deposition by hadronic showers in the scintillating tiles. The second one is defined by intrinsic features of the calorimeter, like inter-calibration, nonuniformity in the light collection for different fibers in the cell, non-linear response due to shower fluctuations in depth, energy leakage, cracks and so on.

An analysis of the performance of $5.6 \lambda_I$ prototype from data that were obtained in the combined test run using the 40 MHz readout electronics, has been compared in detail with simulation results using different software packages for the simulation of hadronic shower development. The data have been fitted by the quadratic sum of the stochastic and constant term that result in $\sigma(E)/E = (79.2 \pm 2.9)\%/\sqrt{E} \oplus (10.11 \pm 0.45)\%$ as shown in Figure 1.

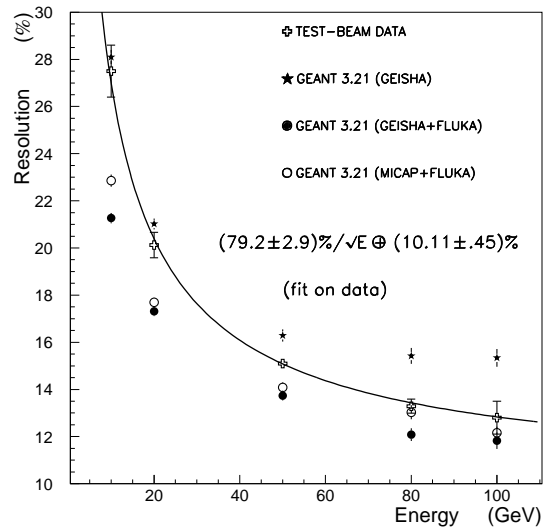


Figure 1: Resolution function on energy.

References

- [1] LHC-B Letter of Intent, CERN/LHCC 95-5.
- [2] The LHCb Technical Proposal, CERN/LHCC 98-4.

The relative non-linearity of pion and proton response with the ATLAS tile hadronic calorimeter

S. Constantinescu², S. Dita¹, Collaboration ATLAS

¹NIPNE-HH, Particle Phys. Dept.

²NIPNE-HH, Computing Dept.

The better understanding of the physics on which the hadron calorimeters are based and the analysis of the factors that determine their performances present a special interest and can be very useful in improving the existing simulation codes for hadronic showers.

In our previous comparative analysis of the Tile Calorimeter response to pions and protons we have shown that the ratio between pion and proton response has a value higher than unity for all the studied incident energies and pseudorapidities and the Monte Carlo simulations of the Tile Hadronic Calorimeter response, based on the G-CALOR hadronic shower simulation package [1], are in very good agreement with the data. We have concluded that our results are confirming the suggestion of Gabriel et al. [2], obtained by simulations, about the presence of a smaller pure hadronic fraction for pions than for protons since our calorimeter is non-compensating with $e/h > 1$.

Taking into account our previous results we have devoted a special interest to a detailed comparison of the relative non-linearity of the response given by protons and pions. In Figure 1, the normalized (to the 100 GeV point) relative non-linearity of the pion and proton response is shown as a function of the beam energy at different pseudorapidities. The very good linearity of the pion response can be seen. The non-linearity for pions seen in the experimental data is less than $\pm 1\%$ while the G-CALOR predicts also a good linearity for pions but the non-linearity ($\pm 2\%$) is slightly higher than the one obtained experimentally.

For protons the non-linearity of the response is a little higher than for pions and the better linearity of pions as well in the data as in G-CALOR simulations can be observed in Figure 1. This result can be seen for all the energies and all the pseudorapidities taken into account.

Expressing the relative non-linearity of pions (protons) of energy E - $R_\pi(E)$ ($R_p(E)$) - as a function of the pure hadronic fraction of pions (protons) F_h^π (F_h^p) and using the ratio between the pure hadronic fraction of pions and protons given by [2] :

$$F_h^\pi / F_h^p = 0.83 \quad (1)$$

we have obtained finally, taking into account the intrinsic constant of our calorimeter ($e/h > 1$), a smaller variation with the energy of the relative linearity for pions than for protons :

$$dR_\pi/dE < dR_p/dE \quad (2)$$

Thus, the better linearity of the pion response, seen as well in the data as in simulations, is another argument in the favor of the relation (1) given by Gabriel and al. [2].

Thus, firstly we have observed a higher calorimeter response to pions than to protons of the same energy and we have considered that this is an experimental confirmation of the result of Gabriel et al. [2] concerning a smaller pure hadronic fraction for pions than for protons. Now, the experimental data concerning the linearity of the response to pions and protons, confirm once more the smaller pure hadronic fraction for pions than for protons and even more, the obtained data about the linearity can be used as an argument in the favor of a similar energy dependence for the two hadronic fractions $F_h^\pi(E)$ and $F_h^p(E)$, e.g. for a constant ratio - $F_h^\pi(E)/F_h^p(E)$ - less than unity.

References

- [1] T.A. Gabriel and C. Zeitnitz, Nucl. Inst. and Meth. A 349 (1994) 106
- [2] T.A. Gabriel et al., Nucl. Inst. and Meth. A 338 (1994) 336

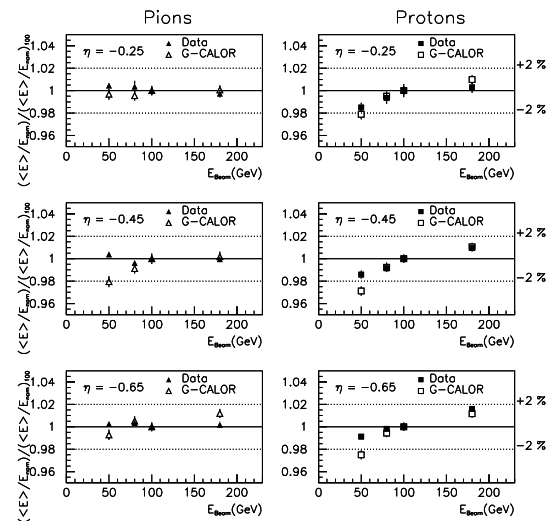


Figure 1: The normalized (to the 100 GeV point) relative non-linearity of pion and proton response as a function of beam energy at different pseudorapidities.

Transverse momentum distributions of J/Ψ , Ψ' , Drell-Yan and continuum dimuons produced in Pb-Pb interactions at the CERN-SPS

C. Alexa¹, V. Boldea¹, S. Constantinescu², S. Dita¹, Collaboration NA50

¹ NIPNE-HH, Particle Phys. Dept.

² NIPNE-HH, Computing Dept.

Muons pairs produced in Pb-Pb interactions at 158 GeV/c per nucleon are used to study the transverse momentum distributions of the J/Ψ , Ψ' and dimuons in the mass continuum. Preliminary results on the p_T distribution of J/Ψ mesons produced in Pb-Pb collisions have been published [1, 2]. In this report the analysis of p_T distributions of J/Ψ , Ψ' , Drell-Yan (DY) and muon pairs in the mass continuum between 2.1 and 2.7 GeV/c² (the intermediate mass region or IMR) are presented. The analysis uses the high statistics data sample of Pb-Pb collisions collected at the CERN SPS in 1996. A detailed description of the layout of NA50 experiment can be found in [3]. The present analysis is based on a new selection method, made possible thanks to the excellent 1996 beam conditions and to the different anti-halo detectors. Details on data taking conditions and event selection can be found in [4]. The final event samples contain 170.10⁶ triggers and $\sim 19.10^4$ J/Ψ events in 1996 and 60.10⁶ triggers and $\sim 5.10^4$ J/Ψ events in 1995.

In order to investigate the transverse momentum distributions of muon pairs produced as a function of the centrality of the collisions, the events are divided into subsamples according to the transverse energy of the collision, E_T . For J/Ψ and IMR events, the size of the samples allows 15 centrality bins, while for Ψ' and DY events, as well as for the J/Ψ events collected in 1995, the number of bins is limited to 5. The $\langle p_T \rangle$ and $\langle p_T^2 \rangle$ values have been determined for muons pairs of different origins: intermediate mass region (IMR), the J/Ψ and Ψ' decays and Drell-Yan mechanism. The $\langle p_T^2 \rangle$ values obtained for different mass intervals are plotted in Fig.1, as a function of E_T .

From the analysis we observed that the $\langle p_T^2 \rangle$ values for the Ψ' are higher than for the J/Ψ . For the J/Ψ the values $\langle p_T \rangle$, $\langle p_T^2 \rangle$, $\langle M_T - M \rangle$ and the inverse slope parameter, T, exhibit a similar trend as a function of E_T : an initial increase followed by a flatter behaviour. The comparison of the 1995 and 1996 results suggests that the $\langle p_T^2 \rangle$ values of the J/Ψ , for the most central events are not affected by

re-interaction effects due to the thickness of the target. The change of the p_T distributions with the centrality of the collisions agrees with what is expected from interactions in the initial state.

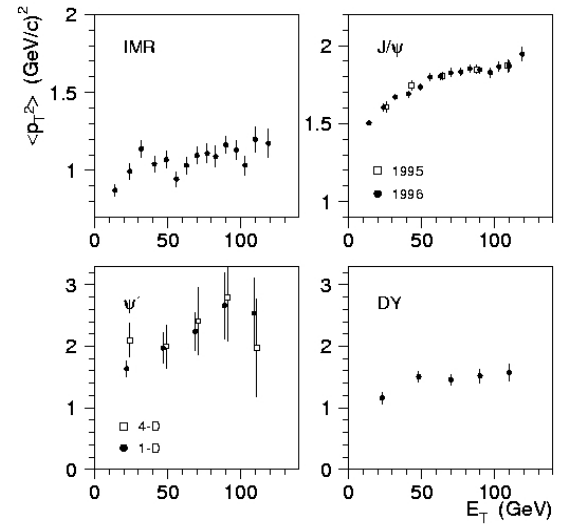


Figure 1: $\langle p_T^2 \rangle$ as a function of the transverse energy for several muon pair mass intervals. For the J/Ψ the 5 open squares correspond to the 1995 data sample. The error bars are only statistical. For Ψ' , both the 1-D and 4-D deconvolution results are shown.

References

- [1] NA50 Collaboration, M.C.Abreu et al., Phys.Lett. A 638 (1998) 261c;
- [2] NA50 Collaboration M.C.Abreu et al., Nucl.Phys. A 654 (1999) 640c;
- [3] NA50 Collaboration, M. C. Abreu et al., Phys. Lett. B 410 (1997) 327;
- [4] NA50 Collaboration M.C.Abreu et al., Phys. Lett. B 450 (1999) 456

ATLAS discovery potential study of the charged heavy leptons pair production via Drell-Yan mechanism

C. Alexa¹, S. Dita¹, Collaboration ATLAS

¹NIPNE-HH, Particle Phys. Dept.

The Z decay parameters measured at LEP have demonstrated that there exist only three light neutrinos coupling to the Z with Standard Model couplings. The simplest supposition is then that the lepton sector comprises these three light neutrinos and their charged counterparts. However, many theoretical models, such as composite models [1], left-right symmetric models [2], grand unified theories [3], technicolor models [4], superstring-inspired models [5], and models of mirror fermions [6], predict the existence of new particles with masses around of the scale 1 TeV and allow the possible existence of new generation of fermions. Charged heavy leptons pair production at LHC is dominated by the Drell-Yan process and by gluon-gluon fusion. The total production cross section for $pp \rightarrow \dots \rightarrow L^+L^-$ is presented in fig.(1). The studied process was $pp \rightarrow q\bar{q} \rightarrow Zl \rightarrow L^+L^- \rightarrow (e^+Z^0)(e^-Z^0)$ where $Z^0 \rightarrow dijet$, and $Br(L \rightarrow eZ^0) = 1/3$ according to [7].

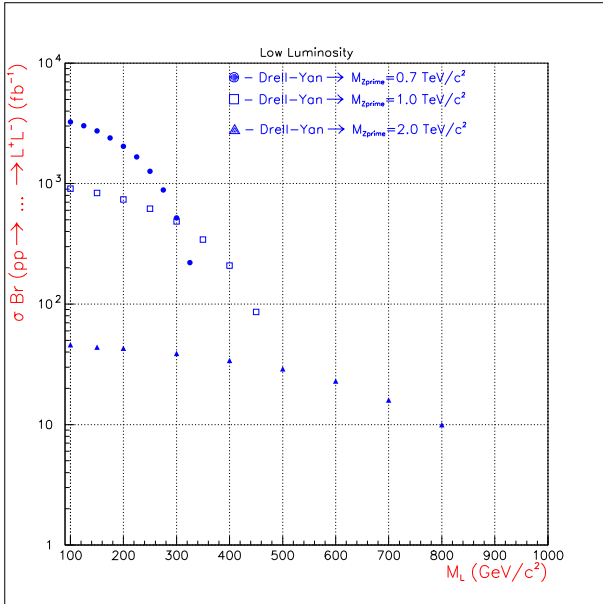


Figure 1: The total cross section for the charged heavy leptons pair production via Drell-Yan and gluon-gluon fusion mechanisms.

We have used PYTHIA [8] as the event generator and ATLFASST [9] for the detector response. The background is given by the production of: $t\bar{t}$, ZZ , WZ , W^+W^- , $ZQ\bar{Q}$. We succeed to reduced significantly the background by a selection based mainly on a best reconstruction of the two Z bosons and

$p_T^{miss} < 20 GeV$. In fig.(2) we present the obtained significance of the signal, for an integrated luminosity of $30 fb^{-1}$.

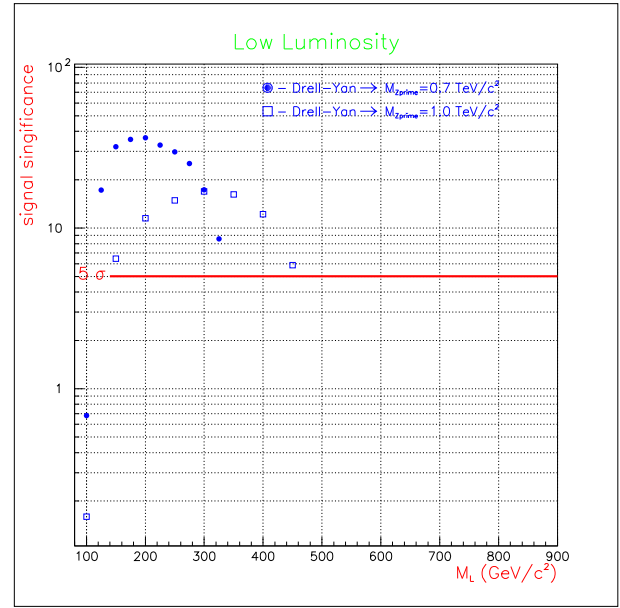


Figure 2: Signal significance for the charged heavy leptons pair production via Drell-Yan mechanism, the simulated process was $pp \rightarrow Zl \rightarrow L^+L^- \rightarrow (e^+Z^0)(e^-Z^0)$ and $Z^0 \rightarrow dijet$.

References

- [1] L. Abbot and E. Fahri, Phys. Lett **101B**(1981)69; Nucl. Phys. **B189**(1981)547
- [2] G. Senjanovic, Nucl. Phys. **B153**(1979)334
- [3] P. Langacker, Phys. Rep. **72**(1981)185
- [4] S. Dimopoulos, Nucl. Phys. **B168**(1981)69; J. Ellis et al., Nucl. Phys. **B182**(1981)529
- [5] J. L. Hewet and T. G. Rizzo, Phys. Rep. **183**(1989)193
- [6] J. Maalampi, K. Mursula and M. Roos, Nucl. Phys. **B207** (1982)233
- [7] G. Azuelos and A. Djouadi, Z.Phys. **C63**(1994)327
- [8] T. Sjöstrand, Comp. Phys. Comm. **82** (1994) 74
- [9] D. Froidevaux, L. Poggioli and E. Richter-Was, ATLAS internal notes PHYS-96-079 and PHYS-98-131.

Spin alignment of $K^*(892)^\pm$ mesons in nC interactions at 58 GeV

A.N. Aleev², T. Ponta¹, T. Preda¹, Collaboration EXCHARM

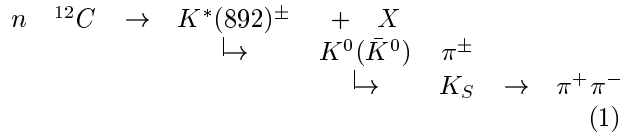
¹ NIPNE-HH, Particle Phys. Dept.

² JINR, Dubna

The inclusive hadroproduction of $K^*(892)^\pm$ has been studied since more than 30 years, but the role of meson spin in the production dynamics is still not understood in details. Spin phenomena in inclusive reactions with non-polarized beam and target are described by spin density matrix ρ of the final state particle. The ρ_{00} element represents relative intensity of vector mesons with zero z -component of the spin. A deviation of ρ_{00} from the value $\frac{1}{3}$ indicates spin alignment. A number of phenomenological models is suggested [1] to predict spin behavior in vector-meson inclusive hadroproduction.

The spin alignment of $K^*(892)^\pm$ mesons produced inclusively in neutron beam has been studied for the first time in the EXCHARM experiment [2]. The analysis has been performed using 184.4×10^6 neutron-carbon interactions recorded in the experiment.

The strange resonances $K^*(892)^\pm$ have been selected by their decays into neutral kaon and charged pion:



The neutral kaons have been identified via decays of short lived mode $K_S \rightarrow \pi^+ \pi^-$. A pair of opposite charged particles (V^0) has been considered as a K_S candidate depending on: distance between the V^0 tracks, momentum ratio of the positive track to the negative ones, Čerenkov identification of the particles.

Each combination of a K_S candidate with an additional track has been regarded as $K^*(892)^\pm$ candidate if it meets some geometrical and identification requirements.

Signals of decays have been estimated as a result of the $K_S \pi$ -mass spectrum approximation in the region of 0.74-1.20 GeV/ c^2 by the following expression representing a superposition of background $BG(M)$ and signal $BW(M)$ with relative rate a .

$$\frac{dN}{dM} = BG(M)[1 + aBW(M)]. \quad (2)$$

The evaluation of ρ_{00} is based on the vector-meson decay angular distribution

$$W(|\cos \theta|) = \frac{3}{2}[1 - \rho_{00} + (3\rho_{00} - 1)\cos^2 \theta], \quad (3)$$

where the angle θ is the polar angle of π^\pm momentum-vector in the decay $K^*(892)^\pm \rightarrow K^0 \pi^\pm$. The key assumption that the background has no spin alignment

and could be used for relative acceptance corrections has been proved independently.

The $K^*(892)^\pm$ inclusive production and the background have been simulated separately by FRITIOF model (with no spin alignment). Charged particle tracking through the setup was realized in GEANT-based program.

The obtained ρ_{00} dependences on P_T are shown in Fig.1.

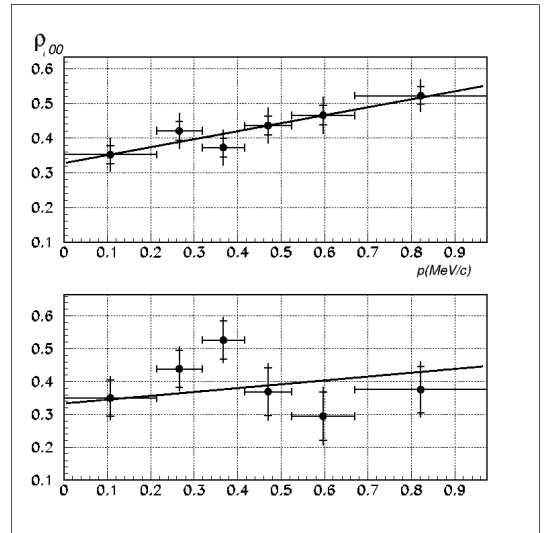


Figure 1: P_T -dependence of the spin density matrix element ρ_{00} for $K^*(892)^+$ (a) and $K^*(892)^-$ (b) in the transversity frame.

Spin density matrix element ρ_{00} for leading vector mesons $K^*(892)^+$ has been measured to be $\rho_{00} = 0.424 \pm 0.011(stat) \pm 0.018(sys)$. This value deviates from the value of $\frac{1}{3}$ indicating the spin alignment of $K^*(892)^+$ produced inclusively in neutron-carbon interactions at 57 ± 9 GeV.

References

- [1] T. DeGrand, H.I. Miettinen, *Phys. Rev.* **D24** (1981) 2419 ;
T. DeGrand, J. Markkanen, H.I. Miettinen, *Phys. Rev.* **D32** (1985) 2445.
- [2] A.N. Aleev et al. *Instrum. Exp. Tech.* **4** (1999) 1.

Health and Environmental Physics

Routine surveillance of environmental radioactivity in the influence area of the Institute during 2000

D. C. Breban¹, R. O. Dumitru¹

¹ IFIN-HH, Life and Environmental Physics Department

The radioactivity measurements were performed according to the Monitoring Concept for nuclear units in IFIN-HH, which provides the type, the locations and sampling frequency of the environmental factors that were analyzed.

The working group has been involved in a project supervised by the IAEA, concerning QA/QC for Nuclear Analytical Techniques.

Samples of water, sediment, soil, vegetation and aerosols have been analyzed for both gross beta and gamma activity, as follows: 1004 samples of potential radioactive water, surface, drinking and underground water; 18 sediment and 72 soil samples; 9 samples of spontaneous vegetation and 8 samples of milk, 3 samples of vegetables.

We analyzed for gross beta and gamma activity 42 samples of radioactive liquid effluents from the two nuclear units CPR and STDR.

Airsols samples have been monitored twice a month, the maximum concentration of the total beta activity was of 9.2 mBq per cube meter air (absolute error: 4.4).

Gross beta activity for samples of drinking water and surface water, was always below the maximum allowed concentration (1Bq/l), respectively below the the warning limit of 1.85 Bq/l.

The maximum value of the gross beta activity recorded for the sewage water (reactor Canal) was 1.92 Bq/l (absolute error: 0.22 Bq/l) (95influence on the

surface water downstream the spillflow was observed, gross beta value determined for this sample being below the detection limit (0.30)Bq/l.

Gamma spectroscopy analyses performed on annual composite samples of sewage water showed an average activity concentration for Cs-137 of 2.0mBq/l (absolute error: 0.5 mBq/l), values close to those determined for the surface water samples 4.2 (absolute error: 0.5).

Co-60 was detected in the sewage water and sediment collected at the sewage spillflow, with an activity concentration of 8.0.mBq/l (absolute error: 1.0 mBq/l) and 129Bq/kg (absolute error: 15 Bq/kg) dry mass, respectively.

For the surface water and sediment samples collected downstream the discharge site, the Co-60 concentration was of 5.5 mBq/l (absolute error: 0.9 mBq/l), respectively below the detection limit (9 Bq/kg).

Gross beta values for cultivated vegetation and milk samples collected from the living area were in the same range to those recorded in the previous years. The concentration level recorded was: 46 Bq/l (absolute error: 4 Bq/l) for milk samples, 55 Bq/kg (absolute error: 4 Bq/kg) fresh mass for tomatoes, 79 Bq/kg (absolute error: 7 Bq/kg) for cabbage, 152 Bq/kg (absolute error: 9 Bq/kg) of potatoes.

Since July, a trimestial surveillance of the Fort area has started. Samples of soil and vegetation were analyzed for gamma spectroscopy.

Large DNA analysis by pulse field gel electrophoresis

D. Fologea¹, O. Csutak²

¹ IFIN-HH, Life and Environmental Physics Department

² University of Bucharest, Faculty of Biology

Conventional gel electrophoresis of DNA molecules allows a good separation up to 50 kbp (kilobase pairs). However, in ordinary situations, all molecules larger than 20 kbp will present the same mobility in a static electric field, so that the separation seems to be impossible. The separation range could be extended reducing the agarose concentration to as low as 0.1% and the separation is allowed up to several hundreds kbp.

In order to overload these limits, a lot of researcher attempted to exploit the size-dependent relaxation, by periodically changing the orientation of the electric field, so that the DNA must change conformation and reorient before it can migrate in the direction of the electric field.

A lot of additional electric fields are involved in

pulse field gel electrophoresis. The simplest way to achieve large molecule DNA separation is to alternate two opposite electric field (Field Inversion Gel Electrophoresis). The switching interval and the electric field involved will give the final resolution.

The aim of this paper is to describe an experimental setup that allows a separation of DNA molecules up to 2 Mbp. For this, a fully computer controlled device was build. The parameters as time ramp, switching intervals and pause intervals for reverse and forward migration can be software varied. The test was performed using a *S. cerevisiae* 288C marker and DNA chromosomes extracted from yeast with xenodegradative capability. The results showed a separation limit up to 2.2 Mbp, comparable with other techniques of electrocaryotyping.

A metabolic derivation of tritium transfer factors in animal products

D. Galeriu¹, A. Melintescu¹, N. M. J. Crout², N. A. Bersford³, S. R. Peterson⁴, M. van Hess⁵

¹ IFIN-HH, Life and Environmental Physics Department

² Nottingham University, UK

³ CEH UK

⁴ LLNL USA

⁵ SCK-CEN Belgium

Tritium is a potentially important environmental contaminant arising from the nuclear industry. Because tritium is an isotope of hydrogen, its behaviour in the environment is controlled by the behaviour of hydrogen. Chronic releases of tritium to the atmosphere, in particular, will result in tritium-to-hydrogen (T/H) ratios in plants and animals that are more or less in equilibrium with T/H ratios in the air moisture. Tritium is thus a potentially important contaminant of plant and animal food products. The transfer of tritium from air moisture to plants is quite well understood. In contrast, although a number of regulatory agencies have published transfer coefficient values for tritium transfer from diet to a limited number of animal products, a fresh evaluation of these transfers needs to be made.

In this paper we present an approach for the derivation of tritium transfer coefficients which is based on the metabolism of hydrogen in animals in conjunction with experimental data on tritium transfer. The derived transfer coefficients separately account for trans-

fer to and from free (i.e. water) and organically bound tritium.

The predicted transfer coefficients are compared to available data independent of model development. Agreement is good, with the exception of the transfer coefficient for transfer from tritiated water to organically bound tritium in ruminants, which may be attributable to the particular characteristics of ruminant digestion.

We show that transfer coefficients will vary in response to the metabolic status of an animal (e.g. stage of lactation, digestibility of diet, etc.) and that the use of a single transfer coefficient from diet to animal product is not appropriate for tritium. It is possible to derive concentration ratio values which relate the concentration of tritiated water and organically bound tritium in an animal product to the respective concentrations in the animals diet. These concentration ratios are shown to be less subject to metabolic variation and may be more useful radioecological parameters than transfer coefficients.

Dose contribution from metabolized organically bound tritium after chronic tritiated water intakes in humans

A. Trivedi¹, D. Galeriu², E. S. Lamothe¹

¹ Chalk River Laboratories, AECL, Canada

² IFIN-HH, Life and Environmental Physics Department

Our earlier study of acute tritiated water intakes in humans has demonstrated that the dose contribution from metabolized organically bound tritium is less than 10% of the body water dose. To further demonstrate that the dose contribution from the organically bound tritium per unit intake of tritiated water is the same, regardless of whether the intake is acute (all at once) or chronic (spread over time), urine samples from six male radiation workers with chronic tritiated water intakes were collected and analyzed for tritium.

These workers have a well-documented dose history and a well-controlled tritium bioassay database, providing assurance that their tritium intakes were in the form of tritiated water. Each month for a full calendar year, urine samples were collected from each exposed worker. The monthly concentration of tritium-in-urine for each exposed worker was no lower than 104 Bq L⁻¹ but no higher than 105 Bq L⁻¹. These urine samples were analyzed for tritiated water and organically bound tritium to determine the ratio of these tritiated species in urine. The average ratio of tritiated water

to organically bound tritium in urine for each exposed worker was 330-129 (range, 297-589).

In calculating the dose to these workers, we assumed that, under steady-state conditions, the ratio of the specific activity of tritium (3H activity per gH) in the organic matter and water fractions of urine is representative of the ratio of the specific activity of tritium in the organic matter and water fractions of soft tissue. A mathematical model was developed and used to estimate the dose increase from the metabolized organically bound tritium based on the ratio of tritiated water to organically bound tritium in urine.

The resulting average dose from the organically bound tritium was 6.9-3.1% (range, 4.7-9.9%) of the body water dose for the six male workers, and agrees well with the value obtained from our acute tritiated water intakes study in humans. The observed dose contribution from organically bound tritium, relative to body water dose, is in agreement with current recommendations of assigning 10% of total body water dose for organically bound tritium in soft tissues after tritiated water intakes.

FDNH - the tritium module in RODOS

D. Galeriu¹, A. Melintescu¹, C. O. Turcanu¹, W. Raskob²

¹ IFIN-HH, Life and Environmental Physics Department

² IKET-FZK, Germany

Under the auspices of its RTD (Research and Technological Development) Framework Programmes, the European Commission has supported the development of the RODOS (Real-time On-line DecisiOn Support) system for off-site emergency management. The project started in 1989 focusing on PWR/LWR type accidents and using experience from the Chernobyl accident. In 1997 it was realised that tritium should be included in the list of radionuclides, as large tritium sources exist in Europe and to allow a potential expansion of the RODOS system for application on future fusion reactor accidents. The National Institute for Physics and Nuclear Engineering (IFIN-HH) in Romania - in close co-operation with the Research centre Karlsruhe (FZK) - was charged to develop the tritium module, based on previous experience in environmental tritium modelling and the operation of CANDU reactors in Romania (with potential tritium accidents).

At present, the Food and Dose Module Hydrogen (FDMH) - for tritium applications - is integrated and documented in the RODOS system. It calculates the time dependent tritium concentration (as tritiated water or organically bound tritium) in crops (as much as 22 different species) and up to 12 animal products, inhalation doses and ingestion dose from up to 34 diet items for various groups of the population and for up to 2520 locations around the source, following an accidental emission of tritiated water. FDMH incorporates many improved techniques in radiological assessment and makes intensive use of interdisciplinary research. It is developed in a modular structure with a variable time grid according to the physical processes. Differing from other models, using generic transfer parameters or parameters fitted on individual experiments, FDMH derives tritium transfer rates based on physical and physiological process anal-

ysis, using scientifically accepted results from interdisciplinary research on, among others, land-atmosphere interaction, water cycle in the soil-plant-atmosphere system, plant physiology, photosynthesis, growth and hydrogen metabolism in mammals. A unique feature of FDMH is the coherent modelling of tritium uptake by plant canopies and its conversion to organic matter, using a physiological plant parameter data base which can reproduce plant growth under various pedoclimatic conditions. By this approach, the difficulties of scaling from leaf to canopy are avoided and the model parameters are tested by concomitant reproduction of plant growth, using an appropriate crop growth model - developed at process level. In order to predict the tritium transfer in animal products in the absence of a complete experimental database, results from basic research on hydrogen metabolism in mammals is applied. Both forms of tritium are considered and the transfer and the conversion from tritiated water (HTO) or organics (OBT) in feed to HTO and OBT in animal products is explicitly introduced. Incorporating the environmental tritium dynamics with time steps ranging from less than one hour up to days, FDMH illustrates seasonal and diurnal effects on public dose related to the time of the accident. Due to the novel modelling approach, FDMH can be easily customised for any European site and can predict the time evolution of tritiated water or organically bound tritium in such details that it can be easily used in establishing countermeasures.

The present model as integrated in the RODOS platform contains a database for Central Europe but is not directly coupled to real-time weather prognosis data, due to external constraints. In order to increase the model flexibility and reliability some upgrades are now on going and an international, stand alone version is in preparation.

IFIN-HH occupational exposure monitoring in 2000

M. Puscalau¹

¹ IFIN-HH, Life and Environmental Physics Department

The Human Monitoring Laboratory from IFIN-HH, Life Sciences and Environment Department, performs its activity in accordance with the new National Basic Regulations on Radiological Safety. In 2000 it was accredited by the National Commission for the Control of Nuclear Activities on the basis of the Quality Manual respecting the requirements of SR EN 45001 Standard.

In 2000, a total of 527 persons from IFIN-HH and 72 from hospitals were monitored in order to identify and quantify the gamma emitting radionuclides - one of the source of human exposure.

The annual collective effective dose for all monitored workers from IFIN-HH, in 2000, amounts to 360.4 person-mSv. Table 1 gives the distribution of the workers and the annual collective effective dose for every Department from IFIN-HH, in 2000.

Also, very important from the radiation protection point of view is the Table 2 that gives the distribution of the annual effective dose for the personal from IFIN-HH, in 2000, in intervals of increasing dose.

Conclusion : no worker from IFIN-HH exceeded, in 2000, the annual effective dose limit for the occupational exposure, mainly the value of 20 mSv.

DEPARTMENT	PERSONS	COLLECTIVE EFFECTIVE DOSE (person-mSv)
TIESR	37	40
TANDEM	99	21.6
CPR	77	177
S220	29	9
CSMC	14	12.2
RN	36	5.4
S360	45	19.2
CICLOTRON	36	20.4
SUA	87	13
STDR	41	21.7
S140	52	17.5
RASPEN	10	3.4

Table 1: Department annual collective effective dose distribution

DOSE INTERVAL (mSv)	WORKERS CONCERNED
0 - 0.2	478
0.3 - 0.9	0
1 - 1.9	12
2 - 2.9	7
3 - 3.9	10
4 - 4.9	5
5 - 5.9	5
6 - 6.9	5
7 - 7.9	1
8 - 8.9	1
9 - 9.9	0
10 - 10.9	1
11 - 11.9	1
12 - 12.9	1
> 13	0

Table 2: Annual effective dose distribution

Consequence assessment of a hypothetical nuclear accident at Kozloduy NPP (VVER - 440) based on drill ("Oltenia-99", Romania)

G. Mateescu¹, D. Slavnicu¹, T. Craciunescu¹, C. Turcanu¹, A. Gheorghiu¹, D. Gheorghiu¹

¹ IFIN-HH, Life and Environmental Physics Department

In order to test and verify the results of the adaptation of RODOS expert system on Romanian conditions, an accident scenario at VVER 440 NPP (Kozloduy - Bulgaria) was considered which served as basis for the international drill "Oltenia 99". The drill was organized by Central Command Unit for Nuclear Accidents and Fall of Extra Atmospheric Objects (CCAN-COC) and was held in May 1999 under the monitoring of the International Atomic Energy Agency (IAEA). Using this accident scenario, the RODOS system functionality was tested on the Romanian database and the chief system performances were assessed in a critical manner.

The application consisted in using two modules of RODOS system (PRTY 3.13): QUICKPRO/ATSTEP for atmospheric dispersion and deposition calculations and EMERSIM/EARLYCONS for early emergency simulation.

The main objectives were to set up countermeasure areas, Fig.1 shows iodine tablets area, the committed effective dose for all pathways, the committed dose for thyroid and number of lethal cases in open air conditions, see Fig.2. In case of protective actions, the number of cancer deaths, as stochastic effects, is 3, instead of 10 when no actions were taken. That proves the beneficial impacts of protective actions.

The experience gained during the drill "Oltenia 99" showed that would be preferable that decision-makers receive the results of calculations in other place that RODOS operation place. Having in mind the complexity of the RODOS system, the further exercises and the application of the system in drills will help to adapt RODOS to actual needs of decision makers and also a special attention should be paid in the training of personnel who will operate the system.

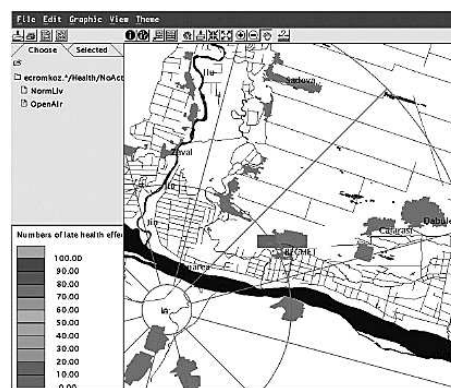


Figure 1: Iodine Tablets Area.

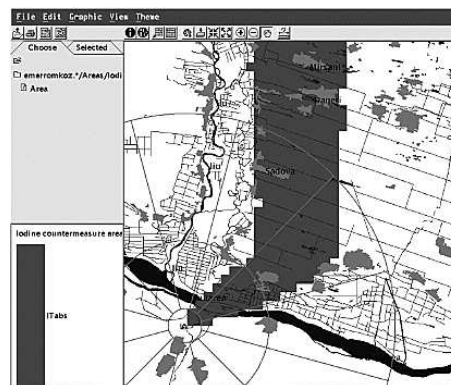


Figure 2: Cancer cases when no actions were taken.

A genetic approach to shape reconstruction in limited data tomography

C. Turcanu¹, T. Craciunescu¹

¹ IFIN-HH, Life and Environmental Physics Department

The paper proposes a new method for shape reconstruction in computed tomography. Unlike nuclear medicine applications, in physical science problems we are often confronted with limited data sets: constraints in the number of projections or limited angle views. The problem of image reconstruction from projection may be considered as a problem of finding an image (solution) having projections that match the experimental ones. In our approach, we choose a statistical correlation coefficient to evaluate the fitness of any potential solution. The optimization process is carried out by a genetic algorithm.

The algorithm has some features common to all genetic algorithms but also some problem-oriented characteristics. One of them is that a chromosome, representing a potential solution, is not linear but coded as a matrix of pixels corresponding to a two-dimensional image. This kind of internal representation reflects the genuine manifestation and slight differences between two points situated in the original problem space give rise to similar differences once they become coded. Another particular feature is a newly built crossover operator: the grid-based crossover, suitable for high dimension two-dimensional chromosomes. Except for the population size and the dimension of the cutting grid for the grid-based crossover, all the other parameters of the algorithm are independent of the geometry of the tomographic reconstruction.

The performances of the method are evaluated on a phantom typical for an application with limited data sets: the determination of the neutron energy spectra with time resolution in case of short-pulsed neutron emission (Fig. 1). The genetic reconstruction is presented in Fig. 2. The qualitative judgement and also the quantitative one, based on some figures of merit, point out that the proposed method ensures an improved reconstruction of shapes, sizes and resolution in the image, even in the presence of noise.



Figure 1: Phantom.

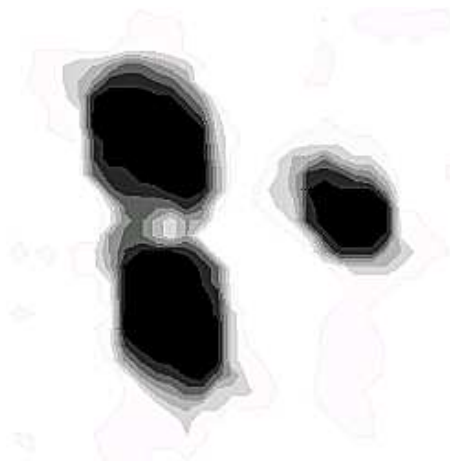


Figure 2: Reconstruction.

Applied Physics

Integrated graphical user interface for the back-end software sub-system

E. Bădescu¹, M. Caprini¹

¹ NIPNE-HH, Department of Applied Nuclear Physics

The ATLAS data acquisition and Event Filter prototype "-1" project [1] was intended to produce a prototype system for evaluating candidate technologies and architectures for the final ATLAS DAQ system on the LHC accelerator at CERN. Within the prototype project, the back-end sub-system encompasses the software for configuring, controlling and monitoring the data acquisition (DAQ).

The back-end sub-system includes core components and detector integration components. One of the detector integration components is the Integrated Graphical User Interface (IGUI), which is intended to give a view of the status of the DAQ system and its sub-systems (Dataflow, Event Filter and Back-end) and to allow the user (general users, such as a shift operator at a test beam or experts, in order to control and debug the DAQ system) to control its operation.

The functional, constraint and quality user requirements for the IGUI are presented in [2]. The IGUI is intended to be a Status Display and a Control Interface too, so there are three groups of functional requirements: display requirements (the information to be displayed); control requirements (the actions the IGUI shall perform on the DAQ components); general requirements, applying to the general functionality of the IGUI. The constraint requirements include requirements related to the access control (shift operator or expert user). The quality requirements are related to the portability on different platforms.

The IGUI has to interact with many components in a distributed environment. The following design guidelines have been considered in order to fulfil the requirements: use a modular design with easy possibility to integrate different sub-systems; use Java language for portability and powerful graphical features; use CORBA interfaces for communication with other components. The actual implementation of Back-end software components use Inter-Language Unification (ILU) for inter-process communication. Different methods of access of Java applications to ILU C++ servers have been evaluated (native methods, ILU Java support, Java IDL). Finally Java IDL was chosen, having as main advantage the independence of CORBA implementation.

The interaction between the IGUI and other back-end components is presented in [3]. The IGUI reads the list of partitions from the Inter Process Communication (IPC) server and the user can select one of them. In interaction with the Resource Manager server the type of the access control is decided. The run

control and data-flow configurations are read from the configuration database. The information about the sub-systems or components status (run control status, lists of Process Manager agents and processes, Data-Flow modules statistics) is read from the Information Service (IS) or is automatically obtained using the IS notification mechanism. The run parameters can be set by the user and are stored in the Information Service server. Through the IGUI the user can send commands to the Run Control main components (DAQ Supervisor and Root Controller). The user can send commands to the MRS (to change the filter or subscription criteria, to set the log control). The IGUI can be a client of the Process Manager, allowing to start auxiliary processes (monitoring tasks, bookkeeping tasks, etc).

IGUI is designed as a Java application (JFrame). On the left side of the frame are displayed the Main Commands and below some major Run Parameters, such as run and event number. On the right side can be chosen different Panels: Run Parameter panel, showing all the run parameters and allowing user to set them; Run Control panel (tree and status for each controller with the possibility to send commands to a particular controller); DAQ Supervisor panel (DAQ Supervisor expert commands); Process Manager panel (list of PMG agents and processes); MRS panel; Data Flow panel (data flow configuration and parameters). Other panels could be added, displaying the status of other DAQ components or sub-systems. On the bottom of the main frame there is a MRS message display panel, showing all the received MRS messages.

References

- [1] G.Ambrosini et al., "The ATLAS DAQ and Event Filter prototype "-1" project", Computer Physics Communications, vol. 110, pp. 95-102, May 1998.
- [2] S. Camara, M. Caprini, L. Moneta, "User Requirements for the Integrated Graphical User Interface of the Atlas DAQ/EF Prototype -1", ATLAS DAQ Technical Note 144, <http://atddoc.cern.ch/Atlas/Notes/144/Note144-1.html>
- [3] "DAQ/EF Prototype -1 Project Back-End Summary Document", ATLAS Note ATLAS-DAQ-2000-001, <http://documents.cern.ch/cgi-bin/setlink?base=atlnot&categ=Note&id=daq-2000-001>

Quality assurance and quality control of nuclear analytical techniques

Emanuela Cincu^{1,2}

¹ Technical responsible of the Romanian Project

² NIPNE-HH, Department of Applied Nuclear Physics

Background: Test and analytical laboratories in East and Central European countries need to prove the reliability and credibility of their economic, environmental, medical and legal decisions and their capacity of issuing reliable, verifiable reports. These demands imposed by the European Community aimed at avoiding a possible barrier to trade for the developing countries. In June 1999, in order to help Member States to develop according to EU objectives and the overall situation of the European market, the International Agency for Atomic Energy (IAEA) launched a new co-operation programme designed to help the nuclear analytical laboratories in nuclear institutions and universities of Member States by training in the use of some Nuclear Analytical Techniques (NAT) that include: alpha, beta and gamma-ray spectrometry, radiochemical and neutron activation analysis, total reflection X-ray fluorescence.

Project objective: The Regional IAEA Project, named "Quality Assurance/Quality Control of Nuclear Analytical Techniques" (NAT) aims at implementing the QA principles via a system of defined consecutive steps leading to a level on which the QA system is self-sustainable for formal accreditation or certification and satisfies the EU technical performance criteria; the requirements are in accordance with the new ISO/IEC 17025 Standard/Dec.1999 "General requirements for the competence of testing and calibration laboratories" - First edition.

Participation of IFIN-HH: The Horia Hulubei National Institute for Nuclear Physics and Engineering was admitted for participation in the IAEA Project in June 1999 account taken of its experience in the QA and metrology fields and its performance in the fields of beta and gamma-ray spectrometry, and radiochemical and neutron activation analysis, employed in both basic research and applications for external clients. Two working groups of specialists with the QA and Standardization & Metrology Departments and six analytical groups with the departments of Nuclear Applied Physics, Life Physics and Ionising Radiation Metrology are involved in the RER 2/004 Project. The latter 6 groups deal with gamma-ray spectrometry, analysis of the total beta-ray spectrum, neutron activation and radiochemical analysis.

Project plan: IFIN-HH follows the IAEA Project plan consisting of participation in the IAEA training workshops and proficiency tests and elaboration of QA

documents 2-3 times /year. In the year 2000 we elaborated part of the QA technical operation procedures and QA Procedures of general interest, namely: "Organization, Sample registration", "Report of results", "Relations with Clients" and other QA-Procedures according to the ISO/IEC 17025 Standard. In April - May 2000 all analytical working groups successfully participated in the Proficiency Test 1 organized by IAEA. The 2nd series of Proficiency Test measurements are scheduled for May-June 2001.

The Progress Report no.2 (the 3rd in the PR series) was the last document prepared in 2000; by means of the last 4th and 5th Progress Reports that will be prepared in April-June 2001 the contents of the typical accreditation dossier of each group taking part in the Project will be established. The QA System and QA Manual (previously elaborated according to European Norms 45001), will also be updated according to the ISO/IEC 17025 Standard requirements.

The final objective of the activity in 2001 (the last year of the project) consists of preparing valid "accreditation dossiers" with a view to securing certification/accreditation from the national accreditation/regulatory body; we need to operate efficiently and effectively and as soon as possible on a certified basis and ensure high performance in the current applications on the clients' samples coming from various fields, including medicine, environment, industry, forensics, geology and archeology.

After the previous steps and evaluations by IAEA experts, IFIN-HH got a quite good position, ranking 5th among the participating countries. Also due to its deep involvement in the Project, IFIN-HH proposed to IAEA to organize a training course on internal auditing, which plays a major part in the efficient and credible implementation of a QA System. As a result, IFIN-HH is pleased and honored to organize the first International Workshop on Internal Auditing that will be held May 2001 in Bucharest under auspices of the International Atomic Energy Agency.

Participating in the "QA/QC of Nuclear Analytical Techniques" project is part of our Institute's efforts to keep up with the European QA level in applications, as well as in the Standardization & Metrology fields; the training and accreditation of the analytical laboratories involved in the project will improve the institute's credentials as to the current offer of the nuclear field to modern Romanian society.

The conclusions on the Th internal contamination by ingestion using animals

M. Ciubotariu¹, A. Danis¹, G. Dumitrescu²

¹ NIPNE-HH, Nuclear Engineering and Vacuum Department

² NIPNE-HH, Life Sciences Department

The paper presents the results obtained in the Th internal contamination study by ingestion. We investigated the Th biodistribution, retention and elimination using the fission track method as high sensitivity analysis method and Wistar-London breed rats as experiment animals.

Three Wistar-London breed rats (RAT 1, RAT 2 and RAT 3) were contaminated with a Th amount corresponding to an Annual Limit Intake using a Th solution. The animals, up to their sacrifice, were kept in normal life conditions and under permanent observation. The rats were sacrificed at different time intervals after their contamination: RAT 1 = 2 days, RAT 2 = 7 days and RAT 3 = 14 days, respectively. Immediately, after sacrifice, the vital organs of the rats were sampled. These samples were weighed, calcined and re-weighed. The evacuations, for each of the three rats, were sampled every 24 hours: urine on the filter paper and all excrements balls. These samples were weighed before and after calcination. The organs and the elimination samples were analysed by track detection using the fission track micromappings technique.

The fission track method is the method which can visualize the distribution of the investigate fissionable element (U, Th, etc.) in the vital organs of the contaminated rats. This advantage of the fission track method, used in our experiment, led us to conclude:

- the Th was retained in all vital organs of the contaminated rats, in particularly in liver, lung, stomach and small intestine;
- all investigated organ samples presented a non-uniform Th distributions, but only the RAT 1 organs presented a lot of inclusions which were

ranging from 1 ppm up to 24 ppm Th concentrations. For the others two rats, the Th distribution were non-uniform too, but without inclusions. The absence of inclusions for the RAT 2 and RAT 3 which were sacrificed at 7 days and 14 days, respectively, after contamination shows that the rat organisms tend to gather the Th in inclusions because Th is considered as "intruder element" and must be eliminate;

- the elimination of the Th intake was higher by urine than by excrements. For all rats, Th was eliminated in proportion of aprox. 98 per cent in the first three days after their contamination. The micromappings of the elimination samples during these three days presented a non-uniform Th distribution with a lot of inclusions with concentrations were ranging from 35 ppm up to 1300 ppm for the urine samples and from 6.6 ppm up to 28.9 ppm for the excrements samples;
- from the medical state point of view, the blood test, for the three rats internal contaminated by ingestion with Th revealed the normal values of the hemoglobin and a exponential increase of the leukocyte values (leukocytosis) without toxic granules.

It is note that the results obtained in the study of Th internal contamination by ingestion using the fission track method could be useful and important in a conception of certain biological and medical studies regarding internal contamination with fissionable elements (U, Th, Pu, etc.) which require a numerous subjects for investigation. For such studies our data can be helpful for the establishing the steps as well as the critical organs which need to be investigated.

Use of the Coulomb excitation by light and heavy ions for quantitative analysis

L. Craciun¹, E. Dragulescu², P.M. Racolta¹, C. Serbanut², V. Tripadus¹

¹ NIPNE-HH, Applied Nuclear Physics Department

² NIPNE-HH, Nuclear Physics Department

It is well known in many cases thin layers with specific properties fulfil the same demands as former bulk materials and, although they seem to be more expensive, the general tendency has proven them to be cheaper. Therefore it might be a permanent task for physicists to develop methods, so far only applied in scientific laboratories, to a standard that might be feasible and economically justified to use them to a much larger extent. The reason for the very slow introduction of new analytical techniques is certainly the fear that instruments and apparatus used in basic research do not fulfil the standards of reliability, permanent availability and easy handling, which are important requirements for industrial applications [1 - 3].

The knowledge of the slowing down of ions in traversing matter is of fundamental importance in methods of materials analysis using beams of charged atomic particles, Depth perception follows directly from the energy lost by the probing particles and the energy loss affects both quantitative and compositional analysis. The physics of energy loss phenomena is very complex, involving many kinds of interactions between the projectile ion, target nuclei, and target electrons. Because of their significance in many fields of physics, these phenomena have been subject to intense studies since the beginning of the century. The theoretical treatment has been reviewed, among others, by Bohr (1948), Whaling (1958), Fano (1963), Jackson (1962,1975), Bichel (1970), Sigmund (1975), Ahlen (1980), Littmark and Ziegler (1980), Ziegler (1977, 1980), Ziegler et al. (1985). The experimental methods have been reviewed and investigated by, e.g., Chu (1979), Brauer (1987), Mertens (1987), Powers (1989).

- Two well known phenomena can be used for the production of γ -rays in bombardments with charged projectiles:

a) nuclear reactions involving incident energies near and above the Coulomb barrier; in this case γ -rays arise from the de excitation of the product nuclei.

b) Coulomb excitation for incident energies below the Coulomb barrier; here the excitations of the nucleus by the interaction of its Coulomb field with that of the bombarding nucleus is a purely electromagnetic process. In the first stage of this project, the theoretical considerations and their consequences for analytical possibilities will be considerate. The overwhelming majority of the excitations in the Coulomb exci-

tation are the electricquadrupole transitions (E2). All particularities of this type of transitions will be evaluated.[4,5]. 8A dedicated beam line with the target chamber and spectrometric setups has been realized and experimented, in order to compete with European standards . The experimental thick-target yields and detection limits for 20 elements in many matrices will be analyzed. Coulombian excitation by different charged particles, like p, ⁹Be, ¹¹B, ¹⁴N, ³⁵Cl will be experimented.

- A special attention will be allocated for CE by heavy ions (³⁵Cl, 55 MeV). For this quantitative analysis, because of the energy range, the used formulae from the Bethe equation for stopping power cannot be applied and then we propose a new methodology after the actual programs and theories [7,8,9].

- To test the validity of our approximation, some standard samples from the " Bureau Communautaire de Reference" in Brussels will be used. The heavy-ion beams will be produced at the IFIN-HH Tandem, 8 MV on terminal.

References

- [1] K.Bethge, Accelerators in materials research, (1995 Kluwer Academic Publishers, Proceedings of the NATO Advanced Study on "Application of Particle and Laser Beams in Materials Technology", 287-381
- [2] J.P.F. Sellschop, S.H. Connell, Elemental isotopic and structural analysis using ion beams, Nucl. Instr. Methods in Phys. Res.B85 (1994), p.1-20
- [3] G. Blondiaux, J.L. Debrun, Charged particle activation analysis, Ed. J.R.Tesmer, M.Nastasi, 1995, Materials Research Society, 9800 McKnight Road, Pittsburg, PA 15237 USA, p. 205-230
- [4] B. Borderie, J.N. Barrandon, B. Delaunay, M. Basutcu, "Use of Coulomb excitation by heavy ions (³⁵Cl, 55 MeV) for analytical purposes: possibilities and quantitative analysis", Nuclear Instrument Methods 163, 1979, p.441-451
- [5] E. Dragulescu, M. Ivascu, R. Mihiu, D. Popescu, G. Semenescu, Coulomb excitation of levels in ¹⁴³Nd and ¹⁴⁵Nd Nuclear Physics A 419 (1984); 148-162.

On the radioactivity of water and sediments from the Danube river significant cross sections during autumn 1998

I.I. Georgescu¹, Gh.D. Baran¹, A.I. Pantelica², M.N. Salagean², A.G. Scarlat²

¹University "Politehnica", Faculty of Industrial Chemistry

²NIPNE-HH, Department of Applied Nuclear Physics

Gamma-ray spectrometry method was used to determine ^{137}Cs , ^{226}Ra , ^{228}Ra and ^{40}K activity concentrations of bottom sediments and surface water (suspended matter) collected from significant verticals of two Danube cross sections by the National Institute of Meteorology and Hydrology (INMH) in Bucharest, during November 1998. The Danube cross sections studied were Bazias, km 1072.4 (at the Danube entrance in Romania) and Ceatal Izmail, km 80.9 (at the beginning of Danube delta). Five significant verticals at Bazias (from the left bank to the middle of the river) and nine at Ceatal Izmail (from the right bank to the left one) were investigated. Numeration of these virtual (approximately equidistant) verticals (V_i) starts from the Romanian bank (the left side at Bazias and the right side at Ceatal Izmail). The same "packet" of water was considered in the two locations at a time interval of 8 days.

For ^{137}Cs , a higher mean level was found at Bazias than at Ceatal Izmail (of about 2 times for sediments, and 2.7 times for water). ^{137}Cs maximum values of (12.70.5) Bq kg⁻¹ in sediments and (8.81.8) Bq m⁻³ in water were determined.

Concerning the natural radioactivity of ^{226}Ra , ^{228}Ra and ^{40}K , maximum values of (40.10.5) Bq kg⁻¹ for ^{226}Ra , (43.01.5) Bq kg⁻¹ for ^{228}Ra and (61212) Bq kg⁻¹ for ^{40}K in sediments at Ceatal Izmail were measured. For sediments, the ^{226}Ra , ^{228}Ra and ^{40}K mean

levels were determined to be higher at Ceatal Izmail than at Bazias (of about 1.6, 1.7 and 1.5 times, respectively), while for water no notable differences between the two cross sections were observed.

The variation of the radioactivity on different significant verticals of the investigated cross sections was put in evidence in the case of sediments. For ^{137}Cs , activity concentration values at Bazias are found to be similar with those at Ceatal Izmail on verticals from the same (left) side of the river, except for V_3 of about 3 times higher. At Ceatal Izmail, a rather constant level was measured for ^{137}Cs , except for the verticals from V_1 to V_3 on the right side of the river, with values of about 8 times lower. Concerning ^{226}Ra , ^{228}Ra and ^{40}K in sediment samples, at Ceatal Izmail higher levels (of about 1.5-2.5 times) were determined on the verticals from V_1 to V_3 . At Bazias, approximately uniform distribution was found for ^{226}Ra and ^{228}Ra , while values of about 2 times higher were determined for ^{40}K on the verticals c (the left and central part of the river).

In the case of water, no significant variation was determined, except for ^{226}Ra at Ceatal Izmail, with a higher level on the verticals V_1 and V_2 (maximum of (37.6 4.5) Bq m⁻³ on V_1).

The radionuclide distribution in a cross section can be correlated with the mineralogical structure of the bed river and the possibility to retain ions in the crystallographic lattice.

Instrumental neutron activation analysis of some fossil samples from romanian sites

A.I. Pantelica¹, M.N. Salagean¹, I.I. Georgescu², M.D. Murariu-Magureanu², A.G. Scarlat¹

¹ NIPNE-HH, Department of Applied Nuclear Physics

² University "Politehnica", Faculty of Industrial Chemistry

During the fossilization process, elemental contents of the buried materials are modified by different physical, chemical and biological factors, such as ground water flow and degree of aeration, chemical composition of the soil, bacterial activity, the process being influenced by the climatical conditions. Bone tissue, by the calcium phosphate mineral (hydroxyapatite) in the external part and organic component (fat and collagen) in the inner part, has proved to be a proper substrate for minor elements accumulation. The uniform increasing of certain elemental concentrations during the fossilization process is generally used in paleoscience for the age dating 1-4.

Instrumental neutron activation analysis (INAA) method was used by us to investigate Al, As, Au, Ba, Br, Ca, Co, Cr, Cs, Fe, Hf, K, Mg, Mn, Na, Ni, Rb, Sb, Sc, Se, Sr, Th, U, V, Zn, and of the rare earth elements Ce, Eu, La, Lu, Nd, Sm, Tb, Yb contents of two different fossil materials discovered in Romania during 1995-1996: *Elephas primigenius* mammoth mandible bone (1.5-2 million years age) and *Pecten solarium* shell (20-25 million years age). Mammoth mandible bone samples were taken both from the external and the internal part of the bone. Shell fragments were taken in association with the surrounding rock samples. Irradiations were carried out at the VVR-S reactor in Bucharest (neutron fluence rate $2.3 \times 10^{12} \text{ cm}^{-2} \text{ s}^{-1}$) and at the TRIGA reactor in Pitesti (neutron fluence rate $5 \times 10^{13} \text{ cm}^{-2} \text{ s}^{-1}$).

For the mammoth mandible bone (relative high contents of U and P) corrections were done for the uranium fission and $(n,\gamma)\beta^-$ contribution to Ce, La, Nd and Sm concentrations, and for the phosphorus interference in Al determination. It was taken in account that ^{141}Ce , ^{140}La , ^{147}Nd , ^{153}Sm isotopes are originated not only by the neutron activation reactions of these elements, but also from the β^- decay chains of the uranium fission products; for ^{153}Sm , spectral interference with 103.65 keV X-ray of ^{239}Pu (by β^- decay of ^{239}Np from uranium $(n,\gamma)\beta^-$ activation reaction) occurs⁵. In the case of Al, phosphorus interference is due to the $^{31}\text{P}(n,\alpha)^{28}\text{Al}$ reaction.

The majority of the analyzed elements in mammoth mandible bone are found to be in a higher concentration in the external than in the internal part of

the bone: the highest concentration ratios are determined for the rare earths elements Tb (147), La (84), Eu (80), Ce (76), and relative high concentration ratios are obtained for Nd (38), Sc (30), Lu (20), Yb (14), U (12.5), Co (11.4). Lower concentrations in the external part of the bone, in rapport to the internal part were determined only for Al, Rb, K and Sr, while about the same concentration values were measured for Ca and Mg. Uranium content of $(320 \pm 8) \mu\text{g g}^{-1}$ was found comparable to $610 \mu\text{g g}^{-1} \text{U}_3\text{O}_8$ of the *Elephas planifrons* bone from the Pleistocene period¹. It is in agreement with the anthropological estimated age for the analyzed mammoth sample.

For the shell fossil, by comparing with recent marine shells from the Romanian Black Sea coast, elemental concentrations correspond to the following ratios: Sc (67), Eu (20), Cr (16.5), Co (15.8), Fe (14.3), Al (11), Zn (10.8), Sm (8.1), Ce (5.1), Ba and La (4.1), Mn (3.8), Th (2.3), Mg (1.7); similar concentrations were determined for Ca and Na, while a lower value for Br (ratio of 0.025) was obtained.

This is a preliminary study of the Romanian fossils from the Tertiary era, in order to try a correlation between the anthropological estimated age and the microelemental contents.

References

- [1] Z. Goffer, *Archaeological Chemistry*, ch. 16, John Wiley&Sons. Inc., N.Y., 1980.
- [2] R.B. Parker, H. Toots, *Geological Society of America Bulletin*, Vol. 81 (1970) 925.
- [3] Cs.M. Buczko, J. Czikai, J. Nemeskery, *Acta Physica Academiae Scientiarum Hungaricae*, 53, (1-2) (1982) 165.
- [4] G. Wesse, F.H. Ruddy, C.E. Gustafson, H. Irvin, *Archaeological Chemistry II*, Giles F. Carter, Editor, Eastern Michigan Univ., *Advances in Chemistry Series*, 171 American Chemical Society, Washington DC, 1978.
- [5] P. Ila, P. Jagam, G. K. Muecke, *J. Radioanal. Chem.*, 79 (1983) 215.

The preliminary studies on production of Pd-103 therapeutic isotope at the U-120 cyclotron

D. Dudu¹, V. Popa², P.M. Racolta³, Dana Voiculescu³

¹ NIPNE-HH, Cyclotron Laboratory

² NIPNE-HH, Nuclear and Vacuum Engineering

³ NIPNE-HH, Applied Nuclear Physics Department

All the radioisotopes used in nuclear medicine are produced artificially using either a nuclear reactor or a cyclotron. By attaching suitable chemical labels to the radioisotopes, radiopharmaceuticals are obtained, which can be made to seek a desired organ by taking part in the metabolic processes. When radiopharmaceuticals are injected into the human body and specifically taken up by an organ of choice, a lack of uptake, or delay in uptake, denotes loss of function in the organ [1,2].

Therapeutic radioisotopes are used in a range of different techniques and which can be divided into teletherapy, brachytherapy or radiopharmaceutical methods.

Although the majority of the radioisotopes used in nuclear medicine have been produced from research reactors for over 45 years and the methods are generally well established, several new initiatives and developments have occurred recently.

One example is ^{103}Pd which is one of the few accelerator generated isotopes to be in common use for therapy, in this case as a short-lived isotope for permanent implant treatment of prostate cancer. Historically, ^{103}Pd used to be generated via the $^{102}\text{Pd}(n,\gamma)^{103}\text{Pd}$ reaction which relied on the availability of 1% naturally abundant ^{102}Pd in an enriched form and its moderately high neutron capture cross section. However this method would not produce sufficient amounts of this short-lived isotope, which needed regular, supply cycle of 2-4 weeks. So a new method was devised based on the reaction $^{103}\text{Rh}(p,n)^{103}\text{Pd}$ by using the accelerators with rather low energy protons (8-18MeV). Starting with 1987 the encapsulated ^{103}Pd source became commercially available in the USA, where a company now operates more than 10 dedicated accelerators to produce this nuclide. Recently a manufacturer in Europe also brought his patent type of ^{103}Pd seed implants to the world market [1,2].

The primary objective of the present Project is to extend the related applications for radioisotope production of our U-120 Cyclotron (p, d, 14MeV max. energy). The preliminary experiment were made using the stacked foil activation technique. Four stacks containing high purity 25 μm thick Rh foils were irradiated in the external beam of the U-120 Cyclotron. The incident energy of protons was 14MeV. The X-ray complexes of the de-excitation of the ^{103}Rh daughter

nuclei (K α and K β) and γ -line 39.7keV were analyzed.

Specific technologies will be developed for the construction materials used in production target, target chemistry, the transport and interaction of particle beams and irradiation conditions. The existing technology, in the world, for the electrodeposition of Rh onto metal plates (Cu, Al etc.) and chemical removal of Rh, the electroplating of Pd on graphite sheet or an adsorption of Pd on a resin will be studied also.

It is also expected that using theoretical and experimental investigation carried out in the framework of this project, the existing knowledge related to the cross-section and yield of nuclear reactions: $^{103}\text{Rh}(p,n)^{103}\text{Pd}$ and $^{103}\text{Rh}(d,2n)^{103}\text{Pd}$ well be extended.

A special attention will be paid to the collaboration between our institute and medical research centers in order to perform, for the first time in our country, this ^{103}Pd clinical using and to establish the standard procedures for its uses. ^{103}Pd is a short-lived radioisotope and therefore is very difficult to obtain it from other countries. The production cost of this isotope will be an important aspect. The research will be finalized with quality assurance (QA) procedure standards. According to specific objectives mentioned above, the work plan for this project is the following:

A) Design and adaptation of a dedicated beam line at IFIN-HH Cyclotron for the ^{103}Pd experiments.

B) Experiments to choose the optimum beam parameters and to select between protons and deuterons beams.

C) Experiments to choose and optimise the target and irradiation conditions.

D) Experiments to establish the procedures for the post irradiation characterization of the ^{103}Pd radioisotope according to the radiobiologic rules and the requests of medical specialists.

This project is partially financed by AIEA Vienna.

References

- [1] M.S.Porazzo at all., Int. J. Radiat. Oncol. Biol. Phys. 23(1992)1033
- [2] A. Hermanne at all., Study on production of ^{103}Pd and characterisation of possible contaminants in the proton irradiation of ^{103}Rh up to 28 MeV, NIM B 170(2000)281-292

Project of positron source at the U-120 cyclotron Bucharest. Status report

L. Craciun¹, D. Dudu², N. Miron³, V. Popa⁴, P.M. Racolta¹, V. Tripadus¹, Dana Voiculescu¹

¹ NIPNE-HH, Applied Nuclear Physics Department

² NIPNE-HH, Cyclotron Laboratory

³ LISES-Laboratory, Chisinau, Moldova

⁴ NIPNE-HH, Nuclear and Vacuum Engineering

Positron annihilation spectroscopy has emerged as a highly sensitive, nondestructive probe to study the nature, concentration and spatial distribution of defects in materials [1-9]. The U-120 cyclotron is a classical variable energy machine, 120 cm diameter magnetic poles, able to accelerate protons and deuterons up to 14 MeV and α -particles up to 27 MeV.

The ⁴⁸V and ²²Na positron sources production dedicated to off-line experiments has basically two options for placing the Ti and Mg foil targets. The first is to place the target inside the cyclotron's chamber, just near the extraction plate.

The second position is in the beam line, immediately after the first group of two focusing lens, where the beam intensity may reach 20 μ A. The reactions used were ⁴⁸Ti(p,n)⁴⁸V and ²⁴Mg(d, α)²²Na, the incident proton and deuteron beams energy was 14 MeV.

We used these sources for testing the performances of our installations and detectors in Doppler broadening measurements on copper, lead, aluminium and indium. The ²²Na source will be used in positron lifetime measurements with a fast coincidence device equipped with two fast detectors from LISES - Laboratory - Moldavia [10, 11].

The positron source project is now in its initial stage. Our target proposal is basically a thin aluminium disk foil fixed between two aluminium plates, all rotating with a speed around 5 rev/s in the beam. We chose this solution with the rotating foil, because it looks more reliable than a fixed thin foil cooled by some fluid. The nuclear reaction ²⁷Al(p,n)²⁷Si with decays β^+ 100% by emitting positrons having the maximum energy at 3.85 MeV with a half-time of 4.16 s will be used. For radiation dose reasons, it is recommended to place this target inside the cyclotron's room and to drive out the positron beam only.

The positron beam has to be transported out of the cyclotron's room, where the radiation level is very high, into another experimental room, to assure low background for performing high accuracy

measurements.

This transport line will be designed in the next stages of the project. One solution we are analyzing now is the bunching after the electrostatic extraction system and then accelerating it in a chain of resonant cavities, in order to compress the transportation efficiency.

For annihilation experiments we need to tune the incident positrons energy, in order to adjust the annihilation depth, and also we like to control the beam's spot from a few mm down to a few microns as well as to control the spot position.

Building such a facility on-line with our cyclotron opens new perspectives for our positron applications.

References

- [1] R. Howell et al., Appl. Phys. Lett., 40, 751(1982)
- [2] A.P. Mills, J. Appl. Phys., 23, 189(1980)
- [3] A. Seeger, Materials Science Forum 255(1997)1-34
- [4] D.M. Schrader, J. Radioanalyt. And Nucl. Chem., 210(1996)435
- [5] R.E. Bell et al, Phys. Rev. 90(1953)64
- [6] S. Hansen et al. Appl. Phys. A65(1997)47
- [7] Graff et al., J. Appl. Phys., A33(1984)59
- [8] H. Schneider et al., Phys. Rev. Lett. 71(1993)2707
- [9] A. Kawasuso, S. Okada, Phys. Rev. Lett. 81(1998)2695
- [10] N.F. Miron, J. Nucl. Mater, 230(1996)247
- [11] P.M.Racolta et al., Nucl. Instr. Methods in Phys, B139(1998)461

A new strategy for wear and corrosion measurements using ion beam based techniques

D. Dudu¹, V. Popa², P.M. Racolta³, Dana Voiculescu³

¹ NIPNE-HH, Cyclotron Laboratory

² NIPNE-HH, Nuclear and Vacuum Engineering

³ NIPNE-HH, Department of Applied Nuclear Physics

An efficient and precise method for wear testing is Thin Layer Activation (TLA) [1-3], which is based on the production of a thin layer of radioisotopes in the component surface by bombardment with a charged particle beam. These radioisotopes disintegrate with the emission of a characteristic gamma radiation that can be detected with thallium activated sodium iodide NaI(Tl) detectors. Since the material loss due to wear or corrosion is directly proportional to the loss in radioactivity of the activated surface, the wear/corrosion can be monitored in real time. Alternatively the increase of the activity of the removed material debris collected in an oil bath of engine or in a filter also gives a measure of wear. The application of TLA and UTLA (ultra TLA - by recoil implantation) techniques presupposes the establishment of the optimum working and measuring conditions for the following stages: irradiation, post irradiation, and "in situ" measurements.

Having in view the diversity of components subjected to wear or corrosion, for TLA-based studies, dedicated beam lines for in-air or vacuum irradiation and translating/rotating target holders must be developed around the U-120 Cyclotron. The project of these improvements has been finished.

The modified IFIN-H.H U-120 cyclotron from Bucharest is a classical variable energy machine that can accelerate protons up to 14 MeV, deuterons up to 13.5 MeV, and alpha particles up to 27 MeV. At this machine, TLA has mainly been used for studies of various parts of running machines on test benches such as 2piston - rings and linear cylinders, also for lubricant characterization. [4-6].

The main advantage of TLA compared to conventional techniques for wear measurements is its ability to perform continuous in situ wear measurements of engine components, such as cylinder liners and piston rings, without the need to dismantle the components investigated. In addition high wear sensitivity and resolution of wear down to nano meters dimensions is guaranteed.[6]

Although the level of activity used in TLA lies under the limit of the range considered to be safe from the point of view of radiation protection, industry hesitates to use this technique mainly due to psychological reasons with respect to the handling of radioactive material. Recognizing this problem we have decided

to offer to industry wear/corrosion measurements using TLA and UTLA in the form of a "complete package". This means that surface activation of components in our accelerators and the subsequent wear measurements in the engine test facility are performed on the same site without the need of transportation of activated components over long distances. This enables industry to obtain reliable wear data in a short time without building on expensive test bed and without the need of handling radioactive material. This objective will be performed in collaboration with the specialists from CNRS-CERI Orleans -France and JRC-IAM Ispra, Italy.

Some experiment in order to develop the UTLA method for wear and corrosion studies have been started. The tandem Van de Graaff accelerator - 8 MV on terminal will be use, in this project, in order to characterize the surface layers and tribological phenomena (Cu, Sn, Ce etc. migration) by other ion beam based techniques RBS, NRA, PIXE, CE, HICE and ERDA techniques.

References

- [1] Asher J. (1994) MeV ion processing applications for industry, Nucl. Instrum. Methods B 89, 315
- [2] Constantinescu B, Ivanov E.A., Pascovici G., Popa-Simil L.and Racolta P.M. (1994) Thin layer activation technique at the U-120 cyclotron of Bucharest. Nucl. Instrum. Methods B 89, 828.
- [3] Fehsenfeld P., Kleinrahm A. And Schweikert H., (1992) Radionuclide technique in mechanical engineering in Germany. J. Radioanal. Nucl. Chem. 160, 141.
- [4] Racolta P.M. (1995) Nuclear methods for tribology, App. Radiat. Isot. 46, No. 6/7, 663
- [5] Racolta P.M., Popa-Simil L. and Alexandreanu B. (1996), Ion beam -based studies for tribological phenomena, Nucl. Instr. Meth. B 113, 420.
- [6] Lacroix O, Sauvage T, Blondiaux G., Racolta P.M., Popa-Simil L. and Alexandreanu B. (1996), Metrology conditions for thin layer activation in wear and corrosion studies, Nucl. Instr, Meth, A 369, 427

Fast XRF analysis of mineral elements in dental composites

E.A. Preoteasa¹, B. Constantinescu¹, E. Preoteasa²

¹ NIPNE-HH, Bucharest, Romania

² Helident Ltd. Bucharest, Dental Surgery Branch, Bucharest, Romania

Dental composites, made by particles of glass, ceramics or quartz embedded in an organic polymer matrix, extensively replaced silver amalgam in tooth fillings and enabled new applications for restorative dentistry. Long-term alteration of dental fillings together with market pressure motivates the development of composites at a high rate, largely by progress of materials forming their mineral phase. Therefore, dental composites constantly bring at the interface with enamel and dentine new elements foreign to the organism, whose biological action has not been studied. Atomic and nuclear methods for surface multielemental analysis have been used in dental research [1] but not for composites. X-ray fluorescence (XRF) is suited for the fast microanalytical screening of the elements and of their changes at the biomaterial's surface [2, 3].

The potential of radioisotope-excited XRF for the analysis of dental composites has been examined. Flat disk-shaped samples of composites have been prepared and polymerized chemically or by irradiation with intense 420-500 nm light. The measurements were performed with a spectrometric chain containing a 30 mCi source of ²⁴¹Am, a Si(Li) detector, and a multichannel analyzer. The spectra were accumulated for 2000-6000 sec. The characteristic X lines were integrated and normated to source lines.

The following $Z \geq 20$ elements were detected in the studied composites: Ba only in Charisma (Kulzer) and Pekafill (Bayer); Zr, Ba, Yb in Tetric Ceram, and Ca, Ba, Yb together with traces of possibly Ti and Fe in Ariston (both from Vivadent); Zr, Hf in Valux Plus (3M Dental); and Sr, Ba together with some trace element, seemingly Cu, in F2000 Compomer (3M Dental) and with other trace elements like Ca, Fe in Surefil (Dentsply). Among older materials, Concise (3M Dental) contained only light ($Z < 20$) undetectable elements, while in Evicrol (Spofa) and Alphaplast (DGM) were evidenced only Ca and Fe. With the exception of Charisma and Pekafill, XRF evidenced a specific elemental composition in each biomaterial (Fig. 1). Yb in Tetric Ceram and Ariston enters as YbF_3 that releases F⁻ for protection of enamel and dentine. Yb, Zr, Ba, Hf improve the radiological opacity of the materials. Some elements may accompany

others as contaminants.

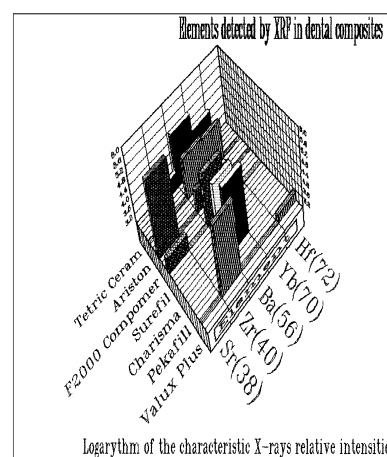


Figure 1: Logarithmic plot of the uncorrected relative intensities for characteristic X-rays of dominant elements in dental composites.

The results suggest that XRF excited with soft γ photons is valuable especially for fast analysis of dominant inorganic elements with $Z \geq 20$. Although the identification of trace elements was not always certain due to spectral overlap, the method is very useful for a fast multielemental analysis of composites. It could be used also for the expertise of these biomaterials (e.g. in customs and commercial applications).

References

- [1] V. Valkovic, M. Jaksic, J. Krmpotic-Nemanc, *Biol. Trace Elem. Res.*, 375 (1987)
- [2] H. Herglotz, L.S. Birks (eds.), *X-Ray Spectrometry*, Marcel Dekker, New York (1978)
- [3] N.G. West, *Trends Analyt. Chem.* **3**, 199 (1984)

Gamma and proton degradation in optical transmission materials

B. Constantinescu¹, C. Nicolescu¹, C. Teodorescu¹, F. Constantin¹, L. Rădulescu¹, M. Drăgușin¹, V. Moise¹

¹ NIPNE-HH, Department of Applied Nuclear Physics

Ceramic materials are anticipated to play very important roles in developing nuclear fusion reactors, where they will be used under heavy irradiation environments (neutrons, gamma-rays, protons, helium and other ions) for substantial periods for the first time. Three key ceramic materials being considered are Al₂O₃, BeO and AlN; while publications dealing with these materials are available, the database is incomplete and uncertainties are large concerning the solubilities, diffusivities, trapping and release of tritium in materials, particularly during irradiation. Among the important applications of fiber optics envisioned for the near future are light pipes for monitoring Tokamak fusion reactor plasma conditions. These applications will make unprecedented demands for hardness against optical attenuation induced by moderate to very high doses of gamma rays and neutrons. In particular, fibers for these tasks will be required to maintain good transmission over the entire visible range (400 - 700 nm). We intend to start a general programme on gamma and proton induced degradation in optical transmission materials, including windows and optical fibres. As a first step, we shall concentrate on assessing the suitability of SiO₂ based materials. The main characteristics of Bucharest irradiation facilities are:

- IRASM IRRADIATOR: 200 kCi ⁶⁰Co "swimming pool" irradiation source, minimum 2 kGy/h with an isotropic dose rate up to 1 Gy/s, ethanol chlorine benzene dosimetry, ionization chamber dosimetry, ESR dosimetry;

- HVEC 8 MV FN TANDEM: protons up to 16 MeV and 200 nA, alpha particles up to 21 MeV and 50 nA, O, C, N ions approximately 100 MeV up to 50 nA;

- DISKTRON (600 kV, ECR source): hydrogen isotopes up to 600 keV and tens of microamperes.

The following main milestones for the project have been achieved for 2000:

- Designing a gamma irradiation chamber, acting underwater, allowing various temperatures (20-300° C) on the sample; this involves finding adequate solutions for dosimetry, heating system and UV absorption and radioluminescence apparatuses (including their information transmission systems) acting in a very intense gamma ray field in the water pool of the ⁶⁰Co irradiator;

- Designing a high energy proton irradiation chamber, acting in high vacuum, allowing various tempera-

tures on the sample in the presence of irradiation proton beam heating (1 mA × 1 MeV = 1 W); this involves finding adequate solutions for dosimetry, heating system and UV absorption and radioluminescence apparatuses working in high vacuum conditions.

During an experiment of PAA (Proton Activation Analysis) on gold coins at our TANDEM, we have tested the maximum intensity of 15 MeV proton beam which can be obtained now on a metallic target: 200 nA. To upgrade this value, some improvements, especially for the ion source and the low energy transport system inside the accelerator, have been decided. The existing usual dosimetry at the TANDEM can be also used for our future experiments. As concerning the radioactivity induced by 15 MeV protons in the samples, our conclusions are:

- for iron: the main radioactivity is - for iron: the main radioactivity is from (91.72%) ⁵⁶Fe(p,n)⁵⁶Co (T_{1/2} = 77.4 d): 10 μ Ci/μ A × hour, which means for 100 ppm Fe at 10¹⁷ protons 5 nCi and at 10¹⁸ protons 50 nCi. Under the level of 100 nCi for ⁵⁶Co, the handling rules are not severe.

- for copper: the main radioactivity is from (30.9%) ⁶⁵Cu(p,n)⁶⁵Zn (T_{1/2} = 245 d): 2.5 μ Ci/μ A × hour, which means for 100 ppm Cu at 10¹⁷ protons 1.25 nCi and at 10¹⁸ protons 12.5 nCi.

- for magnesium: the radioactivity comes from ²⁴Na (T_{1/2} = 15 h), which disappears after 4-5 days and, more important, from (10%) ²⁵Mg(p,³He)²²Na (T_{1/2} = 2.6 y): 20 nCi/μ A × hour, which means 100 nCi at 10¹⁷ protons and 1000 nCi at 10¹⁸ protons for a sample with magnesium as main component (e.g. sapphire). The main problem is the influence on luminescence and absorption measurements (background?).

- for sodium: the main radioactivity is from (100%) ²³Na(p,d)²²Na, which a contribution of 0.5 nCi for 100 ppm Na at 10¹⁷ protons and 5 nCi at 10¹⁸ protons.

- for other possible impurities (Ca, Cr, F, etc) after 100 hours cooling time the radioactivity disappears. The main problem related to the presence of the radioactivity (gamma, X-rays, electrons) in the samples is its influence on luminescence and absorption measurements.

For optical fibers metal jacketed the composition of the jacket is essential (especially the presence of Fe, Cu, Ni generates problems). As concerning the semiconductor lasers, the presence of a relatively thick metallic jacket must be considered as an impediment for our experiment.

Wet storage of nuclear spent fuel from nuclear research reactor WWR-S, IFIN-HH

A. C. Dragolici¹, A. Zorliu¹, C. Petran¹, I. Mincu¹

¹ NIPNE-HH, Nuclear Research Reactor, 76900 Bucharest, Romania

Nuclear research reactor WWR-S of IFIN-HH was commissioned on 29 July 1957 and shut down on December 1997. Now it is in Conservation State. During the 40 years of function, the reactor worked on about 150.000 hours at variable powers between 5W and 3500KW, producing a total power of 9510MWday. After 20 years of operation a large number of spent fuel elements became available for storage exceeding the stocking capacity of the small cooling pond near reactor. Therefore, in 1980 was commissioned the nuclear spent fuel repository that contains at present all the fuel elements burnt in the reactor during years, minus 51 S-36 fuel assemblies which are conserved in the cooling pond. This repository contains 4 identical ponds, each of them having the depositing capacity of 60 fuel assemblies. Every pond having the outside sizes of 2750mm (length) x 900mm (breadth) x 5700mm (depth), is made from a special aluminum alloy (AlMg₃), with the walls thickness of 10mm and bottom thickness of 15mm. Pond's lids are made from cast iron having the thickness of 500mm, they provide only the biological protection for the maintenance personnel. A 1.5m concrete layer provides the lateral biological protection of the ponds. Over the fuel elements in every pond we can find a 4.5m water layer, which play the role of biological protection and coolant. Inside the ponds exists an aluminum rack, which contains 60 places for fuel storage. The rack net step was determinate from critical considerations and it is equal with the rack net step from the cooling pond near the reactor. To have supplementary protection in the case of an accident which can destroy the entire rack and put together all the fuel elements thus forming critical mass, cadmium plates were placed on the ponds bottom for a better neutron absorption. Exploitation of cooling pond near the WWR-S reactor which has the identical structure with that of nuclear spent fuel repository, demonstrate the reliability and robustness of this type of repository. The ponds are supplied with distilled water from reactor tank No 1. The spent fuel assemblies used in the WWR-S reactor and stored in this repository contain two types of fuel: the EK-10 153 pieces and the S-36 70 pieces. The EK-10 and S-36 fuel assemblies have the same shape but distinct numbers of fuel roads and different percentage of U-235 enrichment. So, the EK-10 contains 16 fuel roads and 10Total activity of the fuel assemblies is about 10.69×10^4 Ci. The most important fission products in fuel roads are Sr-90 and Cs-137. Depending on fuel

assembly type the calculated values of the activity of these elements are:

1. EK-10, Sr-90 $\rightarrow 7.14 \times 10^3$ Ci; Cs-137 $\rightarrow 7.67 \times 10^3$ Ci
2. C-36, Sr-90 $\rightarrow 8.21 \times 10^3$ Ci; Cs-137 $\rightarrow 8,08 \times 10^3$ Ci

From the gamma spectrometry analysis performed on water samples from storage ponds it was observed the dominant presence of Cs and of various another nuclides. The presence of Cs in the water is due to fuel roads flaws, the appearance of pores and cracks because of fuel manipulation in active core of the reactor or in the storage pond or because of corrosion pits due to a low quality of water. The manufacturer have specified the water conditions for the EK-10 and S-36 fuel assemblies, which they believe will avoid corrosion problems are displayed in table 1.

Table 1: Water parameters.

Parameter	EK-10	C-36
pH	5,5 - 7,5	5,5 - 6
conductivity	5 μ S/cm	2-3.3 μ S/cm
constant residuals	8 mg/l	1 mg/l
corrosion products	-	1 mg/l
Cl ⁻	-	0,02 mg/l
O ₂	-	8 mg/l

The IAEA recommends values of 1 μ S/cm, but values up to 2 μ S/cm might be accepted if the chlorine, copper and sulphate concentrations are very low. To maintain this parameters of the water in concordance with IAEA recommendations, it was designed and realised a filtration installation for the distilled water produced at the reactor. Till this installation will be assembled the water chemistry is permanent monitored and if the quality is not good it will be replaced. An other problem is the detection of fuel assemblies with leakages. For this purpose was designed a special device for detecting and isolation of fuel assemblies with flaws. We intend to elaborate a solution to confine the leaky fuel in a sealed aluminum cladding and after that to re-store it in the pond. Through this methods of detection, isolation and through a strictly water conditions we hope to extend the storage period till 30-40 years until the properly technology of final disposal will be choosed and approved.

Ref.: Workshop on Characterization, Management and Storage of Spent Fuel from Research and Test Reactors

Molecular dynamics in bitumen compounds. A combined study by NMR and neutron scattering techniques

R. Grosescu¹, V. Tripadus¹, L. Craciun¹, M. Peticila², O. Muresan¹

¹ National Institute of Physics and Nuclear Engineering - Horia Hulubei, Bucharest-Magurele

² Center of Technical Research and Informatics for Roads, Bucharest

The comparative studies by the combined NMR and neutron scattering techniques opened new possibilities for the investigations of the molecular structures and molecular dynamics in liquids as well as in solids. One of the first works of this type, reported in the literature was carried out in our Institute on supercooled liquid phenol [1].

Later, the idea was extended to molecular crystals by a joint research project, between IPNE-Bucharest and Max-Planck Institute-MD Heidelberg, using advanced solid-state NMR and stronger neutron fluxes [2]. Here, we report preliminary results of the combined NMR and neutron scattering investigations on bitumen compounds that are micellar structures with important industrial applications. The goal of the study is to bring information about the molecular dynamics in various phases of these compounds and on this basis to test and/or improve their microscopic models.

The neutron scattering measurements were carried out at IBR-2 high flux reactor at JNIR-Dubna. The neutron energy in the incident beam was 4.43meV and scattering angles ranged from 6° to 134°.

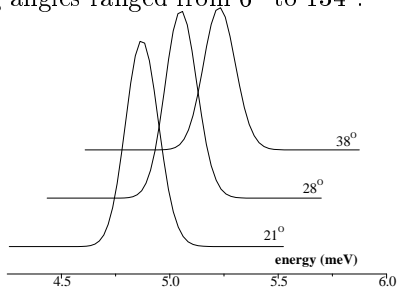


Figure 1: The quasielastic neutron scattering lines at different angles

The scattered neutron spectra at room temperature are shown in Fig. 1, for several angles. The quasielastic peak gives direct information about the molecular dynamics via the linewidth dependence on the transfer momentum k^2 . On this basis we calculated an overall diffusion constant $D_n = 1.26 \cdot 10^{-7} \text{ cm}^2/\text{s}$. D_n is a superposition of contributions from the various rotational diffusions as well as the Translational diffusion. The neutron scattering data can hardly distinguish between them. This ambiguity can be partially removed by the information brought in by NMR.

The temperature dependence of the NMR spin-lattice relaxation time T_1 of ESSO-bitumen, measured at $\omega_o/2\phi = 25 \text{ MHz}$ indicates several particular features (see fig. 2):

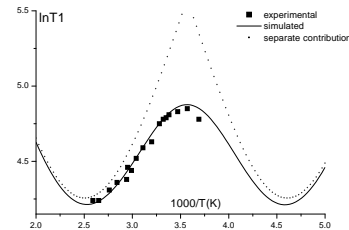


Figure 2: Temperature dependence of the spin-lattice relaxation time T_1

a) The relaxation process cannot be explained by a single relaxation mechanism. The superposition of two V-type mechanisms produces a reasonable agreement with experimental data;

b) These two-mechanisms should be associated with two simultaneous and independent reorientational molecular motions characterized by the correlation times $\tau_c(i) = \tau_c(i) \cdot \exp[E_a(i)/kT]$ cu $i=1,2$. According to this model, by a fitting procedure, we found $\tau_c(1) = 20.10^{-9} \text{ s}$, $\tau_c(2) = 0.44 \cdot 10^{-9} \text{ s}$ at $T=293 \text{ K}$.

A better insight of the molecular motion process is reached if one observes that the NMR and neutron scattering outputs are not independent. In the particular case of reorientational motions mentioned above, they are related by "the ellipse of diffusions":

$$(a_1)^2/\tau_c(1) + (a_2)^2/\tau_c(2) = 6 \cdot D \quad (1)$$

where a_1 and a_2 are the radii of the molecular fragments involved in the motion and D is the overall diffusion constant.

For the particular case of the ESSO-bitumen eq. (1) leads to $a_1 \leq 10 \text{ \AA}$ and $a_2 \leq 1.5 \text{ \AA}$. These values can be used to identify the moving fragments. In general, eq. (1) can be an useful tool whenever the system is heterogeneous and complex. NMR delivers $\tau_c(1)$ and $\tau_c(2)$, the neutron scattering delivers $D = D_n$ and eq.(1) sets limits on a_1 and a_2 which are used to test models for microdynamics.

References

- [1] V. Tripadus et al., J. Chem. Phys. 60, 2832 (1974)
- [2] R. Grosescu et al., J. Mag. Res., 53, 213, (1983)

Tracers, Radiopharmaceuticals and Radiometry

Standardization of a large area alpha and beta sources with a window-less multi-wire proportional counter

E.L. Grigorescu¹, Maria Sahagia¹, A.C. Razdolescu¹, A. Luca¹, C. Ivan¹

¹ NIPNE-HH

In The Radionuclide Metrology Group of IFIN-HH, a measurement system was assembled and tested for the absolute standardization of large area alpha and beta sources. Such sources are employed to calibrate a variety of contaminometers. A window-less multi-wire proportional counter, donation of the "Laboratoire National Henri Becquerel" (LNHB), Saclay-France, was used, with pure methane as flowing gas. The needed electronics (high voltage, amplifier, discriminator, counter, clock, MCA) was a CANBERRA one.

Point and extended sources of ^{241}Am , $^{90}\text{(Sr + Y)}$ and ^{204}Tl were standardized. The variation of the counting rate with high voltage provided "plateaus"

of (300-500) V, with a slope of (0.1-1.5)% for 100 V. The efficiency of the counter for a point beta source and a central area of (100x150) mm^2 , varied with less than 0.2%. To avoid spurious pulses, adequate threshold and working high voltage were chosen, and a imposed 10 μs dead-time was inserted in the counting channel. A procedure for the threshold correction was established.

A combined uncertainty of maximum $\pm 2\%$ was obtained, a quite acceptable value for extended sources. These results, together with the results obtained by romanian specialists in LNHB, with an identical counter, but using argon/methane mixture will be published.

The experiment was realised in the frame of the IFIN-HH long term collaboration agreement.

Standardization of ^{152}Eu

E.L. Grigorescu¹, Maria Sahagia¹, Anamaria Cristina Razdolescu¹, A. Luca¹, C. Ivan¹

¹ NIPNE-HH

^{152}Eu was standardized in the frame of a BIPM international comparison with 23 participating laboratories. In the Radionuclide Metrology Group from IFIN-HH, the ^{152}Eu solution was standardized using a $4\pi\beta - \gamma$ coincidence method in the "beta-efficiency extrapolation" variant. The coincidence system contained as detectors, a $4\pi\text{PC}$ and a NaI(Tl) . Choosing an adequate "gamma-window" in the gamma channel, good linearity and a slope of only -4% were obtained for the extrapolation graphs. The standardization was

facilitated by the important fraction of conversion electrons associated with the electron-capture transitions. The resulted radioactive concentration value at the reference time was 579.4 kBq/g with a combined uncertainty of only 1 which may be considered satisfactory in regard to the complex decay-scheme of ^{152}Eu . The mentioned result is only 0.5% lower than the mean of the comparison. The aim of this experiment was to help assure the International Traceability and the participation to the international Mutual Recognition Agreement.

Obtaining of ^{99}Mo - ^{99m}Tc gel - generator based on zirconium molybdate

N. Negoita¹, Catalina Cimpeanu¹, Maria Sahagia¹

¹ NIPNE-HH, CPR Department

The radioisotope ^{99m}Tc is used in nuclear medicine for radiodiagnosis. This radioisotope results from beta desintegration of ^{99}Mo ($t_{1/2} = 66\text{h}$) which is obtained by irradiation of the natural MoO_3 with thermic neutrons at Nuclear Reactor or by extraction from fission fragments. Since 1997, in our Department, the ^{99}Mo - ^{99m}Tc generators, using fission sodium molybdate ($\text{Na}_2^{99}\text{MoO}_4$) as raw material which is adsorbed on alumina column, are manufactured and delivered regularly to the hospitals. At present we are concerned with the obtaining of the ^{99}Mo - ^{99m}Tc gel generator using as raw material ^{99}Mo obtained by irradiation at Nuclear Reactor because:

- ^{99}Mo is strongly-bounded with Zr in a solid stable matrix (zirconium molybdate);
- use of MoO_3 irradiated at the Nuclear Reactor which is obtained at a low cost as compared with fission ^{99}Mo ;

- obtaining of generators with higher chemical, radio-chemical and radionuclidic purity than the classic generators with alumina column; the radionuclidic purity is very high because the beta-gamma and alfa fission products are not present;

- the practical knowledges accumulated in classic generator is production;

The paper presents first results obtained in our Department: obtaining of ^{99}Mo by irradiation of MoO_3 in Triga reactor SSR-14MW SCN Pitesti; chemical processing of the irradiated target (obtaining of sodium molybdate - ^{99}Mo); obtaining of the Zr- ^{99}Mo matrix (zirconium molybdate form); obtaining of gel-generator; qualitative and quantitative analysis, chemical and radiochemical analysis for sodium pertechnetate eluates - ^{99m}Tc . The results require further research for obtaining of new generators, gel-generators ^{99}Mo - ^{99m}Tc , with higher quality than classic generators and smaller prices.

Model of calculation for an optimized $^{188}\text{W}/^{188}\text{Re}$ generator

Catalina Cimpeanu¹, I. Mihalcea², Corina Simion¹

¹ NIPNE-HH CPR Department

² University of Bucharest, Romania

The stable isotopes of the natural W are: ^{180}W (0,12%); ^{182}W (26,3%); ^{183}W (14,28%); ^{184}W (30,7%); ^{186}W (28,6%).

By irradiation in Nuclear Reactor with termic neutrons the following radionuclides have been obtained: ^{181}W ; ^{185}W ; ^{187}W ; ^{188}W .

The nuclear reactions are of (n, γ) type [1].

When target is enriched W (98% in ^{186}W), the radionuclides formed are: ^{187}W ; ^{188}W .

This paper presents a model of calculation for the following parameters [2]:

- specific activity of all radionuclides obtained by irradiation in both cases - (W natural, respectively enriched 98% W);

- k(%) - relative abundance for ^{187}W ;

- specific activity for ^{188}Re - the daughter radionuclide in $^{188}\text{W}/^{188}\text{Re}$ generator system;

- T_{max} - "maximum time" - the time when specific

activity of the ^{188}Re is maximum or time between two elutions.

In order to establish the optimum irradiation and usable conditions of the $^{188}\text{W} / ^{188}\text{Re}$ generator system as well as the accumulation curves for ^{188}W , the dependence of specific activity function on irradiation parameters (time, neutron fluency) has been studied and the obtained results are presented.

References

- [1] Radiochimia si chimia proceselor nucleare. Editura tehnica 1963. A.N.Murin, V.D. Nefedov, V.P.Snedov.
- [2] Compusi marcati si radiofarmaceutici cu aplicatii in medicina nucleara. A.Balaban, I.Galateanu, G.Georgescu, L.Simionescu 1974.

Obtaining of ^{188}W sodium tungstenate ($\text{Na}_2\ ^{188}\text{WO}_4$) using WO_3 and W metallic (natural and enriched in ^{186}W)

Catalina Cimpeanu¹, Corina Simion¹, I. Mihalcea²

¹ NIPNE-HH, CPR Department

² University of Bucharest, Romania

This paper presents an obtaining method of $\text{Na}_2\ ^{188}\text{WO}_4$ by irradiation with termic neutrons in Nuclear Reactor TRIGA SSR-14MW Research Institute Pitesti, using as raw material WO_3 and W metallic (natural and enriched in ^{186}W –98%). $\text{Na}_2\ ^{188}\text{WO}_4$ is an acceptable chemical form for obtaining $\text{Na}\ ^{188}\text{Re}\ \text{O}_4$ (sodium perrenate).

^{188}Re obtained is carrier free. Two targets were prepared and irradiated. The first target was natural WO_3 and the second, was 98% enriched in ^{186}W metallic W target. ^{188}W is obtained as a result of the following nuclear reactions: $^{186}\text{W}(\text{n}, \gamma)\ ^{187}\text{W}(\text{n}, \gamma)\ ^{188}\text{W}$. After irradiation and cooling (21 days) the targets were chemically processed [1].

From $\text{Na}\ ^{188}\text{W}\ \text{O}_4$ obtained, we have separated $\text{Na}\ ^{188}\text{Re}\ \text{O}_4$ by using a preliminary MEK extraction, following by an elution on a acid alumina (Al_2O_3) column [2]. The $\text{Na}\ ^{188}\text{Re}\ \text{O}_4$ separated was sterilized by filtering through a 22 μm Millipore filter.

We have determinated for final product following physico-chemical parameters: pH value, radiochemical and radionuclidic purity, specific activity, sterility, pyrogenity.

All parametrs were very good except specific ac-

tivity, because the bad parameters of irradiation and a very long (21 days) cooling time: pH-6; radiochemical and radionuclidic purity > 99%; specific activity for ^{188}Re -8,9MBq/g W for first target - WO_3 (after 21 days of cooling), respectively 74 MBq/g W for second target - W (98% enriched in ^{186}W) (after 21 days of cooling); the product were sterile and apyrogene.

References

- [1] M.R.A. Pillai, P.R. Unni, K. Kothari, A.R. Mathakar, "Production and radiochemical processing of therapeutic radionuclides", International Seminar on Therapeutic Application of Radiopharmaceuticals, Hyderabad, India, 18 - 22.01.1999.
- [2] F.F.Knapp, Jr. A.L.Beets and S.Mirzadeh, "Use of a new tandemm cation/anion exchange system with clinical seale generators provides high specific volume solutions of $^{99\text{m}}\text{Tc}$ and ^{188}Re ", International Symposium on Modern Trends in Radiopharmaceuticals for diagnosis and Therapy - Lisabona Portugalia 1998.

Obtaining of ^{186}Re sodium perrenate ($\text{Na } ^{186}\text{ReO}_4$). The study of variation $^{186}\text{Re} / ^{188}\text{Re}$ ratio in time

Catalina Cimpeanu¹, I. Mihalcea², Madalina Cruceru¹

¹ NIPNE-HH CPR Department

² University of Bucharest Romania

^{186}Re and ^{188}Re , two strong beta and week gamma emitters having halflives of 3.775 days and respectively 17.005 hours are intensively studied as promising radionuclides for brachytherapy and mainly as radiopharmaceuticals, due to their similar chemical behavior with ^{99m}Tc [1].

The paper presents the following operations and experimental results: obtaining of the irradiated targets, chemical processing, characterization of the final products, perrenate solution, and new trials of improvement of work.

The irradiation were performed in the TRIGA SSR -14 MW Reactor of the Nuclear Research Institute Pitesti.

The targets were prepared by precise weighting using pure materials (99% purity level).

The primary packing were flame sealed quartz vials, introduced in aluminium capsules sealed by electron beam welding.

For obtaining of ^{186}Re , natural metal (^{185}Re , 37.1% and ^{187}Re , 62.9%) powder was used.

The nuclear reactions are: $^{185}\text{Re} (n,\gamma) ^{186}\text{Re}$; $^{187}\text{Re} (n,\gamma) ^{188}\text{Re}$.

A mixture of ^{186}Re and ^{188}Re resulted. Two targets of Re natural metallic were prepared and irradiated. After irradiation and cooling (9, respectively 3

days), the targets were processed. The final product obtained was sodium perrenate solution ($\text{Na } ^{186}\text{ReO}_4$).

This solution was sterilized by filtering through a 22 μm Millipore filter. For final product the following physico-chemical parameters have been determined: pH value, radiochemical and radionuclidic purity, specific activity [2], sterility, pyrogenity.

All these parameters were very good: pH-6; radiochemical and radionuclidic purity >99%; specific activity for ^{186}Re - 166,5GBq/g Re for first target (after 9 days of cooling), respectively 3330 GBq/g Re for second target (after 3 days of cooling); the product were sterile and apyrogene.

References

- [1] M.R.A. Pillai, P.R. Unni, K. Kothari, A.R. Mathakar, "Production and radiochemical processing of therapeutic radionuclides", International Seminar on Therapeutic Application of Radiopharmaceuticals, Hyderabad, India, 18 - 22.01.1999 .
- [2] M. Sahagia, A. M. Razdolescu, L. Grigorescu, A. Luca, C. Ivan, "Absolute standardization of ^{186}Re , ^{188}Re solutions by $4\beta - \gamma$ coincidence method", International report IFIN - HH .

^{88}Re - AntiCEA MAB. Preparation and biological evaluation

V.V. Lungu¹, G. Mihailescu¹, D. Niculae¹

¹ NIPNE-HH

Monoclonal antibodies are the most recent candidate molecules for the radiopharmaceutical preparation used in radioimmunotherapy and radiodiagnostic, function of the used radionuclide. Our study presents results in: i) ^{188}Re labelling of Monoclonal Anti-Human Carcinoembrionic antigen clone C6G9 (anti-CEA Mab) and ii) Biological evaluation of ^{188}Re -antiCEA Mab on tumour bearing animals. The steps in labelling process are: 1) prereduction of -S-S- bridges of antiCEA-Mab molecule with ascorbic acid in $\text{pH} = 5$, 2) preparation of the reducing system for $^{188}\text{ReO}_4^-$ in presence of Sn^{2+} ions excess and 3) coupling ^{188}Re (red) to -SH groups of biomolecule.

The specific reactions of each above steps are controlled by: incubation time and temperature, pH , molar ratio ^{186}Re : antiCEA- Mab. The incubation at 37°C temperature, 20 hour time and $\text{pH} = 5$ for samples of ^{188}Re :antiCEA with molar ratio 1,6:1 leads to a 85-90% labelling yield

^{188}Re -antiCEA purified samples by gel elution chromatography method were i.p. injected on tumour bearing animals. The sample radioactivity was 1.2 mCi/0.2 ml. The biodistribution registered at 4, 24 and 48 hours post injection presents a maximum accumulation in tumour at 24 h after injection. ($\Lambda_{\text{tumour}}/\Lambda_{\text{blood}} = 6.2:1$ was the activity ratio after 24 h post injection.

Standardization of ^{89}Sr

Anamaria Cristina Razdolescu¹, Maria Sahagia¹, Ph. Cassette², E.L. Grigorescu¹, A. Luca¹, C. Ivan¹

¹ NIPNE-HH, Bucharest-Magurele

² LNHB, CEA-DIMRI, Gif sur Yvette CEDEX, France

^{89}Sr was standardized in the frame of a BIPM international comparison. In the Radionuclide Group from IFIN-HH, the ^{89}Sr solution was standardized by two different methods: TDCR-liquid scintillation method and coincidence tracing method with ^{60}Co .

The TDCR equipment of modular type contained a MAC-3 module produced by LNHB-Saclay. This module contains the circuits for the coincidence, dead time and gate functions. The DETECSZ program (LNHB) was used to obtain the activity concentration, at the

reference time, as 26.09 ± 0.21 kBq g⁻¹. The tracing method provided a general extrapolation curve with a final value of 26.58 ± 0.28 kBq g⁻¹ on the reference time. The results obtained by the two independent methods, TDCR and efficiency tracer method, agree within the limits of the stated uncertainties. In applying the tracer method, additional checks, regarding the determination of beta efficiency, confirmed the proper choice of the extrapolation interval and of the extrapolation relation.

Precise measurement of the activity of ^{186}Re , ^{188}Re radiopharmaceuticals

Maria Sahagia¹, Anamaria Cristina Razdolescu¹, E.L. Grigorescu¹, A. Luca¹, C. Ivan¹

¹ NIPNE-HH

National traceability was assured for the activity of the radiopharmaceuticals containing ^{186}Re , ^{188}Re and $^{186}\text{Re} + ^{188}\text{Re}$ mixtures along the whole chain: production, distribution, using, hospitals.

The corresponded radioactive solutions were standardized by using the $4\pm\text{PC}-\gamma$ method applied for "triangular" decay scheme radionuclides.

The relations between the $4\pm\text{PC}$ beta efficiency of the ground level disintegration, $\varepsilon\beta_n$, and the mean efficiency N_c/N_γ were determined experimentally and calculated. The obtained results agree, in the limit of

uncertainties, and are concordant with reported literature data.

The response of the Centronic IG12/20A ionisation chamber and other radioisotope calibrators was determined for ^{186}Re , ^{188}Re and calculated for their mixture.

The separate contributions of the gamma rays and bremsstrahlung radiations in response were evaluated. The efficiencies of the ionisation chamber for bremsstrahlung radiations were calculated. Comparison with the literature data confirmed the results obtained.

Obtaining of high specific activity ^{186}Re , ^{188}Re perrenates to be used for biomolecule labeling

Catalina Cimpeanu¹, Corina Anca Simion¹, Maria Sahagia¹

¹ NIPNE-HH, CPR Department

^{186}Re and ^{188}Re , two strong beta and week gamma emitters, having halfives of 3.775 days and respectively 17.005 hours, are intensively studied as promising radionuclides for brachytherapy and mainly as radiopharmaceuticals, due to their similar chemical behavior with ^{99m}Tc . The paper presents the following operations and experimental results: obtaining of the irradiated targets, chemical processing, characterization of the final products, perrenate solution, and new trials of improvement of work.

The irradiations were performed in the TRIGA

SSR - 14 MW Reactor of the Nuclear Research Institute Pitesti.

In the case of ^{186}Re , natural metal (^{185}Re , 37.1% and ^{187}Re , 62.9%) powder was used. A mixture of ^{186}Re , ^{188}Re resulted.

In the case ^{188}Re , the aim of the work was the obtaining of a $^{188}\text{W} / ^{188}\text{Re}$ generator, so tungsten targets were prepared. The first sample was natural WO_3 and the second was a metallic W (98% enriched in ^{186}W) target.

Table 1: Characterization of the final products, perrenate solutions

Characteristics	$\text{Na}^{186}\text{ReO}_4$ solution		$\text{Na}^{188}\text{ReO}_4$ solution	
	Target 1	Target 2	Target 1	Target 2
Radionuclidic purity%	99.9	99.9	99.9	99.9
Radiochemical purity%	99.9	99.9	90	99
PH value	5.5	6.0	6	6
Total volume (ml)	9	13	15	15
Total activity (MBq)	1665	333000	8.9	7.4
Specific activ. (MBq/mg)	166.5	3330	-	-
Radioactive concentration (MBq/ml)	185	25900	0.594	0.494

High specific activity $^{186,188}\text{Re}$ perrenate was obtained.

Regarding $^{188}\text{W} - ^{188}\text{Re}$ generator for which low ^{188}W activities were obtained and a relatively low extraction yield was reached, after using the recommend irradiation

conditions, we tried to obtain the gel generator, by using a ZrWO_4 - gel column. The compound ZrWO_4 was obtained in our laboratory by chemical synthesis. We mention that the ^{186}Re perrenate obtained in our laboratory was successfully used for labeling of the G immunoglobulin.

Waste Management and Site Restoration

Durability of cemented waste in repository and under simulated conditions

F. Dragolici¹, M. Nicu¹, L. Lungu¹, C. Turcanu¹, Gh. Rotarescu¹

¹ NIPNE-HH, Waste Management Department, 76900 Bucharest, Romania

The research activities performed by Department of Radioactive Waste Management is focused on the LLAW treatment products obtained by chemical precipitation and on the conditioning of these products by cementation. The individual mechanisms participating on the chemical precipitation process are directly dependent on the precipitate properties and structure, which are connected with the initial system composition and the precipitation procedure. In the case of conditioning by cementation, the chemical nature and proportion of the sludges or concentrates affect both the hydrolysis of the initial cement components and the reactions of metastable hydration constituents, as well as the mechanical strength and chemical resistance of the hardened cemented matrix. Generally, the study of the precipitation products and their behaviour during cementation and the long-term disposal is extremely difficult because of the system complexity (phase composition and structure) and the lack of the non-destructive analytical methods. For a more detailed characterization, Mossbauer Spectroscopy as a complementary analytical method was XRD, performed for precipitates and cemented matrices.

The following systems are considered:

- iron precipitates obtained during LLAW treatment;
- structural modifications in the iron hydrated oxides induced by foreign cations;
- influence of precipitation procedure on the decontamination factors;
- dry and hydrated cement systems;
- cementation of sludge chemical components;
- influence of organic complexants on the cemented matrix performances and structure;
- influence of mineral additives on the concrete;
- durability of cemented waste in repository and under simulated conditions.

Mossbauer investigation of iron species formed in precipitation systems simulating LLAW treatment, revealed that the iron compounds obtained by fast neutralization (as in radioactive aqueous waste treatment) have a different structure compared with iron oxides and hydroxides prepared by slow addition of the reactants when intermediate forms may be precipitated and redissolved many times during a long process reaching the equilibrium. Considering the iron precipitation in a system having other di- or tri-valent cations, Mossbauer spectra put in evidence the structural modifications induced by the foreign cations precipitating together with iron ions, but to identify the mutual influences a complementary analysis method

as XRD was necessary to use. The selected matrices are normal cement and concrete compositions with and without mineral additives (bentonite and volcanic tuff) as reference samples, the conditioned matrices prepared with radioactive sludge non-active components (iron hydroxides and phosphate, calcium phosphate and copper ferrocyanide) and non-active matrices prepared with organic acids and salts (oxalic, citric, tartaric, EDTA). Radioactive effluents containing complexing agents as oxalic and citric acids are generated during the radioactive decontamination operation using chemical methods. The studies performed until now have as object to establish the upper level concentration of some decontamination solutions as citric acid, tartaric acid, oxalic acid, ammonium oxalate and sodium citrate which can be contained in the cement conditioning matrix, and do not affect its mechanical performances. The research programme requires detailed identification of the complex phenomena involved, long investigation times and extending of basic data determined from laboratory tests in simplified conditions. The basic information on the waste matrix are obtained by: X-Rays Diffraction, Mossbauer Spectroscopy, Inelastic Neutron Scattering, Small Angle Neutron Scattering and mechanical strength tests. In the inelastic neutron scattering experiments taken on DIN-2PI time of flight spectrometer at the fast pulsed reactor IBR-2 of the Frank Laboratory of Neutron Physics at JINR Dubna, the microdynamics of cement mixtures was studied. The samples of CaOSiO_2 mixed both with H_2O and D_2O were prepared in IFIN HH. The data are analyzed in terms of the generalized vibration density spectra (GVDS) derived from double differential cross section. The hydrated cement matrix in presence of fresh precipitate of ferric hydroxide ($\text{Fe}(\text{OH})_3$), phosphate ($\text{Fe}_2(\text{PO}_4)_3$) and NaCl are also investigated. Also, in present are developed Small Angle Neutron Scattering researches at IBR-2 Dubna, which will provide informations about the cement paste hydration and the structure of the investigated systems (porosity, water behaviour and influence, etc.). All samples were positioned in five points of Baita-Bihor repository and kept 1,2,5 and 10 years before mechanical and structural characterization. These results will be compared with results obtained for the same type of samples kept in laboratory conditions. The presumed alteration of mechanical and physic-chemical properties will be correlated with a non-destructive analysis of the matrix with thermal resistance tests and leaching experiments.

Standardisation

Standardization of a large area alpha and beta sources with a window-less multi-wire proportional counter

E.L. Grigorescu¹, Maria Sahagia¹, A.C. Razdolescu¹, A. Luca¹, C. Ivan¹

¹ NIPNE-HH

In The Radionuclide Metrology Group of IFIN-HH, a measurement system was assembled and tested for the absolute standardization of large area alpha and beta sources. Such sources are employed to calibrate a variety of contaminometers. A window-less multi-wire proportional counter, donation of the "Laboratoire National Henri Becquerel" (LNHB), Saclay-France, was used, with pure methane as flowing gas. The needed electronics (high voltage, amplifier, discriminator, counter, clock, MCA) was a CANBERRA one.

Point and extended sources of ^{241}Am , $^{90}\text{(Sr + Y)}$ and ^{204}Tl were standardized. The variation of the counting rate with high voltage provided "plateaus"

of (300-500) V, with a slope of (0.1-1.5)% for 100 V. The efficiency of the counter for a point beta source and a central area of (100x150) mm^2 , varied with less than 0.2%. To avoid spurious pulses, adequate threshold and working high voltage were chosen, and a imposed 10 μs dead-time was inserted in the counting channel. A procedure for the threshold correction was established.

A combined uncertainty of maximum $\pm 2\%$ was obtained, a quite acceptable value for extended sources. These results, together with the results obtained by romanian specialists in LNHB, with an identical counter, but using argon/methane mixture will be published.

The experiment was realised in the frame of the IFIN-HH long term collaboration agreement.

Standardization of ^{152}Eu

E.L. Grigorescu¹, Maria Sahagia¹, Anamaria Cristina Razdolescu¹, A. Luca¹, C. Ivan¹

¹ NIPNE-HH

^{152}Eu was standardized in the frame of a BIPM international comparison with 23 participating laboratories. In the Radionuclide Metrology Group from IFIN-HH, the ^{152}Eu solution was standardized using a $4\pi\beta - \gamma$ coincidence method in the "beta-efficiency extrapolation" variant. The coincidence system contained as detectors, a $4\pi\text{PC}$ and a NaI(Tl) . Choosing an adequate "gamma-window" in the gamma channel, good linearity and a slope of only -4% were obtained for the extrapolation graphs. The standardization was

facilitated by the important fraction of conversion electrons associated with the electron-capture transitions. The resulted radioactive concentration value at the reference time was 579.4 kBq/g with a combined uncertainty of only 1 which may be considered satisfactory in regard to the complex decay-scheme of ^{152}Eu . The mentioned result is only 0.5% lower than the mean of the comparison. The aim of this experiment was to help assure the International Traceability and the participation to the international Mutual Recognition Agreement.

Appendix

Publications	133
In Journals	133
Books and Chapter in Books	138
Preprints	138
International Conferences	139
PhD Theses	145
Scientific Exchanges	145
Foreign Visitors	145
Invited Seminars	146
Visits Abroad	146
Seminars Abroad	148
Research Staff	149
Author Index	153

Publications

In Journals

Adam Gh., Adam S.

Data analysis in positron spectroscopy
Proceedings of the International Symposium on Advances in Nuclear Physics, D. Poenaru and S. Stoica, Eds., World Scientific, Singapore, 2000, pp.399-406

Adam Gh., Adam S.

Reliable operations on oscillatory functions
Computer Physics Communications **125** (no. 1-3), 127-141 (2000)

S.Akhmadaliev, ..., V.Boldea, S.Constantinescu, S.Dita, D.Pantea et al. (ATLAS - Tile & DAQ Collab.)

Results from a new combined test of an electromagnetic Liquid Argon calorimeter with a hadronic Scintillating-Tile calorimeter
Nucl. Instr. and Meth. A449, (2000) 461-477.

A.N.Aleev, T.Ponta, T.Preda et al., EXCHARM Collaboration

A measurement of transverse polarization of lambda hyperons produced in nC reactions in the EXCHARM experiment
Eur.Phys.J.C13:427-432, 2000

A.N.Aleev, T.Ponta, T.Preda et al., EXCHARM Collaboration

Spin Alignment of $K^*(892)^\pm$ mesons produced in neutron carbon interactions
Phys.Lett.B485:334-340, 2000

C.Alexa, V.Boldea, S.Constantinescu, S.Dita, et al., NA50 Collaboration

Charmonium production production in Pb-Pb collisions
Nucl. Phys. A663 (2000) 765

C.Alexa, V.Boldea, S.Constantinescu, S.Dita, et al., NA50 Collaboration

Dimuon and charm production in nucleus - nucleus collisions at the CERN SPS
Eur. Phys. J. C14 (2000) 443

C.Alexa, V.Boldea, S.Constantinescu, S.Dita, et al., NA50 Collaboration

Evidence for deconfinement of quarks and gluons from the J/Ψ suppression pattern measured in Pb+Pb collisions at the CERN SPS
Phys. Lett. B477 (2000) 28

C.Alexa, V.Boldea, S.Constantinescu, S.Dita, et al., NA50 Collaboration

Low mass dimuon production in proton and ion induced interactions at the SPS
Eur. Phys. J. C13 (2000) 69

C.Alexa, V.Boldea, S.Constantinescu, S.Dita, et al., NA50 Collaboration

Strangeness measurements in NA50 experiment with Pb projectiles
Nucl. Phys. A663 (2000) 721

P.Amaral, ..., V.Boldea, S.Constantinescu, S.Dita, D.Pantea et al. (ATLAS - Tile Collab.)

Hadronic shower development in Iron-Scintillator Tile calorimetry
Nucl. Instr. and Meth. A443, (2000) 51-70.

M. Avrigeanu, G.S. Anagnostatos, A.N. Antonov, J. Giapitzakis

On dynamics of two-neutron transfer reactions with the Borromean nucleus ${}^6\text{He}$
Phys. Rev. C **62**, 017001 (2000)

S. Berceanu and A. Gheorghe

Boson exapansions for Kähler orbit
Rom. Jour. Phys. **45**, Nos 3-4, 285-288 (2000)

S. Berceanu and M. Schlichenmaier

Coherent state embeddings, polar divisors and Cauchy formulas
J. Geom. Phys. **34** 336-358 (2000)

R. Bimbot, A. Khoumri, A. Fahli, S. Barbey, T. Benfoughal, M. Mirea, A. Hachem, G. Fares, R. Anne, H. Delagrange, C. Tribouillard, Y. Georget and J.C. Foy

Stopping Powers of Gases for 40 MeV/u Tellurium Ions
Nuclear Instruments and Methods B **170**, 329-335 (2000)

V.Bondarenko, T. von Egidy, K.Honzatko, I.Tomandl, D.Bucurescu, N.Mărginean, J.Ott, W.Schauer, H.-F.Wirth, C.Doll

Nuclear structure studies of ${}^{123}\text{Te}$ with (n, γ) and (d, p) reactions
Nucl. Phys. **A673**, 85 (2000)

B.Lauss, A.M.Bragadireanu, M.Iliescu, C.Petrascu, et al.

First measurements at the DAΦNE Φ -factory with DEAR experimental setup
Nucl. Instr.&Methods in Phys.Res. **A482 (2000) 306-**

- I.M.Brancus, B.Vulpescu, A.Bercuci, A.F.Badea, H.Bozdog, M.Duma, M.Petcu, J.Wentz, H.Rebel, A.Haungs, H.J.Mathes, M.Roth**
Measurements of charge ratio of atmospheric muons
Acta Phys.Polon.B31, p.465-470, 2000
- D.Bucurescu, T.von Egidy, H.-F.Wirth, N.Mărginean, U.Köster, G.Graw, A.Metz, R.Hertenberger, Y.Eisermann**
Study of ^{119}Te structure with the (\vec{d}, t) reaction
Nucl. Phys. A674, 11 (2000)
- D.Bucurescu, T.von Egidy, H.-F.Wirth, N.Mărginean, U.Köster, W.Schauer, I.Tomandl, G.Graw, A.Metz, R.Hertenberger**
Study of ^{121}Te structure with the (\vec{d}, t) reaction
Nucl. Phys. A672, 21 (2000)
- I. Caprini, L. Micu, C. Bourrely**
Improvements to the method of dispersion relations for B nonleptonic decays
Phys.Rev. D62, 034016 (2000).
- I.Caprini, J. Fischer**
Convergence of the expansion of the Borel intgral in perturbative QCD improved by conformal mapping
Phys. Rev. D62, 054007 (2000).
- I.Caprini**
Dispersive and chiral symmetry constraints on the light meson form factors
Eur.Phys.J.C13:471-484 (2000).
- A.S. Cârstea, D. Grecu, Anca Vişinescu,**
Multiple scales and bilinear approach for 1-D nonlinear lattices
Roumanian Journal of Physics 45 301-307 (2000).
- A.S. Cârstea**
Extension of the bilinear formalism to supersymmetric KdV-type equations
Nonlinearity 13 1645-1656 (2000).
- A.S. Cârstea**
On the dynamics of rational solutions for 1-D Volterra system
CRM Proceedings and Lecture Notes 25 65-72 (2000).
- A.S. Cârstea**
Weakly localized and supersymmetric structures in nonlinear evolution equations
Roumanian Journal of Physics 45 309-315 (2000)
- J.M.Link, ..., D.Pantea et al. (FOCUS Collab.)**
A measurement of lifetime differences in the neutral D meson system
Phys. Lett. B485, (2000) 62-70.
- J.M.Link, ..., D.Pantea et al. (FOCUS Collab.)**
Measurements of the Σ_c^0 and Σ_c^{++} mass splittings
Phys. Lett. B488, (2000) 218-224.
- J.M.Link, ..., D.Pantea et al. (FOCUS Collab.)**
Search for CP violation in D^0 and D^+ decays
Phys. Lett. B491, (2000) 232-239.
- C.Ciortea, S.Dobrescu, D.Ioanoviciu, G.Baciu, A.I.Badescu-Singureanu, D.Dumitriu, A.Enulescu, D.Fluerasu, N.Gligan, A.B.Radu, R.Ruscu, L.Schächter, S.Z.Szilagyi, and S.Enescu**
RECRIS and future experiments with slow highly charged ions at NIPNE-Bucharest
RIKEN Review, 31 59 (2000)
- I.I.Cotăescu and M. Vişinescu**
Remarks on the radial Klein-Gordon equation in Taub-NUT-like geometries
Annals of West Univ. Timișoara: Theor.Math. and Comp.Phys. 3, 49 (2000)
- I.I.Cotăescu and M. Vişinescu**
Schrödinger quantum modes on the Taub-NUT background
Mod.Phys.Lett.A 15, 145 (2000)
- C.Craciun, M.Sahagia, C.Turcus, A.Stoichioiu, D.Aranghel, F.Scarlat N.Verga**
The response of LiF:Mg, Ti detectors in a 7 MeV photon beam
Romanian Journal of Physics, 45, 1-2(2000)121-127
- Crasovan L.-C., Malomed B. A., Mihalache D., Mazilu D., Lederer F.**
Stable solitons of quadratic Ginzburg-Landau equations
Physical Review E 62, 1322-1327 (2000)
- P. Crochet and the FOPI collaboration**
Sideward flow of K^+ in Ru+Ru and Ni+Ni reactions at SIS energies
Phys. Lett. B 486, 6 (2000)
- Darmanyan S., Crasovan L.-C., Lederer F.**
Double-humped solitary waves in quadratically nonlinear media with loss and gain
Physical Review E 61, 3267-3269 (2000)
- D. B. Ion and M. L. D. Ion**
A new interpretation of two photon entangled experiments via quantum mirrors
Rom. Journ. Phys. 45 (2000) 3-14
- D. B. Ion and M. L. D. Ion**
Limited entropic uncertainty as a new principle in quantum physics
Phys. Lett. B474 (2000) 395-401
- D. B. Ion and M. L. D. Ion**
Plane SPDC-quantum mirror
Rom. Journ. Phys. 45 (2000) 15-23
- D. B. Ion and M. L. D. Ion**
Strong evidences for correlated nonextensive quantum statistics in hadronic scatterings
Phys. Lett. B482 (2000) 57-64

- A. M. Bruce, J. Simpson, D. D. Warner, C. Baktash, C. Barton, M. A. Bentley, M. J. Brinkman, R. A. Cunningham, L. Frankland, T. N. Ginter, C. J. Gross, R. C. Lemmon, B. MacDonald, C. D. O'Leary, S. M. Vincent, R. Wyss, C. H. Yu and N. V. Zamfir
Two - Neutron Alignment and Shape Changes in ^{69}As
Physical Review C **62**, 027303(2000)
- R. Grzywacz, C. H. Yu, Z. Janas, S. D. Paul, J. C. Batchelder, C. R. Bingham, T. N. Ginter, C. J. Gross, J. McConnell, M. Lipoglavsek, A. Piechczek, D. Radford, D. J. Ressler, K. Rykaczewski, J. Shergur, W. B. Walters, E. F. Zganjar and C. Baktash, M. P. Carpenter, R. V. F. Janssens, C. E. Svensson, J. C. Waddington, D. Ward
In - Beam Study of the $N = Z$ Nucleus ^{66}As Using the Decay Tagging Technics
Proceedings of the Nuclear Structure 2000 Conference, East Lansing, Michigan, U. S. A., 15 - 19 August 2000, Nuclear Physics, under press
- Nuclear Structure of fp Shell Odd - Odd $N = Z$ Nuclei Interpreted with IBFFM
Proceedings of the International Workshop "Selected Topics on $N = Z$ Nuclei", Lund University, June 6 - 10, 210 - 215(2000), Lund University Press
- C.Foin, A.Gizon, D.Barneoud, J.Genevey, J.Gizon, D.Santos, F.Farget, P.Paris, C.F.Liang, D.Bucurescu, A.Plochocki
New investigation of the decay of the high-spin isomer in ^{151}Er
Eur. Phys. J. **A8**, 451(2000)
- R. A. Gherghescu and G. Royer
Macroscopic-microscopic energy of rotating nuclei in the fusion like deformation valley
Int. Journal of Modern Physics, **9**, 1:51-66(2000)
- R. A. Gherghescu, G. Royer
Fusion for synthesis of $^{304}\text{120}$
Journal of Optoelectronics, **8**, 4: 37-44(2000)
- Grigore D. R.
On the Quantization of the Gravitational Field
Class. Quant. Grav. **17**, 319-344 (2000)
- Grigore D. R.
The Standard Model and its Generalisations in Epstein-Glaser Approach to Renormalisation Theory
Journ. Phys. A **33**, 8443-8476 (2000)
- A.Haungs and KASCADE collaboration
First results of the air shower experiment KASCADE
Nucl.Phys.B (Proc.Suppl.), vol.87, p.414-416, 2000
- M. Ionescu-Bujor, A. Iordachescu, D. Bucurescu
Decay scheme and magnetic moment of a new isomeric state in ^{86}Y
Phys. Rev. C **62**, 014306 (2000)
- M. Ionescu-Bujor, A. Iordachescu, F. Brandolini, M. De Poli, N. Mărginean, N.H. Medina, Zs. Podolyak, P. Pavan, R.V. Ribas, S.M. Lenzi, A. Gadea, T. Martinez
g factors of the $\frac{7}{2}^+$ and 14^+ isomers in $^{175,176}\text{W}$
Phys. Lett. B **495**, 289 (2000)
- Isar A., Sandulescu A., Scheid W.
Dissipative tunneling through a parabolic potential in the Lindblad theory of open quantum systems
European Physics Journal D **12**, 3-10 (2000)
- Isar A., Sandulescu A., Scheid W.
Purity and decoherence in the theory of open quantum systems
Romanian Journal of Physics **45**, Nr. 3-4 (2000)
- Isar A.
Dissipative tunneling through a potential barrier in the Lindblad theory of open quantum systems
Romanian Journal of Physics **45**, Nr. 3-4 (2000)
- A.Olariu, T.Badica, I.V.Popescu, C.Besliu, M. Bele, Gh.Lazarovici
"Compositional Studies of Ancient Copper from Romanian Territories"
J. Radioanal, Nucl. Chem., **3** (2000) 599
- C.Stihi, I.V.popescu, G.Busuioc, T.Badica, A.Olariu, G.Dima
"Particle Induced X-Ray Emission (PIXE) analysis of Basella Alba L leaves"
J. Radioanal, Nucl. Chem., **246** (2000) 445
- G.Dima. L.Manea, I.V.Popescu, T.Badica, A.Olariu, C.Stihi
"PIXE Analysis of Ca and P in the Downer Cow Syndrome"
Int. J. of PIXE **9** (2000)
- I.V.Popescu, T.Badica, A.Olariu, C.Besliu, R.Rodman, O.Militaru, I.Stefanescu, M.Petre
"Aerosol Samples Elemental Analysis from some Romanian Urban Regions"
Preprint J. FiM 2000
- M. Mihai, I.V. Popescu
"Mathematical Considerations Regarding the Stability of Trace Elements Systems by Polynomial Regression"
J. Radioanal, Nucl. Chem., **245** (2000) 455
- Ixaru L. Gr., De Meyer H., Vanden Berghe G.
Highly accurate eigenvalues for the distorted Coulomb potential
Physical Review E **61**, 3151-3159 (2000)
- Ixaru L. Gr.
CP methods for the Schrödinger equation
Journal. Comp. and Appl. Math. **125**, 347 (2000) (invited paper in the Millenium issue)
- V.M Karnakhov, C. Coca, V.I Moroz
Investigation of the Narrow Structure $K(1630)$ Decaying into the $K_s^0\pi^+\pi^-$ System
Physics of Atomic Nuc. **63** (2000)588, Translated from *Yadernaya Fizika* **63** (2000)652

- J.M.Link, ..., D.Pantea et al. (FOCUS Collab.)**
Preliminary FOCUS results on charmed hadrons spectroscopy
Nucl. Phys. A663-664, (2000) 651c-654c.
- A.Luca, M.Etcheverry, J.Morel**
Emission probabilities of the main γ - rays of ^{237}Np in equilibrium with ^{233}Pa
Applied Radiation and Isotopes 52, 3(2000)481-486
- A.Luca, P. de Felice, G.Tanase**
Low level gamma spectrometry by beta-gamma coincidence
Applied Radiation and Isotopes 53, 1-2, (2000)221-224
- Marghitu S., Dinca C., Rizea M., Oproiu C., Toma M., Martin D., Iliescu E.**
Non-destructive beam characterization at an electron source exit
Nuclear Instruments and Methods in Physics Research B161-163, 1113 (2000)
- N.Mărginean, D.Bucurescu, C.A.Ur, D.Bazzacco, S.Lunardi, S.M.Lenzi, C.Rossi Alvarez, G.de Angelis, A.Gadea, D.R.Napoli, M.De Poli, P.Spoloare**
First identification of excited states in the $T_z=1/2$ nucleus ^{81}Zr
Phys. Rev. C61, 024310 (2000)
- N.Mărginean, D.Bucurescu, Ghe.Căta-Danil, I.Căta-Danil, M.Ivaşcu, C.A.Ur**
High-spin states in the ^{94}Nb nucleus
Phys. Rev. C62, 034309 (2000)
- Melnikov I. V., Panoiu N.-C., Mihalache D.**
Localized multidimensional femtosecond optical pulses in an off-resonance two-level medium
Optics Communications 181, 345-351 (2000)
- Mihalache D., Mazilu D., Crasovan L.-C., Malomed B. A., Lederer F.**
Azimuthal instability of spinning spatiotemporal solitons
Physical Review E 62, R1505-R1508 (2000)
- Mihalache D., Mazilu D., Crasovan L.-C., Malomed B. A., Lederer F.**
Three-dimensional spinning solitons in the cubic-quintic nonlinear medium
Physical Review E 61, 7142-7145 (2000)
- Mihalache D., Mazilu D., Crasovan L.-C., Torner L., Malomed B. A., Lederer F.**
Three-dimensional walking spatiotemporal solitons in quadratic media
Physical Review E 62, 7340-7347 (2000)
- J.R.B. Oliveira, E.W. Cybulska, N.H. Medina, M.N. Rao, R.V. Ribas, W.A. Seale, F.R. Espinoza-Quinones, M.A. Rizzutto, D. Bazzacco, F. Brandolini, S. Lunardi, C.M. Petrache, Zs. Podolyak, C. Rossi Alvarez, C.A. Ur, G. de Angelis, D.R. Napoli, P. Spoloare, A. Gadea, D. De Acuna, M. De Poli, E. Farnea, D. Foltescu, M. Ionescu-Bujor, A. Iordachescu**
High-spin state spectroscopy of ^{143}Dy
Phys. Rev. C 62, 064301 (2000)
- Panoiu N.-C., Mihalache D., Mazilu D., Crasovan L.-C., Melnikov I. V., Lederer F.**
Soliton dynamics of symmetry-endowed two-soliton solutions of the nonlinear Schrödinger equation
Chaos 10, 625-640 (2000)
- Panoiu N.-C.**
Anomalous diffusion in two-dimensional potentials with hexagonal symmetry
Chaos 10, 166-179 (2000)
- Pantelică A., Sălăgean M., Georgescu I.I., Murariu-Măgureanu M.D., Scarlat A.G.**
Neutron activation analysis of some fossil samples from Romanian sites
J. Radioanal. and Nucl. Chem., Vol.224, No. 3, 2000, 579-582
- N. Pauwels, F. Clapier, P. Gara, M. Mirea and J. Proust**
Experimental Determination of Neutron Spectra Produced by Bombarding Thick Targets: Deuterons (100 MeV/u) on ^9Be , Deuterons (100 MeV/u) on ^{238}U and ^{36}Ar (95 MeV/u) on ^{12}C
Nuclear Instruments and Methods B 160, 315-327 (2000)
- A.A.Korshennikov, M.S.Golovkov, A.Ozawa, E.A.Kuzmin, E.Y.Nikolskii, K.Yoshida, B.G.Novatskii, A.A.Ogloblin, I.Tanihata, Z.Fulop, K.Kusaka, K.Morimoto, H.Otsu, H.Petrascu and F.Tokanai**
Observation of an Excited State in ^7He with an Unusual Structure
RIKEN Accelerator Progress Report, 34 62 (2000)
- A.A.Korshennikov, M.S.Golovkov, A.Ozawa, K.Yoshida, I.Tanihata, Z.Fulop, K.Kusaka, K.Morimoto, H.Otsu, H.Petrascu, F.Tokanai, D.D.Bogdanov, M.L.Chelnokov, A.S.Fomichev, V.A.Gorshkov, Y.T.Oganessian, A.M.Rodin, S.I.Sidorchuk, S.V.Stepantsov, G.M.Ter-Akopian, R.Wolski, W.Mittig, P.Roussel-Chomaz, H.Savajols, E.A.Kuzmin, E.Y.Nikolskii, B.G.Novatskii, A.A.Ogloblin**
Superheavy Hydrogen ^5H , Spectroscopy of ^7He
RIKEN Accelerator Progress Report, 34 61 (2000)

- M.Petrascu, I.Tanihata, K.Morimoto, T.Kobayashi, K.Katori, I.Cruceru, M.Giurgiu, A.Isbasescu, H.Petrascu, R.Ruscu, M.Chiba, S.Nishimura, A.Ozawa, T.Suda, K.Yoshida, C.Bordeanu**
Search for Neutron Pair Pre-Emission in the Fusion of ^{11}Li Halo Nuclei with Si Targets
RIKEN Accelerator Progress Report, **34** 63 (2000)
- Petrovici A., Schmid K.W., Faessler A.**
Microscopic aspects of shape coexistence in ^{72}Kr and ^{74}Kr
Nuclear Physics A665, 333 (2000)
- Petrovici A.**
Shape coexistence phenomena in medium mass nuclei
In: Proceedings of the Int. Symposium "Advances in Nuclear Physics", Eds. Poenaru D. and Stoica S., World Scientific (2000) p. 352
- D. N. Poenaru, B. Dobrescu, W. Greiner, J. H. Hamilton and A. V. Ramayya**
Nuclear quasi-molecular states in ternary fission.
Journal of Physics G: Nuclear and Particle Physics **26**, L97-L102 (2000)
- B.Adeva, M.Iliescu, M.Pentia, C.Petrascu, T.Ponta, et al. (DIRAC Collab.)**
Test of chiral perturbation theory with DIRAC at CERN
Acta Physica Polonica B31 (2000) 2571-2579
- B.Lauss, A.M.Bragadireanu, M.Iliescu, C.Petrascu, T.Ponta, et al. (DEAR Collab.)**
The DEAR experiment on DAΦNE
Acta Physica Polonica B31 (2000) 2257-
- M.Augsburger, A.M.Bragadireanu, M.Iliescu, C.Petrascu, T.Ponta, et al. (DEAR Collab.)**
The DEAR case
Nucl. Phys. A, vol. 663-664(1-4)(2000) 561-564
- Racolta P.M.**
Effect of chromium nitride coating on the corrosion and wear resistance of stainless steel
Applied Surface Science 47-64, p. 156, 2000
- F. Rami and the FOPI collaboration**
Isospin-tracing: A probe of non-equilibrium in central heavy-ion collisions
Phys. Rev. Lett. **84**, 1120 (2000)
- A.C.Razdolescu, E.L.Grigorescu, M.Sahagia, A.Luca, C.Ivan**
Standardization of ^{169}Yb by the $4\pi\beta - \gamma$ method
Applied Radiation and Isotopes **52**, 3(2000) 505-508
- H.Rebel and KASCADE collaboration**
The origin of high energy cosmic rays displayed by the energy spectrum and elemental composition
Acta Phys.Polon.B31, p.323-334, 2000
- M.A. Rizzutto, M.N. Rao, W.A. Seale, J.R.B. Oliveira, E.W. Cybulska, N.H. Medina, R.V. Ribas, F.R. Espinoza-Quinones, D. Bazzacco, F. Brandolini, S. Lunardi, C.M. Petrache, Zs. Podolyak, C. Rossi Alvarez, C.A. Ur, G. de Angelis, D.R. Napoli, P. Spolaore, A. Gadea, D. De Acuna, M. De Poli, E. Farnea, D. Foltescu, M. Ionescu-Bujor, A. Iordachescu, A. Chatterjee, A. Saxena, L. Sajo-Bohus**
The $\pi h_{11/2} \otimes \nu h_{11/2}$ yrast band in odd-odd ^{140}Tb
Phys. Rev. C **62**, 027302 (2000)
- P. Roussel, Ch.O. Bacri, V. Borrel, E. Kashy, C. Stephan, L. Tassan-Got, D. Beaumel, M. Bernas, F. Clapier and M. Mirea**
Light Particles Emitted with Very Forward Quasi-Projectiles and the Mechanism in the Fragmentation of 44 MeV/a.m.u ^{40}Ar
Journal of Physics G **26**, 1641-1654 (2000)
- Rykaczewski K., Batchelder J. C., Bingham C. R., Davinson T., Ginter T. N., Gross C. J., Grzywacz R., Karny M., MacDonald B. D., Mas J. F., McConnell J. W., Piechaczek A., Slinger R. C., Toth K. S., Walters W. B., Woods P. J., Zganjar E. F., Barmore B., Ixaru L. Gr., Kruppa A. T., Nazarewicz W., Rizea M., Vertse T.**
Proton emitters ^{140}Ho and ^{141}Ho : probing the structure of unbound Nilsson orbitals
Physical Review C **60**, 011301-1-011301-5, (2000)
- M.Sahagia, A.C.Razdolescu, E.L.Grigorescu, A.Luca, C.Ivan**
The standardization of a ^{204}Tl solution
Applied Radiation and Isotopes **52**, 3(2000)487-492
- L. Schächter, K. Stiebing, S. Dobrescu, A.I. Badescu-Singureanu, S. Runkel, O. Hohn, L. Schmidt, A. Schempp and H. Schmidt-Böcking**
Influence of the secondary electrons emitted by a cylindrical metal-dielectric structure on the Frankfurt 14 GHz electron cyclotron resonance ion source performances
Rev. Sci. Instrum., **71** 918 (2000)
- Paraoanu Gh.-S., Scutaru H.**
Fidelity for multimode thermal squeezed states
Physical Review A **61**, 022306-1-022306-4 (2000)
- C.Signorini, A.Andrighetto, M.Ruan, J.Y.Guo, L.Stroe, F.Soramel, K.E.G.Löbner, L.Müller, D.Pierroutsakou, M.Romoli, K.Rudolph, I.J.Thompson, M.Trotta, A.Vitturi, R.Gernhauser, A.Kastenmüller**
Unusual near-threshold potential behaviour for the weakly bound nucleus ^9Be in elastic scattering from ^{209}Bi
Phys. Rev. C **61**, 061603(R) (2000)

Stefanescu E., Sandulescu A., Scheid W.

The collisional decay of a Fermi system interacting with a many-mode electromagnetic field
International Journal of Modern Physics E, 17-50 (2000)

M. Vişinescu

Generalized Taub-NUT metrics and Killing-Yano tensors
J.Phys.A: Math.Gen. **33**, 4383 (2000)

M. Vişinescu

On the Taub-NUT spinning space
Fortschr.Phys. **49**, 229 (2000)

B.Vulpescu, J.Wentz, I.M.Brancus, H.Rebel, A.F.Badea, H.Bozdog, M.Duma, A.Haungs, H.J.Mathes, M.Petcu and M.Roth

Measurements of the charge ratio of atmospheric muons in the range 0.2-1.0 GeV/c by observing the decay electrons from muonic atoms
Nucl.Phys.B (Proc.Suppl.), vol.87, p.528-529, 2000

Books and Chapter in Books

A.S. Cârstea, D. Grecu, Anca Vişinescu

Rational solutions of a mixed KdV+mKdV and Benjamin-Ono equation
"Nonlinearity, Integrability and all that: Twenty years after NEEDS '79" editors M. Boiti, L. Martina, B. Prinari, G. Soliani, World Scientific, 2000 pg.82-89.

A.S. Cârstea

Bilinear formalism for supersymmetric KdV - type equations
"Nonlinearity, Integrability and all that: Twenty years after NEEDS '79" editors M. Boiti, L. Martina, B. Prinari, G. Soliani, World Scientific, 2000 pg.75-82.

D. N. Poenaru and S. Stoica (Eds.)

Advances in Nuclear Physics, Proc. of the International Symposium celebrating 50 years of institutional physics research in Romania
(World Scientific, Singapore, 2000) , pp. i-xiii and 1-433.

Carmen Postolache, Cristian Postolache

Introducere in ecotoxicologie
ARS DOCENDI

Racolta P.M.

Status and Perspectives at the Cyclotron IFIN-HH Bucharest for Diagnostic and Therapeutic Radionuclides Production
Report on the 1-st Research Co-ordination Meeting of the Co-ordinated Research Project on "Standardized High Current Solid Targets for Cyclotron Production of Diagnostic and Therapeutic Radionuclides", Brussels, Belgium, 27-30 nov. 2000

Racolta P.M.

Surface modification of materials by ion implantations for industrial and medical applications
IAEA-TECDOC-1165, July 2000, INIS Clearinghouse

Stefanescu E.

Sisteme Disipative, 128 pp., ISBN 973-27-0707-0
(Ed. Academiei Române, Bucuresti, 2000)

M. Vişinescu

Killing-Yano tensors on manifolds admitting "hidden" symmetries
Proceedings of International Symposium on Advances in Nuclear Physics, Bucharest (1999), World Scientific, Singapore (2000)

Preprints

Adam Gh., Adam S.

Increasing reliability of Gauss-Kronrod quadrature by Eratosthenes' sieve method
Preprint ICTP-Trieste, IC/2000/70 (2000), 20 pp.

S. Amato, ..C. Coca, D. D Dumitru, G. Giolu, C. Magureanu, R. Petrescu, S.Popescu, T. Preda, A. Rosca, V. Rusu et al., (LHCb Collaboration)

LHCb Calorimeters Technical Design Report
CERN/LHCC/2000-0036

M. Bonnet..C. Coca, D.D Dumitru, G. Giolu, C. Magureanu, S. Popescu, R. Petrescu et al.,
The hadron calorimeter prototype design and construction
LHCb 2000-035 public, <http://weblib.cern.ch>

I. Caprini, L. Micu, C. Bourrely

Quark-hadron duality, factorization and strong phases in $B_d^0 \rightarrow \pi^+ \pi^-$ decay
CPT-2000/P.4064, hep-ph/0010314.

P. Ball, . . . I. Caprini, . . .

B decays at the LHC

Preprint CERN-TH-2000-101

A. Cimpean, C. Coca, D. D Dumitru, D.T Dumitru, C. Magureanu

A proposal for High Voltage Power Supply System for HCAL of LHCb experiment

LHCb 2000-092 public, <http://weplib.cern.ch>

C. Coca, C. Magureanu et al.

A proposal for high voltage power supply system for HCAL of LHCb experiment

LHCb-2000-092

C. Coca, T. Preda, A. Rosca et al.

The hadron calorimeter prototype beam-test results

LHCb-2000-036

C. Coca, T. Preda, A. Rosca, I Ajinenko et al.,

The hadron Calorimeter Prototype Beam-test Results

LHCb 2000-036 public, <http://weplib.cern.ch>

I.I. Cotăescu and M. Vişinescu

The Dirac field in Taub-NUT background

hep-th/0008181, to appear in Int.J.Mod.Phys.A (2001)

D. Grecu, Anca Vişinescu

Multiscale analysis of a Davydov model with an harmonic long range interaction of Kac-Baker type

nlin.SI/0010019

Grigore D. R.

The Renormalization Theory of the Non-Abelian Gauge Theories in the Causal Approach

hep-th/0010226

Grigore D. R.

Wess-Zumino Model in the Causal Approach

hep-th/0011174

M. Mirea, O. Bajeat, F. Clapier, F. Ibrahim, A.C. Mueller, N. Pauwels and J. Proust

Modeling a Neutron Rich Nuclei Source

IPNO DR 00-32, IPN-Orsay

International Conferences

C.Alexa, V.Boldea, S.Constantinescu, S.Dita, et al., NA50 Collaboration

J/Ψ suppression in ultrarelativistic heavy-ion collisions

at 9th International Conference on Nuclear Reaction Mechanisms, Villa Monastero, Varenna, Italy, June 5-9, 2000

C.Alexa, V.Boldea, S.Constantinescu, S.Dita, et al., NA50 Collaboration

Φ production in Pb-Pb collisions at 158 GeV/c per nucleon in the NA50 experiment

at the XXXVIII International Winter Meeting on Nuclear Physics, Bormio, Italy, January 24-29, 2000

C.Alexa, V.Boldea, S.Constantinescu, S.Dita, et al., NA50 Collaboration

Centrality dependence of the J/ψ suppression in Pb-Pb collisions at 158 GeV/c

at the Hadron Structure 2000, Stara Lesna, Slovakia, Oct. 2-8 2000

C.Alexa, V.Boldea, S.Constantinescu, S.Dita, et al., NA50 Collaboration

Charmonium suppression in Pb-Pb collisions and Quark-Gluon deconfinement

at Structure of the Nucleus at the Dawn of the Century, Bologna, Italy, May 29-June 3, 2000

C.Alexa, V.Boldea, S.Constantinescu, S.Dita, et al., NA50 Collaboration

Evidence for deconfinement from the J/Ψ suppression pattern in Pb-Pb collisions by the NA50 experiment

at Quark Confinement and the hadron Spectrum IV, Vienna, Austria, July 3-8, 2000

C.Alexa, V.Boldea, S.Constantinescu, S.Dita, et al., NA50 Collaboration

J/Ψ suppression in Pb-Pb collisions at CERN SPS

at the XXX International Symposium on Multiparticle Dynamics, Lake Balaton, Hungary, Oct 9-15, 2000

C.Alexa, V.Boldea, S.Constantinescu, S.Dita, et al., NA50 Collaboration

Latest results from NA50 on J/ψ suppression and multiplicity distributions in Pb-Pb collisions at 158 GeV/c

at the XXXVIII International Winter Meeting on Nuclear Physics, Bormio, Italy, January 24-29, 2000

C.Alexa, V.Boldea, S.Constantinescu, S.Dita, et al., NA50 Collaboration

Recent results on intermediate mass dimuon production

at 4th Rencontres du Vietnam, Hanoi, Vietnam, July 19-25, 2000

C.Alexa, V.Boldea, S.Constantinescu, S.Dita, et al., NA50 Collaboration

Relative Production of the Phi vector meson in heavy ion collisions

at Strangeness 2000, Berkeley, California, July 20-25, 2000

C.Alexa, V.Boldea, S.Constantinescu, S.Dita, et al., NA50 Collaboration

Results from the NA50 experiment on J/Psi suppression in Pb-Pb collisions at the CERN SPS

at the IX International Workshop on Multiparticle Production, "New Frontiers in Soft Physics and Correlations on the Threshold of the Third Millennium", Torino, Italy, June 12-17, 2000

C.Alexa, V.Boldea, S.Constantinescu, S.Dita, et al., NA50 Collaboration

Results on open charm from NA50

at Strangeness 2000, Berkeley, California, July 20-25, 2000

C.Alexa, V.Boldea, S.Constantinescu, S.Dita, et al., NA50 Collaboration

Searching for QGP: the J/Ψ probe in the NA50/CERN experiment

at the 7th. Conference on Intersections of Particle and Nuclear Physics, Quebec City, Canada, May 22-28, 2000

A. Andronic and FOPI collaboration

Collective Flow in Heavy Ion Collisions at SIS Energies

Deutsche Physikalische Gesellschaft Meeting, Dresden, March 20 - 24, Germany, 2000

G.S. Anagnostatos, A. Vahlas, J. Giapitzakis, A.N. Antonov, M. Avrigeanu

Light exotic nuclei: A new explanation of halo

in Proc. Int. Conf. on Nuclear Structure and Related Topics, Dubna, Russia, June 6-10, 2000 (in press)

M. Avrigeanu, A.N. Antonov, H. Lenske, I. Ștețcu, V. Avrigeanu

Analysis of multistep direct reactions to the continuum with realistic effective NN interactions (invited talk)

in Proc. 9th Int. Conf. on Nuclear Reaction Mechanisms, Varenna, Italy, June 5-9, 2000, edited by E. Gadioli (Ricerca Scientifica ed Educazione Permanente, Suppl. 115, Milano, 2000), p. 171-180

M. Avrigeanu, I. Ștețcu, V. Avrigeanu

Effective Interactions for Preequilibrium Reactions Studies

"Workshop on Nuclear Reaction Data and Nuclear Reactors: Physics, Design and Safety", The Abdus Salam International Centre for Theoretical Physics, Trieste, 13 March 2000 - 14 April 2000

A.F.Badea, H.Rebel, M.Zzazyan, I.M.Brancus, A.Haungs, J.Oehlschlaeger

A simulation based study of Linsley's approach to infer the elongation rate and fluctuations of the EAS maximum depth from the arrival times distributions

17-th European Cosmic Rays Symposium, ECRS, Lodz, Poland, July 24-28, 2000

A.F.Badea

Why we measure muon arrival time distributions in Extensive Air Showers

NATO Advanced Study Institute "Nuclei far from the stability and Astrophysics", Predeal, Romania, August 28- Sept.8, 2000

I. Berceanu and DRACULA collaboration

Fluctuation phenomena for dissipative processes in $^{19}F + ^{27}Al$ system

7-th International Conference Nucleus-Nucleus Collisions, Strasbourg, July 3 - 7, France, 2000

S. Berceanu and A.Gheorghe

Holomorphic quantization and equations of motion generated by algebraic Hamiltonians,

invited talk by S. Berceanu at the Third International Workshop on Wavlets, Quantization and Differential Equations: Theory and Applications, University of Havana, Cuba, May 2-6, 2000

S.Bianco, ..., D.Pantea et al.

New FOCUS results on charm mixing and CPV

"International Conference on CP Violation Physics", Ferrara, Italy, Sept. 18-22, 2000

G.Boca, ..., D.Pantea et al.

Recent results from E831-FOCUS

"Heavy quarks at fixed target", Rio de Janeiro, Brasil Oct. 9-12, 2000

I.M.Brancus

Phenomenology of Extensive Air Showers

NATO Advanced Study Institute "Nuclei far from the stability and Astrophysics", Predeal, Romania, August 28- Sept.8, 2000

F.Brandolini et al.

Spherical and deformed states in $N \approx Z 1f_{7/2}$ nuclei

Proc. International Workshop "Selected Topics on $N \approx Z$ nuclei" (Pingst 2000), Lund, (2000) p. 70

F. Brandolini, S.M. Lenzi, C.A. Ur, D. Bazzacco, R. Menegazzo, P. Pavan, C. Rossi Alvarez, N.H. Medina, R.V. Ribas, N. Mărginean, D.R. Napoli, G. de Angelis, M. De Poli, T. Martinez, A. Algara-Pineda, A. Gadea, E. Farnea, D. Bucurescu, M. Ionescu-Bujor, A. Iordachescu, J.A. Cameron, S. Kasemann, I. Schneider, J.M. Espino, A. Povos, J. Sanchez-Solano

Spherical and deformed states in $N \approx Z 1f_{7/2}$ nuclei

Int. Workshop PINGST2000, Selected Topics on $N \approx Z$ Nuclei, June 6th-11th 2000, Lund, Sweden, p.70.

F. Brandolini, S.M. Lenzi, C.A. Ur, D. Bazzacco, R. Menegazzo, P. Pavan, C. Rossi Alvarez, N.H. Medina, R.V. Ribas, N. Mărginean, D.R. Napoli, G. de Angelis, M. De Poli, T. Martinez, A. Algora-Pineda, A. Gadea, E. Farnea, D. Bucurescu, M. Ionescu-Bujor, A. Iordachescu, J.A. Cameron, S. Kasemann, I. Schneider, J.M. Espino

Collective motions in the $1f_{7/2}$ shell

Int. Conf. on Structure of the Nucleus at the Dawn of the Century, Bologna, May 29th - June 3rd, 2000.

D.Bucurescu, I.Cata-Danil, G.Cata-Danil, M.Ivascu, L.Stroe, N.Mărginean, C.A.Ur

Gamma-ray spectroscopy studies at the NIPNE tandem accelerator

Advances in Nuclear Physics, eds. D.Poenaru and S.Stoica, World Scientific, Singapore (2000), p. 344-351

C.Buettner, K.Daumiller, P.Doll, D.Martello, R.Obenland, J.Zabierowski, for KASCADE collaboration

Lateral distributions and production height of muon derived from the muon tracking detector in KASCADE experiment

17-th European Cosmic Rays Symposium, ECRS, Lodz, Poland, July 24-28, 2000

C.Campeanu et al.

Obtaining of high specific activity $^{186,188}\text{Re}$ perhenates to be used for biomolecule labelling

5th International Conference on Nuclear and Radio Chemistry, Pontresina, Suisse, sept. 2000, extended abstract., vol.2, p.750-753

C.Campeanu et al.

Studii asupra posibilitatilor de realizare a unui generator $^{99}\text{Mo} - ^{99m}\text{Tc}$

Conferinta Nationala de Chimie, Caciulata, oct. 2000

I. Caprini

Theoretical constraints on the semileptonic and non-leptonic B-decays

Proceedings of the International Symposium Advances in Nuclear Physics, Bucharest, Romania, World Scientific, 2000, pag.178, eds. D. Poenaru and S. Stoica.

C.Ciortea, S.Dobrescu, D.Ioanoviciu, G.Baciu, A.I.Badescu-Singureanu, D.Dumitriu, A.Enulescu, D.Fluerasu, N.Gligan, A.B.Radu, R.Ruscu, L.Schächter, S.Z.Szilagyi, and S.Enescu

RECRIS and future experiments with slow highly charged ions at NIPNE-Bucharest

National Physics Conference, September 21-23, 2000, Constanța, Romania, Abstracts p.12 (plenary session)

S. Dobrescu, L. Schächter and Al. I. Badescu-Singureanu,

Romanian 14 Ghz Electron Cyclotron Resonance Ion Source - Recris

Romanian National Conference of Physics, September 2000, Constanța, Romania

A. C. Dragolici, A. Zorliu

WET STORAGE OF NUCLEAR SPENT FUEL FROM NUCLEAR RESEARCH REACTOR WWR-S, IFIN-HH

Regional Workshop on Characterization, Management and Storage of Spent Fuel from Research and Test Reactors, Swierk, Poland, 08-12 May, 2001

S.E.Enescu, I.Bibicu, A.Kluger, and V.Tripadus

An Experimental Set-up for Rayleigh Scattering of Mössbauer Radiation

National Physics Conference, September 21-23, 2000, Constanța, Romania, Abstracts p.26 (oral presentation)

S.E.Enescu, I.Bibicu, A.Kluger, and V.Tripadus

Rayleigh Scattering of Mössbauer Radiation on Pyrolytic Graphite

National Physics Conference, September 21-23, 2000, Constanța, Romania, Abstracts p.44 (oral presentation)

S.E.Enescu, I.Bibicu, M.N.Grecu, and A.Kluger

Critical Scattering of Low Energy Gamma Rays on Rb_2ZnCl_4 Around the Normal-Incommensurate Phase Transition Point

National Physics Conference, September 21-23, 2000, Constanța, Romania, Abstracts p.44

F.Fabbri, ..., D.Pantea et al.

Results on charmed Meson Spectroscopy from FOCUS "International Conference on HEP 2000", Osaka, Japan, July 27 - Aug. 2, 2000

F.Fessler, G.Schatz and KASCADE collaboration

Search for PeV Gamma Rays with the KASCADE experiment

International Symp.on High Energy Astronomy, June 26-30, 2000

V.Fugaru

^{169}Yb - DTPA for diagnosis purposes

Balkan Congress of Oncology, Brasov, Romania, september 2000

A.Gadea et al.

In-beam and off-beam studies on ^{52}Fe

International workshop, Selected Topics on N=Z nuclei (Pingst 2000), Lund, 2000 (abstract nr. 125)

Georgescu I.I., Băran Gh.D., Pantelică A.I, Sălăgean M.N., Scarlat A.G.

On the radioactivity of water and sediments from the Danube River significant cross sections during Autumn 1998

Proceedings of the 5th International Conference on Nuclear and Radiochemistry (NR5), Pontresina, 3-8 Sept., 2000, 477 - 479

G. Royer, R. Moustabchir and R. A. Gherghescu

Alpha Emission as an asymmetric fission and super-heavy element decay

invited talk, in Proc. Int. Conf. on Nuclear Reaction Mechanism, June 5-9, 2000, Varenna, Italy

R. A. Gherghescu and W. Greiner

Fusion valleys for the synthesis of superheavy elements
invited talk at Proc. NATO Advanced Summer School: Nuclei far from Stability and Astrophysics, 28 Sept.-10 Oct. 2000, Predeal, Romania

R. Glasstetter, H. Ulrich, K.H. Kampert for KASCADE collaboration

Determination of the energy spectrum and composition of cosmic rays in the knee region from shower size spectra

17-th European Cosmic Rays Symposium, ECRS, Lodz, Poland, July 24-28, 2000

D. Grecu, Anca Vişinescu

Multiscale analysis of a Davydov model with an harmonic long range interaction of Kac-Baker type
"Balkan Physics Union Conference", Veliko Turnovo, august 2000

D. Grecu, Anca Vişinescu, A.S. Cârstea

Higher order approximation in a multi-scale analysis of a Davydov model

Conferința Națională de Fizică, Constanța, sept. 2000

D. Grecu, Anca Vişinescu

Small amplitude localized solutions in a Davydov model with a Kac-Baker long range interaction

"Quantum Field Theory and Hamiltonian Systems", Călimănești, mai 2000

E.L. Grigorescu et al.

Contor proportional multifilar deschis

Conferinta Nationala de Fizica, Constanta, sept. 2000

R. Haeusler, A.F. Badea, H. Rebel, I.M. Brancus for KASCADE collaboration

Experimental studies of the local time profile of the EAS muon component and the influence of the multiplicity of the observed muon arrival time distributions
17-th European Cosmic Rays Symposium, ECRS, Lodz, Poland, July 24-28, 2000

J. H. Hamilton, ... W. Greiner, D. N. Poenaru et al. (total 26 authors)

Behavior of nuclear matter under extreme conditions in fission

invited talk in Fundamental Issues in Elementary Matter, Proc. Internat. Symp. in honor and memory of Michael Danos, (241. W. & E. Heraeus Seminar), Bad Honnef, Germany, 25-29 Sept. 2000

A. Haungs for KASCADE collaboration

Cosmic Ray Physics around the Knee with KASCADE experiment

Chacaltaya Meeting on Cosmic Rays, La Paz, Bolivia, July 2000

A. Haungs for KASCADE collaboration

Towards the energy spectrum and composition of primary cosmic rays in the knee region: methods and results at KASCADE

11-th International Symposium of Very High Energy Cosmic Rays Interactions, Sao Paulo, Brasil, July 2000

Isar A.

Dissipative tunneling through a parabolic potential in the theory of open quantum systems

Communication at the NATO ASI "Nuclei far from Stability and Astrophysics", Predeal, 2000

K.H. Kampert for KASCADE collaboration

Methods of determination of the energy and mass of the primary particles at extensive air shower energies
17-th European Cosmic Rays Symposium, ECRS, Lodz, Poland, July 24-28, 2000

V.M. Karnakhov, C. Coca, V.I. Moroz

Processes with a possible formation of exotic states

Invited talk presented by V.M. Karnaukhov at the "XV International seminar on High Energy Physics problems, Dubna, 25-29 September 2000", <http://relnp.jinr.ru/ishepp/xv/pr/>; Proceedings in print

S.M. Lenzi, D.R. Napoli, M. Axiotis, E. Fabbian, A. Gadea, M. Ionescu-Bujor, A. Iordachescu, N. Mărginean, C.A. Ur, GASP collaboration, EUROBALL collaboration, N-WALL Collaboration

High spin structure of light nuclei

Int. Conf. on Structure of the Nucleus at the Dawn of the Century, Bologna, May 29th - June 3rd, 2000.

A. Luca et al.

Probabilitati de emisie a radiatiilor gamma din lantul $^{237}\text{Np} - ^{233}\text{Pa}$

Conferinta Nationala de Fizica, Constanta, sept. 2000

V. Lungu et al.

Development of ^{188}Re radiolabelling procedures of peptides

Research Coordinating Meeting on Labelling Techniques of Biomolecules for Targeted Radiotherapy, Bombay, India, Jan. 2000

N. Mărginean, C. Rossi Alvarez, D. Bucurescu, C.A. Ur, A. Gadea, S. Lunardi, D. Bazzacco, G. de Angelis, M. Axiotis, M. De Poli, E. Farnea, M. Ionescu-Bujor, A. Iordachescu, S.M. Lenzi, Th. Kroll, T. Martinez, R. Menegazzo, D.R. Napoli, G. Nardelli, P. Pavan, B. Quintana, P. Spolaore

New nuclei around the N=Z line in the A=80-90 region

International School of Nuclear Physics, 22nd Course: Radioactive Beams in Nuclear and Astro Physics, Erice-Sicily, 16-24 September 2000.

V.Mihaila et al.

Paramynobenzoic acid 3, 5-T
7th International Symposium on Synthesis and Applications of Isotopically Labelled Compounds, Dresda, Germany, may 2000

V.Mihaila et al.

Tocopherol methyl-T
7th International Symposium on Synthesis and Applications of Isotopically Labelled Compounds, Dresda, Germany, may 2000

G.Mihailescu et al.

¹⁸⁸Re labelled Anti-CEA-Monoclonal Antibody
Balkan Congress of Oncology, Brasov, Romania, september 2000

M. Mirea

Shell Effects in the Fine Structure of the ¹⁴C Cluster Decay
in 50 Years of Nuclear Shells, Proceedings of the 49th Meeting on Nuclear Spectroscopy and Nuclear Structure, Dubna, Russia, 21-24 April 1999, (Yu. Ts. Oganessian and R Kalpakchieva eds., World Scientific, Singapore, 2000), p. 134-143.

N.Negoita et al.

Biological active Compounds with ³⁵S dysulphide bridges
7th International Symposium on Synthesis and Applications of Isotopically Labelled Compounds, Dresda, Germany, may 2000

N.Negoita et al.

Date preliminară privind obținerea Timinei marcate ca ^{99m}Tc
Conferința Națională de Chimie, Căciulata, oct. 2000

L.Pentchev, K.Daumiller, P.Doll for KAS-CADE collaboration

Complementary use of the muon density and track information for the investigation of the muon component in EAS
17-th European Cosmic Rays Symposium, ECRS, Lodz, Poland, July 24-28, 2000

M.Petrascu, I.Tanihata, T.Kobayashi, A.Isbasescu, H.Petrascu, I.Cruceru, M.Giurgiu, A.Korshennikov, K.Morimoto, A.Ozawa, R.Ruscu, K.Yoshida, C.Bordeanu

Investigation of Neutron Pair Pre-Emission in the Fusion of ¹¹Li Halo Nuclei with Si targets
International Conference RIB00 (Perspective in Physics with Radioactive Isotopes Beams 2000), Hayama, Kanagawa, Japan, Nov. 2000

A. Petrovici

Variational approach to coexistence phenomena in $N \simeq Z$ nuclei; Neutron-proton correlations in medium mass $N \simeq Z$ nuclei
Nuclear Structure for the 21st Century (INT-00-3), Seattle, Washington, USA, 16.-31.10.2000

A. Petrovici

Variational approach to complex nuclear structure
Shell Model 2000, Riken, Japan, 05-08.03.2000

A. Petrovici

Variational approach to coexistence phenomena in $N=Z$ nuclei
Nuclei far from Stability and Astrophysics, Predeal, Romania, 28.-08.09.2000

A. Petrovici

Variational approach to the structure of $N=Z$ nuclei
Shell Model 2000, GSI - Darmstadt, Germany, 02.-03.05.2000

D. N. Poenaru, B. Dobrescu and W. Greiner

Three-Cluster Nuclear Molecules
invited talk, in Clustering Aspects of Nuclear Structure and Dynamics, Proc. of the 7th International Conference, Rab, Croatia, Eds. M. Korolija, Z. Basrak and R. Čaplar (World Scientific, Singapore, 2000), p. 205-212.

D. N. Poenaru, B. Dobrescu, W. Greiner, J. H. Hamilton and A. V. Ramayya

Fission energy surfaces and ternary fission
invited talk in Exotic Nuclear Structures (ENS2000), Proc. Internat. Symp., Debrecen, Hungary, 15-20 May 2000

D. N. Poenaru, B. Dobrescu, W. Greiner, J. H. Hamilton and A. V. Ramayya

New Fission Modes
invited talk, in Fission and Properties of Neutron-Rich Nuclei, Proc. 2nd International Conference, St.Andrews, Scotland, Eds. J. H. Hamilton, W. R. Phillips, H. K. Carter (World Scientific, Singapore, 2000), p. 332-339.

D. N. Poenaru, B. Dobrescu, W. Greiner, J. H. Hamilton and A. V. Ramayya

The quasi-molecular stage of ternary fission
invited talk, in Advances in Nuclear Physics, Proc. of the International Symposium celebrating 50 years of institutional physics research in Romania, Eds. D. N. Poenaru and S. Stoica (World Scientific, Singapore, 2000), p. 91-102.

D. N. Poenaru, W. Greiner, J. H. Hamilton and A. V. Ramayya

Nuclear molecules in ternary fission
invited talk in Fundamental Issues in Elementary Matter, Proc. Internat. Symp. in honor and memory of Michael Danos, (241. W. & E. Heraeus Seminar), Bad Honnef, Germany, 25-29 Sept. 2000

D. N. Poenaru

Ternary and multicluster cold fission
invited talk and co-Director in Nuclei Far from Stability and Astrophysics, Proc. of the NATO Advanced Study Institute, Predeal, August 28-Sept. 8, 2000

B.Adeva, M.Iliescu, M.Pentia, C.Petrascu, T.Ponta, et al. (DIRAC Collab.)

DIRAC experiment at CERN

9-th Int. Conf. on Nuclear Reaction Mechanisms, Varenna, Italy, June 5-9, 2000, Proceedings:367-374

M.Augsburger, A.M.Bragadireanu, M.Iliescu, C.Petrascu, T.Ponta, et al. (DEAR Collab.)

The DEAR experiment

9-th Int. Conf. on Nuclear Reaction Mechanisms, Varenna, Italy, June 5-9, 2000, Proceedings:375-379

E.A.Preoteasa, C.Ciortea, D.Fluerăsu, S.E.Enescu, and E.Preoteasa

Mineral Elements in Composites for Restorative Dentistry. II. Improved Analysis by PIXE

Fourth General Conference of the Balkan Physics Union BPU-4, 22-27 August 2000, Veliko Turnovo, Bulgaria

E.A.Preoteasa, C.Ciortea, D.Fluerăsu, S.E.Enescu, and E.Preoteasa

Mineral Elements in Dental Composites by Atomic and Nuclear Analytical Methods. II. Improved Analysis by PIXE

National Physics Conference, September 21- 23, 2000, Constanța, Romania, Abstracts p.89 (oral presentation)

A.C.Razdolescu et al.

Compararea calibratoarelor comerciale de radioizotopi
Simpozionul Societatii Romane de Radioprotectie, Sinaia, sept.2000

A.Razdolescu et al.

Results obtained in the metrological check of a commercial radioisotope calibrator

International Radiation Protection Association, Hiroshima, Japonia, may 2000

M.Risse for KASCADE collaboration

Test and analysis of hadronic interaction models with KASCADE event rates

11-th International Symposium of Very High Energy Cosmic Rays Interactions, Sao Paulo, Brasil, July 2000

M.Roth, A.Chilingarian, A.Haungs, H.Rebel, A.Vardanyan for KASCADE collaboration

Nonparametric determination of energy and mass primary of cosmic rays and parameter correlations of classified KASCADE events

17-th European Cosmic Rays Symposium, ECRS, Lodz, Poland, July 24-28, 2000

M.Sahagia et al.

Asigurarea calitatii in masurarea activitatii radiofarmaceuticelor

Conferinta Nationala de Chimie, Caciulata, oct. 2000

M.Sahagia et al.

Obtaining of the Therapy radioisotopes at the TRIGA SSR Reactor

Symposion on Synthesis and Applications of Isotopically Labeled Compounds, Dresda, Germany, may 2000

M.Sahagia

Noi radiofarmaceutice cu utilizari in radioterapie

Simpozionul Societatii Romane de Radioprotectie, Sinaia, sept. 2000

S.Sarwar, ..., D.Pantea et al.

Spectroscopy of orbitally excited charm mesons

The Meeting of the Division of Particles and Fields of the American Physical Society "DPF 2000", Columbus, Ohio, USA, Aug. 9-12, 2000

G.Schatz for KASCADE collaboration

Recent results of KASCADE

11-th International Symposium of Very High Energy Cosmic Rays Interactions, Sao Paulo, Brasil, July 2000

L. Schächter, S. Dobrescu, Al. I. Badescu-Singureanu, K. E. Stiebing, S. Runkel, O. Hohn and H. Schmidt-Böcking

Influence of Secondary Electrons on the High Charge State Ion Output of Electron Cyclotron Resonance Ion Sources

Romanian National Conference of Physics, Constanta, September 2000 (Awarded by the Ion Agarbiceanu First Prize of the Romanian Physical Society)

C.Simion et al.

Obtaining of ^{67}Ga cytrate at the U-120 Cyclotrone
5th International Conference on Nuclear and Radio Chemistry, Pontresina, Suisse, sept. 2000

C.Simion

Simularea matematica a unor noi liganzi

Conferinta Nationala de Chimie, Caciulata, oct. 2000

C.A.Ur et al.

Cross-conjugate symmetry in the $f_{7/2}$ shell $N=Z$ nuclei

Proc. International Workshop "Selected Topics on $N=Z$ nuclei" (Pingst 2000), Lund, (2000) p. 252

C.A. Ur, C. Rossi Alvarez, D. Bazzacco, S.M. Lenzi, S. Lunardi, P. Pavan, P. Spolaore, G. de Angelis, M. De Poli, A. Gadea, N. Mărginean, D.R. Napoli, D. Bucurescu, M. Ionescu-Bujor, A. Iordachescu

Study of the symmetric reaction $^{90}\text{Zr}+^{90}\text{Zr}$ at GASP
Int. Conf. on Structure of the Nucleus at the Dawn of the Century, Bologna, May 29th-June 3rd, 2000.

M. Vişinescu

"Hidden" symmetries and Killing-Yano tensors

Invited talk at the Spring School and Workshop "Quantum Field Theories and Hamiltonian Systems", Călimănești, May 2000, to be published in Proceedings, Annals of Univ. Craiova (2001)

M. Vişinescu

Generalized Taub-NUT metrics and Killing-Yano tensors

Invited talk at NATO Advances Research Workshop "Noncommutative Structures in Mathematics and Physics", Kiev, September 2000, to be published in Proceedings, Kluwer Academic Publishers (2001)

J.Weber, R.Glasstetter, K.H.Kampert, H.O.Klages, H.J.Mayer, H.Ulrich for KASCADE collaboration

Determination of chemical composition and mass dependent energy spectra with the analysis of the muon/electron ratio in EAS

17-th European Cosmic Rays Symposium, ECRS, Lodz, Poland, July 24-28, 2000

J.Wentz, A.F.Badea, A.Bercuci, H.Bozdog, I.M.Brancus, H.J.Mathes, M.Petcu, H.Rebel, B.Vulpescu

The relevance of the muon charge ratio for the atmospheric neutrino anomaly.

17-th European Cosmic Rays Symposium, ECRS, Lodz, Poland, July 24-28, 2000

J.Wentz, D.Heck, B.Vulpescu, A.Bercuci

Calculation of atmospheric muon and neutrino fluxes with the air shower simulation code CORSIKA

International Conf. on Neutrino Physics and Astrophysics, Sudbury, Canada June 16-21, 2000.

J.Zabierowski, C.Buettner, K.Daumiller, P.Doll, D.Martello, R.Obenland for KASCADE collaboration

Large muon tracking detector in KASCADE EAS experiment

17-th European Cosmic Rays Symposium, ECRS, Lodz, Poland, July 24-28, 2000

PhD Theses

Călin Alexa

Aplicatii ale cromodinamicii cuantice in studiul interactiilor nucleare ultrarelativiste

Dragos Anghel

Phases and Phase transitions in restricted systems

Sorina Popescu

Neconservarea paritatii in interactiile hadron - hadron

Scientific Exchanges

Foreign Visitors

Cercasov V.

University of Hohenheim, Institute of Physics, Stuttgart, Germany, July 5-15, 2000

Dr O. Gavrishuk

IUCN-Dubna, Federația Rusă

Dr D. Jouan

IPN-Orsay, Franța

Dr V. Karnaukhov

IUCN-Dubna, Federația Rusă

Prof. S.Krasznovsky

KFKI-Budapest, Ungaria

Prof. J. Lefrancois

LAL-Orsay și CERN-Geneva

Dr.H.-J.Mathes

Forschungszentrum Karlsruhe, Institut für Kernphysik, Germany, POB 3640, D-76021, Karlsruhe, Germany

S.P.Ratti

INFN-Sezione di Pavia, Italy

Prof. Dr. H. Rebel

Forschungszentrum Karlsruhe, Institut für Kernphysik, Germany, POB 3640, D-76021, Karlsruhe, Germany

Dr. A. Schopper

CERN-Geneva

Prof. I. Wagner

KFKI-Budapest, Ungaria

Dr. J. Wentz

Forschungszentrum Karlsruhe, Institut für Kernphysik, Germany, POB 3640, D-76021, Karlsruhe, Germany

Invited Seminars

Prof. S.P. Ratti

The strange charm of charm
INFN-Sezione di Pavia, Italia

S.P. Ratti

"The strange charm of charm" April 13, 2000
INFN-Sezione di Pavia, Italy

Visits Abroad

Călin Alexa

CERN, Geneva, Elveția

Călin Alexa

CPPM, Marseille, Franța

Dr. A.F. Badea

Forschungszentrum Karlsruhe, Institut für Kernphysik, Germany POB 3640, D-76021, Karlsruhe, Germany

I. Berceanu

LNS - Catania

A. Bercuci

Forschungszentrum Karlsruhe, Institut für Kernphysik, Germany, POB 3640, D-76021, Karlsruhe, Germany

Venera Boldea

CERN, Geneva, Elveția

Mario Bragadireanu

LNF, Frascati, Italia

Dr. I.M. Brancu

Forschungszentrum Karlsruhe, Institut für Kernphysik, Germany POB 3640, D-76021, Karlsruhe, Germany

D. Bucurescu

Fysik Department, Technische Universität München

D. Bucurescu

University of Padova, Padova, Italy

I. Caprini

Center of Particle Physics, Marseille, France.

I. Caprini

Center of Theoretical Physics, Marseille, France.

I. Caprini

Institute of Physics, Academy of Sciences of Czech Republic, Prague.

I. Caprini

TH Division, CERN, Geneva, Switzerland.

V. Cătănescu

Kirchhoff Institute for Physics - Heidelberg

M. Ciobanu

Kirchhoff Institute for Physics - Heidelberg

Cornelia Coca

CERN, Geneva, Elveția

Cornelia Coca

Osaka, Japonia

Sanda Diță

CERN, Geneva, Elveția

S. Dobrescu

Kernfysich Versneller Instituut (KVI), Groningen, The Netherlands S. Dobrescu Participation at the workshop Kick-off Meeting on Fusion Technology for new Associated Countries organized by the Directorate for Research of the European Commission, March 2000, Garching bei Munchen, Germany L. Schachter Kernfysich Versneller Instituut (KVI), Groningen, The Netherlands

S. Dobrescu

Participation at the workshop Kick-off Meeting on Fusion Technology for new Associated Countries organized by the Directorate for Research of the European Commission, March 2000, Garching bei Munchen, Germany

R. A. Gherghescu

Institut für Theoretische Physik der J. W. Goethe Universität, Frankfurt am Main, Germany, working stage

R. A. Gherghescu

SUBATECH, Nantes, Franta, working stage

Grigore D. R.

Theory Division, DESY, Germany

M. Ionescu-Bujor

INFN, LNL, Legnaro/Padova, Italy

A. Iordachescu

INFN, LNL, Legnaro/Padova, Italy

A. Isbasescu

The Institute of Physics and Chemical Research (RIKEN), Participation in Measurements at the RIKEN-RIPS Accelerator for Radioactive Beams, September 2000, Wako, Saitama, Japan

M. Ivaşcu

University of Padova, Padova, Italy

N. Mărginean

INFN, Padova, Italy

Andrei Micu

ICTP, Trieste, Italia

Andrei Micu

Martin-Luther Univ., Halle, Germania

M. Mirea

Institut de Physique Nucléaire – Orsay, France

D. Moisa

GSI - Darmstadt

Dan Pantea

CERN, Geneva, Elveția

H. Petrascu

INFN-LNS, Catania, Italy, Nov.2000, Colaboration at the MAGNEX Project

H. Petrascu

The Institute of Physics and Chemical Research (RIKEN), Preparation of the experimental set-up and measurements at the RIKEN-RIPS Accelerator for Radioactive Beams, Wako, Saitama, Japan

M. Petrascu

The Institute of Physics and Chemical Research (RIKEN), Preparation of the experimental set-up and measurements at the RIKEN-RIPS Accelerator for Radioactive Beams, Wako, Saitama, Japan

Radu Petrescu

LNF, Frascati, Italia

M. Petriş

GSI - Darmstadt

M. Petrovici

CERN - Geneva

M. Petrovici

GSI - Darmstadt

A. Petrovici

GSI - Darmstadt, Germany

A. Petrovici

INT - Seattle, Univ. Washington, USA

A. Petrovici

Riken, Japan

A. Petrovici

Universität zu Köln, Germany

A. Petrovici

Institut

für Theoretische Physik, Universität Tübingen, Germany

D. N. Poenaru

Department

Physics, Vanderbilt University, Nashville, Tennessee, USA, working stage

D. N. Poenaru

European Commission, Brussels, Belgium, Presentation of the Center of Excellence IDRANAP

D. N. Poenaru

Institut für Theoretische Physik der J. W. Goethe Universität, Frankfurt am Main, Germany, working stage

D. N. Poenaru

Institute "ATOMKI" of the Hungarian Academy of Sciences, Debrecen, invited talk at International Symposium ENS2000

Titus Ponta

LNF, Frascati, Italia

A. Pop

LNS - Catania

Sorina Popescu

CERN, Geneva, Elveția

Sorina Popescu

Ruprech-Karis Univ., heidelberg, Germania

Titi Preda

CERN, Geneva, Elveția

R. Ruscu

The Institute of Physics and Chemical Research (RIKEN), Participation in Measurements at the RIKEN-RIPS Accelerator for Radioactive Beams, September 2000, Wako, Saitama, Japan

L. Schächter

Kernfysich Versneller Instituut (KVI), Groningen, The Netherlands S. Dobrescu Participation at the workshop Kick-off Meeting on Fusion Technology for new Associated Countries organized by the Directorate for Research of the European Commission, March 2000, Garching bei Munchen, Germany L. Schachter Kernfysich Versneller Instituut (KVI), Groningen, The Netherlands

V. Simion

GSI - Darmstadt

Diana Soare

LNF, Frascati, Italia

G. Stoicea

GSI - Darmstadt

L. Stroe

INFN, Padova, Italy

C.A. Ur

University of Padova, Padova, Italy

Dr.B.Vulpescu

Forschungszentrum Karlsruhe, Institut für Kernphysik, Germany, POB 3640, D-76021, Karlsruhe, Germany

Seminars Abroad

A. Andronic

Differential Flow in Heavy Ion Collisions
FOPI Collaboration Meeting, GSI-Darmstadt, 10.10.2000

A. Andronic

Differential Flow
FOPI Collaboration Meeting, GSI-Darmstadt, 04.04.2000

S.Berceanu

Topics on coherent states, Segal-Bargmann-Hall transform, Toeplitz operators and D-modules,
a series of two hours talks delivered in the Seminary of "Operator Theory" of S. Berceanu and A. Gheondea at the Institute of Mathematics Simion Stoilow at the Romanian Academy, the first one on January 24, 200

S.Berceanu

Holomorphic differential operators with polynomial coefficients on Kähler coherent state orbits
seminar at the Insitute of Mathematics, University of Technology, Darmstadt, Seminary on "Complex Analysis" of Karl-Hermann Neeb, November 9, 2000

S.Berceanu

Linear dynamical systems on Kähler coherent states orbits
invited talk at the Universidad National Autonoma de Mexico, Instituto de Matematicas, Unidad Cuernavaca, May 10, 2000.

S.Berceanu

Symplectic area of geodesic triangles and coherent state
seminar at the Berkeley, CA, USA, in the Seminary on Symplectic Geometry of Alan Weinstein, May 23, 2000; seminary at the Doppler Institute, Czech Technical Univesity in Prague, Faculty of Nuclear Science and Physical Engineering, Seminar of Mathematical Physics of J. Tolar, oct. 17, 2000

I. Caprini

Quark-hadron duality, factorization and strong phases in $B_d^0 \rightarrow \pi^+ \pi^-$ decay
Institute of Physics and Charles University, Prague, Czech Republic, 20.11.2000

I. Caprini

Quark-hadron duality, factorization and strong phases in $B_d^0 \rightarrow \pi^+ \pi^-$ decay
Triangle Meeting on Particle Physics, Viena, 1-2 december 2000

R. A. Gherghescu

Target-projectile pairs for the synthesis of superheavy nuclei
GSI- Darmstadt, 20 Noiembrie, 2000

H.Petrascu

Investigation of Neutron Pair Pre-Emission in the Fusion of ^{11}Li Halo Nuclei with SI targets
CINFN-LNS, Catania, Italy, Nov.2000

M. Petrovici

Isospin dependence of squeeze-out
FOPI Collaboration Meeting, GSI-Darmstadt, 10.10.2000

M. Petrovici

RPC Tests
FOPI Collaboration Meeting, GSI-Darmstadt, 09.10.2000

M. Petrovici

Transition from in-plane to out-of-plane emission for Au+Au collisions
FOPI Collaboration Meeting, GSI-Darmstadt, 04.04.2000

A. Petrovici

Variational approach to coexistence phenomena in medium mass nuclei
Kernphysikalisches Kolloquium, IKP - Univ. Köln, Germany, 04.05.2000

G. Stoicea

Incident Energy and A_{part} Dependence of Flow in Au+Au and Xe+CsI
FOPI Collaboration Meeting, GSI-Darmstadt, 10.10.2000

Research Staff

Basic Physics

Nuclear Physics

Ivaşcu Marin, Petraşcu Marius, Semenescu Gheorghe, Bădică Teodor, Bucurescu Dorel, Haţeganu Cornel, Calboreanu Alexandru, Dobrescu Şerban, Buţă Apostol, Borcea Cătălin, Popescu V. Ion, Iordăchescu Alexandru, Ionescu Bujor Manuela, Drăgulescu Emilian, Petrovici Alexandriana, Ion B. Dumitru, Ponta Titus, Diţa Sanda, Boldea Venera, Zamfir Nicolae, Olariu Silviu, Schachter Leon, Pădureanu Ion, Isbăşescu Alina, David Ioana, Berceanu Ionela, Brîncuş Ileana, Cojocaru Viorel, Simon Victor, Grama Cornelia, Duma St. Marin, Ruscu Radu, Enulescu Alexandru, Piticu Ion, Lazăr Ioana, Corcalciuc Valentin, Ciortea Constantin, Dumitrescu Radu, Penţia Mircea, Dorobanţu Ion, Coca Cornelia, Pantea Dan, Avrigeanu Marinela, Cutoiu Dan, Bădescu Singureanu Alex, Iacob Victor Eugen, Cţa Danil Gheorghe, Avrigeanu Vlad Gabriel, Pantelică Dan, Petcu Ileana, Pop Amalia, Flueraşu Daniela, Pîrlog Marian, Bejan Anca Bogdana, Preoteasa Eugen, Petrache Costel, Gherghescu Radu, Cotorobai Florin Valeri, Petraşcu Horia, Radu Mihai, Legrand Iosif Charles, Căta Danil Irina, Mirea Mihail Doloris, Nica N. Ninel, Szilagyi Szabolcs Zoltan, Ur A. Călin A. Alexandru, Petraşcu Cătălina Oana, Olariu Agata, Preda Titi, Sabaiduc Vasile, Andronic N. Anton, Ionescu M. Remus Amilcar, Alexa R. Călin, Dumitru M. Dana Elena, Stroe Lucian, Iliescu Mihail, Negoită Florin, Savu Iulia Diana, Moiso Nicoleta, Fologea Daniel, Răduţă Adriana Rodica, Stoicea Gabriel, Răduţă Alexandru Horia, Ionescu Maria Adriana, Groza Radu Liviu, Ion Mihai Laurian, Bragadireanu Alexandru, Ion Mihail, Dumitrescu Gabriela, Scîntee N. Nicolae, Petriş D. Mariana, Bastea T. Sorin, Popescu I. Răzvan, Vaman Georgeta, Vulpescu Bogdan, Kusko Cristian, Popescu Sorina, Rădulescu Aurel, Drafta George, Anghel Dragoş Victor, Badea Aurelian Florin, Tăbăcaru Gabriel, Toader Cristian Florenti, Beldiman Anne Marie, Albu Mihaela, Andreoiu Corina, Stetcu Ionel, Borcan Cristina, Radu Florin, Oros D. Ana Maria, Mitrică Ionel, Popa Gabriela, Petre Marian.

Theoretical Physics

Micu Mircea, Grecu Dan, Iosifescu Mircea, Vişinescu Mihai, Ixaru Liviu, Rădescu Eugen, Răduţa Apolodor, Săndulescu Aureliu, Diţa Petre, Micu Liliana, Angelescu Nicolae, Scutaru Horia, Caprini Irinel, Grama Nicolae, Adam Gheorghe, Mihalache Dumitru, Apostol Marian, Grigore Radu Dan, Ceauşescu N. Valentin, Cîrstoiu Florin Cornel, Vişinescu Anca, Adam Sanda, Gheorghe I. Alex Cezar, Stratan Gheorghe, Bundaru Mircea, Stoica Sabin, Silişteanu Ion, Delion Doru Sabin, Isar Aurelian, Săndulescu Nicolae, Buzatu

Florin Dorian, Ursu Ioan, Enachi Nicolae, Costache Gheorghe, Bîrsan Vasile Victor, Florescu Adrian, Băran Virgil, Mişicu Şerban Dragos, Despa Florin, Popa Mircea, Horoi Mihai, Bulboacă Iosif, Costin Ovidiu, Baboiu Daniel Marian, Pănoiu Nicolae Coriolan, Manoliu I. Mihaela, Iancu V. Edmond, Doloc A. Lida, Fircă Radu Gabriel, Moldoveanu Florin, Vaman Diana, Paradanu Gheorghe Sorin, Cârstea Adrian Ştefan, Mihuş Izabela Ramona, Schiaua Claudiu Cornel, Acatrinei Ciprian Sorin, Cune Liviu Cristian, Crasovan Lucian Cornel, Răduţă Cristian, Ispas Simona Georgiana.

Applied Physics and Technological Development

Applied Physics

Berinde Alexandru, Constantinescu Olimpiu, Caprini Mihai, Ciobanu Mircea, Ivanov Eugen, Racolţa Petre Mihai, Galeriu Dan, Mateescu Gheorghe, Vamanu Vasile Dan, Bengulescu Dumitru, Grosescu Radu, Caraghergheopol Gheorghe, Ciuş Mihai, Niculescu Dumitru, Sălăgean Maria, Cătănescu Vasile, Pantelică Ana, Prada Benone, Niculescu Alexandru, Bozdog Horia Pavel, Constantinescu Bogdan, Grabari Valeriu, Ploştinaru Dan, Saidel Maria Alice, Păunescu Niculina, Catană Dumitru, Cîncu Manuela, Stan Sion Cătălin, Constantin Florin, Tripăduş Vasile, Goran Benone, Rusu Alexandru, Bădescu Elisabeta, Georgescu Rodica Maria, Bartoş Daniel, Petcu Mirel Adrian, Măgureanu Constantin, Stănescu Samoil Petre, Niculescu Mihaela Lili, Mocanu Nicolae, Lupu Mihaela, Tarta Petru Dorinel, Nicolescu George, Gheorghiu Adriana, Mihai Nelu, Vasilescu Angela, Popa Simil Liviu, Timofte Laurenţiu, Mărgineanu Romul Mircea, Crăciunescu Teddy, Dumitru Radu Octavian, Slavnicu Stelian Dan, Ioan Petre, Scarlat Anişoara, Edu Gabriel, Enăchescu Mihaela, Drăghici Daniela Victoria, Gheorghiu Dorina, Rădulescu Mihaela, Bratu Eugen, Todor A. Aurel Dorin, Ivan P. Adrian, Apostoaei Andrei Iulian, Arsenescu N. Remus, Manciu Felicia Speranţa, Breban Domnica Cristina, Ţurcanu Catrinel Octavia, Niculae Carmen Georgeta, Bugoi Roxana Nicoleta, Radu Alina, Mărginean Nicolae Marius, Pavel Eugen, Dumitru Dionis, Ciobanu Ileana, Acasandrei Valentin Teodor, Ianculescu M. Cristian, Alexandru Bogdan, Casaru George, Rusu Claudiu, Dănilă Bogdan, Mihăilescu Lucian, Muntele Claudiu Iulian, Udrea Şerban Alexandru, Melintescu Mirela Anca, Crăciun Liviu, Cuturela Doru, Cristea Ion, Zaharia Petre, Mitru Aurel, Dobre Nicolae, Matache Mihaela.

Technological Development

Nuclear Methods and Instruments

Pîrlogea Paul, Andruscenco Paul, Ţarină Eneea, Aldea

Adriana, Lira Cristian, Ciulei Dumitru, Popa Mircea Alexandru, Cîmpean Adrian, Botoș Clara, Crăciun Marian Virgil.

Radiation Detectors and Dosimetric Methods

Rebigan Florian, Julier Georgeta, Sandu Miron, Cruceru Ilie, Turcuș Caliopia, Păunică Tatiana, Staicu Maria, Sandu Elena, Stîngă Doru, Călin Marian Romeo, Pușcălău Mirela Angela, Crăciun Cornelia Nicoleta, Stochioiu Ana, Lungu Claudiu Teodor, Moiseev Tamara, Aranghel Dorina, Borca Camelia Nicoleta, Timiș Cozmin Nicolae, Glodariu Tudor, Mihai Felicia, Muntele Iulia Cristina, Mangiac Dan Octavian.

Vacuum Equipments and Clean Environments

Bătulescu Cornel, Giolu Gheorghe, Manoil Alexandru, Duță Viorel, Popa Victor, Ursescu Constantin, Mateescu Gheorghe, Aculai Augustin, Rădulescu Gheorghe, Guță Tudor Dragoș, Ighigeanu Daniel Paul, Iancu Dumitru, Serbina Leonard, Rusen I. Ion, Andrieș Mihail, Tudor Gheorghe.

Technological Transfer

Nuclear Facilities

Mărculescu Augustin, Nicolescu Constantin, Cojocaru Emil, Teodorescu V. Emanoil, Alecu Ana, Rădulescu Laura.

Tandem-Operation

Marinescu Liviu, Bordeanu Cristina, Dumitru Gabriel, Dima Răzvan.

Cyclotron-Operation

Dudu Dorin, Boțilă Emil.

Nuclear Facilities and Services of National Interest

Radioisotope Production Center

Negoită Nicolae, Grigorescu Leon, Gîrd Eugen, Sahagia Maria, Borza Virginia, Lungu Valeria, Mihăilă Vasile, Iliescu Victor, Fugaru Viorel, Postolache Cristian, Ivan Constantin, Simion Corina Anca, Munteanu Răzvan, Manea I. Simona Eugenia, Neacșu V. Elena, Grosu Cătălina, Răzdolescu L. Anamaria, Mihăilescu Gabriela, Tătar Laura Dalida, Barna Cătălina Mihaela, Cruceru Mădălina, Chiper Diana, Chariton Delfina, Luca Aurelian, Petrașcu Anca Maria, Niculae Dana, Corol Delia Irina, Dragomir Andrei Vasile, Chirvășoiu Gheorghe, Chirvășoiu Adriana.

Reactor, Radwaste Treatment-Station (RWTS) + National Repository (RWNR)

Reactor Research

Gîrlea Ion, Gîrlea Cristina, Mocioiu Doru, Ene Daniela, Ilas Dănuț, Kelerman Cristian, Tigău Nicoleta, Tigău Florin Dănuț.

Reactor-Operation

Crăciun Lucia, Olteanu Alexe Ioan, Zorliu Adrian, Mincu Gh. Ion, Petran Corneliu, Aranghel Tudor, Dragolici Cristian, Rîpeanu Randus Florin, Iliescu Nicolai.

RWTS-RWNR - Research

Turcanu Corneliu, Popovici Constantin, Dragolici Felicia Nicole, Nicu Mihaela Daniela, Mihai Cosmin.

RWTS-RWNR - Operation

Postelnicu Constantin, Rotărescu Gheorghe, Cazan Ioan Lucian, Lungu Florina Laura, Morar Dumitru Nicolae, Guran Victor, Dinu Dorel.

Technological Irradiation

Gașpar Emilian, Daniș Ana, Popescu Corneliu, Staicu Leon, Dorcioman Dorin, Radu Rodica, Diniescu Lucreția, Ciungan Beniamin, Rucăreanu Ion, Ponta Corneliu, Kluger Alexandru Victor, Drăgușin Mitică, Moraru Rodica, Pătrașcu Sanda, Pascu Maria, Lăzărescu Toma, Andrieș Constantin, Păunică Iosif, Ciubotariu Mariana, Lucaci Adriana, Enescu G. Sanda Elena, Popescu Aurora, Dorcioman Radu, Pop Dan, Mureșan Raluca Anca, Moise Ioan Valentin, Militaru Otilia, Popovici Gelu, Ilie Theodor, Roncea Cristina, Andrieș Emilia, Rotaru Păstorita Rodica, Copelciuc Angela, Cernisov Mihaela.

Computing and Data Exchanging Center

Zamfirescu Ion, Moldovan Nicolae, Cărbunaru Octavian, Mazilu Dumitru, Rizea Margarit, Manu Valentin, Dăneț Anton, Mirică Micșunica, Ciupitu Eugen, Angelescu Gabriela Paula, Andrieș Sorin, Constantinescu Serban.

Quality Assurance

Domșa Ioana, Brancovici Sibila, Livadaru Mariana, Dogaru Gheorghe.

Radiation Protection

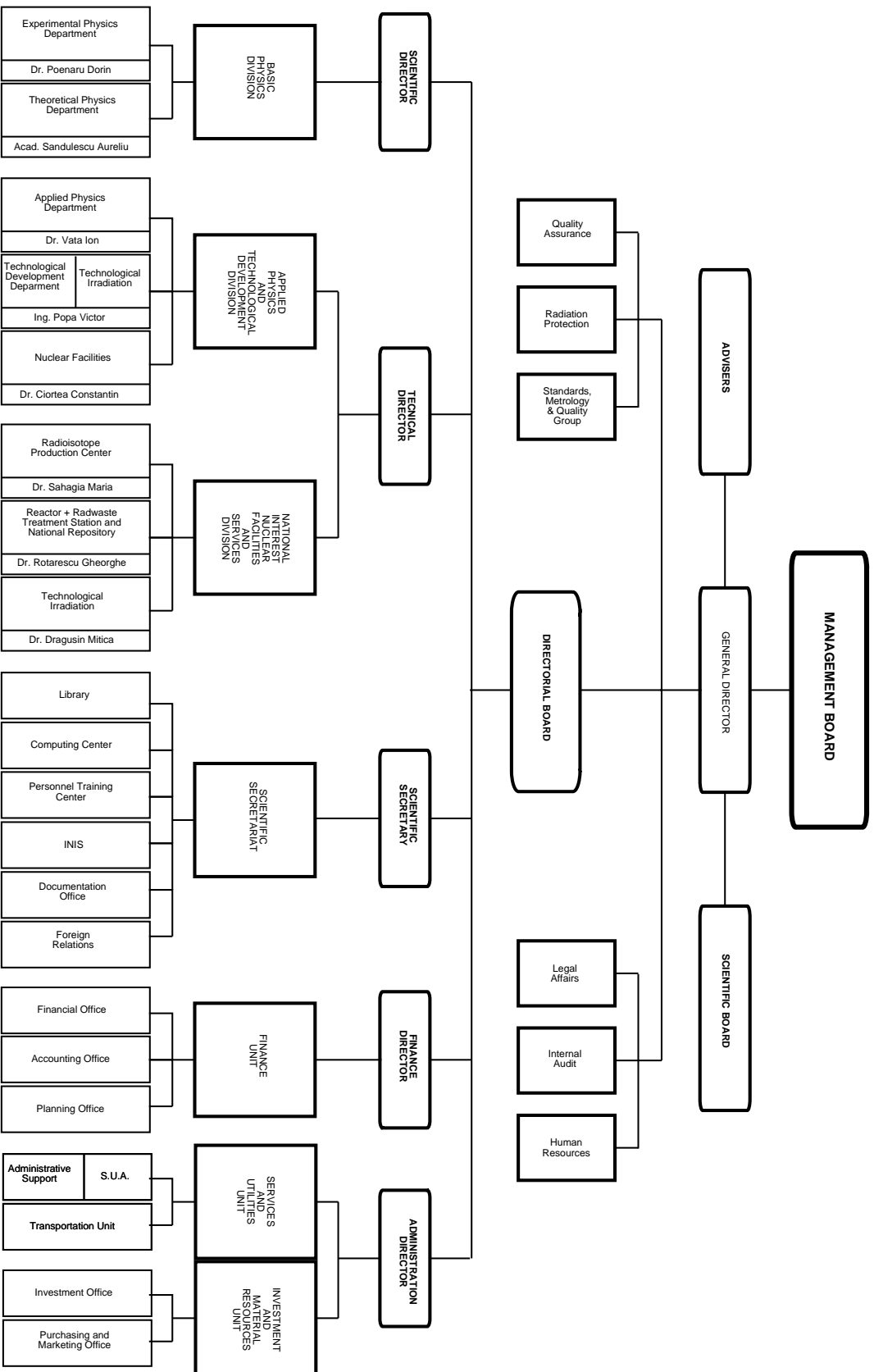
Floare Gabriel, Bejenaru Sorin, Frujinoiu Cătălin, Preda Mihaela, Iordache Elena, Sacota Valeriu, Oatu Carmen.

Standards, Metrology, Quality

Vâlcov Nicolai, Macrin Rodica, Dobrescu Corvin, Purghel Lidia, Diviricean Maria, Bercea Sorin, Iancso Georgeta, Celarel Aurelia, Avram Corina Carmen, Barbu Mircea, Iliescu Elena, Hurezeanu Dorina, Iancu Rodica, Kelerman Cristina Raluca, Costin Aurelia Monica.

INTERNAL ORGANIZATION

HORIA HULUBEI NATIONAL INSTITUTE OF PHYSICS AND NUCLEAR ENGINEERING - IFIN-HH, Bucharest



Author Index

Assunção, M.	53	Căta-Danil, I.	23
Adam, Gh.	14, 15	Cătănescu, V.	64, 65, 70
Adam, S.	14, 15	Chiba, M.	58
Aiftimiei, C.	51, 52	Cimpeanu, Catalina	115–118, 122
Ajinenko, I.	79	Cincu, Emanuela	98
Aksenov, V. L.	34	Ciobanu, M.	43, 64, 65, 70
Aleev, A. N.	83	Ciortea, C.	46–48
Alexa, C.	77, 78, 81, 82	Ciubotariu, M.	62, 99
ALICE, Collaboration	64, 65, 70	Clapier, F.	38
Andronic, A.	39, 40, 68, 70	Coc, A.	53
Anton, L.	14	Coca, C.	79
Appelshäuser, H.	70	Colci, M.	27, 42
Aranghel, D.	55	Coniglione, R.	69
ATLAS, Collaboration	74, 77, 80, 82	Constantinescu, A.	58, 66
Avriganu, M.	35	Constantinescu, B.	106, 107
Avriganu, V.	35–37	Constantinescu, S.	74, 77, 78, 80, 81
Baciu, F.	28	Constantin, F.	107
Badea, A. F..	51, 52	Courtin, S.	53
Badica, T.	45, 59	Craciunescu, T.	93, 94
Baran, Gh. D.	101	Craciun, L.	100, 104, 109
Bădescu, E.	97	Crasovan, L.-C.	17–19
Beck, C.	53	Crout, N. M. J.	89
Becker, F.	33	Crucearu, I.	41, 58, 66
Beijers, J. P. M.	38	Crucearu, Madalina	118
Berceanu, I.	68, 69	Csutak, O.	88
Bercuci, A.	52	Curceanu, C.	73
Berdermann, E.	43	Danis, A.	62, 99
Bersford, N. A.	89	Daues, H.	70
Besliu, C.	28	David, I.	47
Bibicu, I.	46	Desmedt, A.	55
Blank, B.	33	Devismes, A.	70
Blume, C.	70	Dima, G.	45, 59
Boldea, V.	74, 77, 78, 81	Dinca, C.	20
Borcea, C.	33	Dinescu, L.	47
Bordeanu, C.	58, 66	Dita, S.	74, 77, 78, 80–82
Bouchez, E.	33	Diță, P.	10
Bourrely, C.	11	Dobrescu, S.	50
Bozdog, H.	52	Dorcioman, D.	63
Bragadireanu, M.	73	Dragolici, A. C.	108
Brancus, I. M.	51, 52	Dragolici, F.	125
Brandenburg, S.	38	Dragulescu, E.	28, 29, 100
Brandolini, F.	25	Drăgușin, M.	107
Braun-Munzinger, P.	41, 43, 70	Drentje, A. G.	50
Breban, D. C.	87	Dudu, D.	103–105
Bucher, D.	70	Duma, M.	41, 43, 51, 52, 68, 69
Bucurescu, D.	23, 25	Dumitrescu, G.	99
Busuioc, G.	59	Dumitriu, D. E.	44, 47
Caprini, I.	11, 12	Dumitru, R. O.	87
Caprini, M.	97	Emsallem, I.	33
Caragheorghopol, G.	43	Enescu, S. E.	46–48
Cassette, Ph.	120	Enulescu, Al.	46
Catanescu, V.	43	d'Erasmus, G.	68
Căta-Danil, Gh.	23, 27, 30	Etzkorn, M.	31, 32

EXCHARM,Collaboration	83	Katori,K.	58
Faessler,A.	24	Kiener,J.	53
Fey,M.	53	Klini,Argyro	60
Finck,Ch.	70	Kluger,A.	46
Fischer,J.	12	Kobayashi,T.	58
Fleurot,F.	53	Korichi,A.	53
Fluerasu,D.	47, 48	Korten,W.	33
Fologea,D.	88	Kozlov,Zh.A.	56
FOPI,Collaboration	39, 40	Kriembardis,G.	53
Fotakis,C.	60	Kunz,R.	53
Fraiquin,H.	50	Lamothe,E. S.	90
de France,G.	33	Lanzanò,G.	68
Galanopoulos,E.	53	Laurent,H.	38
Galeriu,D.	89–91	Lauter,H.	34
Genevey,J.	33	Lazarescu,M.F.	61
Georgescu ,I.I.	101, 102	Lebreton,H.	38
Gheorghiu,A.	93	Lechner,R.	55
Gheorgiu,D.	93	Lechner,R.E.	54
Gherghescu,R.A.	26	Le Coz,Y.	33
Ghita,R. V.	61	Lederer,F.	17–19
Giurgiu,M.	58, 66	LeDu,D.	53
Glodariu,T.	37	Lefebvre ,A.	53
Grama,C.	9, 53	Leifels,Y.	39, 40
Grama,N.	9	Leiner,V.	31, 34
Greco,M.N.	46	Lenzi,S.M.	25
Greiner,W.	26	Lewitowicz,M.	33
Grigore,D. R.	13	Lister,T.	70
Grigorescu,E.L.	113, 114, 120, 121, 129, 130	Lopez-Martens,A.	53
Grosescu,R.	109	Luca,A.	113, 114, 120, 121, 129, 130
Guaraldo,C.	73	Lucas,R.	33
Gyorgy,Eniko	60	Lucherini,V.	73
Haas,F.	53	Lungu,L.	125
Hamilton,J.H.	26	Lungu,V. V.	119
Hammer,J. W.	53	Macovei,I.	33
Hannachi,F.	53	Magureanu,C.	79
Harissopulos,S.	53	Mahmoud,T.	70
Hauschild,K.	33	Malcherek,D.	53
Herrmann,N.	39–41, 70	Malomed,B. A.	17–19
van Hess,M.	89	Manea,A.S.	61
Hildenbrand,K.D.	39–41	Marghitu,S.	20
Hurstel,A.	33	Mărginean,N.	25
Iftimia,I.	28	Martin,D.	20
Iliescu,E.	20	Mateescu,G.	93
Iliescu,I.	73	Mathes,H. J.	52
Immé,G.	68	Mărginean,N.	23
Ion,D.B.	75, 76	Mazilu,D.	17–19
Ionescu-Bujor,M.	25	Medina,N.H	25
Ion,M.	55	Melintescu,A.	89, 91
Ion,M.L.	75, 76	Melnikov,I. V.	17, 18
Iordăchescu,A.	25	Meunier,R.	53
Isbasescu,A.	57, 58, 66	De Meyer,H.	16
Ivan,C.	113, 114, 120, 121, 129, 130	Micu,L.	11
Ivaşcu,M.	23	Mihailescu,G.	119
Iwai,Y.	44	Mihailescu,I.N.	60
Ixaru,L. Gr.	16	Mihalache,D.	17–19
Jianu,E. D.	45, 59	Mihalcea,I.	116–118
Kanai,Y.	44	Mincu,I.	108

Mirea, M.	38	De Poli, M.	25
Miron, N.	104	Ponta, T.	73, 83
Mitrica, B.	52	Pop, A.	68, 69
Moisă, D.	28, 41–43, 67–69	Popa, V.	103–105
Moise, V.	107	Popescu, I. V.	45, 59
Morimoto, K.	58, 66	Postolache, C.	54
Morishita, Y.	44	Preda, T.	79, 83
Moritz, P.	43	Preoteasa, E.	48, 49, 106
Murariu-Magureanu, M. D.	102	Preoteasa, E. A.	48, 49, 106
Muresan, O.	109	Puscalau, M.	92
NA50, Collaboration	78, 81	Qaim, S. M.	36
Napoli, D. R.	25	Raciti, G.	68
Negoita, F.	33, 49, 57, 60, 61	Racolta, P.	28
Negoita, N.	115	Racolta, P. M.	100, 103–105
Negreț, Al.	30, 63	Radu, F.	31, 32, 34
Nicolescu, C.	107	Radulescu, A.	54
Niculae, D.	119	Rădulescu, L.	107
Nicu, M.	125	Rahkila, P.	33
Nikitenko, Yu. V.	34	Ramayya, A. V.	26
Nishimura, S.	58	Raskob, W.	91
Nishi, Y.	58	Rădulescu, A.	56
Oehlschlaeger, J.	51	Razdolescu, A. C.	113, 129
Olariu, A.	45, 59	Razdolescu, Anamaria Cristina	114, 120, 121, 130
de Oliveira, F.	33	Râpeanu, S.	56
Oncescu, M.	62	Rebel, H.	51, 52
Oproiu, C.	20	Reimer, P.	36
Ozawa, A.	58	Reisdorf, W.	40
Padureanu, I.	54	Rejmund, M.	33
Pagano, A.	68	Reygers, K.	70
Panoiu, N.-C.	17, 18	Ribas, R. V.	25
Pantaleo, G.	68	Ristoscu, Carmen	60
Pantea, D.	74, 77	Rizea, M.	20
Pantelica, A. I.	101, 102	Rodrigues, G.	50
Pantelică, D.	33, 49, 57, 60, 61	Rosca, A.	79
Paradellis, T.	53	Rossi Alvarez, C.	25
Pauwels, N.	38	Rotarescu, Gh.	125
Pavan, P.	25	Rousseau, M.	53
Pădureanu, I.	55, 56	Rowley, N.	53
Peitzmann, T.	70	Ruscu, R.	58, 66
Pelissier, C.	53	Rusu, C.	23
Petcu, M.	52	Sahagia, Maria	113–115, 120–122, 129, 130
Peterson, S. R.	89	Saint-Laurent, M. G.	38
Peticila, M.	109	Salagean, M. N.	101, 102
Petran, C.	108	Santo, R.	70
Petrascu, H.	57, 58, 66	Sapienza, P.	69
Petrascu, M.	57, 58, 60, 66	Scantei, N.	57
Petre, M.	45, 59	Scarlat, A. G.	101, 102
Petriș, M.	41, 43	Schächter, L.	50
Petrovici, A.	24	Schicker, R.	70
Petrovici, M.	39–41, 43, 68–70	Schmid, K. W.	24
Piatelli, P.	69	Schmitte, T.	32
Pieper, J.	55	Schreyer, A.	31, 32
Pinston, J.	33	Schukraft, J.	43
Plakida, N. M.	14	Sedykh, S.	70
Plompen, A. J. M.	35–37	Semenescu, G.	28
Podolyak, Zs.	25	Semenov, V. A.	56
Poenaru, D. N.	26	Serbanut, C.	100

Serbanut,G. C.	28, 29	Tripadus,V.	100, 104, 109
Serbanut,I.	29	Trivedi,A.	90
Simion,Corina	116, 117	Tudorica,A.	57, 58, 60
Simion,Corina Anca	122	Turcanu,C.	93, 94, 125
Simion,V.	43, 68, 69	Turcanu,C. O.	91
Simon,R.S.	70	Ur,C.A.	23, 25
Sirghi,D.	73	Vainos,N.	60
Slavnicu,D.	93	Vanden Berghe,G.	16
Stachel,J.	70	Voiculescu,Dana	103–105
Stanoiu,M.	33	Vulpescu,B.	52
Staudt,G.	53	Weigmann,H.	37
Stelzer,H.	43, 70	Weil,J.	53
Stihi,C.	45, 59	Wentz,J.	52
Stochioiu,A.	47	Wessels,J.	70
Stoicea,G.	39–41, 43	Westerholt,K.	31, 32
Suda,T.	58	Windelband,B.	70
Syromyatnikov,V	34	Winkelmann,O.	70
Szilner,S.	53	Xu,C.	70
Tanihata,I.	58, 66	Yamazaki,Y.	44
Tatischeff,V.	53	Yoshida,K.	58
Teodorescu,C.	107	Zabel,H.	31, 32
Theisen,Ch.	33	Zamfirescu,I.	9
Thibaud,J.P.	53	Zegers,R.G.T.	38
Toma,M.	20	Del Zoppo,A.	68, 69
Torner,L.	17	Zorliu,A.	108